Theses and Dissertations--Molecular and Cellular Biochemistry

Molecular and Cellular Biochemistry

2021

Reversible Glucan Phosphorylation in the Red Alga, *Cyanidioschyzon merolae*

Corey Owen Brizzee

University of Kentucky, corey.brizzee@gmail.com

Author ORCID Identifier:
https://orcid.org/0000-0001-8659-7407

Digital Object Identifier: https://doi.org/10.13023/etd.2021.216

Right click to open a feedback form in a new tab to let us know how this document benefits you.

STUDENT AGREEMENT:

I represent that my thesis or dissertation and abstract are my original work. Proper attribution has been given to all outside sources. I understand that I am solely responsible for obtaining any needed copyright permissions. I have obtained needed written permission statement(s) from the owner(s) of each third-party copyrighted matter to be included in my work, allowing electronic distribution (if such use is not permitted by the fair use doctrine) which will be submitted to UKnowledge as Additional File.

I hereby grant to The University of Kentucky and its agents the irrevocable, non-exclusive, and royalty-free license to archive and make accessible my work in whole or in part in all forms of media, now or hereafter known. I agree that the document mentioned above may be made available immediately for worldwide access unless an embargo applies.

I retain all other ownership rights to the copyright of my work. I also retain the right to use in future works (such as articles or books) all or part of my work. I understand that I am free to register the copyright to my work.

REVIEW, APPROVAL AND ACCEPTANCE

The document mentioned above has been reviewed and accepted by the student's advisor, on behalf of the advisory committee, and by the Director of Graduate Studies (DGS), on behalf of the program; we verify that this is the final, approved version of the student's thesis including all changes required by the advisory committee. The undersigned agree to abide by the statements above.

<div align="right">

Corey Owen Brizzee, Student

Dr. Matthew Shawn Gentry, Major Professor

Dr. Trevor Creamer, Director of Graduate Studies

</div>

REVERSIBLE GLUCAN PHOSPHORYLATION IN THE RED ALGA,
CYANIDIOSCHYZON MEROLAE

_____

DISSERTATION
_____

A dissertation submitted in partial fulfillment of the
requirements for the degree of Doctor of Philosophy in the
College of Medicine at the University of Kentucky

By
Corey Owen Brizzee
Lexington, Kentucky
Director: Dr. Matthew S. Gentry, Professor of Molecular and Cellular
Biochemistry
Lexington, Kentucky
2021

ABSTRACT OF DISSERTATION

REVERSIBLE GLUCAN PHOSPHORYLATION IN THE RED ALGA,
CYANIDIOSCHYZON MEROLAE

Starch and glycogen are an essential component for the majority of species and have been developed to maintain homeostasis in response to environmental changes. Water-soluble glycogen is an excellent source of quick, short-term energy in response to energy demands. In contrast, plants and algae have developed the macromolecule starch that is elegantly suitable for their dependence on external circumstances. Semi-crystalline starch is water-insoluble and inaccessible to most amylolytic enzymes, thus plants and algae have developed a coordinated system so that these enzymes can gain access to the denser starch energy cache. Starch-like semi-crystalline polysaccharides are also found in red algae, termed floridean starch, and are located outside the plastid in the cytosol. Floridean starch resembles a unique class of polyglucans, intermediate of higher plant starch and mammalian glycogen. Reversible glucan phosphorylation is essential in facilitating normal degradation of starch in many higher plants. However, there is a knowledge gap in regards to this process in other starch-containing organisms such as algae. The relationship between phosphorylation and dephosphorylation activity on the structural consequences of starch are still in their infancy as well.

One such organism that produces floridean starch is the thermophilic red microalga, *Cyanidioschyzon merolae,* which has been rapidly advancing as a model organism. Several studies have shown that *C. merolae* contains a minimal set of genes required to metabolize a semi-crystalline carbohydrate called semi-amylopectin. Amongst this conservative set of genes, we identified a single glucan phosphatase (laforin) and a putative glucan dikinase (GWD), suggesting that reversible glucan phosphorylation may also be present in *C. merolae* as a means to metabolize their 'floridean starch'. Therefore, we proposed that the genetically manipulatable *C. merolae* provides an excellent model organism to study the basic functions of enzymes involved in reversible glucan phosphorylation and how they affect the main constituent of starch.

Our work is the first to show specific effects of reversible glucan phosphorylation in a red algal system. In addition, a sole glucan dikinase (GWD) and phosphatase (laforin) are responsible for phosphorylation and dephosphorylation of semi-amylopectin type floridean starch in *C. merolae.* They both are highly specific to the C6-hydroxyl of glucose moieties of semi-amylopectin and the loss of either enzymatic activity significantly affects the fine structure of

amylopectin and thus granule morphology. Loss of C6-phosphate content of semi-amylopectin in Δgwd lines results in suboptimal organization of semi-amylopectin indicating that C6-phosphate is required for proper synthesis and degradation in *C. merolae*. In the case of $\Delta laforin$ lines, without proper maintenance of C6-phosphate, too much C6-phosphate content can equally be as detrimental to amylopectin organization and thus plant vitality. Proper packing of amylopectin likely has direct biological effects in *C. merolae* as seen through prolonged energy deprivation. Loss of GWD or laforin in *C. merolae* resulted in excessive nutrient-scavenging which led to the depletion of critical photosynthetic pigments required to recover cell proliferation upon reintroduction of light.

These studies highlight the critical function and conservation of reversible glucan phosphorylation and its effect on starch structure in *C. merolae.*

KEYWORDS: Starch, Reversible glucan phosphorylation, granule morphology, glucan dikinase, glucan phosphatase, *Cyanidioschyzon merolae*

Corey Owen Brizzee

April 7, 2021
Date

REVERSIBLE GLUCAN PHOSPHORYLATION IN THE RED ALGA,
CYANIDIOSCHYZON MEROLAE

By
Corey Owen Brizzee

Dr. Matthew Shawn Gentry
Director of Dissertation

Dr. Trevor Creamer
Director of Graduate Studies

April 7, 2021
Date

DEDICATION

For my sister Jamie, my wife Brittany, and my family

thankful for Savita Sharma for helping me with my projects and spending countless hours in the microscopy room. Thank you to Dr. Andrea Kuchtova, Dr. Katy Brewer, Annette Uittenbogaard, Zoe Simmons, Kit Donohue, Lyndsay Young, and Tiantian Chen whose friendship and laughter have helped me through the years.

This work would not have been possible without our outside collaborators. During my first couple years in graduate school, I went to Tokyo, Japan to learn from Drs. Kan Tanaka and Imamura Sousuke. The lessons I learned from them were the foundation of my work. Invaluable work was done by Dr. Jean-Luc Putaux of Universitè Grenoble Alpes, France, and the help of Dr. Nicolas Szydlowski and Stanislas Helle of Universitè de Lille, France. I am also extremely grateful to Dr. Timothy Meerloo and Ying Jones at the Electron Microscopy Facility of UCSD, California. I would also like to thank Dr. Felix Nitschke for all his NMR work with starch samples from *C. merolae.*

I wouldn't be in science if it weren't for my loving sister Jamie. I miss you and your laughter every day and hope you're looking down on me and are proud. I am eternally grateful for all the love and support from my parents Mike and Narda, and my brother Michael.

Finally, I am so lucky and grateful for my wife Brittany. Her love, support, intelligence, and humor got me through the good and bad times throughout graduate school. She has not only made me a better scientist but also a better man and without her drive, this work would not be possible.

TABLE OF CONTENTS

LIST OF TABLES

LIST OF FIGURES

CHAPTER 1. *CYANIDIOSCHYZON MEROLAE* AND CARBOHYDRATE METABOLISM

1.1   Introduction

Essentially all living organisms rely on the uptake of carbon to sustain life. Environmental changes drive organisms to stockpile energy for times when resources are not available. The storage of energy is widely in the form of carbohydrates and lipids which can be consumed for different purposes. For fast mobilization of carbon, organisms typically utilize carbohydrates, whether glycogen in animals or starch in plants. Starch is the central carbohydrate storage molecule in photosynthetic organisms such as higher plants, green algae, and red algae. Starch also plays a central role in many aspects of our daily lives as it is a major source of our caloric intake as well as a feedstock for biofuels.

Glycogen is a polysaccharide made up of short linear chains of glucose linked by α-1,4-glycosidic bonds with continuous α-1,6-branches throughout. The evenly distibruted branching nature along with the shorter glucan chains render glycogen water-insoluble for quick access by amylolytic enzymes. Starch is comprised of two main components, amylopectin and amylose. Similar to glycogen, amylopectin is also an α-1,4-linked polymer; however, it has clustered α-1,6 branches along with longer glucan chains and is the main constituent of starch (70-90%). The long clustered chains form double helices with neighboring chains, producing semi-crystalline layers that exclude water rendering the starch granule water-insoluble. Amylose, the minor component of starch, 10-30%, is a predominantly linear α-1,4-linked polymer with very rare α-1,6 branch points and is thought to intwine through the amorphous regions between the crystalline layers. The insolubility of starch also prohibits access for most amyloytic enzymes, therefore, higher plants have developed a coordinated system of reversible glucan phosphorylation to gain access to the energy-dense cache. However, there is a knowledge gap in regards to this process in other starch-containing organisms such as algae.

Recently, microalgae have been of increasing interest due to their capability for producing a variety of high-yield bioproducts, such as starch, which can be used

to generate biofuels without competing as a food resource. In addition to their potential biofuel applications, microalgae have become exciting model organisms to understand fundamental mechanisms of carbohydrate metabolism with rapidly advancing genetic, biochemical, and cell biology tools.

This chapter characterizes and discusses the history of the thermophilic red microalga, *Cyanidioschyzon merolae* (*C. merolae*), and the advances that led it to become a model organism. In addition, this chapter provides a literature review regarding metabolism of carbohydrates, such as glycogen and starch as well as the enzymes involved in their synthesis and degradation. The role of reversible glucan phosphorylation for the mobilization of glucose from starch will be emphasized as several alterations of this cycle lead to an accumulation of starch.

C. merolae provides one of the simplest networks to define how crystalline storage glucans are synthesized and mobilized for utilization. Amongst this simple network of genes, the identification of a single glucan phosphatase and a putative glucan dikinase led us to hypothesize that reversible glucan phosphorylation is conserved in *C. merolae* and might be one of the earliest forms of this process studied to date. Therefore, we designed this study to characterize starch dephosphorylation and phosphorylation activity from biochemistry of the enzymes in question, to cell biology of *C. merolae,* to the floridean starch itself.

The results of this study will lead to innovative approaches applicable to polyglucosan storage disease in humans to enhancing/modifying starch processing and utilization in higher plants. Such novel approaches create new options to enhance starch degradation *in vitro*, increase starch production *in vivo*, and design starch crops and algal systems with valuable functionalities in food and nonfood areas.

1.2   Overview/Discovery of *Cyanidioschyzon merolae*

C. merolae was first discovered by Paolo De Luca and colleagues in 1978 when investigating material from a fumarolic mouth of Campi Flegrei (Phlegraean Fields), which is a large supervolcano just west of Naples, Italy (1). In 1978, De Luca described this novel species as a club-shaped unicellular alga that exhibits a blue-green color, is 1-3 μm in diameter, and is absent of a cell wall (1). *C. merolae*

was profoundly different than the more common *Cyanidium caldarium* that inhabits Campi Flegrei as it was found to contain only one mitochondrion, one chloroplast, and one nucleus. A unicellular rhodophyte (red algae), *C. merolae* is classified under the order Cyanidiales (interchangeably with "Cyanidia") of red algae. Red algae are classified by several attributes; eukaryotic cell, absent of a flagella, an α-1,4- α-1,6-linked glucan produced in the cytosol, presence of accessory pigments such as phycoerythrin or phycocyanin, plastids with unstacked thylakoids, and plastids lacking an external endoplasmic reticulum (2). Cyanidia consist of three genera, *Cyanidioschyzon, Cyanidium,* and *Galdieria.* These Cyanidiales are commonly found to inhabit sulfuric hot springs throughout Yellowstone National Park (USA), Italy, and Japan. They are also the only photosynthetic eukaryotes that dominate in thermoacidophilic areas which are said to represent ancient earth environments (3). Interestingly to date, the genera, *Cyanidioschyzon* and *Cyanidium* are comprised of a single species, *C. merolae* and *C. caldarium,* while the genus *Galdieria* possesses four species (*G. sulphuraria, G. maxima, G. partita,* and *G. daedala*) (3). Like most Cyanidiales, *C. merolae* optimally grows at 42°C with a pH ranging 2-3 while dominating humid environments such as springs and pools. In contrast, Cyanidiales *Galdieria* and *Cyanidium* thrive in relatively dry habitats (rock faces, vents, etc.). There are also many defined morphological and biochemical differences between the three Cyanidiales genera (4, 5). **Figure 1-1** presents the current knowledge of the morphological differences, mode of cell proliferation, presence or absence of a cell wall, chloroplast shape and number, type of storage glucan, presence or absence of vacuoles, and nutritional patterns between the three genera in Cyanidiales.

    C. merolae is the smallest Cyanidiale with an oval, club-like shape that reproduces by binary fission (cytokinesis), which is unlike the other Cyanidia (6). Due to this reproduction method, it is thought that *C. merolae* is the most primitive species in the order (7). *G. sulphuraria* was found to uniquely grow heterotrophically and mixotrophically in contrast to the obligate photoautotrophs, *C. caldarium* and *C. merolae* (8-11). More recently however, evidence was found that *C. merolae* could utilize exogenous organic compounds as a respiratory

substrate to varying degrees of effectiveness (12). Sato and Colleagues found that *C. merolae* could grow heterotrophically in the dark in the presence of glycerol suggesting that the nutritional status of *C. merolae* is "ecological rather than physiological (12)."

1.2.1 Path to a Model Organism

After the discovery of *C. merolae* in the late 1970s, much research has been done in regards to the forementioned morphological differences of each Cyanidiale genera (13, 14). From the late 1980s to early 1990s, all three genera where in the midst of confusing terminology and classification until the pioneering work by Dr. Tsuneyoshi Kuroiwa and colleagues. *C. merolae* possesses several characteristics that make it an attractive model organism to define organelle division, including that it can be serial thin-sectioned for electron microscopy and it is unicellular with a small diameter (15). The ultrastructure of *C. merolae* is also simple as it consists of one plastid, nucleus, and mitochondrion per cell which has led to unique advantages to study organelle-DNA as well as mitochondrial and chloroplast divisions. Additionally, *C. merolae* can be easily synchronized so that one can study how light/dark cycles impact cellular processes (14, 16, 17). In 1992, organelle DNA was isolated from *C. merolae* and biochemically characterized via density centrifugation to show the *C. merolae* genome is the smallest of the Cyanidiale genera by at least 60% (13). In the mid-1990s, Kuroiwa and colleagues identified the first structural basis of the mechanism of plastidial and mitochondrial division by visualizing a plastid- and mitochondria-dividing ring (PD- and MD-ring), respectively (18). These findings were quite valuable as visualization of organelle division in higher organisms cannot be easily observed. For example, even in *E. coli* the MD-ring is not observed by electron microscopy (EM); however, Kuroiwa and colleagues utilized immuno-gold EM to define the process in *C. merolae* and identify the presence of division-associated proteins located at the bridge between the daughter cells (19).

Successful isolation of organelle DNA from *C. merolae* led to complete genome sequencing of the mitochondrion and then shortly thereafter, the plastid (20, 21).

In 2004, the complete nuclear genome of *C. merolae* 10D was published providing not only the first complete sequenced algal genome but also information on basic and essential genes that support multiplication and differentiation of organelles in photosynthetic eukaryotes (22). At 16.5 Mbp, the nuclear genome of *C. merolae* is dramatically smaller that the genome of other photosynthetic model organism genomes with *Chlamydomonas reinhardtii* (green algae) having 120 Mbp and *Arabidopsis thaliana* (thale cress) having 157 Mbp. The nuclear genome of *C. merolae* represents one of the smallest nuclear genomes among all photosynthetic eukaryotes (22). The 16.5 Mbp sequence of the 20 chromosomes in *C. merolae,* transcribe 5,331 genes in which 86.3% are expressed and the genome contains only 26 genes containing introns (3, 22). The simple gene composition and low genetic redundancy of *C. merolae* allow for simplified genome annotation and gene prediction as well as making the organism an excellent model to study the evolution of fundamental mechanisms essential for survival through multiple comparative genetic studies (8, 22, 23). The comparative genomic data has been invaluable to characterizing the differences in photosynthetic mechanisms of red algae compared to those of green plants (green algae and land plants). Dr. Kuroiwa's team also has established many biochemical and cell biology techniques such as protein isolation, cell synchronization, immunofluorescence, transmission electron microscopy, and immuno-electron microscopy (22, 24, 25). In addition, there has been many cell-cycle manipulations performed in *C. merolae* and its mitotic cell division has been documented in numerous reports (23).

The advancements of genetic manipulation in *C. merolae* have flourished in the last two decades and are imperative for furthering the potential of a model organism. In 2004, Dr. Kan Tanaka and colleagues developed a mutant screen to identify selectable marker genes and conditions that could be utilized for a nuclear transformation system (26). Results of the screen identified that 5-fluoroorotic acid (5-FOA) inhibited growth of *C. merolae* cells similarly to that found in yeast which were also uracil auxotrophs (27). Further screening of potential mutants resistant to 5-FOA in the presence of uracil identified a mutant clone, M4, with a frameshift mutation in the *URA5.3* gene (26). Using the M4 strain as a host for nuclear

transformation, wild-type *URA5.3* DNA was cloned into a plasmid and introduced by electroporation which successfully reverted the mutated *URA5.3* gene by recombinant recombination (26). DNA introduction into *C. merolae* was later improved by polyethylene glycol (PEG)-mediated transformation for transient gene expression (28). The first successful gene-targeted knockout employed both the M4 strain and PEG-mediated transformation to target a transcriptional factor, MYB1, associated with nitrogen assimilation genes (29).

Several inducible transgene expression protocols have also been developed utilizing heat-shock and nitrogen-sensitive systems (30, 31). More recently, a multiple gene-targeting transformation system was developed utilizing a chloramphenicol-selection system in addition to the previously mentioned *URA* selection system. Sequential transformations resulted in a double knock-in of HA-tagged cyclin-1 and FLAG-tagged cyclin-dependent kinase A (CDKA) (32). There also has been improvements in the host strain since 2004 due to the spontaneous reversion mutations of the M4 strain frequently occurring which can lead to many false positives for genetic selection (33). Recently in 2015, a new mutant strain, termed T1, was developed where the *URA5.3* gene is completely deleted and has been successfully used as a 'backgroundless' selection for transformants (33). The T1 strain is now more commonly used in reverse genetic experiments as Chapter 3 and 4 will describe.

1.2.2 Photosynthesis in *C. merolae*

Photosynthesis is the most fundamental process which is critical for all forms of live, especially plants and algae. The concept of photosynthesis has been around since 1779 where the first demonstration of photosynthesis as a light-driven process was described by Dr. Jan Ingenhousz (34). Photosynthesis is the process of using light energy to convert carbon dioxide, water, and other small amounts of inorganic salts into carbohydrates, amino acids, lipids, and other organic material. Photosynthesis is the only photochemical process known to store the energy of visible light in the form of chemical energy (35). One of the most central events to ever occur in the development of life on earth was oxygenic

photosynthesis. I will refer to oxygenic photosynthesis as 'photosynthesis' for the remainder of this work as the development of advanced eukaryotic organisms did not take place until free oxygen rose to sufficient levels in our atmosphere (36). The general overall reaction of photosynthesis is:

$$n\text{CO}_2 + n\text{H}_2\text{O} \rightarrow (\text{CH}_2\text{O})_n + n\text{O}_2$$
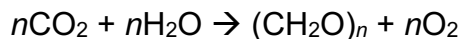
as $(\text{CH}_2\text{O})_n$ is the formula for a hexose sugar (n = 6). Photosynthesis producing oxygen as the oxidant is common amongst algae and plants, and has inheritance from cyanobacteria through endosymbiosis; however, the components and molecular mechanisms vary between cyanobacteria, green algae and plants, and red algae (37).

1.2.2.1 Light-harvesting pigments

For light energy to be stored it must first be absorbed by the photosynthetic pigments of the organism. The photosynthetic pigments then supply their energy to the core pigments in the reaction center complexes that then transmit excitation energy to the reaction centers. Photosynthetic eukaryotic microorganisms are usually divided based on their light-harvesting photosynthetic pigments: Chlorophyta (green algae) and Rhodophyta (red algae) for example. Generally, Chlorophyta possess chlorophyll *a* and *b* as well as several carotenoids while Rhodophyta possess chlorophyll *a* and *d*, phycobiliproteins (phycoerythrin and phycocyanin) and carotenoids. Red algae are one of the most primitive eukaryotic algae and their photosynthetic machinery represents a transitional state between cyanobacteria and higher eukaryotes (38). A key difference between green algae and red algae is the absence of chlorophyll *b* which is an important accessory light-harvesting pigment in green algae and plants (39). In the case of *C. merolae*, three types of pigment exist: chlorophyll *a,* phycobiliproteins, and carotenoids (**Figure 1-2**). Chlorophyll *a* is present in both core photosystems I and II as it is the major light-harvesting pigment in *C. merolae* (39). In an absorption spectrum, chlorophyll *a* can also be seen at two different absorption wavelengths due to different interactions with proteins (**Figure 1-2**). As mentioned above, the major difference between red algal antenna systems from green plants are the absence of chlorophyll *b* and the use of phycobilisomes as the light-harvesting antenna system

for photosystem II (PS II) similarly to that of cyanobacteria. Phycobilisomes are large protein complexes encoded by the chloroplast genome and are integrated into the core of PS II that have several rods that emanate from the core (40). The major phycobiliproteins that make up the rods of phycobilisomes found in *C. merolae* are phycocyanin and allophycocyanin giving it, its 'blue-green' color as *C. merolae* does not possess the red pigment phycoerythrin (41). Phycobilisomes are primarily associated with PS II and in *C. merolae* it was found that the organization of the supramolecular structures in the thylakoid membranes permits efficient energy transfer between the phycobilisomes to both photosystems (42). PS II splits water, releases oxygen and transfers electrons to the electron acceptor, plastoquinone (43). Light-driven photosystem I (PS I) mediates the transfer of electrons from cytochrome c_6 to ferredoxin (44). Associated with PS I are chlorophyll *a*-binding proteins termed, Lhcr, which serve as peripheral antennae for PS I and are encoded by the nuclear genome (40). PS I generates the electrons to reduce $NADP^+$ to NADPH which is then utilized for the reduction of CO_2 to organic carbon (44). Cytochrome c_6 transfers the electrons from the cytochrome b_6f complex to PS I creating a proton gradient that drives ATP synthesis from ADP and P_i (39). ATP and NADPH are critical components that act as energy carriers for the Calvin cycle which incorporates inorganic carbon into organic molecules.

1.2.3 Carbon fixation and utilization

Carbon fixation is carried out through the Calvin cycle and begins with the action of ribulose-1,5-bisphosphate carboxylase/oxygenase (RuBisCO, CMV013C/CMV014C) (45). RuBisCO catalyzes the reaction of CO_2 and ribulose-1,5-bisphosphate fixing CO_2 into two organic triose-phosphate molecules, 3-phosphoglycerate (3-PGA). Then utilizing the ATP and NADPH produced by the light photosystems, the two molecules of 3-PGA are reduced to two molecules of glyceraldehyde-3-phosphate (GAP) by 3-phosphoglycerate kinase (PGK, CMJ305C) and 3-phosphoglyceraldehyde dehydrogenase (GAPA, CMJ042C), respectively (45). GAP can be interchanged with its isomer, dihydroxyacetone phosphate (DHAP), by catalysis of triosephosphate isomerase (TPI, CMQ172C)

and both of these triose phosphates are essential for the production of organic compounds (46). These organic compounds are synthesized in the plastid then act as building blocks in many subcellular locations for the production of carbohydrates, lipids, organic acids, and fatty acids. My work focuses on soluble and insoluble storage sugars, so I will further elaborate on these aspects of carbohydrate metabolism.

1.3   Carbohydrate Metabolism

The following sections provide a literature review into the synthesis and degradation of organic carbon following photosynthesis and carbon dioxide assimilation. The fate of photosynthates such as GAP and DHAP can be converted into soluble storage compounds, soluble/insoluble polysaccharides, or can be metabolized for the synthesis of immediate cell material (45). Becoming soluble storage sugars as well as soluble and insoluble polysaccharides (i.e., glycogen and starch, respectively) entails photosynthates progressing through pathways such as gluconeogenesis where they can be catalyzed into hexoses (6 carbon sugars). Downstream carbon metabolism of triose phosphates in *C. merolae* are quite similar to that of other photosynthetic eukaryotes such as green algae and land plants however there are several differences in type and localization of enzymes involved (47, 48). Studies by Moriyama et al. 2014 and Mori et al. 2016 do a spectacular job detailing these differences of carbohydrate and lipid metabolism in *C. merolae* (47, 48).

1.3.1   Soluble storage carbohydrates

Triose phosphates produced through photosynthesis and carbon fixation are used to produce soluble or insoluble storage carbohydrates following efficient relocation to the cytosol by a triose-phosphate translocator (49). 'Storage' carbohydrates embody an accumulation of carbon with no immediate role and assumed to be used at times when needed, e.g., periods of darkness. Soluble carbohydrates are often known as 'compatible solutes' which are low molecular weight molecules often involved in acclimation to various abiotic stresses (50). Interestingly, *C. merolae* possesses a soluble sugar called floridoside (2-O-α-D-

galactopyranosylglycerol) and an isomeric form (isofloridoside) that can have an osmotic role analogous to sucrose in land plants which acts an osmoprotectant and major soluble source of carbon (51, 52). In addition, the biosynthetic pathway of (iso)floridoside also includes a phosphorylated intermediate ((iso)floridoside-P) which is thought to take place in the cytosol along with insoluble storage carbohydrates (49). This is in contrast to higher plants and green algae as the fixed carbon from insoluble to soluble moieties does not have to be exchanged across a plastid membrane in *C. merolae.* (Iso)floridoside is not exclusive to red algae but is a general characteristic of Cyanidiales. (Iso)floridoside production is thought to be catalyzed by (iso)floridoside phosphate synthase (FPS) from UDP-galactose and glycerol 3-phosphate in *C. merolae (46).* UDP-glucose is epimerized to UDP-galactose by UDP-glucose 4-epimerase (CMA041C) in the cytosol and the ratio of each sugar nucleotide could be an important determinant of the fate of carbon allocation (49). However, Barbier et al. 2005 identified key biosynthetic enzymes involved in floridoside biosynthesis, one being galactosyltransferase (Floridoside Phosphate Synthase, FPS), which was initially not found in the *C. merolae* genome although mentioning several other potential biosynthetic enzymes could be involved (8). Another interesting caveat is that floridoside and cell-wall polysaccharide biosynthesis are linked due to the common precursor UDP-galactose although *C. merolae* does not have a cell wall (53). More recently in *G. sulphuraria,* two enzymes were identified with homology to trehalose 6-phosphate synthase/phosphatase that also acted as active (iso)floridoside phosphate synthase/phosphatase fusion proteins (50). There are two similar enzymes encoded in the *C. merolae* genome (CMO053C and CMI293C) that suggests that floridoside biosynthesis may occur similarly as in *G. sulphuraria* (46, 50). Therefore, there are still many questions to be answered on the presence, importance, and biosynthesis of floridoside in *C. merolae* as well as its relationship to insoluble carbohydrate reserves*.*

1.4 Storage polysaccharide metabolism

1.4.1 Glycogen, Starch, and Floridean starch structure

Almost all living organisms store energy in some dense form of a carbohydrate polymer. Whether in the form of glycogen or starch, these macromolecules are chemically similar as they are all comprised of glucose molecules linked together by glycosidic bonds, yet they differ in many important structural features that effect their physiochemical properties (54). Glycogen is a cytosolic polysaccharide produced in the majority of (archae)bacterial, fungal, and animal species. In glycogen, glucose moieties are joined via α-1,4-glycosidic linkages with a continuous pattern of α-1,6-glycosidic linkages, or branches, every 12-14 residues. The continuous, relatively high degree of branching throughout the glycogen particle tends to result in shorter linear chains and a homogeneous water-soluble polysaccharide (55). In addition, the continuous branching nature causes physical constraints as the glycogen particle grows giving glycogen a theoretical size limit of approximately 40 nm in diameter that can accommodate 55,000 glucose residues (**Figure 1-3A)** (56).

Starch is a storage carbohydrate that is a functional equivalent of glycogen produced in almost all photosynthetic organisms (57). Starch is made as a granular ultrastructure that ranges from 1μm to over 100μm (58). Starch is a heterogeneous blend of two major molecules, amylose and amylopectin, and both constituents consist of glucose polymers of although each has their own distinct branching pattern. Amylopectin is responsible for 75-90% of the starch granule while amylose comprises 10-25% of starch. Amylose is a largely linear glucose polymer with very few α-1,6-glycosidic branches and is thought to be interspersed within the amorphous regions of amylopectin (59-61). In contrast to amylose, amylopectin is responsible for the dense nature of starch and is discontinuously branched by α-1,6-glycosidic linkages every 12-25 glucose residues. The clustered nature of branch points along with the long glucose chains results in neighboring chains forming double helices that exclude water, giving native starch a layered structure with alternating regions of amorphous and crystalline matter and a semicrystalline

nature (60, 62-64). The interior architecture of starch granules is characterized by 'growth rings' that correspond to the layered regions of concentric semi-crystalline (120-400 nm thick) lamellae separated by amorphous (loosely disordered) regions. These layers alternate with a repeat distance of 9-10 nm (**Figure 1-3B)** (65).

The arrangement of double helices differentiate starch structures into three allomorphs; A-type starches are typically found in cereal starches (wheat, barley, etc.) and lower plants, B-type starches are found in storage organs of dicots such as potato tubers and in assimilatory starches from potato and *Arabidopsis thaliana*. The C-type structure is a mixture of both the A-type and B-type allomorphs found in a single starch granule and are typically found in legumes (66). A-type allomorphs are dense, containing less intracrystalline water formed from short lateral chains and close branch points while the B-type allomorphs are formed by amylopectin with long side chains and more distant branch points allowing for more water molecules between double helices (67). In regards to the amount of water molecules in a unit cell for these two types of allomorphs, B-type structures contain 36 water molecules while A-type structures only contain four (67). Thus, the hydration level has major effects on crystallinity and other physiochemical properties of the starch granule.

Starch can typically be characterized by its biological function within an organism based on whether it's short-term (transitory) or long-term (storage). For many higher plants, starch is mainly produced in the chloroplasts of leaves where a portion of carbon-assimilated products of photosynthesis are incorporated into transitory starch (63). Roots, tubers, and seeds are characteristic of non-photosynthetic organs that can also store long-term storage starch within amyloplasts by sucrose transported from the leaves of a plant (63, 68). Short-term transitory starch accumulation occurs within typically a 12-hour photoperiod whereas long-term storage starch accumulation can be months to years in length. Remobilization of storage starch is utilized for high-energy demanding processes such as germination and sprouting (63).

A starch-like molecule referred to as floridean starch or amylopectin granules can also be produced by photosynthetic red algae and their non-photosynthetic

derivatives from secondary endosymbiosis of a red algal ancestor, like some members of apicomplexa (e.g., *Toxoplasma gondii*) as well as dinoflagellates (69-71). Unlike starch in higher plants and green algae, floridean starch is synthesized and stored outside the plastid in the cytosol, a key characteristic of red algae (2, 69). In wild-type *C. merolae,* the glucan structure and granule morphology consists of semi-amylopectin-type α-glucans alone with no detectable amylose and approximately 0.2 μm glucan granules. Floridean starch differs from that of green algae and higher plants not only by location but also by the apparent lack of amylose with some minor exceptions (49). These starch granules are very different from those found in most other red and green algae as well as higher plants, which are generally greater than 1 μm in size. For example, in *A. thaliana*, starch granules from wild-type leaves were approximately 1 to 2 μm in diameter after a regular 12-hour photoperiod and the size increases to 2 to 3 μm in diameter after 180 hours of continuous light (72). To put this in perspective, starch granules found in *A. thaliana* leaves are as large as an entire *C. merolae* cell.

The molecular structure of the *C. merolae* floridean starch was analyzed by chain-length distribution analysis and size-exclusion chromatography. These analyses confirmed the presence of semi-amylopectin-type α-glucans and a proportion of short chains (DP $\leq$ 8) of < 22% and of long chains (DP $\geq$ 37), 4-8% in total (73). This finding is in stark contrast to the other genera of Cyanidiales (*G. sulphuraria* and *C. caldarium*) that produce glycogen-type polysaccharides that have a hardly detectable proportion of long chains and a very high proportion of short chains (74, 75). Semi-amylopectin type glucans found in *C. merolae* are also different compared to the typical chlorophyta amylopectin found in green algae as well as vascular plants such as rice which have a higher proportion of long chains around 6-12% (73). As mentioned previously, for most chlorophyta, the crystalline structures are classified in three types (type A, B, and C), for *C. merolae* the crystalline pattern resembled an A-type pattern although the diffraction signals from X-ray diffraction (XRD) were low (73). Another interesting finding was that wild-type *C. merolae* starch granules do not contain long-range lamellar order, as defined by small angle x-ray scattering (SAXS), like that found in green algae and

13

higher plants. Due to its chain-length distribution, semi-amylopectin is thought to be an intermediate between glycogen and chlorophyta amylopectin. In fact, *C. merolae's* polyssacharide resembles that of semi-amylopectin type produced in several species of cyanobacteria including *Cyanobacterium* sp. NRBC 102756, *Cyanothese* sp. ATCC 51142 and *Cyanobacterium* sp. CLg1 (76, 77). While these studies have characterized the glucan type synthesized by *C. merolae*, there are still many questions regarding the nature of cytosolic polyssacharide metabolism in red algae and those alike.

1.4.2 Minor polysaccharide components

Proteins, lipids, and phosphate are additional components that are found in glycogen and starch at low levels. Unlike proteins and lipids, phosphate is the only known natural covalent modification of starch and levels vary widely amongst species (78). As discussed below, the level of starch phosphorylation can vary from 0.1% to 1%. In principal, each glucosyl residue carbon could be esterified with a phosphate group with the exception of those linking glucose chains (78). Intriguingly, phosphorylation occurs only on a few specific sites of a glucosyl residue. Phosphate is found in glycogen as monophosphate esters at the C2-, C3-, and C6-hydroxyls of glucose moieties at equal quantities, but there is only 1 phosphate per 600-1500 glucose residues depending on tissue source (79-81). Additionally, the source of glycogen phosphate remains a mystery (82). It has been reported that glycogen synthase (GS) could incorporate phosphate from UDP-glucose in a rare side reaction to the C2- and C3-hydroxyls; however, there was no evidence to support a monophosphate incorporation at the C6-hydroxyl (79, 83).

Monophosphate esters were shown to be present in starch since the beginning of the 1900s and later were found to be mainly present in the amylopectin fraction of starch (84, 85). In 2000, Blennow and colleagues located the monophosphate esters in the amorphous region of the amylopectin (86). Covalently bound phosphate esters reside largely on the C6- and C3-positions of glucosyl residues though trace amounts have been reported on the C2-position (85, 87, 88).

Although phosphorylation at the C2-position was detected in the 1970s, it has not been detected since in many subsequent publications involving *Arabidopsis* leaf starch and potato tuber starch (85, 89). The identification of the phosphorylated sites was confirmed via NMR and biochemical analyses including amylolytic- and acid-hydrolysis products (85, 89-92). 70-80% of all phosphate content found in starch is esterified at the C-6 position (90). The level of phosphorylation varies in the storage starches with cereal starches containing very minute amounts, e.g. corn has ~0.03 phosphoesters per thousand glucose residues, whereas starch from potato tubers are highly phosphorylated with 2.34 phosphoesters per thousand glucose residues (93). Interestingly, phosphorylated α-glucan chains are typically longer hence tuber starches typically have long chains are highly phosphorylated and the crystalline type (type A or B) can be predicted by the degree of phosphorylation (86). Amylopectin can possess more than one phosphate group on an α-glucan chain but no phosphate groups are found on the non-reducing end or closer than nine glucose moieties from an α-1,6 branch (94).

Molecular models of phosphate incorporation display evidence towards the restructuring of double helices in crystalline starch (95). A phosphoester at the C6-position does not cause a steric strain in between double helices while the C3-phosphoester induces a significant steric effect and strain in double helices preventing optimal crystalline packing (95). Although the level of phosphorylation in starch is moderately low, it has significant impacts on normal polysaccharide metabolism, mobilization, solubilization, as well as physicochemical properties in which I will revisit in later sections.

1.4.3 Carbohydrate-Binding Modules – Important feature of carbohydrate metabolizing enzymes

Before I embark on polysaccharide metabolism and the enzymes that are essential for efficient biosynthesis and degradation, there is an important feature that many of these enzymes possess. α-glucan metabolizing enzymes often have non-catalytic domains that aid in substrate specificity and increase the interaction with carbohydrates known as carbohydrate-binding modules (CBMs) and

previously known as starch-binding domains (SBDs) (96). CBMs are grouped into 88 families currently by their sequence similarities and SBDs are only found in 15 of those families (http://www.cazy.org) (97, 98). There are many SBDs that are uncharacterized to date; however, approximately 90% of the SBDs belong to enzymes with non-amylolytic functions (96). Almost all CBMs consist of roughly 30-200 (~100 on average) residues with a conserved distorted β-barrel topology even though there are significant differences in their respective amino acid sequences (96). CBMs non-covalently interact with their substrates often by aromatic tryptophan and tyrosine residues however other residues may exist (99). Chapter 4 and 5 will discuss the CBM families 20 and 45, respectively.

1.4.4 Starch synthesis

For all α-glucans, whether glycogen, starch or floridean starch, they all begin with a glucosyl-nucleotide that provides the fundamental glucose building blocks for construction and is a major rate-limiting step in the biosynthetic pathway. Green algae and higher plants produce starch within the chloroplast from the precursor ADP-glucose. ADP-glucose is a glucosyl-nucleotide synthesized by the action of ADP-glucose pyrophosphorylase (AGPase, EC 2.7.7.27) which condenses ATP and glucose 1-phosphate and releases inorganic pyrophosphate (PPi). On the other side of the polyssacharide spectrum, glycogen is made from the precursor UDP-glucose in eukaryotes however ADP-glucose in glycogen-synthesizing prokaryotes in which plastids evolved. The synthesis of UDP-glucose is analogous to ADP-glucose as it is a product of the condensation of UTP and glucose 1-phosphate by the enzyme, UDP-glucose pyrophosphorylase (EC 2.7.7.9). Thanks to several completely sequenced genomes (including *C. merolae*), the pathway in which red algae synthesize floridean starch confirms a UDP-glucose based route as there is an absence of genes encoding AGPase (22, 100).

Initiation of glycogen synthesis is well-known and was elucidated in the 1980s (101). First, glycogen initiation takes place by a specialized initiation step where glycogenin (UDP-Glc:glycogenin glucosyltransferase, EC 2.4.1.186) self-glucosylates using the glucose from UDP-glucose to create an α-1,4 linked primer

chain for glycogen synthase (GS, EC 2.4.1.11) to begin elongating (55). GS elongates the primer chain by repetitively transfering glucosyl residues to the non-reducing end. The growth of the glycogen molecule is progressed by repeat actions of chain-elongation (GS) and chain-branching via a glycogen branching enzyme (BE, EC 2.4.1.18).

Much of the research in regards to starch metabolism has been conducted on *A. thaliana* leaves and cereal endosperms. Molecular and genetic data convincingly show green algae and land plants contain numerous isoenzymes involved in the formation of starch (69, 100, 102). Unlike glycogen, the initiation of a starch granule is thought to be more complex as the precursor is hypothesized to be an ordered pre-amylopectin cluster structure (71, 103). Analogous to glycogen, the glucosyl residue of ADP-glucose is transferred to the non-reducing end of a preexisting primer by soluble starch synthases (SSs, EC 2.4.1.21). Glucose from ADP-glucose can be converted to starch polymers by three classes of enzymes: starch synthases (SSs), starch-branching enzymes (SBEs, EC 2.4.1.18), and debranching enzymes (DBEs, EC 2.4.1.41). Briefly, SSs are the major work horses as they sequentially elongate the non-reducing ends of α-glucan chains, terminal regions of those α-glucan chains can then be added to adjacent chains (α-1,6 linked) by SBEs, and finally some of those branches can be trimmed by debranching enzymes beginning the structure of the starch granule (104). Disruption of the fine structure of amylopectin and/or amylose alters the morphology, physicochemical properties, and sometimes the overall starch granule ultrastructure is lost.

1.4.4.1   Starch synthases

There are muliple isoforms of SSs conserved in almost all plant tissues and there are five major classes (granule-bound starch synthase (GBSS), SSI, SSII, SSIII, and SSIV) that can be identified based on their actions (105). While classes SSI – SSIII are primarily responsible for the elongation of α-glucan chains at the outer starch regions, most reports indicate the unique involvement of SSIV and GBSS in starch granule initiation and amylose synthesis in *Arabidopsis,* respectively.

17

The role of SSIV in starch granule initiation has been highlighted since 2007 when Roldan et al. identified mutants of *ss4* in *Arabidopsis* contained a dramatically reduced number of starch granules (1-2) per plastid compared to 5-7 in wild-type plants (106). Despite the decreased number of starch granules in *ss4* plastids, the granule(s) were significantly bigger than wild-type and thus there was no defect in total polysaccharide levels. Transitory starch granules in *Arabidopsis* chloroplasts are typically flattened and disc-like (discoid), but starch granules in *ss4* mutants were larger and more spherical in nature. Interestingly, both starch synthesis and degradation rates were decreased in *ss4* mutants which was attributed to the reduced amount of granular surface for metabolism (106, 107).

Amylose, the minor constituent of starch, is synthesized by granule-bound starch synthase, GBSS. It elongates short maltooligosaccharides into longer, linear α-glucans (amylose) inside of the amylopectin matrices (108). Interestingly, the activity of GBSS is correlated with its association with starch, hence 'granule-bound', thus is widely localized within the starch granule and its activity seems to be secondary to amylopectin synthesis (109). Organisms with either a lack or alteration of GBSS result in amylose-free starch which is called *waxy* starch (109, 110). *Waxy* starch from cereals (maize, rice, barley, wheat, etc.) have been of increasing interest due to their advantageous industrial applications like pasting properties and gelatinization temperatures (110, 111).

1.4.4.2 Starch branching enzymes (SBE)

SBEs are enzymes responsible for the formation of α-1,6 branches in amylopectin (as well as the rare occurence in amylose) by cleaving an α-1,4 linkage of an α-glucan chain and transferring the cleaved fragment in an α-1,6 manner to a different position of the same chain or an adjacent chain (112). There are three isoforms of SBEs subdivided into two major classes of SBEs found in plants, SBEI and SBEII (EC 2.4.1.18). The role of SBEI in starch metabolism is still poorly understood as downregulation of SBEI has minimal effects on starch metabolism in *Solanum tuberosum* (potato) (113). In contrast, SBEII contains two isoforms, SBEIIa and SBEIIb, which have different expression patterns in cereals. SBEIIa is essential for starch synthesis in maize leaves as mutant lines have

reduced branching compared to wild-type however the branching pattern of endosperm starch was indistinguishable from wild-type (112). In contrast, SBEIIb expression seems to be restricted to the endosperm as *sbe2b* mutant lines have normal leaf starch metabolism and branching.

1.4.4.3   Debranching enzymes (DBE)

One of the most important features of starch/amylopectin is its semicrystalline nature distinct from glycogen by the distribution of α1,6 branches. Intriguingly, debranching activity occurs throughout starch synthesis and degradation and DBEs are specific for α1,6 hydrolysis but are classified by their substrate preference: isoamlylase type (ISA, EC 3.2.1.68) and pullanase (PUL, EC 3.2.1.41) (114). The final structure of amylopectin requires trimming by DBEs and are essential for the cluster structure. In higher plants, there are generally four DBEs; ISA1, ISA2, ISA3, and PUL (102). Mutants of ISA1 (*isa1*) results in a lack of structured amylopectin and the α-glucans have increased branching which is unable to form crystalline structures and remains water-soluble, much like glycogen; however, to discern this type of glucan in plants, it is named phytoglycogen (115). ISA1-deficient mutants are referred to as *sugary-1* mutants in maize and rice (115-119). PUL and ISA3 are mainly involved in starch degradation and have a negligible role in synthesis (120-122).

1.5   Starch degradation of transitory starch

Degradation of transitory starch is a critical process in photosynthetic organisms especially in unicellular algae and leaves of higher plants as they are presented with diurnal fluctuations. Polysaccharides synthesized during the day act as a short-term reserve that can be mobilized at times when photosynthesis is not available, i.e., darkness. The products from polysaccharide degradation provide an abundance of sugars, mainly maltose, malto-oligosaccharides, and low amounts of glucose and glucose 1-phosphate that provide the necessary energy for growth and maintenance of the organism. The native starch granules physical structure has major effects on the action of carbohydrate-active enzymes as they are responsible for the transition of starch granules from insoluble to soluble

19

phases (123). A hallmark study to screen for mutants with impaired starch degradation using the model organism *A. thaliana* spear-headed research to identify the enzymes involved (124). Mobilization of plastidial starch in higher plants requires several enzymes with several isoforms localized to different areas of a cell that are involved in disassembling starch granules. In this section, the main focus will be on studies that pertain to transitory starch degradation.

1.5.1 β-amylases (BAM), a.k.a. exo-hydrolases

Starch degradation revolves around the hydrolysis of α-1,4- and α-1,6-glycosidic bonds to release products for metabolism. The most prominent hydrolysis of α-1,4-glucans during starch degradation is catalyzed by the exo-hydrolase, β-amylase (EC 3.2.1.2) that releases β-maltose from the non-reducing end of at least four glucosyl residues in length chain (68). The *Arabidopsis* genome encodes for numerous β-amylase-like proteins, nine in total (BAM1-9), however only four are localized to the chloroplast (125, 126). Of the four plastidial β-amylase-like proteins, BAM1 and BAM3 have been shown to possess amylolytic activity and contribute to starch degradation although only the *bam3* mutant leads to a starch excess phenotype. Interestingly, the double *bam1 bam3* mutant has a more severe starch excess phenotype than the single *bam3* mutant suggesting a functional overlap in degradation (127). Initially, BAM2 was characterized as having little to no catalytic activity; however, BAM2 was later found to be quite unique existing as a tetramer and requiring potassium for catalytic activity (128, 129). To date, the function of BAM2 in starch degradation is unknown as there is no observable phenotype although BAM2 likely plays an important role that has yet to be discovered (127, 129). Despite recombinant BAM4 having no amylolytic activity, *bam4* displays a starch excess phenotype thus is speculated to have a facilitatory or regulatory role by interacting with different proteins involved in starch metabolism (127).

1.5.2 α-amylases (AMY) a.k.a endo-hydrolases

α-amylases (AMY, EC 3.2.1.1) are endo-amylolytic enzymes that also hydrolyze α-1,4-glycosidic bonds; however, they act on internal bonds of starch or glycogen releasing either linear or branching α-glucans. The *Arabidopsis* genome encodes for three α-amylase-like proteins (AMY1, 2, and 3) but only AMY3 is targeted to the plastid. Although AMY3 is localized to the chloroplast in *Arabidopsis,* the *amy3* mutant as well as the *amy1 amy2 amy3* triple mutants do not display a starch excess phenotype suggesting that α-amylases are not necessary for transitory starch degradation (130). Following studies discovered in the presence of a DBE mutant background, AMY3 could also release soluble branched oligosaccharides which could be a compensatory mechanism employed in *A. thaliana* (131, 132). In contrast to transitory starch breakdown in *Arabidopsis,* α-amylases play a key role in starch degradation in cereal endosperm facilitating seed germination (133).

1.5.3 Debranching enzymes (DBE)

In addition to their essential role in trimming α-glucans for starch biosynthesis, DBEs are also critical for efficient and complete degradation of starch. β-amylase activity is impeded by α-1,6 branch points thus requiring the action of DBEs such as isoamylases (ISA) and limit dextrinase (LDA). ISA3 and LDA (also pullulanase) release short chains (3-5 glucose units) from branch points left over from β-amylolysis with non-redundant functions. In *Arabidopsis,* the *isa3 lda* double mutant displays a severe starch excess phenotype over single mutants of *isa3* or *lda* and accumulates soluble branched oligosaccharides that are absent in the single mutants (131).

1.5.4 Disproportionating enzymes (DPE) and α-glucan phosphorylases (PHS/Pho)

The products of starch degradation by DBEs, α-amylases, and β-amylases results also in longer malto-oligosaccharides (MOS) in the chloroplast that have to be further metabolized in order to be exported to the cytosol. Disproportionating

enzyme1 (DPE1/D-enzyme, EC 2.4.1.25) is a plastidial α-1,4 glucanotransferase that transfers one α-1,4-linked glucan chain to another, or to glucose (134). Essentially, DPE1 can fashion longer end products of starch degradation facilitating further β-amylase activity while producing reduced end products for exportation to the cytosol. DPE1 is able to catalyze multiple MOS reactions and generates a mixture of linear α-glucans (135). Loss of DPE1 in *Arabidopsis* results in an excess of MOSs (especially maltotriose) in leaves at night and a mild starch excess phenotype which could indicate the accumulation of maltotriose may inhibit starch degradation (135). In the green algae *Chlamydomonas,* a mutant defective in *dpe1* (*sta11* mutant) accumulated MOS during light photoperiods and displayed a low starch phenotype suggesting that this enzyme could be involved in both starch synthesis and degradation (109, 136).

As previously mentioned, glucose 1-phosphate (G1P) is present as an end product of starch degradation in low amounts. α-glucan phosphorylases (PHS1/Pho1, EC 2.4.1.1) catalyze the phosphorolytic cleavage of the terminal residue from nonreducing ends of α-glucans yielding G1P. This reaction is reversible suggesting a possible role of phosphorylases in starch synthesis and degradation (137). Most plants studied thus far have two isoforms of phosphorylase, PHS1/Pho1 and PHS2/Pho2, localized to the chloroplast and cytosol, respectively (137). Similar to β-amylases, phosphorylases cannot bypass branch points and are known to act on long MOSs greater than DP of 4 (138). In *Arabidopsis*, mutants lacking PHS1 activity have no starch excess phenotype compared to wild-type plants (137).

In addition to DPE1 and PHS1, there are cytosolic isoforms as well, DPE2 and PHS2, respectively. DPE2 differs from that of DPE1 as it is specific for the β-anomeric form of maltose (end product of β-amylase) (139). DPE2 uses maltose as a glucosyl donor to multiple acceptors like glucose, maltose, or glycans and releases the other glucose molecule (140, 141). *dpe2* mutants in *Arabidopsis* display a starch excess phenotype and accumulate significant quantities (200x) of maltose in the cytosol compared to wild-type (140, 141). DPE2 and PHS2 have been indicated in interactions with cytosolic heteroglycans composed of several

different, variously linked sugars such as arabinose, galactose, glucose, fucose, mannose, and rhamnose. These heteroglycans can reach sizes up to approximately 70 kDa in the cytosol and can also serve as substrates for PHS2 (140, 141).

1.5.5 Reversible Glucan Phosphorylation Overview

Due to the insoluble nature of starch, a phase transition must be made at the granule surface in order to transition from an insoluble to a soluble state. This transition is important to allow efficient binding of starch degradation enzymes. Degradation of starch is facilitated by a cyclic process known as reversible glucan phosphorylation that begins by disrupting the granular surface by phosphorylation. Glucose phosphorylation creates steric hinderance between the amylopectin helices and causes the glucose chains to unwind. The covalent addition of phosphate helps to initiate degradation by amylolytic enzymes discussed above by allowing access to the starch granule (132). More internal phosphate groups impede further degradation by amylolytic enzymes thus require their removal by glucan phosphatases to complete the degradation of a lamellar level, resetting the cycle (**Figure 1-4**). Reversible glucan phosphorylation is essential to rapidly access the energy-dense sugars in the starch granule and enhances the degradative process.

1.5.5.1 α-Glucan, Water Dikinases (GWD)

As mentioned previously, an important constituent of starch is the presence of phosphate mainly at the C6- and C3-positions of glucosyl residues which have a significant impact on mobilization, solubilization, and physicochemical properties of starch. The enzymes responsible for the phosphorylation of starch were identified as α-glucan, water dikinase (GWD1, EC 2.7.9.4) and phosphoglucan, water dikinase (GWD3/PWD, EC 2.7.9.5) and both are localized to the chloroplast (142, 143). Glucan dikinases belong to a family of phosphotransferases that use a unique mechanism to phosphorylate glucosyl residues of amylopectin (142). Glucan dikinases phosphorylate α-glucans according to the following equation described in (142):

$$\alpha\text{-glucan} + \text{ATP} + H_2O \rightarrow \alpha\text{-glucan-}P_\beta + \text{AMP} + P_\gamma i$$
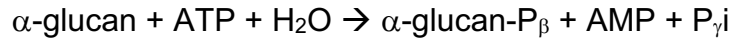
Research on GWD progressed rapidly from the discovery of the genes encoding glucan dikinases first described by Priess and Somerville in 1991 when they published the results of an *Arabidopsis* mutant screen designed to identify Starch Excess (*sex*) mutants (124). In 1998, the Kossmann lab cloned the gene of a starch granule-bound protein they named R1 and demonstrated that reduced levels of R1 in *Solanum tuberosum* (potato) resulted in decreased starch phosphorylation (144). In contrast to known kinases, a paper by the Steup and Kossmann labs in 2002 definitively demonstrated that potato R1 is an α-glucan water dikinase (GWD1) that transfers the β-phosphate of ATP to starch. A conserved histidine residue is responsible for accepting the β-phosphate of ATP creating a phosphohistidine intermediate following nucleotide binding and hydrolysis of the γ-phosphate (78). It has been proposed that the GWD protein contains two autophosphorylation sites; however, other than the conserved histidine residue in the phosphohistidine domain the other remains a mystery (145).

Multiple groups identified a second starch dikinase that is dependent on the phosphorylating action of GWD1, named phosphoglucan, water dikinase (GWD3/PWD), and other groups have demonstrated that GWD1 phosphorylates the C6-hydroxyl on the glucose moiety which triggers C3 phosphorylation by PWD (90, 146, 147). A cytosolic form of GWD (GWD2) is also encoded in the *Arabidopsis* genome that phosphorylates amylopectin *in vitro* and acts similar to GWD1 (C-6 specificity); however, it does not seem to play a role in transitory starch degradation (148). More recently, a *gwd2* mutant of *Arabidopsis* showed drastically lower water-soluble sugars and proline contents in the response to osmotic stress revealing a potential biological role for the first time (149).

Both GWD1 and PWD proteins contain similar domains like a N-terminal chloroplast targeting peptide roughly 75-80 amino acids in length, a C-terminal catalytic domain with significant homology to the nucleotide binding and phosphohistidine domain of phosphate, pyruvate dikinase (PPDK, EC 2.7.9.1) and phosphoenolpyruvate synthase (PPS, EC 2.7.9.2) (150, 151). A major difference

between GWD1 and PWD are the carbohydrate binding modules (CBMs) found between the N-terminal chloroplast targeting peptide and the C-terminal catalytic domain. Canonical GWD1 (as well as GWD2) from *Arabidopsis thaliana* and *Solanum tuberosum* possess tandem CBMs of family 45 which have uniquely been identified in only GWDs and plastidial α-amylases (152). There are two conserved tryptophan residues that act as binding/interaction sites and there is commonly a 200-amino acid linker spanning the two CBMs. PWD contains a single CBM of family 20 in the N-terminal region and is one of the earliest and most well characterized CBMs to date (153).

The importance of GWD1 in transitory starch turnover was shown in transgenic potato plants with reduced R1 levels and the *Arabidopsis* mutant *sex1* that has a severe starch excess phenotype in leaves after normal and prolonged periods of darkness, respectively (144, 150). PWD mutants in *Arabidopsis* also have a starch excess phenotype, but it is less severe of that from GWD mutants (143). GWD mutant plants often display severely compromised growth in contrast with PWD mutant plants that have minor effects on growth. Additionally, C6 phosphorylation by GWD may minorly compensate for the loss of PWD *in vitro* (154).

The direct effect of phosphate-induced solubilization by glucan dikinases was shown by phosphorylating maltodextrins *in vitro* as they have structural characteristics mimicking starch (123). Although C6 phosphorylation is modeled for localized disruption of double helical packing, C3 phosphorylation can affect orientation of neighboring glucosidic bonds by a greater steric hindrance which could destabilize the double helices themselves (95, 134, 155). The knowledge that amylopectin is phosphorylated rather than amylose could explain the apparent substrate specificity of GWD for α-1,6 branches (156). On the other hand, if amylose chains are long enough GWD can act on them accordingly to a lesser degree. Furthermore, GWD preferentially phosphorylates longer chains of amylopectin (DP >30) and can phosphorylate both allomorph types (A and B) although activity towards type B is higher (123). GWD was also found to prefer crystalline substrates due to the observation that phosphorylation activity essentially disappeared in a reaction with identical soluble maltodextrins (123).

PWD phosphorylation specificity at the C3-position is unique since phosphorylation at this position is rarely found anywhere else in nature. Furthermore, PWD can also phosphorylate non pre-phosphorylated substrates like maltodextrins thus it is likely that PWD activity is judged by physical rather than chemical parameters (157). Phosphorylation activity is essential for initiating starch degradation at the granule surface as demonstrated by GWD and PWD activity stimulating starch breakdown by β-amylases and isoamylases (ISA3) (158). β-amylases were shown to preferably act on solubilized maltodextrins compared to crystalline maltodextrins further suggesting the importance of solubilization prior to amylolytic activity (123). The GWD protein was also suggested to be redox-regulated in vitro via two conserved cysteine residues that form a disulphide bridge. Although this was observed in vitro, there are no observations of this being the case *in vivo* (159).

Transitory starch is phosphorylated during synthesis and degradation but the levels of phosphorylation are dramatically higher during starch degradation at night (160). Although there has been substantial evidence of the importance of glucan dikinases in starch degradation, the role of glucan phosphorylation during synthesis is still being defined. GWD-deficient mutants have a progressive accumulation of starch suggested from several diurnal cycles with impaired degradation, but the rate of synthesis is also affected (161). Elongation activity by starch synthases *in vitro* is also higher when native starch granules have been pre-phosphorylated with GWD (161). Altering starch phosphate content has been shown in several reports to alter starch synthesis activity (162). This result is similar to a report on GWD1 suppression in potato tubers led to the simultaneous down-regulation of starch synthesizing genes SBEII, SSII, and SSIII (163). In *A. thaliana* leaves, C6- and C3-phosphate were found in starch produced during a single 12-hour photoperiod suggesting that glucan dikinases are active during synthesis as well (63). We may not observe this activity as glucan phosphatases may transiently maintain certain levels of phosphate content in starch for proper packing of the starch granule.

1.5.5.2   Glucan Phosphatases

Complete transitory starch degradation requires the removal of phosphate groups from the starch granule by glucan phosphatases. β-amylase activity is impeded by more internal phosphate groups and in order for complete starch hydrolysis, these phosphate esters must be removed (158, 164). In *Arabidopsis*, there are two glucan phosphatases responsible for the subsequent dephosphorylation: Starch Excess 4 (SEX4) and Like Sex Four 2 (LSF2). Both glucan phosphatases share an N-terminal dual-specificity phosphatase (DSP) domain and are localized to the chloroplast (165). DSPs are a heterogeneous group of enzymes capable of dephosphorylating phosphate esters at both serine/threonine and tyrosine residues of proteinacious substrates in addition to non-protein substrates such as polysaccharides, lipids, and nucleotides (166). DSPs utilize a catalytic cysteine residue in the active site CX_5R motif similarly to classical protein tyrosine phosphatases (PTPs) that performs a nucleophilic attack on the phosphoester of the substrate (167). The DSP active site construction is more shallow but broader than classical PTPs and thus more accommodating to different phosphorylated residues (167, 168). Glucan phosphatases have a signature DSP motif, CζAGΨGR, that defines these members from other DSPs (169). DSP members are also classified based on their sequence similarities and appended domains (170).

The SEX4 protein and *Arabidopsis* mutants in *sex4* have been well characterized over the past twenty years (164, 171-177). SEX4 contains a N-terminal chloroplast targeting peptide, a DSP domain, a C-terminal CBM of family 48, and a C-terminal motif (169, 178). It has been shown that SEX4 binds to carbohydrates such as glycogen, amylopectin, and native starch granules as well as preferential dephosphorylating activity towards C6-phosphate esters while also possessing activity against the C3-position (175, 179). The mechanism behind substrate specificity of SEX4 has been extensively studied since the elucidation of its structure (PDB 3NME) (178). SEX4 has multiple features that are unique compared to other DSP containing phosphatases. The tertiary structure of SEX4 has many interdomain interactions including an intricate formation of a continuous binding pocket between the DSP active site and the glucan binding region of

CBM48. Additionally, a previously unrecognized C-terminal motif that interacts with the DSP domain was discovered that is suggested to be critical for stability (178). Subsequent structural studies identified the mechanism for C6 specificity of SEX4 by solving the crystal structure of SEX4 bound to maltoheptaose and phosphate (PDB 4PYH) (175). The continuous binding pocket between the DSP and CBM48 uniquely positioned maltoheptaose in a C6-specific orientation.

Sex4 mutants in *Arabidopsis* possess a progressive starch excess phenotype that is around 50% of that found in *sex1* (GWD1) mutant plants, suggesting that GWD phosphorylation is the initial step in starch degradation. In addition to the excess starch found in *sex4* mutant plants, there is also a large accumulation of soluble phospho-oligosaccharides that are not found in wild-type plant leaves (164). The soluble phospho-oligosaccharides are likely starch degradation intermediates and the result of hyperphosphorylated surface glucans that are liberated by endo-amylolytic enzymes such as AMY3 or ISA3 which would normally be acted on by SEX4 *in vivo.* Phospho-oligosaccharide accumulation decreases in double mutants lacking SEX4 with either AMY3 or ISA3 and are undetectable when GWD activity is lost (164). The starch morphology of *sex4* starch granules were significantly different than wild-type starch granules. Unlike the flat, discoid granules found in wild-type plants, *sex4* starch granules were larger and rounded (180). SEX4 span is highly conserved and homologs span from higher plants to green algae (77).

LSF2 is also localized to the chloroplast and was identified based on its similarities to the DSP domain of SEX4. LSF2 is a unique glucan phosphatase in that it lacks a CBM and only possesses a N-terminal chloroplast targeting peptide, a DSP domain, and C-terminal motif. Although it lacks a CBM, it possesses three surface binding sites (SBSs) that bind and engage starch, which essentially replace the CBM (181). LSF2 can dephosphorylate potato amylopectin, purified phospho-oligosaccharides (from *sex4* mutant), and exclusively dephosphorylates the C3-position of glucosyl residues of native starch (179). Similarly, to SEX4 from *A. thaliana*, the structure was solved of LSF2 with (PDB 4KYQ) and without maltohexaose and phosphate (PDB 4KYR) (181). The structure of LSF2 bound to

maltohexaose showed one of the SBSs was an aromatic-rich interface in the active-site channel responsible for majority of the interaction with maltohexaose. The structures of SEX4 and LSF2 revealed that a structured α-helical V-loop may be a unique characteristic of glucan phosphatases (178, 181). In contrast to SEX4, the positioning of the bound glucan was C3 oriented with a significant distance to the C6-hydroxyl of a glucose residue, displaying a mechanism for exclusive C3 specificity (181).

A surprising finding was that *lsf2* mutants do not display a starch excess phenotype compared to wild-type plants although the amount of C3-phosphate was increased. Unlike SEX4-deficient *Arabidopsis* plants, there was no accumulation of phospho-oligosaccharides suggesting that phospho-oligosaccharide accumulation may be a distinct SEX4 phenotype (179). The double *lsf2 sex4* mutant displayed a greater starch excess phenotype, compromised growth, and phospho-oligosaccharides accumulated at 30% less compared to that of the single *sex4* mutant. It is unlikely LSF2 is essential for starch degradation in leaves of *Arabidopsis* under normal circumstances since there are no other known defects. SEX4 activity could compensate for the lack of LSF2 activity being sufficient for normal starch degradation in experimental growth conditions. It was proposed that LSF2 acts during the day to reduce phosphate at the C3-position and net phosphate incorporation is a balance between glucan kinases and phosphatases (179).

Like Sex Four 1 (LSF1) is also encoded in the *A. thaliana* genome and is similar to SEX4 as it contains a N-terminal chloroplast targeting peptide, a DSP domain, and a C-terminal CBM of family 48. Additionally, LSF1 includes a PDZ protein interaction domain and a domain of unknown function (DUF). Similar to *sex4* mutants, *lsf1* mutants display a starch excess phenotype, albeit to a lesser extent, throughout the diurnal cycle; however, there is no accumulation of phospho-oligosaccharides, a reduction in AMY3 expression, nor a major alteration in starch granule morphology (180). Although LSF1 binds to starch granules *in vivo*, it is not an active glucan phosphatase as it lacks conserved residues in the DSP active site, the CX_5R consensus motif, responsible for engaging glucan chains and

directing them to the active site for dephosphorylation (171). More recently, LSF1 was shown to act as a scaffold for β-amylases, BAM1 and BAM3, facilitating degradation (182). LSF1 is found in higher land plants but is absent in green and red algae. SEX4 and LSF2 orthologs are highly conserved throughout chloroplastida from land plants to single-celled green algae like *Chlamydomonas reinhardtii;* however, are absent in prokaryotes and glycogen metabolizing eukaryotes (171).

The first glucan phosphatase described was a glucan phosphatase found in humans called laforin and is the founding member of glucan phosphatases. Mutations of a gene encoding for laforin, *EPM2A*, is in part responsible for the rare and fatal neurodegenerative epilepsy known as Lafora disease (LD). A hallmark of LD is the accumulation of aberrantly branched and hyperphosphorylated insoluble glucans known as Lafora bodies (LBs) in the cytoplasm of nearly all cell types (183). The LBs were found to have similar physicochemical properties to amylopectin (184). Human laforin is quite unique being the only phosphatase in the human genome to contain a CBM. Laforin shares general features with SEX4 found in plants as they both contain a CBM and a DSP domain. However, laforin contains a N-terminal CBM of the family 20 and a C-terminal DSP domain which is not only an inverted orientation compared to SEX4, the CBM is different as well. Therefore, it is likely that these two glucan phosphatases underwent separate evolutionary fusion events yielding different homologues (185).

Laforin can bind and dephosphorylate glycogen and potato amylopectin *in vitro* and can dephosphorylate both the C6- and C3-positions although the C3-position is preferred. Laforin dephosphorylation specificity is almost exactly the opposite of SEX4 (176). While SEX4 and laforin are not orthologues, they both share common structural similarities and involved in carbohydrate metabolism therefore they were suggested to be functional equivalents of one another (185). Indeed human laforin rescued the starch accumulation of the *sex4-3* mutant phenotype in *Arabidopsis* when transforming human laforin fused to a chloroplast targeting peptide (185). Interestingly, laforin was originally thought to be conserved in only vertebrate genomes; however, laforin orthologues were found in five additional protists

including *Toxoplasma gondii* and *Cyanidioschyzon merolae* (185)*.* Furthermore, both *T. gondii* and *C. merolae* produce floridean starch in the cytosol therefore laforin-like activity is likely required for normal metabolism of semicrystalline carbohydrates.

1.6 Floridean starch metabolism in *C. merolae*

This section will highlight the current knowledge on floridean starch metabolism in *C. merolae* as well as featuring my work on a glucan dikinase and glucan phosphatase found in the *C. merolae* genome. The forementioned observations in higher plants such as *Arabidopsis* have paved the way in biochemically and biologically understanding certain enzymatic functions in regards to the biosynthesis and degradation of starch and glycogen. Compared to higher plant model organisms that require 30-40 genes for starch, protists such as *T. gondii* and *C. merolae* seemingly have the bare minimum set of genes (~12) required to metabolize plant-like semicrystalline carbohydrates (**Figure 1-5**) (69).

1.6.1 Synthesis and degradation of floridean starch in *C. merolae*

As a reminder, the α-glucans, glycogen and starch, are synthesized through coordinating functions of glycogen/starch synthases and branching enzymes which are able to form $\alpha-1,4$- and $\alpha-1,6$-glycosidic bonds. The additional novel function of isoamylase-like debranching activity during amylopectin synthesis reflects a major difference between glycogen and starch metabolism.

Rhodophytes uniquely synthesize floridean starch in their cytosol using the UDP-glucose based pathway similar to that of eukaryotic glycogen metabolism. Although this may be true for most rhodophytes, Cyanidiales are an interesting clade as *C. merolae* produces floridean starch that is absent of amylose while *G. sulphuraria* and *C. cyanidium* produce glycogen-type glucans. Glycogenin acts as a self-glucosylating primer for the subsequent actions of glycogen synthase while starch initiation is thought to begin with an amylopectin cluster (71, 103, 186). Glycogenin-like proteins have been proposed in higher plants known as "amylogenin" but were subsequently dismissed (101). Later a protein homologous to glycogenin called, plant glycogenin-like starch initiation protein 1 (PGSIP1), was

31

identified in the *Arabidopsis* genome that when the expression is reduced results in a reduction of starch content in leaves (187). In the *C. merolae* genome, there are actually four encoded glycogenin-like proteins, *Cm*GLG1 (CMK020C, glycogenin-1), *Cm*GLG2 (CMG174C, glycogenin-2), CMR358C, and CMJ262C. The latter two encode two proteins that are associated with polyglucans of the chloroplast and mitochondrion dividing rings, respectively (188). Through phylogenetic analysis *Cm*GLG1 is assigned to the same group in which PGSIP1 is classified. A 65-fold overexpression of *Cm*GLG1 in *C. merolae* resulted in a 4.7-fold increase in starch content and is regulated by its phosphorylation status by target of rapamycin (TOR) (189). *Cm*GLG2 is grouped with yeast and rabbit muscle glycogenin proteins that are essential for glycogen accumulation (188, 190). Interestingly, a 362-fold overexpression of *Cm*GLG2 only resulted in a 2-fold increase and therefore suggests that *Cm*GLG1 likely plays the major role in floridean starch synthesis in *C. merolae* (189). Regulation of *Cm*GLG2 is currently unknown but similar to *Cm*GLG1, their expression is unaffected by nitrogen deprivation and rapamycin treatments which are starch accumulating conditions therefore it is likely they are both regulated at the post-transcriptional level (191).

Chain elongation and branching follow initiation and the *C. merolae* genome encodes for only one enzyme for each function, CMM317C and CMH144C, respectively. UDP-glucose utilizing starch synthase (CMM317C) found in *C. merolae* and other red algae belong to the glucosyl transferase family (GT5, www.cazy.org) which is distinct compared to GT3 UDP-glucose glycogen synthases found in other species (102). Glucan trimming and reorganization is performed by disproportionating enzymes (DPE1/2) and debranching enzymes (isoamylases-like) and is thought to be one of the distinct reasons why *C. merolae* can produce insoluble crystalline carbohydrates stores. *C. merolae* intriguingly possess two isoforms of DPE-like (CMP352C and CMT204C) and isoamylase-like (CMI294C and CMS197C) enzymes therefore it is tantalizing to suspect specific synthesis and degradation functions between isoforms. The absence of amylose synthesis in *C. merolae* is due to the absence of GBSS in the genome. Instead of GBSS commonly found bound to starch granules, starch phosphorylase

(CMD184C, EC 2.4.1.1) was associated with starch granules. Starch phosphorylase is not normally found within starch granules in higher plants and may have roles in both synthesis and degradation (73).

Genomic comparisons between *C. merolae, G. sulphuraria,* and *T. gondii* reveal a complete set of minimum genes required to metabolize storage α-glucans (8, 69). In contrast to the glycogen-producing *G. sulphuraria,* floridean starch degradation proteins encoded in *C. merolae* and *T. gondii* are similar to green plants and algae. In addition to isoamylase-like proteins, the presence of a GWD-like (CMT547C) protein largely distinguishes plant starch metabolism from that of animal, fungal, and bacterial glycogen metabolism pathways as GWD-like genes are not found in such organisms unrelated to plants (74). Counteracting GWD-like proteins, laforin-like (CMT465C) proteins recycle phosphorylated glucans furthering the degradative process. The presence of such genes reflects the requirement to synthesize and degrade crystalline structures. Products of reversible glucan phosphorylation are generally maltose and MOSs in which the latter are not generated from glycogen in yeast or mammalian cells. Maltose and MOSs are further processed by DPE2 (CMP352C/CMT204C) to mobilize glucose which are encoded in the *C. merolae* genome. No work has been done in regards to reversible glucan phosphorylation in *C. merolae* or in floridean starch producing organisms in general. This works aims to shed light on the utilization of glucan dikinases and glucan phosphatases in floridean starch metabolism in *C. merolae.*

1.6.2 α-Glucan, Water Dikinase characterization in *C. merolae* (Chapter 3)

A single putative glucan dikinase (CMT547C) is encoded in the *C. merolae* genome (NC_010146) on chromosome 20. CMT547C is a 1572 amino acid protein comprised of three N-terminal CBM of the family 45 (CBM45), an α-helical rich linker region, and a C-terminal pyruvate, phosphate dikinase-like (PPDK) catalytic domain comprised of the phosphohistidine (HIS) and nucleotide-binding (NBD) subdomains. The putative 1572 amino acid protein from *C. merolae* was only 24% identical to the prototypical GWD from potato (**Figure 3-3**). We used the criteria that a GWD ortholog must contain CBMs of the family 45 and a PPDK domain

(**Figure 3-1**). Since phosphoglucan, water dikinase (PWD) possesses a CBM of the family 20 (CBM20), we ruled out that this putative glucan dikinase was a PWD ortholog. Additionally, there are no other dikinases encoded in the *C. merolae* genome that possess a CBM20 and a PPDK domain which suggested that *C. merolae* only contains one glucan dikinase similar to a GWD ortholog (**Figure 3-2**). Via sequence alignments, we synthesized the full-length putative GWD ortholog as well as a proposed catalytically inactive mutant (H1162A) and purified recombinant protein from bacteria (**Figure 3-4**). Upon further investigation, our data supports that unlike normal kinases, the putative GWD follows a unique mechanism transferring the β-phosphate of ATP to a glucan substrate. Prior to transferring the β-phosphate to its substrate, the putative GWD creates a phosphohistidine-intermediate as shown through a radiolabeled $β^{33}$-ATP autophosphorylation assay. Mutation of the phosphohistidine residue (H1162) to an alanine effectively abolished autophosphorylation capabilities (**Figure 3-3C**). Through an *in vitro* phosphorylation assay, the putative GWD phosphorylated native wild-type *C. merolae* starch granules while the H1162A mutant could not (**Figure 3-3D**). Utilizing a novel indirect site-specificity assay, we showed that the putative GWD from *C. merolae* exclusively phosphorylates the C-6 position of glucosyl residues of starch (**Figure 3-3E, 3-5**). Overall, our bioinformatic and biochemical data demonstrate that the putative GWD in *C. merolae* is an active glucan dikinase with characteristics resembling a GWD ortholog, which we named *Cm*GWD (**Figure 3-3F**).

In order to investigate the role of GWD in *C. merolae* we successfully knocked out GWD and isolated (propagated) GWD-deficient (Δ*gwd*) strains using an uracil auxotrophic *C. merolae* mutant strain T1 (**Figure 3-7A, B**) (33). In contrast to GWD-deficient (*sex1*) plants of *A. thaliana,* under continuous and diurnal light regimes, there were no growth defects nor observable cell morphology differences compared to wild-type cells (**Figure 3-7, C-F**). To confirm *Cm*GWD phosphorylates the C6-position of glucosyl residues *in vivo,* we examined the phosphate content and the position of phosphates utilizing three separate analytical methods: fluorescence-assisted capillary electrophoresis (FACE) (**Figure 3-12A**), gas

chromatography mass spectrometry (GCMS) (**Figure 3-12B**), and ^{31}P-NMR (**Figure 3-14**). All three methods corroborated that wild-type *C. merolae* starch contained phosphate only at the C6-position which was essentially absent in Δ*gwd,* rendering the latter phosphate free. GWD mutant plants often result in a severe starch excess phenotype conversely in *C. merolae*, we did not observe this phenomenon (**Figure 3-12C**). Under more physiologically-relevant conditions, we subjected both strains to 12-hour/12-hour diurnal conditions and observed that Δ*gwd* cells underwent slightly reduced rates of both synthesis and degradation of starch compared to wild-type (**Figure 3-15A**). There are a couple possible explanations for these results: 1) GWD activity plays an active role in both synthesis and degradation of floridean starch or 2) loss of GWD activity in initiating starch degradation causes poor substrates for subsequent synthesizing enzymes. Although the rates of both synthesis and degradation were reduced in Δ*gwd* cells, the rates were similarly balanced corroborating that found in *sex1* plants (150). We further analyzed the chain-length distribution (CLD) of the floridean starch product produced by Δ*gwd* cells and compared them to wild-type. Starch produced in both continuous (**Figure 3-16**) and diurnal (**Figure 3-15C, D**) conditions displayed a uniquely altered CLD profile which exhibited an abnormal abundance of short chains with a degree of polymerization (DP) 3-7 as well as a decreasing trend in longer chains >35. Particularly, DP3 and DP4 were ~1.5 – 2.0-fold higher compared to the WT CLD profile. These are major differences, 4-5 times higher, than those reported for the *sex1* mutant in *A. thaliana* and G1i line in cassava (33, 192). Our most significant finding was the altered morphology of Δ*gwd* starch granules through scanning (SEM) and transmission (TEM) electron microscopy compared to wild-type. Starch granules from Δ*gwd* lines were vastly heterogeneous in distribution and exhibited larger, deformed and thin granules in contrast to round, uniform and smooth granules of wild-type. There were many regions of depressions in Δ*gwd* starch granules observed by TEM that penetrated towards the core of the granule under both continuous (**Figure 3-18**) and diurnal (**Figure 3-17**) conditions suggesting a progressive defect in these regions.

Due to the overwhelming altered starch morphology observed in Δ*gwd* cells under normal laboratory growth conditions, we hypothesized that utilization of their starch would be compromised under a prolonged period of darkness (i.e. energy deprivation). Under certain environmental stress conditions like prolonged dark stress and nitrogen starvation, it has been shown that *C. merolae* enters a state of quiescence which slows metabolic activity and activates autophagy-like mechanisms as a means to provide nutrients for survival (12, 193). Our work showed the ability of wild-type *C. merolae* to survive over two weeks of prolonged darkness while preserving majority of its photosynthetic pigments and starch. In stark contrast, the loss of GWD in *C. merolae* perturbed starch storage and maintenance as well as over-inducing macroautophagy-like mechanisms resulting in the consumption of major stores of carbon and nitrogen. Consequentially, Δ*gwd* cells were unable to reenter the proliferative cell cycle upon reintroduction of light whereas wild-type cells were able to recover seamlessly (**Figure 3-19**).

1.6.3 Laforin-like characterization in *C. merolae* (Chapter 4)

A single glucan phosphatase, *Cm*laforin (CMT465C), is encoded in the *C. merolae* genome and was discovered back in 2007 (185). *Cm*laforin is a 532 amino acid protein comprised of a N-terminal predicted unstructured region, two CBM20s, and a DSP domain. Due to the orientation of the CBMs to the DSP and the family of CBMs (CBM20 instead of CBM48), this protein is more laforin-like than SEX4 in higher plants. The full-length *Cm*laforin protein is largely insoluble therefore we cloned a truncated version of *Cm*laforin in which we eliminated the predicted unstructured region at the N-terminus of *Cm*laforin (Δ157) and retained the two CBM20s and the DSP (**Figure 4-1A, red asterisk**). Utilizing a novel radiolabeling assay, we can define the specificity of glucan phosphatases (**Figure 4-5**) (169, 174, 179, 181, 194). As mentioned previously, human laforin dephosphorylates the C3- and C6-position of glucosyl residues of substrates; however, the C3-position is preferred. In contrast, our biochemical data show that *Cm*laforin dephosphorylates the C3- and C6-position of glucosyl residues and largely prefers the C6-position (**Figure 4-6**). The specificity of *Cm*laforin resembles that of the

plant glucan phosphatase SEX4. Importantly, this data corroborates the presence of one glucan dikinase and phosphatase in *C. merolae* that preferentially act on the C6-position of glucosyl residues in a starch-like structure which lack phosphates on the C3-position. In order to investigate the role of laforin in *C. merolae* we successfully knocked out laforin (Δ*laforin*) as before in the case of GWD (**Figure 4-7A, B**). In contrast to Δ*gwd* cells, Δ*laforin* cells are approximately 80% the size of wild-type cells in area; however, do not display a proliferative defect under continuous or diurnal light conditions compared to wild-type (**Figure 4-7C, D**).

In SEX4-deficient *A. thaliana* plants, there is a progressive starch excess phenotype as the leaves age (173). We extracted and quantified the starch content of Δ*laforin* cells under continuous light and strikingly observed a substantial decrease (~7-fold) compared to wild-type cells (**Figure 4-8A**). Of the minute starch produced, there was however a 4-fold increase in glucose-bound C6-phosphate content (**Figure 4-8B**). Under more physiologically-relevant conditions, we subjected both strains to 12-hour/12-hour diurnal conditions and observed that Δ*laforin* cells underwent considerably slower rates of synthesis and even more significantly reduced rates of degradation compared to wild-type (**Figure 4-12A**). Both growth conditions, whether continuous or diurnal, produced similar increases in glucose-bound C6-phosphate content (**Figure 4-12B**). Our observation of the nearly absent rate of degradation was more pronounced than those in SEX4-deficient *A. thaliana* plants (164, 172, 173). The starch granules from Δ*laforin* cells under continuous light conditions were morphologically smaller, less spherical in shape, and also had several regions of depressions that seemed to originate from the core (**Figure 4-9**). Under nitrogen deprivation, *C. merolae* is known to accumulate starch within the first 48 hours as it is the primary carbon sink compared to lipids (193). Nitrogen deprivation induced starch accumulation in both wild-type and Δ*laforin* cells; however, Δ*laforin* cells still accumulated only 60% of that in wild-type cells (**Figure 4-10A**). Furthermore, Δ*laforin* starch granule morphology was expressively pronounced compared to granules grown in regular media. There is a considerable alteration of the granular surface exhibiting bulging

37

protrusions compared to the smooth granular surface of wild-type granules (**Figure 4-10C**). This data suggests that phosphate regulation significantly impacts granule morphology during accumulating conditions. In addition to the noticeable starch granule morphology, starch produced in both continuous (**Figure 4-8C**) and diurnal (**Figure 4-12C**) conditions of Δ*laforin* cells displayed an altered CLD profile which revealed an abnormal abundance of short chains with a DP 4-10. This data is similar to the CLD profile that is seen in *sex4* plants of *A. thaliana* compared to wild-type plants (72)*.* Due to severe dysregulation of starch metabolism observed in Δ*laforin* cells under normal continuous and diurnal conditions, we hypothesized that under a prolonged period of darkness, cells lacking laforin would not be able to utilize their starch properly. Our work showed that the loss of laforin in *C. merolae* correlated to the consumption of major stores of carbon and nitrogen in the form of light-harvesting proteins such as phycocyanin and chlorophyll α, and not in the form of starch reserves, as a means to survive (**Figure 4-14, C-E**). Consequentially, Δ*laforin* cells retained more than 60% of their starch but were unable to reenter the proliferative cell cycle upon reintroduction of light. Like the loss of laforin activity in humans, hyperphosphorylated carbohydrates result and are unable to be degraded which cause LD. Further investigations into laforin in *C. merolae* may help to open new avenues for an effective therapeutic strategy for LD patients.

1.7   Future prospectives in *C. merolae*

Recent advances in genomic manipulation in *C. merolae* has allowed us to investigate reversible glucan phosphorylation on an insoluble carbohydrate that is similar to lafora bodies and phytoglycogen that often results from abnormal carbohydrate metabolism. Although the simplistic nature of *C. merolae* is enticing to use as a model organism, there are still many unknowns in regards to cytosolic floridean starch metabolism as well as the regulatory mechanisms associated. In the future, we hope to build on the knowledge of reversible glucan phosphorylation and translate our findings to higher systems such as polyglucosan storage diseases in humans as well as manipulating starch metabolism for industrial applications.
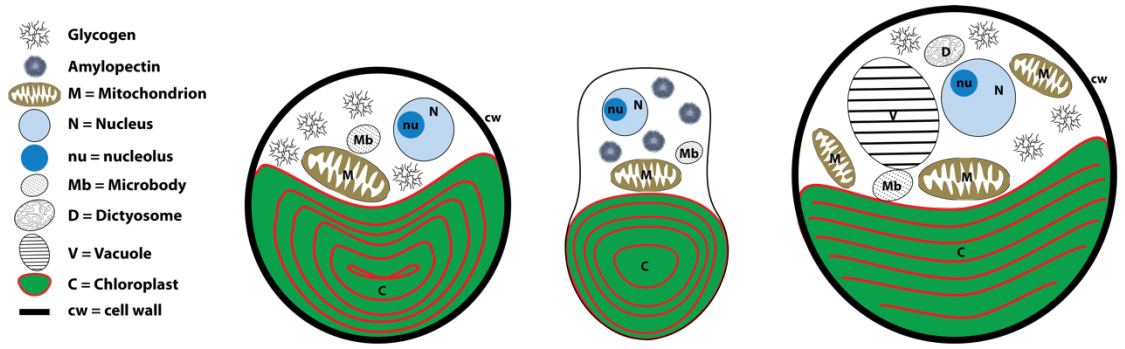
Feature	*Cyanidium caldarium*	*Cyanidioschyzon merolae*	*Galdieria sulphuraria*
Shape	Spherical	Oval, club-like	Spherical
Size (*µm*)	2-5	2-3	3-11
Genome size (Mb)	approx. 35*	16.73	13.78
Reproduction	Endospores	Binary fission	Endospores
Daughter cells	4	2	4-32
Cell wall	Present	Absent	Present
Chloroplast number	One	One	One
Chloroplast shape	Polymorph	Spherical	Multilobed
Mitochondria number	One	One	Multiple
Vacuoles	No	No	Yes
Microbodies	Yes	Yes	Yes
Phycobiliproteins	C-phycocyanin	C-phycocyanin	C-phycocyanin
Storage glucans	Glycogen-like	Amylopectin-like	Glycogen-like
Mixotrophy	No	No	Yes

Figure 1-1 Cyanidiales Comparison
Cytomorphological differences between three model species of the Cyanidiale order. Adapted from Albertano et al. 2000 (4) and morphological descriptions from Merola et al. 1981 (9).
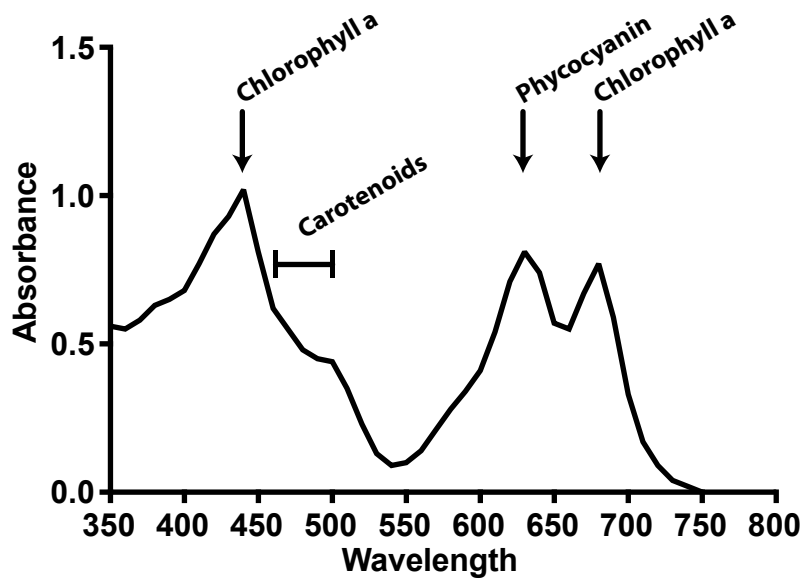
Figure 1-2 Absorption spectra of *C. merolae*
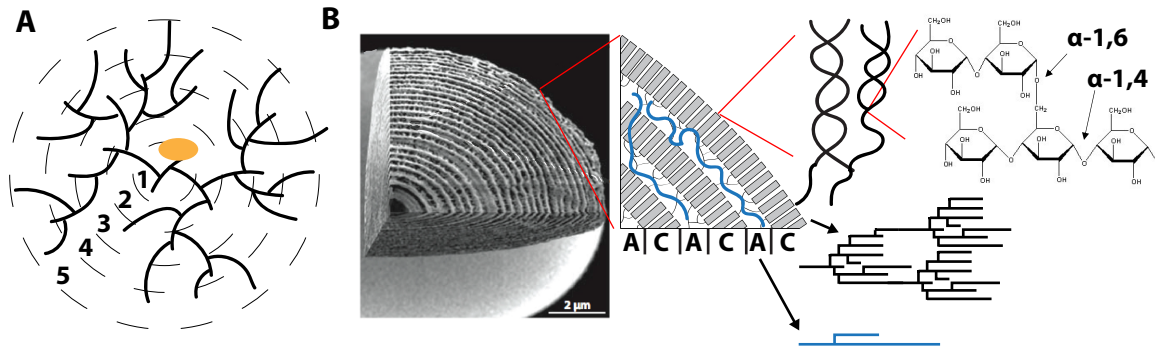
Figure 1-3 Glycogen and Starch structures
A) Structure of glycogen with continuous branching and the formation of tiers. Glycogenin in yellow. **B)** Starch granule macromolecule showing internal growth-ring structure after chemical and enzymatic treatment. The growth rings are made from alternating layers of amorphous (A) and crystalline lamellae (C) with a thickness ~9 nm. The blue linear glucan polymer represents amylose throughout the amorphous region. In contrast, the discontinuous branched amylopectin forms double helices with neighboring glucan chains rendering the starch granule water-insoluble. The chains and branches of both starch and glycogen are comprised of α-1,4-glycosidic linkages and α-1,6-branches (far right). Adapted from Pfister and Zeeman 2016 (63).
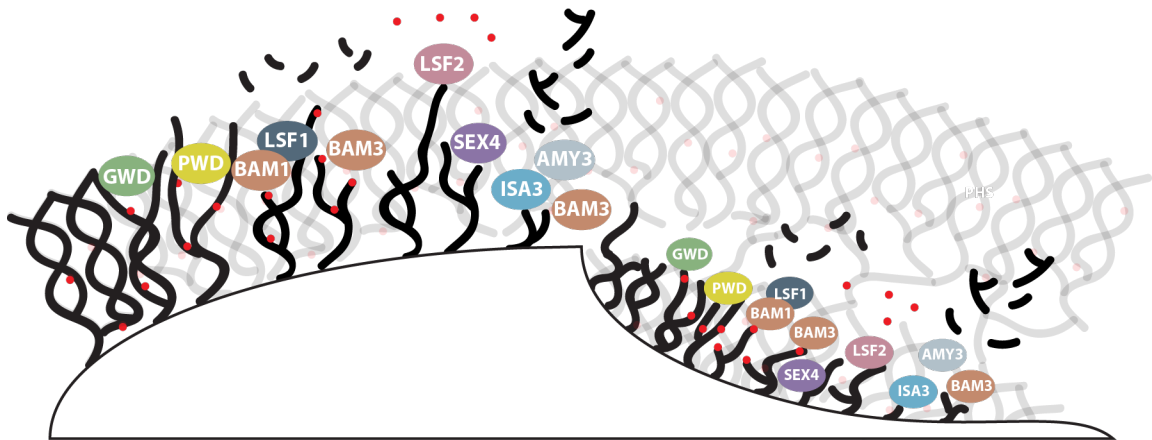
Figure 1-4 Reversible glucan phosphorylation cycle – transitory starch degradation

Current knowledge of the essential reversible glucan phosphorylation cycle of transitory starch degradation. Main steps of the cycle are: phosphorylation of the outer surface by the glucan dikinases, glucan water dikinase (GWD) and phosphoglucan water dikinase (PWD), initiate and solubilize the amylopectin helices. Amylolytic degradation by β-amylase (BAM) and isoamylase (ISA) follows solubilization of amylopectin helices releasing maltose and linear oligosaccharides. Dephosphorylation of hindering phosphate groups by glucan phosphatases, Starch Excess Four (SEX4) and Like Sex Four2 (LSF2), enable further degradation by amylolytic enzymes and resets the cycle for further solubilization.
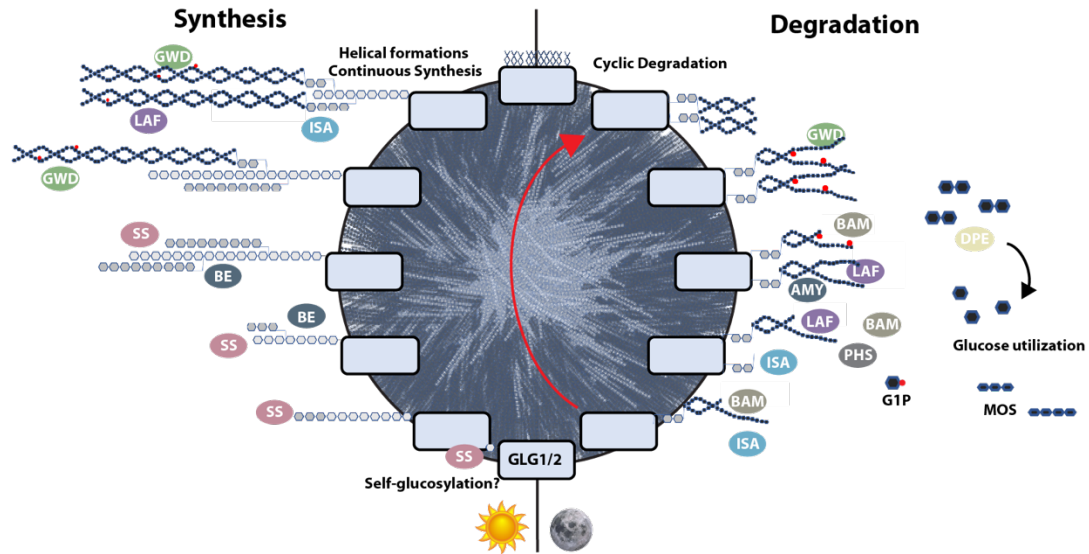
Figure 1-5 Proposed floridean starch metabolism in *C. merolae*
Synthesis of floridean starch in *C. merolae* begins with the self-glucosylation of Glycogenin (GLG). This acts as a primer for glucan elongation and glucan branching activity by starch synthase (SS) and branching enzyme (BE), respectively. Proposed transient phosphorylation and dephosphorylation at the C6-position of glucose moieties by glucan, water dikinase (GWD) and laforin (LAF), respectively. Phosphate content may influence trimming/debranching activity of isoamylase (ISA) and thus crystalline organization of amylopectin during synthesis. Cyclic degradation of floridean starch by reversible glucan phosphorylation is initiated by phosphorylation by GWD which causes solubilization of outer amylopectin helices. Solubilized glucans are then mainly degraded by the amylases, β-amylase (BAM) and isoamylase (ISA), releasing maltose and linear maltooligosaccharides (MOS). The released products are substrates for disproportionating enzyme (DPE) which releases glucose for utilization. α-Amylase (AMY) and phosphorylase (PHS) may also have minor activity during degradation releasing branched oligosaccharides, glucose, and glucose 1-phosphate (G1P). Dephosphorylation by LAF allows for further degradation by amylolytic enzymes and resets the degradation cycle.

CHAPTER 2. MATERIALS AND METHODS

2.1 Identification, synthesis, and purification of α-glucan, water dikinase from *C. merolae*

2.1.1 Bioinformatic identification and synthesis

A BLASTp search was conducted using the *Cyanidioschyzon merolae* Genome Project website (http://czon.jp/blast/blast.html). The PPDK domain from the prototypical *Solanum tuberosum* GWD was used as the query (159). Two BLAST results were identified in *C. merolae,* XP_005539443.1 (CMT547C) and XP_005535692.1 (CMF012C). Amino acid sequences of GWD orthologs were obtained through NCBI, aligned by ClustalW (195), and refined manually using MacVector. Full-length CMT547C was codon optimized, synthesized (Genscript), and subcloned into the protein expression vector pET28b (Novagen) using NdeI and XhoI restriction sties to encode an N-terminal His$_6$ tag, a thrombin cleavage site, and full-length *Cm*GWD. From full-length *Cm*GWD, multiple constructs including truncations and individual domains were synthesized by Genscript. Construct 114-C deleted the unstructured N-terminal region, 345-C construct removed the first CBM45, 511-C construct removed the first CBM45 and the initially characterized DUF, 820-C was the isolated PPDK domain (**Figure 2-1**).

2.1.2 Site-directed mutagenesis

Wild-Type *Cm*GWD in the pET28b vector was used as the template DNA for subsequent mutagenesis by the QuikChange Lightning Site-Directed Mutagenesis Kit (QuickChange Lightning, Agilent; Q5 Site-Directed Mutagenesis, New England BioLabs; GENEWIZ Site-Directed Mutagenesis). The forward primer H1162A-for-ATGCCCGCATTGGCCACTGC and reverse primer H1162A-rev-CCCTGGCAATGGCAATGCTT were used to generate the His1162Ala catalytically inactive construct.

2.1.3 *C. merolae* α-glucan, water dikinase construct expression and purification

*Cm*GWD recombinant proteins were produced in BL21 (*DE3) E. coli* cells (EMD Millipore). Cells were grown in 2xYT media to an OD_{600} of 0.6-0.8, placed on ice for 20 min, induced with 0.4mM isopropyl β-D-1-thiogalactopyranoside (IPTG), grown for 16 hours at 16°C, and harvested by centrifugation. Cells were lysed in lysis buffer (50mM Tris-Cl, 50mM NaCl, 0.1% Triton X-100, 0.1% Tween-20, 2 mM dithiothreitol (DTT), and a PIC tablet (cOmplete, Mini, EDTA-free Protease Inhibitor Cocktail, Sigma-Aldrich 11836170001)) by sonication 5 times for 5 seconds. The lysate was centrifuged and the proteins were purified using immobilized metal affinity chromatography (IMAC) on a Profinia Purification System (BioRad). Proteins were eluted into lysis buffer containing 300mM imidazole and then dialyzed in 3 liters of size exclusion chromatography (SEC) running buffer (50 mM Tris, 50 mM NaCl, 0.05% Triton X-100, 0.05% Tween-20, and 20 mM DTT) overnight at 4°C. Proteins were purified to homogeneity via SEC using an ÄKTA system (GE Healthcare) and a prep grade 16/70 Superose 6 column. Protein purity was determined by SDS-PAGE with Coomassie staining. The purifications typically yielded approximately 2-3 mg/L of *E. coli*.

2.1.4 Cloning, expression, and purification of CBM45 from *Cm*GWD

CBM45 (construct 2.11) from *Cm*GWD, residues 318-469 (UniProt accession No. M1VD00), was expressed from pET28b (Novagen) as an N-terminal His_6 tag fusion. The point mutant W457A was created using a site-directed mutagenesis kit (QuickChange Lightning, Agilent). WT and W457A were expressed in BL21-CodonPlus *E. coli* Rosetta (DE3) competent cells grown at 37°C in 2xYT media to OD_{600} = 0.5 to 0.6, placed on ice for 20 min, induced with 1mM isopropyl β-D-thiogalactopyranoside, cells were then grown at 16°C for overnight, and harvested by centrifugation. For protein purification, cells were lysed in 50 mM Tris-HCl (pH 7.5), 100 mM NaCl, 5 mM βME and 15 mM Imidazole, sonicated and centrifuged to remove debris, and soluble proteins were loaded onto IMAC column (Bio-Rad) using Profinia Purification system (Bio-Rad). His-tagged protein was eluted from

IMAC column by 300 mM Imidazole and dialyzed in size exclusion buffer (50 mM Tris-HCl (pH 7.5), 100 mM NaCl and 5 mM βME) overnight. Following dialysis, size exclusion chromatography was performed by a HiLoad 16/60 Superdex 75 column (GE Healthcare) for final purification equilibrated with size exclusion buffer (50 mM Tris-HCl (pH 7.5), 100 mM NaCl and 5 mM βME). The purifications typically yielded approximately 20-27 mg/L of *E. coli.*

2.2   Biochemical *in vitro* studies of *C. merolae* α-glucan, water dikinase

2.2.1   Autophosphorylation

Auto-phosphorylation activity was performed as described previously (142, 156) with the following modifications. 10 μg of either *Cm*GWD or H1162A was incubated with 10 μCi β^{33}-ATP or γ^{33}-ATP (Hartmann Analytic) separately in Buffer C (50 mM HEPES-KOH pH 7.5, 1 mM EDTA, 6 mM $MgCl_2$, 10% glycerol) for 30 minutes at room temperature. The reaction was terminated by adding 4x SDS sample buffer and denatured for 20 minutes at 30°C. Approximately 8 μg of protein was loaded per well of an SDS-PAGE and the proteins were separated from radiolabel. Autoradiography was detected using a phosphor screen (GE Healthcare) and imaged by a Typhoon FLA 9500 Imager. The Mini-PROTEAN TGX stain-free gel was directly imaged after autoradiography using a ChemiDoc Bio-Rad Imager.

2.2.2   Radiolabeled Phosphorylation Activity Assay

5 pmol of *Cm*GWD and H1162A protein were incubated in a freshly prepared 3x phosphorylation buffer [10x Phosphorylation buffer (500 mM HEPES-KOH, pH 7.5, 10 mM EDTA, 60 mM $MgCl_2$, and 0.5% Triton X-100), 5 mM ATP, 0.1 M DTT, and 10 mg/mL BSA]. Three different types of glucans were used: WT *C. merolae* glucan, Δ*gwd* from *C. merolae,* and *A. thaliana sex1-3* phosphate-free starch. The dried glucans were washed twice with 1 mL of 0.05% Triton X-100 and re-suspended in a volume of water so that the final glucan concentration was 20 mg/mL. 0.25 μCi β^{33}-ATP (Hartmann Analytic) was used per reaction. The samples

46

were mildly agitated to keep the glucan in suspension at room temperature for the indicated times in **Figure 3-3D**. SDS was added to terminate the reaction. Following centrifugation at 3,000 rpm for 5 minutes, the supernatant was aspirated off. The pellet was washed 5-7 times with wash buffer [2% SDS and 2 mM ATP] until no residual radiolabel counts could be detected in the supernatant. The final wash was 100 μl of wash buffer and 5 μl was taken out, added to 3 ml scintillation fluid, and the mixture was quantified on a Packard 1900 TR scintillation analyzer for quality control. The supernatant was aspirated off one last time and up to 100 μl ddH$_2$O was added to re-suspend the glucan. All contents were added into 3 ml scintillation and quantified by the scintillation analyzer. A 'no enzyme' control was used as the background control.

2.2.3 Indirect glucan phosphatase site-specificity assay

A. thaliana sex1-3 starch was washed and phosphorylated as described above with the following modifications. *sex1-3* starch was incubated with a recombinant glucan dikinase (*Cm*GWD) and [β ^{33}P]-ATP at 0.5 μg and 0.5 μCi per milligram of starch, respectively. The reaction was incubated for 5 hours at room temperature with constant mild vortexing to keep starch in suspension. After 5 hours, the starch was pelleted and a second phosphorylation step was initiated. For the second phosphorylation step, fresh recombinant protein was added using these conditions with the total amount of ATP in the reaction lowered to 10 μM and incubated for 16 hours. Following overnight phosphorylation with recombinant protein, the reaction was terminated by the addition of 10% SDS. *Cm*GWD-treated starch was washed with 1 mL 2%SDS/2 mM ATP until label in the supernatant did not change. The starch was washed two more times with 0.05% Triton and finally re-suspended in water to a concentration of 20 mg/mL.

Site-specific dephosphorylation was carried out by the glucan phosphatases LSF2 and SEX4 as well as their catalytically-inactive mutants (C/S). For each phosphatase reaction, 0.6 mg of dikinase treated *sex1-3* starch was incubated with 2 mM DTT, 1x Phosphatase Buffer (100 mM sodium acetate, 50 mM bis-Tris, 50 mM Tris-HCl pH 6.5), 1 mg/mL BSA, 0.05% Triton and 150 ng glucan phosphatase

protein (**Figure 2-2**). The reaction was first carried out with LSF2 for 15 min at room temperature with constant mild vortexing and terminated by the addition of 10% SDS. LSF2 exclusively dephosphorylates the C3-position of glucose moieties therefore LSF2 will remove all of the C3-phoshate before the starch is dephosphorylated with SEX4. The reaction was centrifuged for 5 minutes at max speed and the released radiolabel in the supernatant was quantified by a Packard 1900 TR scintillation analyzer. Following two washes, the starch was then incubated similarly with recombinant *At*SEX4 for 15 min at room temperature. The reaction was terminated by the addition of 10% SDS and the reaction was centrifuged to separate released radiolabeled phosphate. Although SEX4 preferentially dephosphorylates C6-phosphate, SEX4 has the ability to remove C3-phosphate as well. With the C3-phosphate removed already by LSF2, the phosphate released by SEX4 should all be from the C6-position. The reaction was centrifuged for 5 minutes at max speed and the released radiolabel in the supernatant was quantified by a Packard 1900 TR scintillation analyzer. The catalytically-inactive mutants served as background/blanks for each reaction.

2.2.4 Differential scanning fluorimetry (DSF)

Experiments were performed as described (169, 194) using a CFX96 Real-Time PCR system (BioRad) with some modifications. Individual reactions contained 5 µM protein and 5X SYPRO Orange Protein Gel Stain (Invitrogen) with or without maltooligosaccharides. Melting/stability were monitored from 20 to 90°C at a ramp rate of 1°C/50sec. Melting temperatures (T_m) were calculated from a Gaussian fit of the first derivative of the melting curves. Data analyses and binding fits were determined using the Prism software (Graphpad).

2.3 Biochemical *in vitro* studies of *C. merolae* laforin

2.3.1 Site-specific dephosphorylation assays

Phosphate-free *Arabidopsis* (*sex1-3*) was phosphorylated as previously described (**Figure 4-5**) (169, 175). Radiolabel was incorporated into sex1-3 starch with [β ^{33}P]-ATP from Hartmann Analytic. Briefly, phosphorylation was performed

by purified *S. tuberosum* GWD and *A. thaliana* PWD where C6-labeled starch was prepared by including [β ^{33}P]-ATP (0.5 μCi/mg starch) with the GWD incubation and unlabeled ATP with the PWD incubation. C3-labeled starch was prepared by GWD incubation with unlabeled ATP and PWD incubation with [β ^{33}P]-ATP. Unbound phosphate after each phosphorylation round was removed from labeled starch by stopping the phosphorylation reaction with 10% SDS and subsequent washes with 2% SDS/2 mM ATP until radiolabel in supernatant ceases to decrease. The labeled starch was resuspended in water at a concentration of 100 μg starch/μL.

For dephosphorylation of labeled starch, 150 ng of recombinant glucan phosphatase protein at a concentration of 7.5 ng/μL was incubated in a total volume of 150 μL for 15 minutes while on a rotating wheel at room temperature. Phosphatase reactions contained 0.6 mg labeled starch (either C6- or C3-labeled), 1x phosphatase buffer (0.1 M sodium acetate, 0.05 M bis-Tris, and 0.05 M Tris-HCl, pH 6.5), 2 mM DTT, 1 mg/mL BSA, and 0.05% Triton X-100. The reaction was stopped with 10% SDS and after mixed thoroughly by vortex, the sample was centrifuged at 13,000 rpm for 5 minutes to pellet starch. 150 μL of the supernatant was added to 3 mL scintillation liquid, and 33P release was measured by a Packard 1900 TR liquid scintillation counter. For kinetic experiments, time and substrate concentration were varied as indicated. Kinetic parameters were calculated using Prism Software (Graphpad).

2.4   Preparation and materials for *C. merolae* cell biology

2.4.1   2x Modified Allen's (MA2) medium

Culture medium was prepared as previously described (26, 196). Briefly, four solutions were prepared separately and then compiled together to make 2x Modified Allen's (MA2) medium (**Table 2-1**). 100 mL of Solution I, 10 mL of Solution II, 1 mL of Solution III, and distilled water up to 1 L were combined. The pH was then adjusted to 3 with sulfuric acid then the medium was sterilized by autoclaving. After sterilization, the medium was cooled to room temperature and 4 mL of filter-sterilized Solution IV was added to complete the MA2 medium. A separate Solution

I was made for Nitrogen deprivation (-Nitrogen MA2) medium where ammonium sulfate is replaced with 40 mM sodium sulfate.

2.4.2 Genomic DNA extraction methods

2.4.2.1 Hot phenol method

C. merolae genomic DNA was extracted from WT cells as described previously in (196). Briefly, C. merolae cells were harvested by centrifugation at 3,000 rpm for 5 min at 4 °C where supernatant was discarded afterwards. The cell pellet was dissolved in DNA extraction buffer (50 mM-HCl pH 8, 5 mM EDTA, 0.05% (w/v) SDS). An equal volume of Tris-saturated phenol solution is subsequently added (usually 250 µL of solution). The 1:1 mixture is incubated at 65 °C for 10 minutes with frequent mixing followed by centrifugation at 15,000 rpm for 5 minutes at room temperature. The upper aqueous phase is then transferred to a fresh tube and added to an equal volume of PCI (phenol/chloroform/isoamylalcohol (25:24:1)) then centrifuged as above. This step is repeated three times. The DNA is precipitated with 100% ethanol and then dissolved in distilled water. The dissolved DNA is then cleaned of RNA contamination by the addition of RNase A at 37°C for 30 minutes and then purified again by PCI extraction and ethanol precipitation. The final purified genomic DNA is dissolved in distilled water and 50-100 ng is used as template for PCR reactions.

2.4.2.2 TRIzol extraction method

C. merolae cells were harvested by centrifugation at 3,000 rpm for 5 min at 4 °C where supernatant was discarded afterwards. TRIzol reagent (ThermoFisher Scientific, 15596026) was added to cell pellet (3:1 volume of sample collected) and C. merolae cells were lysed by forcing through pipet several times until homogenized. For phase separation, homogenized cell lysate was incubated at room temperature for 5 minutes. Chloroform was added to the homogenized sample (1:5 volume of TRIzol) and the sample was shaken vigorously for 15-30 seconds then incubated for 3 minutes at room temperature followed by centrifugation at 12,000 x g for 15 minutes at 4 °C to further separate phases. The upper aqueous phase was discarded and both the interphase and organic phase

were collected for DNA precipitation. 100% ethanol was used to precipitate DNA from both collected phases (1:3 volume of TRIzol used for initial homogenization) and mixture is inverted several times to mix thoroughly. Following a 3-minute incubation at room temperature, the mixture was centrifuged for 5 minutes at 2,000 x g at 4 °C to pellet DNA. The resulting DNA pellet was washed thoroughly with 0.1 M sodium citrate in 10% ethanol and incubated for 30 minutes at room temperature with occasional inversion. The supernatant is removed after centrifugation at 2,000 x g for 5 minutes at 4 °C and the wash is repeated twice before the addition of 75% ethanol. After a 20-minute incubation at room temperature with occasional inversion and centrifugation, the washed DNA pellet is air dried and resuspended in 8 mM sodium hydroxide.

2.4.3 MA2 gellan gum plates for transformation and colony isolation

Two solutions were separately prepared for making MA2 gellan gum plates for the transformation of *Cyanidioschyzon merolae.* First, Solution A (1.5 g Gerlite (Gellan Gum) in 200 mL of distilled water) and Solution B (70 mL distilled water) were autoclaved. After autoclaving, Solution A was stored in a 65°C water bath to keep Gellan Gum from solidifying. While Solution A was incubating, added 30 mL of Solution I, 3 mL Solution II, and 300 μL Solution III to Solution B (see table 2.1). Cooled Solution B to room temperature and added 1.2 mL of Solution IV and 150 μL sulfuric acid to lower pH to around 2.5. Combined Solutions A and B and immediately poured into 10 cm petri plates. Cooled until the gellan gum has solidified and stored wrapped in aluminum foil @ 4°C.

2.4.4 Corn starch preparation for MA2 gellan gum plates

10 grams of corn starch (Gift from Dr. Kan Tanaka) was suspended in 40 mL of distilled water. The mixture was then vortexed until the corn starch was completely suspended. After suspension, the slurry was centrifuged at 3,000 rpm for 2 minutes at 4°C and supernatant was decanted. The corn starch pellet was then washed in 40 mL 100% ethanol and subsequently vortexed and centrifuged as above. The final washed starch pellet was then fully resuspended in 75%

ethanol up to 50 mL where it could be stored at 4°C with the cap sealed with parafilm to prevent evaporation for up to 6 months.

2.4.5 Spotting corn starch on MA2 gellan gum plates

Aliquot 1 mL of prepared corn starch in 1.5 mL reaction tubes then centrifuge at 1,500 rpm for 1 minute at 4°C and decant supernatant afterwards. Add up to 1 mL 10x Solution I (see table 2.1) and resuspend starch pellet to wash starch. After resuspension, centrifuge starch as above and wash two more times with MA2 medium. On the final wash, add up to 1 mL MA2 medium and resuspend washed starch pellet. Place corn starch spotting template (**Figure 2-3**) underneath the MA2 gellan gum plate and use to guide 15 μL spots of corn starch to plate using a cut pipet tip. Keep corn starch solution resuspended while spotting. Dry for 10-15 minutes in a sterile environment at room temperature. Plates were either used immediately or stored at 4 °C for 24-48 hours, in which plates had to be warmed and dried for 30 minutes prior to use.

2.4.6 PEG4000 solution for polyethylene glycol (PEG)-mediated transformation

30 minutes prior to transformation, Solution I (100 μL, 10x of MA2 medium) and distilled water (300 μL) are added to 600 mg of PEG 4000 (Sigma Aldrich, 81240). PEG 4000 was dissolved at 65 °C for 10-15 minutes and kept at 65 °C until use.

2.5 Gene-targeted knockout procedure of CMT547C (GWD) and CMT465C (laforin)

2.5.1 Generation of linear DNA knockout fragments

Targeted knockout of *gwd* and *laforin* was performed as described by (33) and (197) with the following alterations. The GWD knockout linear DNA was generated in steps. All primer sequences used for the production and validation of gene-targeted knockouts are listed in **Table 2-2.** First, a DNA fragment containing the *URA5.3* gene was generated that contains 897-bp upstream of *URA5.3* and a 484-bp downstream of *URA5.3*. This sequence was amplified using primers URA_-897F: 5'-GAACTGAGGGGCGAACGCAGTC-3'   and   URA_1873R: 5'-

GTCGCGCCACAATCCCTAGCAGC-3' and *C. merolae* 10D genomic DNA as template. Second, the fragments corresponding to ~2 kb of sequence upstream of CMT547C and CMT465C were amplified from the template *C. merolae* 10D genomic DNA by PCR with the following primer sets A and B'. The ~2 kb of sequence downstream of CMT547C and CMT465C were amplified by PCR with the following primer sets C' and D. Primers B' and C' contained 5' complementary sequences (underlined in table 2.2) to primers URA_-897F and URA_1873R used to amplify the *URA5.3* gene present in the WT strain, respectively. These complementary sequences allowed for all three linear DNA fragments (upstream CMT547C/CMT465C DNA, *URA5.3*, and downstream CMT547C/CMT465C DNA) to anneal together essentially by the flanking arm fragments acting as their own primers during PCR overlap extension. The resultant ~6.7 kb linear DNA fragment comprised of the CMT547C/CMT465C upstream region + the *URA5.3* selection marker + the CMT547C/CMT465C downstream region was amplified using primers A and D to generate the >10 μg of DNA needed for transformation. PCR reactions were performed using Q5 High-Fidelity polymerase (NEB). Linear DNA was isolated by gel electrophoresis and subsequently purified using a NucleoSpin Gel and PCR Clean-up Kit (Macherey-Nagel).

2.5.2 Production and validation of genetic knockout lines

Δgwd and $\Delta laforin$ lines were generated as described in (197) with some modifications. Wildtype *C. merolae* 10D cells were maintained in 2x Modified Allen's (MA2) medium (28) at OD_{750} ~1.5 and used as nurse cells to aid in the production of stable transformants. The uracil-auxotrophic T1-strain was used as the host for the production of stable transformants. T1-strain was maintained in MA2 medium supplemented with uracil (0.5 mg/mL) and 5-FOA (0.8 mg/mL). 50 mL T1 cultures were grown to OD_{750} ~0.7 and pelleted by centrifugation at 1000 rpm for 5 minutes after the addition of 0.001% Tween-20 (Sigma-Aldrich P1379). The T1 cells were transformed with a transformation cocktail consisting of PEG4000, 10x Solution I (196), 10 μg of the knockout linear DNA, and 550 μg of carrier DNA (salmon sperm ssDNA, Sigma D7656). T1 transformants were grown

in 40 mL MA2 medium supplemented with uracil (0.5 mg/mL) for 24 hours at 42 °C under continuous light (50 μmol m^{-2} sec^{-1}) with 2% ambient CO_2. After 24 hours, the cells were harvested by centrifugation (1000 rpm for 5 minutes) and the cells were washed twice with plain MA2 medium to wash out the remaining uracil. The transformants were subsequently transferred to corn starch-spotted MA2 gellan gum plates lacking uracil and incubated at 42 °C under continuous light (50 μmol m^{-2} sec^{-1}) in a double-zip AnaeroPouch bag (R686010) with an AnaeroPouch-CO_2 (R682007) (Mitsubishi, ThermoFisher Scientific). Independent clones were isolated after one month and expanded for analysis. Independent lines were screened by PCR using primers GWD_1733F and GWD_2321R producing a 588 bp fragment if GWD was present. For laforin, isolated colonies were screened using primers LAF_864F and LAF_432R producing a 432 bp fragment. To determine if the linear KO construct was incorporated into the T1-host genome, lines were analyzed by PCR using primers GWD_valF and GWD_valR (LAF_valF and LAF_valR) that amplifies the junction of the upstream homologous region of CMT547C/CMT465C and the beginning portion of the *URA5.3* selection marker producing a 276/283 bp fragment, respectively (**Table 2-2**).

2.5.3 Immunoblot analyses of genetic knockout lines

A rabbit anti-*Cm*GWD polyclonal primary antibody was generated by Cocalico Biologicals Inc. Rabbits were immunized with recombinant *Cm*GWD protein corresponding to amino acids 511-4716. The post-boost serum was subjected to antibody purification using a HiTrap NHS-Activated Affinity Column (GE Healthcare) conjugated to *Cm*GWD 511-4716 antigen. The antigen buffer was exchanged into 1 mL coupling buffer (0.2 M $NaHCO_3$, 0.5 M NaCl pH 8.3) at 10 mg/mL. The antigen solution was slowly added to the column and incubated for 4 hours at 4°C. The column was then washed and deactivated through a series of Buffer A (0.5 M ethanolamine, 0.5 M NaCl pH 8.3) and Buffer B (0.1 M Acetate, 0.5 M NaCl pH 4) injections then neutralized with 10 mM Tris pH 7.5. The pH of the column was continuously checked until the pH was ~7.5. The post-boost serum (5 mL, UKY137) was prepared by a brief centrifugation (4,000 rpm for 10 minutes

at 4°C), the supernatant passed through a 0.45 micron filter, and buffer exchanged into 10 mM Tris pH 7.5. The prepared serum was passed through the column three times at 0.3 mL/minute and the antibodies were eluted with an acid fraction, 100 mM glycine pH 2.5 directly into tubes containing 1M Tris pH 8.0 which were then dialyzed against PBS containing 0.2% sodium azide and concentrated to 0.9 mg/mL. The acid fraction was tested against recombinant CmGWD protein.

To immunoblot for endogenous GWD, 2 mL cell cultures of OD_{750}=1.0 were pelleted by centrifugation (3,000 x g for 5 min at 4°C), cell pellets were re-suspended in 1x SDS-loading buffer (50 mM Tris-HCl pH 6.8, 2% SDS, 10% glycerol, 1% β-mercaptoethanol, 12.5 mM EDTA, and 0.02% bromophenol blue), cell lysates were vortexed with a gene disrupter (3 min at 3,000 rpm), and subsequently heated at 95°C for 30 min. Equal volumes were loaded per well in a Mini-PROTEAN TGX stain-free gel (BioRad) and imaged with an ImageDoc Imager (BioRad) for protein load. The gel was then transferred to a PVDF membrane with a TurboBlot system (BioRad). The membrane was probed with the rabbit polyclonal CmGWD primary antibody (1:2000) and then a goat-anti rabbit secondary (Thermo Scientific 65-6120, 1:5000). Immunoblotting for endogenous laforin was performed similarly to CmGWD using a previously developed α-Cm-laforin antibody (185). Images were taken by a ChemiDoc BioRad imager.

2.5.4 *C. merolae* immunofluorescence

For immunofluorescence, cells were fixed, washed and blocked as previously described (185, 198). Briefly, cells were centrifuged for 5 minutes at 800 x g, then pre-fixed in a low salt (10 mM) phosphate buffer (pH 7.5), 30 mM NaCl, 0.5 mM KCl, and 2% (w/v) paraformaldehyde for 5 minutes. Following centrifugation at 2,000 x g for 3 minutes, cells were resuspended with the same pre-fixation buffer at a 1:1 ratio to cell pellet. The cells were fixed by addition of 20 volumes of chilled 85% (v/v) methanol, 15% (v/v) DMSO, 2% (w/v) paraformaldehyde, 1.5 mM NaOH solution for 5 minutes at -20 °C. The fixed cells were washed with methanol and rehydrated and stored in PBS. Cells were blocked in 5% BSA in PBS at room temperature for 15-30 minutes then washed with 0.1% BSA in PBS before

incubation with primary antibody. Cells were probed with 1:1000 α-*Cm*GWD or α-*Cm*laforin polyclonal rabbit antibodies previously described (section 2.5.3 and (185)) followed by 1:1000 AlexaFluor488 goat α-rabbit secondary antibody (Invitrogen). Chloroplasts were visualized by their autofluorescence and immunofluorescence was visualized with a Nikon Eclipse E600 and AxioCam MRm or Zeiss 512 camera at 100x.

2.6 *C. merolae* strains and growth conditions

All cell culture growth and experiments were performed in a CARON Plant Growth Chamber (Model: 7300-22) equipped with a Thermo Scientific MaxQ 2000 CO2-resistant shaker. Cyanidioschyzon merolae 10D was grown in foam-stop Erlenmeyer flasks in 2x Modified Allen's (MA2) medium (196) under ambient 2% CO2 at 42 °C under continuous white light (50 μmol m-2 sec-1) while agitated at 130 rpm (26). Nitrogen deprivation media (-Nitrogen) replaced ammonium sulfate ($(NH_4)_2SO_4$) of MA2 medium with sodium sulfate (Na_2SO_4). For diurnal growth conditions, C. merolae cells were subjected to cycles of 12 hours light (50 μmol m-2 sec-1) /12 hours dark. The URA5.3 deletion strain T1 was used as the parental strain (33). The T1 strain was grown in MA2 medium supplemented with uracil (0.5 mg mL-1) and 5-FOA (0.8 mg mL-1) as described (33).

2.6.1 Prolonged dark stress experiment (Light deprivation)

Cells were cultured in diurnal growth conditions and diluted to OD_{750} ~1.0 in fresh MA2 medium. The cultures were grown for 48 hours under diurnal growth and subjected to continuous dark for 16 days while under ambient 2% CO_2 at 42°C and agitated at 150 rpm. At the end of 16 days, cultures were washed with fresh MA2 medium once, resuspended in identical volumes, and reintroduced to a diurnal light regime for 6 days. Samples were taken at the time points shown in Figure 6 and diluted 1:10 with MA2 medium. Absorption spectrums from 300 nm to 750 nm were quantified using a BioTek EPOCH2 microplate reader and blanked to MA2 medium. All experimental values were the mean ± SD of three lines of WT and Δgwd.

2.7   *C. merolae* glucan extraction and characterization

2.7.1   *C. merolae* glucan extraction and purification

Polyglucans from *C. merolae* cells was extracted as described previously (73) with the following modifications. *C. merolae* cells were pelleted by centrifugation at 4,000 rpm for 15 minutes. The cell pellet was resuspended in starch extraction buffer (10 mM Tris-HCl (pH 8.0) and 10 mM EDTA). The cell suspension was then lysed by sonication 10 times for 5 seconds with an inversion step midway through. The cell extract was centrifuged at 10,000 x g for 20 minutes at 4°C. The insoluble material was resuspended in polyglucan extraction buffer and layered on a 80% percoll density cushion (GE Healthcare), followed by centrifugation at 10,000 x g for 20 minutes at 4°C. The final insoluble polyglucan pellet was washed several times with HPLC-grade water to eliminate percoll remnants and stored at 4 °C in 20% ethanol (**Figure 2-5**).

2.7.2   Amyloglucosidase-dependent Starch Quantification

A 5-10 mL culture of each WT and Δ*gwd* line were pelleted and sonicated 10 times for 5 seconds with an inversion step midway through. Then the sonicated portion was divided into two fractions, amyloglucosidase (AG)-treated and non-treated. 4 μL of amyloglucosidase (5U/μL) from *Aspergillus niger* (Sigma) or buffer was added to corresponding fractions and incubated for 16 hours at 37°C while rotating. Following the incubation, fractions were centrifuged at 4,000 x g for 10 minutes and the supernatants were diluted with two parts water. Equal volumes were used for glucose determination according to the R Biopharm Inc. D-Glucose Kit (Fisher). The absorbance at 340nm of the NADPH product (stoichiometric to glucose) was measured and starch was quantified based on standard curves using glucose standards.

2.7.3   Fluorescence-Assisted Capillary Electrophoresis (FACE)

Identification and quantification of glucose and phosphoglucose moieties via fluorescence-assisted capillary electrophoresis (FACE) was performed as described previously (**Figure 2-4**) (93, 199). For chain length distribution analysis,

native granules were solubilized briefly with NaOH (125 mM final concentration) at 98°C for 10 minutes with occasional inversion. Once solubilized granules cooled to room temperature, the reaction was neutralized with glacial acetic acid and adjusted to optimal pH with 90 mM sodium acetate pH 4.5. Samples were debranched with 5U of High Purity *Pseudomonas sp.* isoamylase (ISA, Megazyme) for 2 hours at 37°C then ISA was deactivated by boiling at 98°C for 10 minutes. After a brief centrifugation at 12,000 x g, 50 μL and 100 μL aliquots were dried in a SpeedVac (Thermo). Dried debranched samples were derived and fluorescently labeled as in Verbeke et al. 2016 (93). Samples were analyzed using an Agilent CE7100 equipped with a Picometrics Zetalif LED-induced fluorescence detector.

2.7.4 Phosphate Content via Gas Chromatography Mass Spectrometry (GCMS)

Equal amounts of purified polyglucans from cells was mildly acid-hydrolyzed with 2M TFA for 2 hours at 98°C and brought to room temperature before neutralization. The reaction was neutralized with a final concentration of 50% MeOH with 100 μM L-norvaline (standard) and dried in a SpeedVac (Thermo). The samples were derivatized by the sequential addition of 20 mg/ml methoxylamine hydrochloride in pyridine, and then N-methyl-trimethylsilyl-trifluoroacetamide (MSTFA). GCMS settings were as reported in (200, 201).

2.7.5 Phosphate content by ^{31}P-NMR

2.7.5.1 Preparation of phosphoglucans from *C. merolae* polyglucan

All NMR preparations and spectrometry were performed by Dr. Felix Nitschke and colleagues at The Hospital for Sick Children in Toronto, Canada. Extracted native granules from *C. merolae* (approximately 180 mg WT starch or 140 mg Δ*gwd* starch) were repeatedly washed with 0.05% sodium azide at room temperature to reduce phosphate that is not covalently linked to glucosyl residues of the starch. Between wash steps, orthophosphate was monitored in the supernatant after the starch was pelleted by centrifugation. Orthophosphate was

determined using the PiColorLock™ Gold Phosphate Detection System (Innova Biosciences) according to manufacturer's instructions. Phosphoglucans were prepared as previously described (202). The purified polyglucan was solubilized applying the following temperature program: 5 minutes at 55 °C, T-gradient to 95 °C in 8 minutes, 10 minutes at 95 °C, and gradual cooling to 55 °C in the presence of a mixture of α-amylase (Roche, pig pancreas) and amyloglucosidase (Megazyme; 20 mg granular starch and 50 U of each enzyme per mL in 50 mM NH_4OAc buffer [pH 6.0]). Again, α-amylase and amyloglucosidase (each 2.5 U per mg starch) are added, followed by 2 hour incubation at 55 °C. Starch digestion was stopped by 10 minute heating at 95 °C prior to cooling on ice. After centrifugation (16,000 x g, 4 °C, 15 minutes) an aliquot of the supernatant (designated 'DIG') was taken for later analysis and the rest passed through a 10 kDa ultrafilter (regenerated cellulose membrane, Millipore). An aliquot of the filtrate (designated '<10kDa') was taken and the remainder subjected to anion exchange chromatography on a 8 mL QFF sepharose (GE Healthcare) column, which was previously washed with 50 mL 1 M ammonium acetate (NH_4OAc, pH 7.0) and equilibrated with 100 mL water. Fractions were collected (designation in parenthesis) during 1) sample application (flow-through, 'FT'), 2) washing with 50 mL water ('W1' and 'W2' each 25 mL), 3) elution with 40 mL 0.2 M NH_4OAc ('E200'), and 4) elution with 60 mL 1 M NH_4OAc ('E1000-1', 'E1000-2', 'E1000-3', each 20 mL). Fractions were lyophilized, dissolved in water, and subjected to further analyses, such as determination of glucosyl residues, total phosphate, free phosphate, and C6 phosphate. Fractions E200, E1000-1, E1000-2, E1000-3 of WT and mutant starch were combined, lyophilized again, dissolved in D_2O, and subjected to NMR analyses.

2.7.5.2 NMR Spectroscopy

All NMR measurements were acquired on a Bruker AV-III 600 MHz spectrometers at 300 K using 5mm sample tubes and D_2O as solvent. All experiments were performed using a ($^1H, ^{13}C, ^{15}N, ^{31}P$)-QCI cryoprobe equipped with a one-axis self-shielding gradient.

C. merolae WT phosphoglucans - The sample had a concentration of 2 mM total phosphate. An ^{31}P-1D spectrum was recoded using continuous proton decoupling, an acquisition time of 1.3 sec, 16384* points and a relaxation delay of 1.3 sec using 24000 scans. The multiplicity-edited HSQC was recorded with 512* x 1024* points, 64 scans, $t_{2,max}$ = 51.3 msec and $t_{1,max}$ = 194.5 msec; the ^{31}P-edited HSQC was recorded with 512* x 1024* points, 256 scans, $t_{2,max}$ = 51.3 msec and $t_{1,max}$ = 194.5 msec; the ^{31}P-edited HSQC with ^{31}P chemical shift evolution was recorded with 512* x 256* points, 1024 scans, $t_{2,max}$ = 51.3 msec and $t_{1,max}$ = 43.5 msec; the ^{31}P-HMBC HSQC was recorded with 2048* x 256* points, 32 scans, $t_{2,max}$ = 204.8 msec and $t_{1,max}$ = 25.6 msec. ^{31}P-1D spectra of phosphoglucans from WT *C. merolae* were also recorded after the addition of 10uL reference compounds (sodium hydrogen phosphate, sodium pyrophosphate, sodium polyphosphate (Merck-Millipore Cat# 1065291000), all in D_2O at 70 mM total phosphate). After each addition, a 1D spectrum was recorded with continuous proton decoupling, an acquisition time of either 819.2 or 655.4 msec, either 8192* or 16384* points and a relaxation delay of 1.3 sec using 1536 scans.

C. merolae △gwd phosphoglucans - The sample had a concentration of 0.24 mM total phosphate. An ^{31}P-1D spectrum was recoded using continuous proton decoupling, an acquisition time of 655 msec, 16384* points and a relaxation delay of 1.3 sec using 40960 scans. The multiplicity-edited HSQC was recorded with 512* x 1024* points, 128 scans, $t_{2,max}$ = 51.3 msec and $t_{1,max}$ = 194.5 msec; the ^{31}P-edited HSQC was recorded with 512* x 256* points, 1024 scans, $t_{2,max}$ = 51.3 msec and $t_{1,max}$ = 48.6 msec; the ^{31}P-edited HSQC with ^{31}P chemical shift evolution was recorded with 512* x 256* points, 1024 scans, $t_{2,max}$ = 51.3 msec and $t_{1,max}$ = 25.6 msec; the ^{31}P-HMBC HSQC was recorded with 2048* x 256* points, 128 scans, $t_{2,max}$ = 204.8 msec and $t_{1,max}$ = 25.6 msec.

All were processed using topspin 3.2 (Bruker Biospin) The 2D spectra were processed using squared sinebell window functions in both dimension resulting in a 4096 by 2048 data matrix. The 1D spectra were processed using line broadening of 1 Hz and zerofilling up to 131072 points.

2.7.5.3 Quantification of total phosphate, free phosphate, and C6-phosphate

For determination of C6-phosphate, aliquots of fractions obtained during anion exchange chromatography were subjected to quantification of glucose and glucose 6-phosphate after acid hydrolysis as previously described (203). Total phosphate in these fractions was determined as orthophosphate subsequent to incubation with Antarctic phosphatase (final volume of 65 uL, 2.5 U Antarctic phosphatase (NEB), 50 mM bis–Tris–propane pH 6.0, 1 mM $MgCl_2$, and 0.1 mM $ZnCl_2$, 17 hours at 37 °C). Orthophosphate was determined using the PiColorLock™ Gold Phosphate Detection System (Innova Biosciences) according to manufacturer's instructions against authentic sodium phosphate. Fraction aliquots used for the quantification of free inorganic phosphate were treated alongside but Antarctic phosphatase was omitted and the mixtures were kept at -20 instead of 37 °C to conserve labile phosphate esters.

2.7.6 Scanning Electron Microscopy (SEM)

Cells are collected by centrifugation (10 min at 500 rcf) and then fixed on a copper grid with lacey carbon (300 mesh, Ted Pella 01895-F) with 1% glutaraldehyde in 20 mM sodium cacodylate (pH 7.2) for 2 h at room temperature. Samples were washed with 1x PBS (pH 7.2) for 20 minutes, three times, and then dehydrated in a graded ethanol series. They were then dried to the critical point, mounted, and then sputter coated with gold and platinum. The samples were examined by using a FEI Quanta 250 field emission scanning electron microscope.

Granules were isolated as described above and prepared in water suspensions for Dr. Jean-Luc Putaux. The drops of dilute granule suspensions were allowed to dry on metal stubs covered with carbon tape. The dried specimens were coated with Au/Pd in a Baltec MED-020 sputter coater and observed in secondary electron mode on a Thermo Scientific Quanta 250 microscope equipped with a field emission gun and operating at 2.5 kV.

2.7.7 Transmission electron microscopy (TEM)

C. merolae cells were centrifuged briefly at 500 rcf and then gently resuspended in TEM fixative (1% para-formaldehyde, and 2.5% glutaraldehyde in 0.1 M sodium cacodylate pH 7.4) and incubated at room temperature for 1 hour. The cells are then washed with fresh TEM fixative, post-fixed with osmium tetroxide and embedded in Epon resin. Ultrathin sections (~70 nm) were cut with a diamond knife in a Leica UC6 microtome and post-stained with periodic acid thiosemicarbazide silver proteinate (PATAg) (204).

Samples were immersed in modified Karnovsky's fixative (2.5% glutaraldehyde and 1% paraformaldehyde in 0.1 M sodium cacodylate buffer, pH 7.4) for 1 hour at room temperature. Cells were stored at 4 °C until shipment to Dr. Timothy Meerloo and colleague Ying Jones. Cells were postfixed in 1% osmium tetroxide in 0.15 M cacodylate buffer for 1 hour and stained en bloc in 2% uranyl acetate for 1 hour. Samples were dehydrated in ethanol, embedded in Durcupan epoxy resin (Sigma-Aldrich), sectioned at 50 to 60 nm on a Leica UCT ultramicrotome, and picked up on Formvar and carbon-coated copper grids. Sections were stained with 2% uranyl acetate for 5 minutes and Sato's lead stain for 1 minute. Grids were viewed using a JEOL 1200EX II (JEOL, Peabody, MA) transmission electron microscope and photographed using a Gatan digital camera (Gatan, Pleasanton, CA), or viewed using a Tecnai G^2 Spirit BioTWIN transmission electron microscope equipped with an Eagle 4k HS digital camera (FEI, Hilsboro, OR).

Native polyglucan granules were washed several times with water and droplets of granule suspensions were deposited onto carbon-coated copper grids freshly glow-discharged in a Pelco easiGlow station. After blotting the excess liquid, the preparations were negatively stained with 2 wt% uranyl acetate, allowed to dry and observed with a JEOL JEM 2100-Plus TEM operating at 200kV and images were recorded using a Gatan Rio 16 camera.

2.7.8 TEM analyses

Transmission electron micrographs of starch granules from continuous and diurnal light regimens were analyzed with ImageJ software

(http://imagej.nih.gov/ij). Measurements were converted from pixels to nm using the 'set scale' function based on scale bars provided. Measurements were then analyzed and graphed using GraphPad Prism8 software, histogram and Tukey box and whisker methods.

Table 2-1 Preparation of *C. merolae* growth media
2x Modified Allen's (MA2) autotrophic media for the growth and maintenance of C. merolae. List of components were adopted from Kobayashi et al. 2010 (196).

	Components	Amount	Concentration	Final Conc. in MA2
Solution I (10x)	$(NH_4)_2SO_4$ *	52.9 g	400 mM	40 mM
	$MgSO_4 \bullet 7H_2O$	10.0 g	40 mM	4 mM
	A6 minor salts (500x)	40 mL	20x	2x
	H_2SO_4	3 mL	-	-
Add water to a final volume of 1000 mL				
*For Nitrogen Deprivation, replace $(NH_4)_2SO_4$ with Na_2SO_4 (20-40 mM)				
Solution II (100x)	KH_2PO_4	10.88 g	800 mM	8 mM
Add water to a final volume of 100 mL				
Solution III (1000x)	$CaCl_2$	14.7 g	1 M	1 mM
Add water to a final volume of 1000 mL				
Solution IV (250x)	$FeCl_3$	0.4 g	25 mM	0.1 mM
	Na_2EDTA	0.7 g	20 mM	0.08 mM
Add water to a final volume of 1000 mL				
Solution IV should be sterilized by filtration with a 0.22 μm filter				
A6 minor salts (500x)	H_3BO_3	2.85 g	46 mM	92 μM
	$MnCl_2 \bullet 4H_2O$	1.8 g	9 mM	18 μM
	$ZnCl_2$	0.105 g	0.77 mM	1.54 μM
	$Na_2MoO_4 \bullet 2H_2O$	0.39 g	1.6 mM	3.2 μM
	$CoCl_2 \bullet 6H_2O$	0.04 g	0.17 mM	0.34 μM
	$CuCl_2$	0.043 g	0.3 mM	0.6 μM
Add water to a final volume of 1000 mL				

Table 2-2 List of gene-targeted knockout and validation primers

Primer Name	Sequence (5' to 3')
*Cm*GWD A	CCGAATTCACTGCTCTGCATGTAACGATAGGG
*Cm*GWD B'	GACTGCGTTCGCCCCTCAGTTCGGAAAACGCTTGACGGTAGCGTGCGAA
*Cm*GWD C'	GCTGCTAGGGATTGTGGCGCGACCGGTCGTTGAATGCGAAGAATTTAAAGTCTGGG
*Cm*GWD D	TAGGTAACGTCGTTCTGAACCACCCAAGGG
*Cm*laforin A	GCAACAACGCCAAACCTATATGATGTGTTGGCAC
*Cm*laforin B'	GACTGCGTTCGCCCCTCAGTTCGCCCAGGTATTACTCCAGTGCGAGATAATGAGG
*Cm*laforin C'	GCTGCTAGGGATTGTGGCGCGACGCGCACAAACCTATATCGGATAGCGATGGTACC
*Cm*laforin D	CCCAGAGACCGGGGTTTGGATTGCTT
GWD_1733F	ACCGCTTCGAAAACAAAGCC
GWD_2321R	ACCGCTTCGAAAACAAAGCC
LAF_864F	GCCAGTGACACAGAGATGCT
LAF_432R	TTCAGACATTGCGGACACGA
GWD_valF	CGCTACCGTCAAGCGTTTTC
GWD_valR	CAGATACACGGTACGCGGAA
LAF_valF	CCTGATTCGGCAGTGACTGT
LAF_valR	CGGATCTTTCCAAGCGCATG
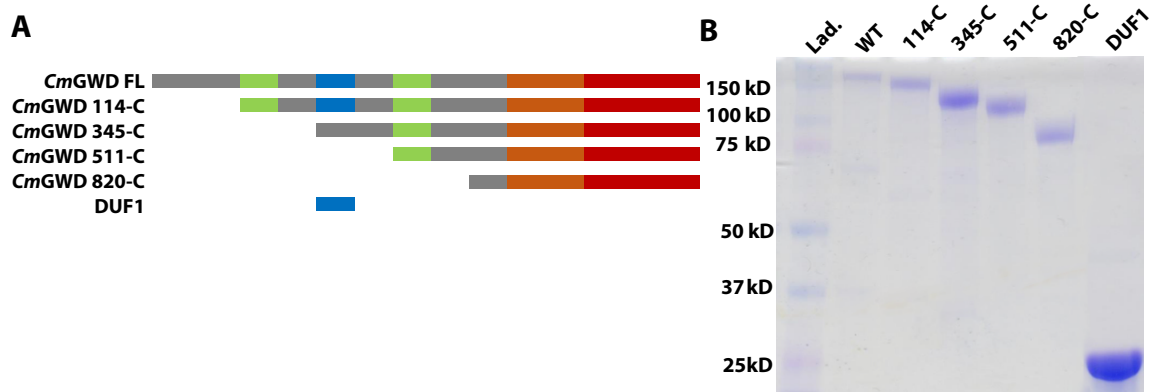
Figure 2-1 Truncated constructs and isolated domains of *Cm*GWD
A) Several truncated constructs were synthesized by Genscript based on bioinformatic analyses identifying regions of disorder and domain boundaries. **B)** Purified recombinant protein visualized via SDS-PAGE. All proteins were >80% pure.
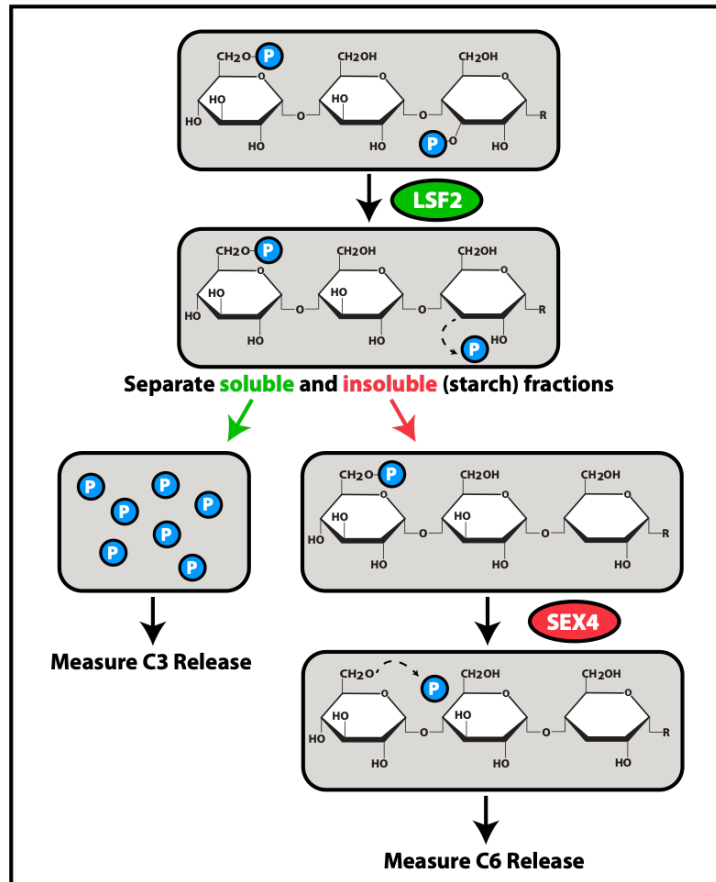
Figure 2-2 Indirect site specificity glucan dikinase assay
Site-specific dephosphorylation was carried out by the glucan phosphatases LSF2 and SEX4. For each phosphatase reaction, 0.6 mg of dikinase treated *sex1-3* starch was incubated with 150 ng glucan phosphatase protein. The reaction was first carried out with recombinant *At*LSF2 for 15 min at room temperature with constant mild vortexing and terminated by the addition of 10% SDS. LSF2 exclusively dephosphorylates the C3-position of glucose moieties therefore LSF2 will remove all of the C3-phoshate before the starch is dephosphorylated with SEX4. The reaction was centrifuged and the released radiolabel in the supernatant was quantified by a Packard 1900 TR scintillation analyzer. Following two washes, the starch was then incubated similarly with recombinant *At*SEX4 for 15 min at room temperature. The reaction was terminated by the addition of 10% SDS and the reaction was centrifuged to separate released radiolabeled phosphate. Although SEX4 preferentially dephosphorylates C6-phosphate, SEX4 has the ability to remove C3-phosphate as well. With the C3-phosphate removed already by LSF2, the phosphate released by SEX4 should all be from the C6-position. The reaction was centrifuged for 5 minutes at max speed and the released radiolabel in the supernatant was quantified by a Packard 1900 TR scintillation analyzer.

Figure 2-3 Corn starch spotting template
White spots are for transformed T1 cells. Black spots are for wild-type *C. merolae* nurse cells.
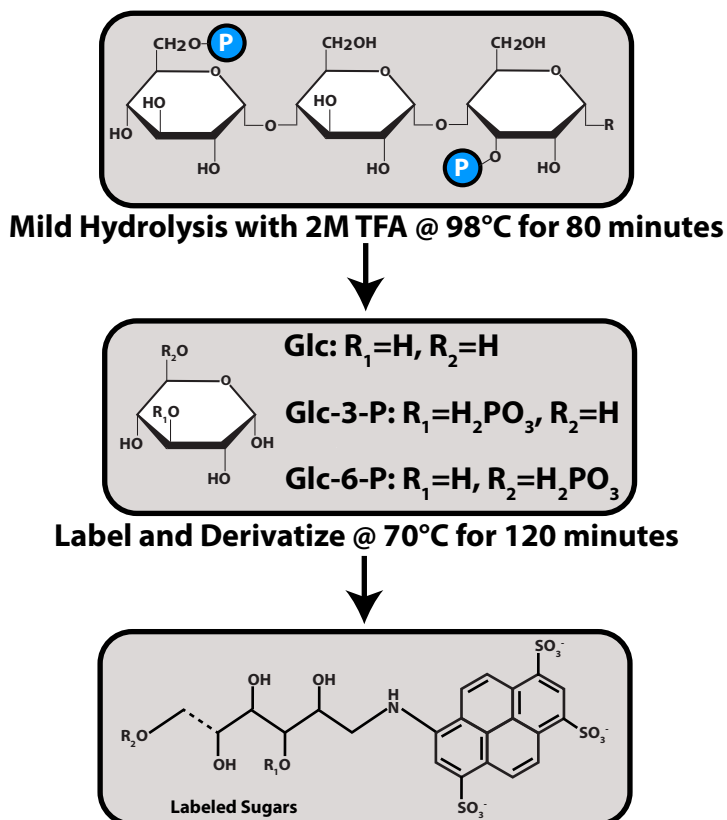
Figure 2-4 Fluorescence-Assisted Capillary Electrophoresis flowchart
Starch was mildly hydrolyzed with trifluoroactetic acid (TFA) to minimize release of phosphates. The remaining glucosyl moieties were then derivatized by reductive amination with the charged fluorophore 8-aminopyrene-1,3,6-trisulfonic acid (APTS). This method facilitates the separation of glucosyl moieties as well as offering high sensitivity. Flowchart adopted from Verbeke et al. 2016 (93).

Pellet C. merolae Culture @ OD$_{750}$ ~ 7.5 to 10

↓

Homogenization

↓

Lyse by Sonication

↓

Percoll Gradient Centrifugation

↓

Collect Starch Pellet

↓

Wash Starch Pellet

↓

Enzymatic Determination of Starch Yield
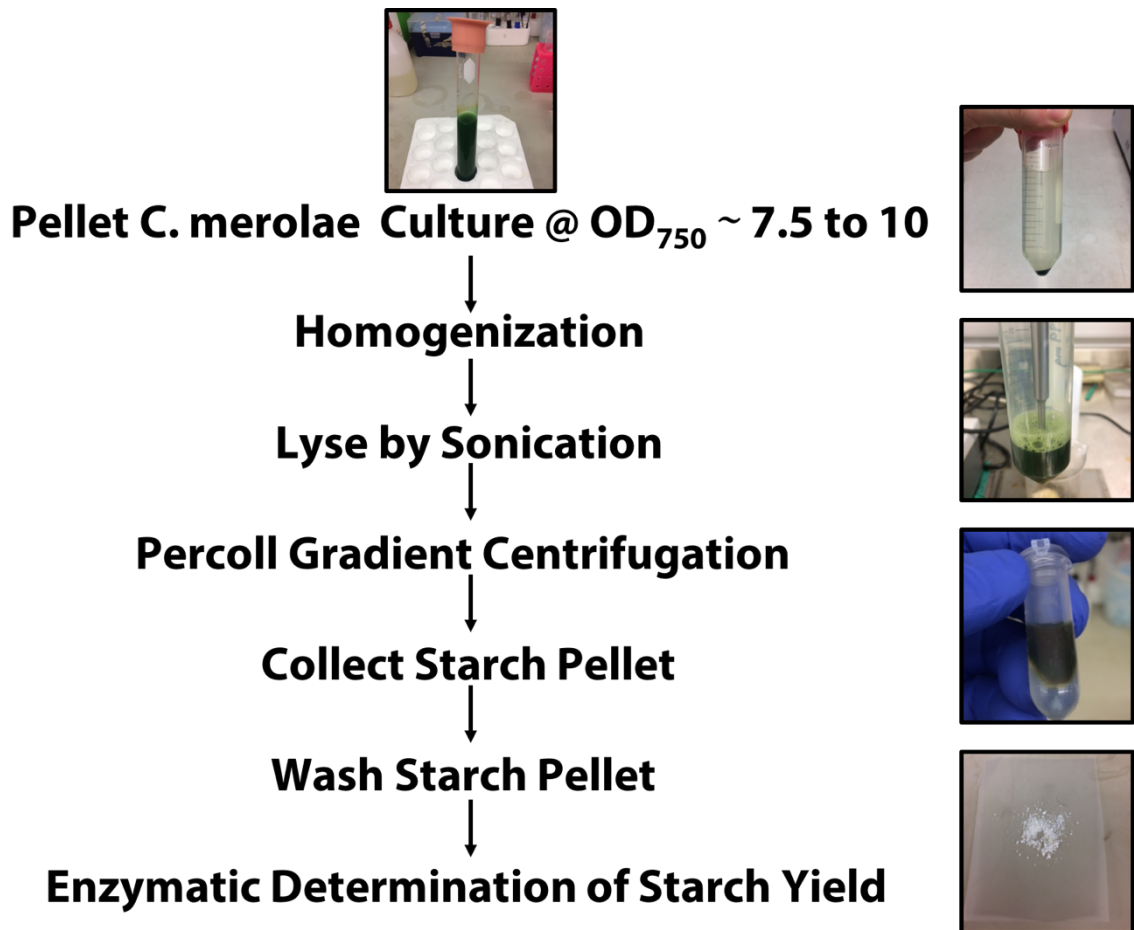
Figure 2-5 *C. merolae* starch extraction flowchart
C. merolae cultures were grown to a sufficient optical density where the cells were then collected and pelleted by centrifugation. The cell pellet was resuspended and homogenized in a mild tris-based extraction buffer as described in Hirabaru et al. 2010 (73). The cells were then lysed by sonication prior to separation of soluble and insoluble material. The insoluble starch fraction was then resuspended in extraction buffer and the starch was purified over a Percoll gradient. After centrifugation, the starch pellet was washed and quantified via a enzymatic glucose assay.

CHAPTER 3. α-GLUCAN, WATER DIKINASE IS REQUIRED FOR NORMAL FLORIDEAN STARCH METABOLISM AND MORPHOLOGY IN THE RED ALGA, *CYANIDIOSCHYZON MEROLAE*

3.1 Introduction

Photosynthetic organisms generate starch during the day as their primary glucose cache and source of carbon (energy) for the subsequent period of darkness to maintain their growth and metabolism. At the onset of darkness, reversible glucan phosphorylation plays a key role in efficient starch degradation and ensuing utilization (68, 95), and recent reports describe an emerging role for this process in starch synthesis (160, 162, 179, 205). Glucan dikinases are the enzymes responsible for initiation of reversible glucan phosphorylation, and subsequently degradation, by phosphorylating the outer edges of the starch granules.

The genes encoding glucan dikinases were first identified in 1991 by the Preiss and Somerville labs when they employed an *Arabidopsis* mutant screen to identify gene losses that were responsible for Starch EXcess (*sex*) phenotypes (124). In 1998, the Kossmann lab cloned the gene of a starch-bound protein named R1 (later named **G**lucan, **W**ater **D**ikinase, GWD) and revealed that reduced R1 levels in potato resulted in decreased starch phosphorylation (144). GWD from potato is comprised of a N-terminal chloroplast targeting peptide (cTP), tandem carbohydrate binding modules (CBMs) of family 45 (CBM45), and a C-terminal catalytic domain exhibiting similarities to bacterial pyruvate, water dikinase (PPS; EC 2.7.9.2) and pyruvate, phosphate dikinase (PPDK; EC 2.7.9.1) (156, 206). Although the catalytic domain is termed PPDK, it is made up of two subdomains, the nucleotide-binding domain (NBD) and a phospho-histidine domain (HIS) (**Figure 3-1**). It is now well known that the majority of higher plant genomes encode for three isoforms of GWD: glucan, water dikinase (GWD1, EC 2.7.9.4) and phosphoglucan, water dikinase (GWD3/PWD, EC 2.7.9.5) are localized to the chloroplast; while GWD2 is localized to the cytoplasm (143, 148, 207). GWD and PWD catalyze the formation of starch phosphate esters at the C6- and C3-

positions of glucose, respectively (90). Once GWD phosphorylates the C6-position, then PWD can phosphorylate the C3-position (146). Glucan dikinases follow a unique catalytic mechanism using ATP, bound by the NBD, as a dual phosphate donor. The glucan dikinases simultaneously transfer the γ-phosphate to water yielding orthophosphate and AMP, while the β-phosphate is used to auto-phosphorylates the catalytic histidine residue in the HIS domain and is then transferred to a glucan substrate (78, 156, 206). PWD and GWD orthologs contain one or two N-terminal CBMs, respectively, which are known to interact with starch granule surfaces (146, 152). The PWD CBM is a CBM20 family member while the N-terminal GWD CBM is a CBM45 (78). This difference is one of the ways to identify a glucan dikinase as either GWD or PWD (78). Glucan dikinases are intriguingly conserved in Archaeplastida and their starch-like producing lineages; however, they are not found in glycogen-containing species such as vertebrates (165, 171).

Plant genomes also encode for two starch phosphatases that oppose the dikinases in the process of reversible phosphorylation: Starch Excess 4 (SEX4) preferentially dephosphorylates the C6-position and Like Sex Four2 (LSF2) exclusively dephosphorylates the C3-position (164, 175, 179, 181). Alternatively, mammals, which synthesize water-soluble glycogen, encode a single glucan phosphatase called laforin that dephosphorylates the C2-, C3-, and C6-positions (169).

The addition of phosphate by GWD to the branched and tightly-wound glucose chains in starch, known as amylopectin, is thought to lead to chain unwinding, and thus amylopectin solubilization (95). This process renders the glucose chains on the outer surface of starch more solvent accessible and accessible to degradation by the successive amylolytic actions of β-amylases and isoamylases. β-amylase releases maltose units until it encounters a more buried phosphate moiety that inhibits its activity and must be removed by a glucan phosphatase (164). Thus, a cyclic pattern emerges of starch phosphorylation, degradation, and dephosphorylation; and then the cycle can repeat successfully. Loss of function mutations in any of the *A. thaliana* genes encoding GWD1, PWD, or SEX4 result

in a starch excess phenotype (146, 150, 173, 192). Along with a starch excess phenotype, GWD mutant starch granules are often larger in size and more varied in size distribution as well as irregular in shape, as compared to wildtype granules (72, 161, 192). While much progress has been made defining this system in higher plants, the complexity and redundency of this system in higher plants is a hinderence to pinpointing the exact contribution of each enzyme to the process of starch metabolism.

The unicellular thermophilic red alga, *Cyanidioschyzon merolae* has been well-characterized both genetically and biologically (25, 208-212). *C. merolae* optimally grows at 42°C with a pH ranging 2-3 and has only one mitochondrion, one plastid, and one nucleus (26). Since its genome was completely sequenced, *C. merolae* has been widely utlilized in multiple comparative genomic studies regarding carbohydrate metabolism as well as studying mitochondrial, plastid, and nuclear division mechanisms (8, 22, 23, 26, 208, 209). *C. merolae* produces and stores floridean starch, a type of starch consisting of semi-amylopectin α-glucans with no amylose (linear glucose chain) content that is stored in the cytosol instead of in a plastid (73). The term "floridean" refers to an α-1,4 and α-1,6 glucan that resembles amylopectin produced outside of the plastid (49, 69). Several reports found that *C. merolae* possesses one of the lowest number of enzymes and enzyme isoforms involved in eukaryotic storage polysaccharide metabolism (69, 100). As such, we previously identified a single glucan phosphatase in the *C. merolae* genome (185) and hypothesized that *C. merolae* provides a uniquely simplified system to define the role of reversible glucan phosphorylation.

Utilizing bioinformatics, biochemical analyses, and cell biology, we demonstrate that *C. merolae* also contains a single glucan dikinase. The *C. merolae* glucan dikinase shares more domain similarity and overall amino acid conservation with GWD compared to PWD, and like GWD it phosphorylates the C6-position of glucose. Mutants lacking GWD (Δgwd) exhibit a dramatic loss of starch-bound glucose 6-phosphate and this phosphorylation loss impacted on both synthesis and degradation of the floridean starch. Additionally, Δgwd floridean starch granules have an aberrant chain-length distribution profile and drastically

altered granule morphologies compared to wild-type. Lastly, under prolonged light deprivation Δ*gwd* cells rapidly deplete major carbon and nitrogen reserves such as photosynthetic pigments (phycocyanin and chlorophyll α) and floridean starch as a stress response. Consequently, Δ*gwd* cells are unable to recover from extended dark stress after losing the light harvesting complexes and carbon reserves, which is unlike their wild-type cells. Ultimately, these deficiencies lead to catastrophic cell death as opposed to cellular quiescence-like states observed in wild-type cells.

3.2 Results

3.2.1 A putative *C. merolae* glucan, water dikinase

Using the GWD1 sequence from *S. tuberosum* (*St*GWD) (144), we searched the *C. merolae* genome to identify a putative glucan kinase. We performed a BLASTp (213) search using *St*GWD in the *Cyanidioschyzon merolae* Genome Project database (czon.jp). This analysis yielded one putative homologue, XP_005539443.1/CMT547C as well as another partial hit, XP_005535692.1/CMF012C (**Figure 3-2A**). Further investigation revealed that the partial hit with CMF012C only shared homology with 200 amino acids of *St*GWD. This partial hit was of the protein family (Pfam), *PPDK_N,* which was the N-terminal AMP/ATP-binding domain of the pyruvate phosphate dikinase domain (**Figure 3-2A**). There was no additional homology or identification of a CBM in CMF012C, thus we eliminated CMF012C as a possible glucan dikinase. Conversely, CMT547C showed 70.7% amino acid homology to the entire PPDK domain as well as 40% amino acid similarity to the entire *St*GWD protein (**Figure 3-2B**). Additional sequence analyses revealed partial identification of two putative CBM45 domains in CMT547C that corresponded to *St*GWD CBMs (**Figure 3-3A**) (156, 214). Furthermore, additional BLASTp searches with CBM20 sequences from *Arabidopsis* PWD (AAU93516.1) (143) and *S. tuberosum* PWD (ACZ66259.1) (215) yielded no hits in the *C. merolae* genome.

Using ClustalW (195), we aligned full-length GWD orthologues from *S. tuberosum* (potato, higher plant)*, A. thaliana* (thale cress, higher plant)*, C. reinhardtii* (green algae)*,* and the putative *C. merolae* GWD (**Figure 3-3A**). The

putative 1572 amino acid GWD from *C. merolae* was 24% identical to the prototypical *St*GWD and only 12% identical to *At*PWD (**Figure 3-3B**)*.* The higher plant GWD orthologs are all localized to the chloroplast and contain a chloroplast transit peptide (cTP) (78, 150). The GWD orthologue in *C. merolae* does not possess a cTP when analyzed using the ChloroP algorithm (216). Despite the low percent identity, the putative GWD sequence is comprised of two tandem domains containing signature aromatic amino acid profile consistent with that of a CBM45 (152). At the C-terminus, there is a putative pyruvate, phosphate dikinase (PPDK) domain that is comprised of a histidine (HIS) subdomain and nucleotide binding (NBD) subdomain with the catalytic phosphohistidine residue located in the HIS subdomain (**Figure 3-3A**) (206, 217). Therefore, we hypothesized that CMT547C encodes for a GWD orthologue that we named *C. merolae* GWD (*Cm*GWD). Additionally, these data strongly suggest that *C. merolae* does not possess a PWD orthologue.

3.2.2 Biochemical properties of *C. merolae* glucan, water dikinase

The wildtype (WT) CMT547C gene and putative catalytic histidine mutant H1162A were synthesized, expressed in *E. coli*, purified via affinity chromatography followed by size-exclusion chromatography, and analyzed by SDS-PAGE. Purification of *Cm*GWD and the H1162A mutant yielded monomeric proteins of the expected ~177 kDa size (**Figure 3-4A, B**). To determine if *Cm*GWD can auto-phosphorylate, the purified proteins were incubated with either $^{33}\beta$-ATP or $^{33}\gamma$-ATP for 30 minutes, reactions were terminated, proteins were separated by SDS-PAGE, and gels were imaged to detect radio-label incorporation into the recombinant protein. There was robust auto-phosphorylation for *Cm*GWD when incubated with $^{33}\beta$-ATP while this signal was absent for *Cm*GWD-H1162A (**Figure 3-3C**). Moreover, there was no auto-phosphorylation detected when either protein was incubated with $^{33}\gamma$-ATP (**Figure 3-3C**). Thus, WT *Cm*GWD autophosphorylates with the β-phosphate, but not with the γ-phosphate from ATP. Additionally, this auto-phosphorylation event is dependent on H1162,

75

demonstrating that *Cm*GWD autophosphorylates as is characteristic of a dikinase mechanism.

Next, we investigated if *Cm*GWD could transfer the β-phosphate to an α-glucan substrate. We purified wild-type *C. merolae* floridean starch and incubated it with *Cm*GWD and ^{33}β-ATP for 0-12 hours. *Cm*GWD phosphorylated native *C. merolae* floridean starch in a time dependent manner with an apparent maximum velocity of 5.63 pmol•min^{-1}•mg glucan^{-1}. Conversely, the H1162A mutant did not incorporate radiolabel (**Figure 3-3D**). These data also demonstrate that *Cm*GWD functions as a canonical glucan dikinase.

As mentioned previously, starch from higher plants contain glucosyl residues that are phosphorylated at the C6- and C3-hydroxyls by GWD and PWD, respectively (90, 143, 146). To assess the specificity of *Cm*GWD, we utilized an indirect *in vitro* assay that employs the glucan phosphatases SEX4 and LSF2 as enzymatic tools to determine where phosphate was added by the dikinase (**Figure 3-5**). We phosphorylated *Arabidopsis sex1-3* starch that is phosphate free (150) with recombinant *Cm*GWD and ^{33}β-ATP in a similar manner as in **Figure 3-3D**. Then, the ^{33}P-labeled starch was dephosphorylated with the glucan phosphatase LSF2, which specifically removes phosphate from C3-hydroxyl groups (179). LSF2 released minimal to no phosphate (**Figure 3-3E**). Conversely, subsequent treatment with SEX4, which prefers removing C6 phosphate over C3 phosphate, released robust levels of ^{33}P (**Figure 3-3E**). As expected, when catalytically inactive glucan phosphatases were utilized there was no phosphate release. These experiments demonstrate that *Cm*GWD exclusively phosphorylates glucose at the C6-position.

Overall, these bioinformatic and biochemical data demonstrate the mechanism of *Cm*GWD and specific activity as a α-glucan, water dikinase. *Cm*GWD is an active glucan dikinase following a similar two-step reaction mechanism as described for *St*GWD (159) that autophosphorylates on H1162 via the β-phosphate of ATP to form a phospho-histidine intermediate. The β-phosphate can then be transferred to the C-6 hydroxyl group of glucose moieties on starch (**Figure 3-3F**).

3.2.3 Localization of *Cm*GWD

Due to floridean starch being localized outside of the plastid in *C. merolae* and the absence of a chloroplast targeting peptide in *Cm*GWD, we hypothesized that *Cm*GWD was located in the cytosol. In order to visualize the localization of *Cm*GWD, we produced a *Cm*GWD rabbit polyclonal antibody raised against recombinant *Cm*GWD protein. The antiserum was affinity purified with a NHS-activated purification column that utilized recombinant *Cm*GWD protein to purify polyclonal antibodies towards *Cm*GWD. The purified α-Cm-GWD antibody was validated by a protein-excess blocking experiment towards whole-cell lysate and purified recombinant *Cm*GWD protein (**Figure 3-6A**). Two identical SDS-PAGE gels were ran and transferred to a PVDF membrane. Prior to addition of the α-Cm-GWD antibody, one of the membranes was blocked with 200 molar excess of recombinant *Cm*GWD protein. Both of the membranes were incubated with α-Cm-GWD antibody and subsequently a secondary goat anti-rabbit antibody, then imaged. Incubation with excess *Cm*GWD protein completely blocked the ability of α-Cm-GWD antibody to detect both recombinant protein and endogenous GWD protein in whole-cell lysates (**Figure 3-6A**). In contrast, α-Cm-GWD antibody was able to recognize recombinant and endogenous GWD protein devoid of excess blocking protein (**Figure 3-6A**).

After the polyclonal antibody was validated, we fixed *C. merolae* cells and probed them with α-Cm-GWD antibody and used an AlexaFluor-488 conjugated secondary α-rabbit antibody to view endogenous GWD localization via immunofluorescence. We also were able to visualize the autofluorescence of the plastid, in CY5 channel, as well as using 4′,6-diamidino-2-phenylindole (DAPI) to stain DNA. The merged images show distinct homogeneous localization of GWD in the cytosol of the cells (**Figure 3-6B**).

3.2.4 Gene-targeted knockout of GWD

To determine the role of *Cm*GWD *in vivo*, we utilized the newly developed uracil auxotrophic strain of *C. merolae* (T1) (33) to delete *CmGWD* gene locus CMT547C. Genomic DNA was extracted from wild-type *C. merolae* cells and used

to amplify DNA flanking CMT547C (*CmGWD*). A linear fragment of DNA was generated via an overlap extension PCR comprised of ~2 kb of genomic DNA 5' to *CmGWD*, the *URA5.3* gene, and ~2 kb of genomic DNA 3' to *CmGWD* (**Figure 3-7A**). The linear DNA fragment targeting *CmGWD* was introduced via PEG-mediated transformation into the T1 strain of *C. merolae* (28). Transformed cells were plated on media lacking uracil to select for successful transformants and individual colonies were expanded into independent lines (**Figure 3-8A, B**). Potential *gwd* knockout lines were first screened via PCR for both the incorporation of *URA5.3* and loss of *CmGWD* (**Figure 3-7B-a and -b**). Lines positive for *URA5.3* and negative for *CmGWD* via PCR were then assessed by immunoblot analysis using a polyclonal antibody raised against *Cm*GWD (**Figure 3-7B-c**). Three lines were PCR positive for *URA5.3* and negative for *CmGWD* and also negative for *Cm*GWD by immunoblotting (**Figure 3-7B-d**).

3.2.5 Cell growth of Δ*gwd* lines in continuous and diurnal light

Three lines that were validated to lack GWD were selected and analyzed under continuous and diurnal light. Wild-type (WT) lines and the three Δ*gwd* lines were cultured under continuous light (50 μmol m^{-2} sec^{-1}) with 2% atmospheric CO_2 and cell numbers were assessed every 24-hours. When grown for 96 hours in continuous light, there were no observable differences in cell growth between WT and Δ*gwd* strains (**Figure 3-7C**). To assess growth curves in diurnal light, cultures were diluted to OD$_{750}$ ~0.5 and cultured using a 12h light (50 μmol m^{-2} sec^{-1}) / 12h dark diurnal light regimen for two weeks. After two weeks of diurnal growth, cultures were diluted back to OD$_{750}$ ~1.0 and cell numbers were assessed every 4-hours for 48 hours. There were no differences in diurnal growth of Δ*gwd* compared to WT (**Figure 3-7D**). Furthermore, through scanning electron microscopy (SEM), we did not observe any distinguishable morphological differences between Δ*gwd* and WT cells (**Figure 3-7E, F**). Overall, knocking out *GWD* in *C. merolae* did not result in an immediately detectable growth defect or observable global cell morphology difference under stable laboratory growth conditions.

3.2.6 Cell morphology via Transmission electron microscopy (TEM)

Although there was no detectable growth defect or observable cell morphology difference, we hypothesized that the internal ultrastructure of WT and Δ*gwd* cells would provide us more insight. Synchronous cultures were grown under a diurnal 12-hour light/12-hour dark regime for 48 hours. An aliquot of cells were taken after each 12-hour period and gently centrifuged and resuspended in a fixative. Our collaborator Dr. Timothy Meerloo and colleague Ying Jones processed the fixed cells and prepared ultrathin sections of WT and Δ*gwd* cells on carbon-coated copper grids. TEM micrographs of *C. merolae* cells exhibited a substantial difference in floridean starch granule morphology (red arrows) in the cytosol of Δ*gwd* cells compared to WT (**Figure 3-9**). The granules in WT cells were uniform and spherical after both 12-hour periods (**Figure 3-9A, B**). In stark contrast, we observed large, deformed granules in Δ*gwd* cells (**Figure 3-9C, D**). The plastids of WT cells also were observed to be more round than Δ*gwd* cells; however, this could be an experimental issue such as the plane of the cells.

To test if the floridean starch morphological differences are as pronounced in cells grown under continuous light, we grew cultures for 48 hours under continuous light and fixed cells as described above. Our collaborator Dr. Jean-Luc Putaux then processed our samples and post-stained with periodic acid thiosemicarbazide silver proteinate (PATAg) (204). This type of stain is analogous to periodic acid-schiff stain used to detect polysaccharides in histological studies (218, 219). Similar to diurnal growth, the floridean starch granules found in WT were uniform and spherical throughout the cytosol whereas granules from Δ*gwd* cells, were large and misshapen (**Figure 3-10A, B,** respectively). Due to the morphological differences in cells that lack GWD, we wanted to characterize the floridean starch produced in Δ*gwd* cells compared to WT.

3.2.7 Loss of GWD results in ablated floridean starch phosphate

Our biochemical analyses indicated that *Cm*GWD phosphorylates starch at the C6-position of glucose moieties. Therefore, to test this function *in vivo*, we utilized fluorescence-assisted capillary electrophoresis (FACE) to determine phosphate

position and quantity for WT and Δ*gwd* floridean starch (**Figure 3-11**). Floridean starch was extracted from cultures grown in continuous light, glycosidic bonds were hydrolyzed with 2M trifluoroacetic acid (TFA), and glucose moieties were treated with 200 mM 8-aminopyrene-1,3,6-trisulfonic acid (APTS) for 16 hours at 42°C (93). FACE analysis of the samples yielded well-resolved hydrolysis products and revealed a peak corresponding to glucose 6-phosphate (G6P) in the WT sample that was absent in the Δ*gwd* samples (**Figure 3-12A, top**). These two samples were also treated with alkaline phosphatase and analyzed by FACE. The alkaline phosphatase treatment eliminated the G6P peak in WT floridean starch and did not change the electrophoretic profile of Δ*gwd* (**Figure 3-12A, bottom**). Peak area was calculated to establish *C. merolae* G6P levels in floridean starch samples. WT *C. merolae* samples contained 0.888 ± 0.05 total phosphoesters per thousand glucose residues. These phosphate levels are similar to the total phosphate levels of *A. thaliana* leaf starch and over 10-fold higher than maize (**Figure 3-13**) (93). Phosphoesters from WT floridean starch at the C6-position accounted for >95% (0.840 ± 0.049 %) of all phosphate content, again verifying that *C. merolae* lacks a PWD ortholog. Conversely, phosphoesters in Δ*gwd* samples were at the sensitivity threshold (0.031 ± 0.01) indicating the lack of GWD ablated detectable G6P hydrolyzed from the sample.

To further confirm the phosphorylation status of *C. merolae* floridean starch, we employed a gas chromatography mass spectrometry (GCMS) method that we recently developed for sensitive quantification of glucose and glucose phosphate esters (201). This method utilizes mild acid hydrolysis and a two-step derivatization protocol to create volatile glucosyl species which can then be separated by gas chromatography (201). The GCMS method confirmed that Δ*gwd* floridean starch possesses drastically reduced phosphate content that were near the level of detection, consistent with FACE analysis (**Figure 3-12B**). These results were further confirmed in collaboration with Drs. Berge Minassian and Felix Nitschke using ^{31}P-NMR, which demonstrates C6 phosphate content again near limits of detection (**Figure 3-14**).

3.2.8 GWD-deficient cells do not display a starch-excess phenotype under continuous light

Multiple studies have found that perturbations in reversible glucan phosphorylation often results in a starch excess phenotype (124, 142, 144, 150, 172). The biological role and biochemical activity of GWD was first determined in potato, where GWD suppression led to a decrease in starch-bound G6P and a starch-excess phenotype (144). A starch excess phenotype was also described in *A. thaliana* when the mutant *sex1* line was found to be defective in glucan, water dikinase activity and displayed three to seven times higher starch levels than wild type (150). To determine if our Δ*gwd* strains also displayed a starch excess phenotype, we quantified the floridean starch content of Δ*gwd* strains and compared those to WT under continuous light using the amyloglucosidase-dependent glucose release assay. While there was a slight trend of more floridean starch in the Δ*gwd* cells under continuous light, we unexpectedly found Δ*gwd* lines did not display a statistically significant increase in floridean starch levels (**Figure 3-12C**). Previous work established that microalga generate substantial amounts of starch under nitrogen deprivation (193, 220, 221). Therefore, we grew WT and Δ*gwd* cells in continuous light in replete conditions and then shifted cells to nitrogen deprivation conditions for 48 hours. We again determined floridean starch levels using the amyloglucosidase-dependent glucose release assay. Under normal nitrogen-replete conditions, there was not a statistical difference in glucan amounts between WT and Δ*gwd* cells (**Figure 3-12D**). Nitrogen-depleted conditions resulted in a marked increase in floridean starch accumulation in both the WT and Δ*gwd* cells with no statistical difference between the two (**Figure 3-12D**). Therefore, unlike other species there is no starch excess phenotype in *C. merolae* lacking GWD.

3.2.9 Floridean starch content and phosphate levels in diurnal conditions

A more physiologically-relevant environment for photosynthetic organisms revolves around daily diurnal cycles. Therefore, we subjected *C. merolae* cells to 12h light/12h dark diurnal cycles and assessed both floridean starch levels and

phosphate content. Using the amyloglucosidase-dependent glucose release assay at 12-hour intervals, we observed that Δgwd cells underwent slower rates of both synthesis (1.46 μg/10^8 cells/hour) and degradation (-1.72 μg/10^8 cells/hour) compared to WT cells (3.30 and -3.60 μg/10^8 cells/hour, respectively) (**Figure 3-15A**). The total amount of accumulated floridean starch during the day was lower than WT cells; however, these levels equalized after a complete 24-hour diurnal cycle displaying a unique regulation/feedback of carbohydrate metabolism similar to that seen in *A. thaliana* (222). We collected cultures at both the end of light and dark periods and employed the GCMS method to assess glucan phosphorylation levels. While WT cells yielded floridean starch samples that contained robust levels of C6-phosphate, floridean starch from Δgwd cells were below the limit of detection (**Figure 3-15B**).

3.2.10 GWD-deficient floridean starch possesses a unique chain-length distribution profile

Due to the almost 50% reduced rates of both synthesis and degradation in Δgwd cells, we performed chain-length distribution (CLD) analysis using FACE to determine whether there were differences in the structure of amylopectin. Synchronous cultures were grown under diurnal light and floridean starch was extracted from cultures at the end of both 12-hour periods. The purified floridean starch granules were debranched via *Pseudomonas sp.* isoamylase after a brief solubilization at 98 °C for 10 minutes. Following isoamylase treatment, the debranched glucans were dried, APTS-labelled, and derivatized in a similar fashion to the acid-hydrolyzed glucose moieties to detect phosphate levels (93, 199). The CLD analysis of WT *C. merolae* debranched glucans under diurnal conditions corroborate previous findings showing a peak degree of polymerization (DP) at 13 glucose moieties (**Figure 3-15C, D**) (73). Conversely, Δgwd glucans displayed a unique CLD profile from cells grown under diurnal conditions compared to WT. Debranched glucans from Δgwd cells exhibited an abnormal abundance of short chains from DP 3-7 as well as a decreasing trend in longer chains >35 although the resolution of these longer chains were low (**Figure 3-15C,**

D). DP 3 and 4 levels are ~1.5 – 2.0-fold higher compared to the WT CLD chromatogram during day and night (**Figure 3-15C, D**) as well as under continuous light (**Figure 3-16**). The peak area fold differences seen here in *C. merolae* are 4-5 times higher compared to *sex1* in *A. thaliana* (150) and the corresponding mutant in cassava (192).

3.2.11 Irregular granule morphology of GWD-deficient cell lines

The unique CLD profile of Δ*gwd* glucans prompted the examination of granule morphology from WT and Δ*gwd* cells. Synchronous cultures were grown diurnally and floridean starch was extracted as previously described. The native floridean starch granules were subjected to morphological analysis by scanning (SEM) and transmission (TEM) electron microscopy. SEM analysis of WT granules confirmed a uniform spherical morphology, corroborating previous findings (73) (**Figure 3-17A**). Granules from Δ*gwd* cells were vastly different exhibiting larger, deformed and thinner granules with a dramatically more heterogeneous size distribution (**Figure 3-17B**). These results are similar to starch granules from *A. thaliana sex1* mutant plants (72, 161).

Utilizing the same native floridean starch granules purified from synchronous cultures grown diurnally, we quantified the morphological differences via TEM. WT granules displayed a round, smooth and uniform morphology; however, Δ*gwd* granules were misshapen with a ruffled shape (**Figure 3-17C, D**, respectively). In addition, the Δ*gwd* granules were often enlarged, severely altered in granular shape, and included several regions of fissure-like depressions (161) (**Figure 3-17D**, arrows). Quantification of the TEM images revealed that Δ*gwd* granules on average are larger in diameter and perimeter compared to WT granules, and Δ*gwd* granules have a considerably broader distribution (**Figure 3-17E-F**). Granules of Δ*gwd* cells from the end of the 12h period of light were ~24% and ~34% larger in diameter and perimeter, respectively (**Figure 3-17E, F**). Similar values are seen at the end of the 12h dark period as well. The mean diameters (nm) were 258 ± 57 and 322 ± 103 for WT and Δ*gwd* granules at the end of the day (mean ± SD; n > 400, each). The maximal diameter of Δ*gwd* granules at the end of the day were

dramatically different and widely distributed compared to WT, measuring 753 nm and 485 nm, respectively (**Figure 3-17E**). The roundness of Δgwd granules were significantly compromised and widely distributed with ~16% decrease on average compared to WT granules (**Figure 3-17G**). Similar results were obtained from floridean starch granules isolated from cells under continuous light growth (**Figure 3-18**). Δgwd granules were thin, enlarged and contained several regions of fissure-like depressions (**Figure 3-18D**, black arrows).

3.2.12 GWD-deficient cells employ detrimental nutrient-scavenging in prolonged dark stress

Under normal 12-hour periods of darkness, i.e., diurnal conditions, Δgwd cells exhibit reduced rates of both starch synthesis and degradation (**Figure 3-15A)** as well as substantially altered granule morphology (**Figure 3-17 and Figure 3-18)**. However, Δgwd cells display a growth rate similar to WT cells (**Figure 3-7C, D**). We hypothesized their ability to utilize floridean starch might be compromised with the imposition of a prolonged period of darkness. We subjected the obligate photoautotrophic WT and Δgwd cultures to a prolonged period of dark stress and monitored key energy-rich storage molecules like floridean starch and photosynthetic pigments, i.e., chlorophyll α and phycobiliproteins.

Dilute cultures were grown under diurnal conditions (12h light/ 12h dark) for 48 hours followed by constant dark while still being supplied with 2% ambient CO_2. At the beginning of the experiment, a threshold optical density (OD_{750}) value of 0.9 for all cultures were chosen in which would mark the end of the dark stress and allow cultures to sufficiently recover. After 16 days, the Δgwd OD_{750} dropped below the threshold and all cultures were reintroduced to diurnal light for six days. Minimal culture samples were collected throughout the experiment and analyzed visually, by spectral scans, and floridean starch levels.

The average OD_{750} of WT and Δgwd cultures were similar for the first 72 hours of dark stress and then considerably deviated (**Figure 3-19A, B**). Δgwd cultures exhibited a continuous decrease in optical density from day three to the end of the dark stress period compared to a markedly slower rate of decline in WT cultures

(**Figure 3-19A**). After 16 days of dark stress, there were striking visual differences between the WT and Δgwd cultures with each of the Δgwd cultures exhibiting a yellowish-green color compared to the light green of WT (**Figure 3-19B**). After 16 days, cultures were collected by centrifugation, gently resuspended in fresh media, and reintroduced to 12h light/12h dark diurnal growth. Two days after the re-introduction of diurnal light, WT cultures displayed an increase in their OD_{750} that quickly became exponential (**Figure 3-19A**). However, Δgwd cultures were unable to recover even after being resuspended in fresh media and reintroduced to diurnal light. Δgwd cultures began lysing and exhibited a further 33% reduction in OD_{750} and cell count from day 16 to day 22 (**Figure 3-19A, B**).

The major carbon storage molecule in *C. merolae* is floridean starch. After 16 days of continuous dark, WT cells degraded only ~50% of their accumulated floridean starch (**Figure 3-19C**). Conversely, Δgwd cells began to degrade glucan stores rapidly by day four and degraded essentially all of their floridean starch before day 16 (**Figure 3-19C**). Under nutrient-deprived stress, it has been documented that *C. merolae* degrades phycobilisomes to maintain metabolic activity by utilizing the phycobilisomes as sources for nitrogen and carbon (223). We quantified the status of two main photosynthetic *C. merolae* pigments, phycocyanin (630 nm) and chlorophyll α (680 nm), throughout the 16 days of extended dark stress. Decreased absorbance began for both 630 nm and 680 nm between day three and five for both WT and Δgwd cells. Beginning on day five, Δgwd cells exhibited a rapid loss of phycocyanin and chlorophyll α compared to WT cells (**Figure 3-19D, E**). WT cells had a decrease of 23% in phycocyanin over the 16-day period while Δgwd cells displayed a 59% loss (**Figure 3-19D**). For chlorophyll α, WT cells degraded a meager 5% while Δgwd cells consumed a considerable 45% of their chlorophyll α content (**Figure 3-19E**). These data suggest Δgwd cells underwent extreme energy deprivation and lost the ability to regulate the depletion of major nitrogen and carbon reserves during prolonged stress which resulted in cell death, in contrast to WT cells which preserved these major reserves for the necessary means to recover when reintroduced to light.

3.3 Discussion

The role of reversible glucan phosphorylation in starch granule homeostasis is an emerging area of research that impacts our understanding of plant energy storage. This study describes an active GWD in the red alga *Cyanidioschyzon merolae, Cm*GWD demonstrating for the first time conservation of the glucan dikinase family across kingdoms. We identified that *Cm*GWD does not contain a chloroplast transit peptide, possesses tandem N-terminal starch binding domains of the CBM45 family and a catalytic PPDK domain comprised of a HIS and NBD subdomain. The catalytic mechanism of *Cm*GWD utilizes ATP as a dual phosphate donor by transferring the γ- and β-phosphate to water and α-glucans, respectively. Mutation of the catalytic histidine residue abolished autophosphorylation as well as glucan phosphorylation activity. *Cm*GWD is highly specific toward the C6-position of glucosyl residues as C3-phosphate levels were insignificant. We generated *C. merolae* lines lacking GWD to elucidate the biological function of GWD. Under continuous light, Δ*gwd* cells showed no growth defect and no overall increase in floridean starch content. Under diurnal conditions, Δ*gwd* cells have 50% slower rates of starch synthesis and degradation. Δ*gwd* floridean starch has a very unique chain-length distribution profile with a higher proportion of short chain glucans DP 3-7, a discontinuous pattern of DP 3 and 4, and a drastically altered granule morphology compared to that of WT in both continuous and diurnal light regimens. Δ*gwd* granules exhibit similar morphologies to that of other starch-excess mutants pertaining to GWD from other model organisms (72, 161, 163). However, this is the first report to show a complete transformation from a round, spherical wild-type granule to a thin, deformed granule. Under prolonged dark stress, Δ*gwd* cells strikingly degrade the majority of their nitrogen and carbon reserves much more rapidly than WT and are unable to recover when light is reintroduced leading ultimately to cell death.

While the overall amino acid similarity between GWD orthologues from *S. tuberosum, A. thaliana, C. reinhardtii,* and *C. merolae* is very low, all GWD orthologues share similar domain structure lending evidence towards functional preservation of glucan phosphorylation in carbohydrate metabolism. The presence

of glucan dikinases and isoamylase-like debranching enzymes are proposed to explain the existence of semicrystalline starch-like polymers (69). Higher plants also utilize an additional glucan dikinase, PWD, to act downstream of GWD further phosphorylating pre-phosphorylated glucans at the starch granule surface increasing the solubility of the glucan chains (143). All photosynthetic model organisms studied thus far, including the green alga *C. reinhardtii*, possess both GWD and PWD. Compared to green algae and plants where there are multiple forms of enzymes, sometimes >30 genes required for starch metabolism, *C. merolae* has a floridean starch metabolism network that is incredibly simple and nonredundant (69, 100, 102). Hence, this species can produce a sufficiently crystalline α-glucan using a minimum set of activities (69).

The α-glucan in *C. merolae* is intermediate between plant amylopectin and glycogen-containing species (73). Therefore, it is likely that C3-phosphorylation evolved to aid in the unwinding of outer glucans from higher plant starch. The crystallinity of floridean starch from *C. merolae* was found to be relatively lower when compared to the green alga, *C. reinhardtii,* that displays a highly ordered amylopectin structure and crystallinity (73). With just one glucan dikinase, C6 phosphorylation of less ordered amylopectin may allow enough solubilization or hydration at the granule surface to allow amylolytic enzymes access to the glucose polymers in *C. merolae*. This is in agreement with the Blennow and Engelsen 2010 model of initial GWD activity affecting helix packing and acting as a "tracker" for local degradation (95).

*Cm*GWD is localized to the cytosol along with the floridean starch granules found in *C. merolae* (**Figure 3-6B**)*.* We previously discovered a laforin-like gene in the genome of *C. merolae,* a 532 amino acid protein named *Cm*laforin also located in the cytosol (185). Laforin was originally thought to be exclusively found in vertebrates; however, it was found in five additional protists including *Toxoplasma gondii* and *C. merolae* (185)*.* It is likely that laforin is a glucan phosphatase that opposes GWD activity in *C. merolae.* Furthermore, in 2007, Gentry et al. discovered that SEX4 and laforin are functional equivalents. Loss of function mutations in any of the genes encoding GWD, PWD, or SEX4 results in varying

starch excess (*sex)* phenotypes. Our results provide exciting evidence that GWD-like activity is required to regulate the metabolism of semicrystalline macromolecules across kingdoms. The simplified genome of *C. merolae* retains the function of reversible glucan phosphorylation by GWD and laforin. Intriguingly, the observed specific C6 phosphorylation by GWD is sufficient to induce hydration and disruption between helices at the granular surface to stimulate breakdown. The absence of PWD and LSF2 in the *C. merolae* genome supports the lack of C3 phosphate in its carbohydrate reserve and may indicate more complex regulation is required for starch species which contain amylose and longer amylopectin chain lengths (74).

The nature of *C. merolae* α-glucan reflects the ancestral structure within Cyanidiales which could have initially accumulated glycogen (as seen in *Galdieria sulphuraria* and *Cyanidium caldarium*) and later evolved starch-like structures gradually (73, 74). *C. merolae* production of an amylose-free semi-amylopectin glucan is in contrast to the other members of the Cyanidiales, *Galdieria sulphuraria* and *Cyanidium caldarium,* which both produce glycogen. Unlike amylopectin and plant starch, glycogen is a water-soluble macromolecule and is stored in the cytoplasm in majority of bacterial, fungal, and animal species (55). Our results contrast those seen in higher plants where loss/reduction of GWD activity does not have a substantial impact on the chain-length distribution profile of native starch granules (150). In *C. merolae,* we observed significant changes in the proportion of DP3 and DP4 in the chain-length distribution profile of Δ*gwd* floridean starch. We also observed, to date, one of the most noticeable transformations in granule morphology by the loss of GWD. Furthermore, our results are complementary to Skeffington and colleagues who discussed the lack of GWD activity during degradation alters the surface of starch granules thereby creating poor substrates for the proceeding biosynthesis of starch (162). In *C. merolae* under continuous light, we observed similar alterations to the chain-length profile as well as granule morphology suggesting that GWD most likely plays a pivotal role in granule remodeling. For example, recombinant starch synthase I from *A. thaliana* had higher activity on wild-type starch granules compared to *gwd* mutant granules

(224). Differential turnover throughout selective areas of the starch granule preferably towards degradation and/or synthesis after numerous diurnal cycles would have pronounced alterations in starch granule morphology (161). This concept seems supported in *C. merolae,* as the loss of GWD results in many regions of fissure-like depressions most likely from differential turnover throughout the surface of the starch granule. One could speculate that this differential turnover may have a crucial effect on an organism's ability to efficiently utilize or regulate starch catabolism during periods of extreme stress such as light deprivation.

The ability of *C. merolae* to live and thrive in particularly extreme environmental conditions require remarkable adaptation mechanisms during unfavorable periods. In this study, we observed the astonishing ability of WT *C. merolae*, which is an ecologically obligate photoautotroph (12), to undergo prolonged dark stress while preserving majority of its photosynthetic pigments (>80%) and floridean starch (~50%) compared to Δ*gwd* cells. The loss of GWD in *C. merolae* perturbed insoluble carbohydrate storage and over-induced nutrient-scavenging mechanisms resulting in the consumption of major stores of carbon and nitrogen. Interestingly, there is evidence that most autophagy-related components are absent in *C. merolae* with the exception of target of rapamycin (TOR1/2) (225). In addition, under nutrient-deprived conditions, TOR is repressed and shown to be a key checkpoint kinase for carbon storage in the form of TAG and floridean starch accumulation (189, 191, 226). Although adaptation mechanisms are relevant for short-term stress conditions, the exact nature of prolonged adaptation mechanisms remain unexplored; however, some light has been shed on apoptotic features in *C. merolae* with the discovery of novel proteins with lytic, transporting, membrane fusion and trafficking functions encompassed in vacuoles (227). Future studies are needed to elucidate the excessive consumption of nitrogen and carbon reserves observed in GWD-deficient *C. merolae* as well as if GWD is a substrate for TOR regulation under nutrient and energy deprived conditions.
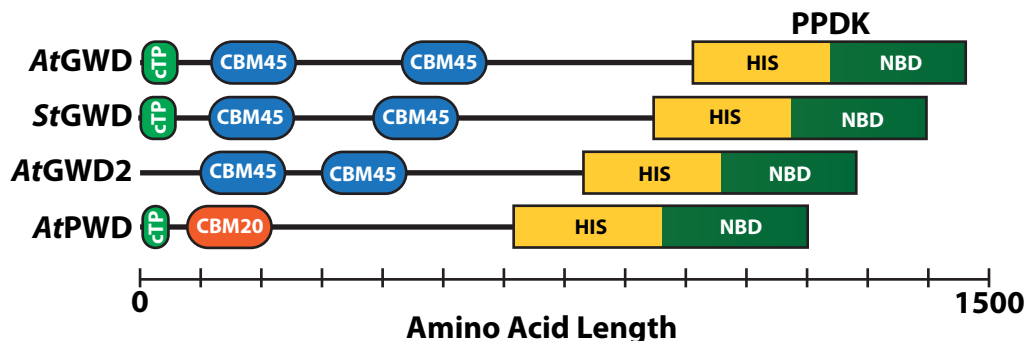
Figure 3-1 Domain structure of glucan dikinases
Domain structures of GWD from *A. thaliana* (*At*) and the prototypical *S. tuberosum* (*St*). GWD is comprised of a chloroplast targeting peptide (cTP), tandem N-terminal CBM45s, a long linker region, and a pyruvate, phosphate dikinase (PPDK) domain. The PPDK domain is comprised of a histidine (HIS) subdomain nucleotide binding (NBD) subdomain with a highly conserved catalytic phosphohistidine residue located in the HIS subdomain. *At*GWD2 is a GWD homologue that bares significant resemblance to *At*GWD, devoid of a 78 amino acid cTP. Therefore, *At*GWD2 is localized in the cytoplasm. *At*GWD3 (*At*PWD) is localized to the chloroplast and is comprised of a cTP, a CBM20, a long linker region, and a PPDK domain.

A)

```
                    Color Key for Alignment Scores
        <40         40-50        50-80        80-200        >=200

    1_
        0      250      500      750      1000      1250

  gn1| CMER|CMT547C  ████████████████████████████████████████
  gn1| CMER|CMF012C                                      ████

                                                  Score      E
  Sequences producing significant alignments:    (bits)   Value

  gn1|CMER|CMT547C starch associated protein R1      480    e-136
  gn1|CMER|CMF012C phosphoenolpyruvate synthase       49    4e-06
```
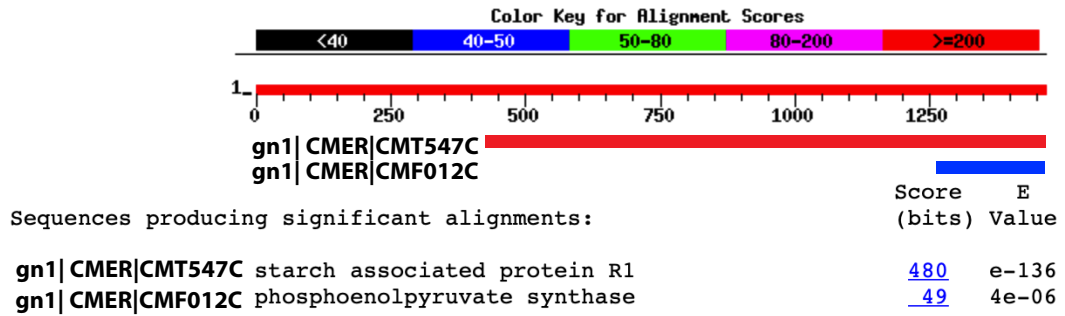
B)

Percent Similarity/Identity			
	_St_GWD	**CBMs**	**PPDK**
C. merolae	40.0/24.0	37.8/23.2	70.7/61

Figure 3-2 Blastp search results of _St_GWD in _C. merolae_ genome
A) Search results of _St_GWD in the _C. merolae_ genome database (http://czon.jp)
yielding two hits, CMT547C and CMF012C. A significant hit (red line) identified
homology to over 1000 amino acids in CMT547C. The partial hit (blue line)
identified homology to 200 amino acids in CMF012C which corresponds to a
_PPDK_N,_ the N-terminal ATP/AMP-binding domain of pyruvate phosphate
dikinase. There was no additional homology or identification of a CBM in
CMF012C. **B)** A putative orthologue to _St_GWD, CMT547C, showed significant
similarity to the PPDK domain (70.7%) as well as the entire _St_GWD protein (40%).
In addition, there was also homology to the N-terminal CBM45s (37.8%), unlike
that of CMF012C.
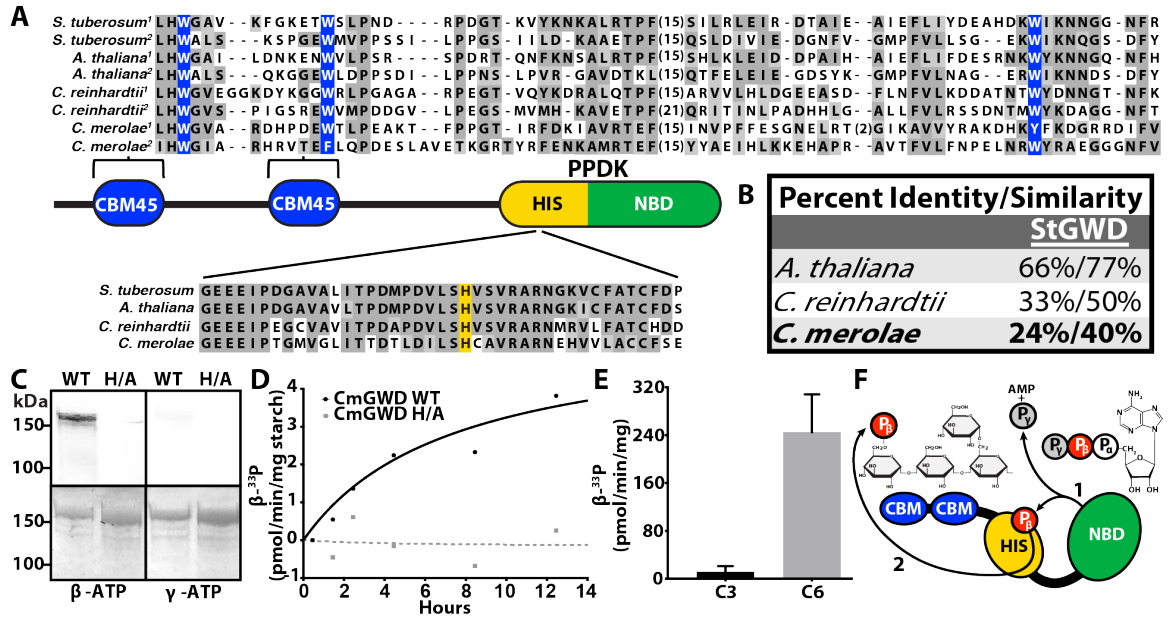
Figure 3-3 Bioinformatics and biochemical analyses of a putative *C. merolae* glucan, water dikinase.

A) Amino acid sequence alignment of α-glucan, water dikinase (GWD) orthologs. Residues boxed in dark gray are identical, while similar residues are boxed in light gray. Residues boxed in blue are highly conserved amongst the CBM45 family and critical for glucan binding. The histidine residue boxed in yellow is the conserved catalytic residue. **B)** Percent identity and similarity of full-length *Solanum tuberosum* GWD compared to those of *A. thaliana*, *C. reinhardtii*, and *C. merolae*. **C)** Autophosphorylation activity from recombinant WT *Cm*GWD and catalytically inactive mutant H1162A (H/A). Top left and right panels: Autoradiography with ^{33}β-ATP and ^{33}γ-ATP, respectively. Bottom Panels: Mini-PROTEAN TGX stain-free imaging protein loading control. **D)** *In vitro* phosphorylation activity measuring ^{33}β-phosphate incorporation (pmol•min^{-1}•mg starch^{-1}) of WT *Cm*GWD and H1162A using native WT *C. merolae* floridean starch granules as the substrate. Black circles: WT *Cm*GWD phosphate incorporation activity. Gray squares: H1162A phosphate incorporation activity. Black and gray lines are curve-fitted to triplicate data points using a Michaelis-Menten model. **E)** Site specificity of *Cm*GWD phosphorylation activity. *C. merolae* floridean starch granules were phosphorylated with *Cm*GWD and subsequently dephosphorylated by Like Sex Four2 (LSF2, black bar), which exclusively releases C3-phosphate, and Starch EXcess4 (SEX4, grey bar), which dephosphorylates both C3-phosphate and C6-phosphate. ^{33}β-phosphate release (pmol•min^{-1}•mg^{-1}) was quantified. **F)** Proposed schematic of the two-step mechanism of action employed by *Cm*GWD. Proposed mechanism adopted from Mikkelsen and Blennow 2005 (159).
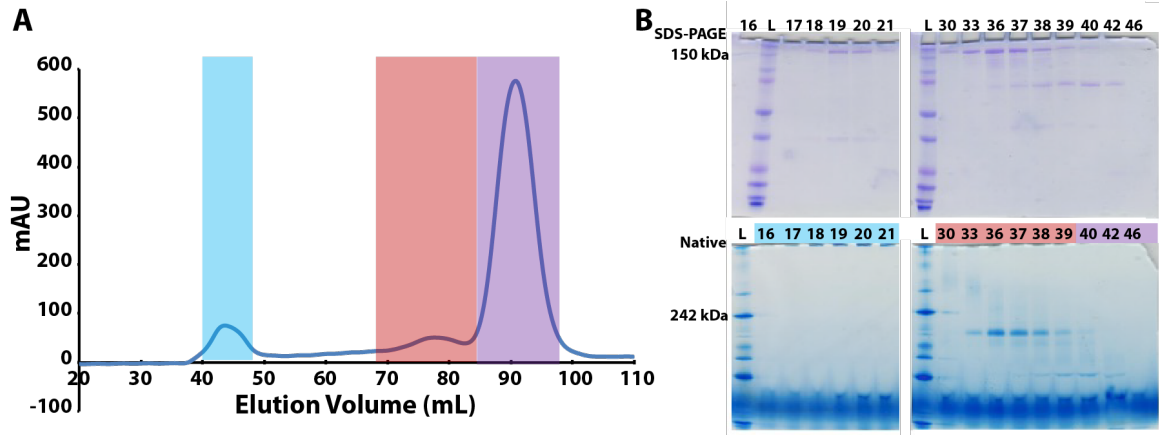
Figure 3-4 SEC, SDS-PAGE, and Native-PAGE of full-length *Cm*GWD
A) SEC elution chromatogram of recombinant full-length *Cm*GWD (~177kDa). **B)** Highlighted fractions were run on SDS- and Native-PAGE gels to check purity and oligomeric status. Both gels were stained with Coomassie Blue. Light blue highlighted fractions (16-21) were aggregated protein. Light red highlighted fractions (33-39) were monomeric protein. Light purple highlighted fractions (40-46) were a large amount of smaller proteins (likely chaperones and heat-shock proteins) co-purified after IMAC purification.
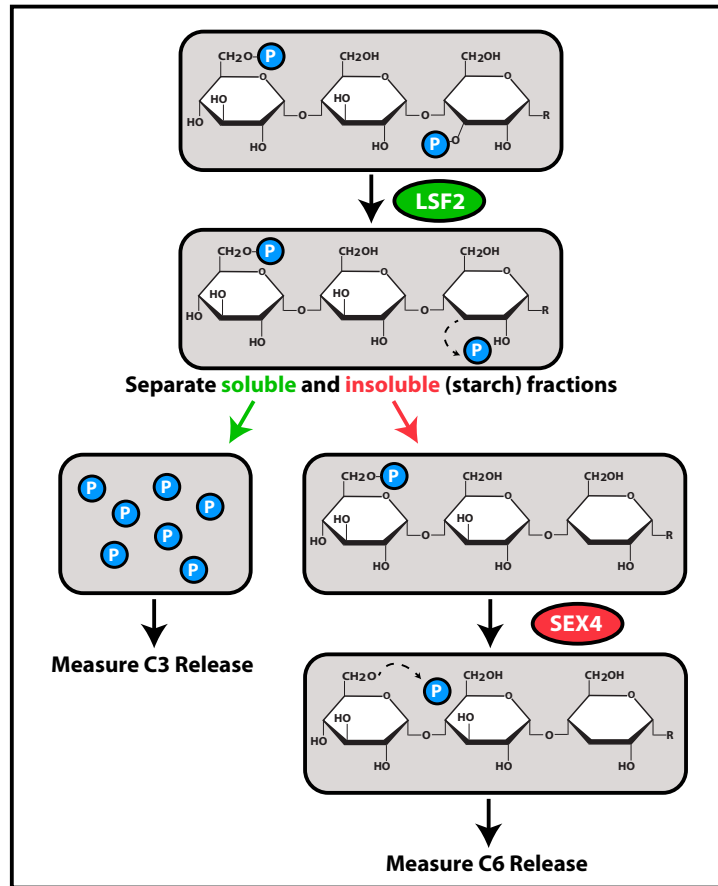
Figure 3-5 Indirect *in vitro* site specificity assay
Flowchart overview of indirect *in vitro* specificity assay utilizing glucan phosphatases, *At*LSF2 and *At*SEX4. Phosphate-free *A. thaliana sex1-3* starch was phosphorylated with a glucan dikinase incubated with β ^{33}P-ATP. After several washes to rid the radiolabeled starch of unbound β ^{33}P-ATP, the starch has either C3, C6, or both positions radiolabeled. Dephosphorylation with *At*LSF2 exclusively removes the C3-phosphate incorporated into starch. The reaction was stopped with SDS and centrifuged to separate the starch from the released C3-phosphate. After centrifugation, the C3-phosphate released in the supernatant was quantified using a scintillation counter. The remaining supernatant was aspirated and the remaining radiolabeled starch was subsequently washed twice with water. The experiment was then repeated using *At*SEX4 which prefers to dephosphorylate C6-phosphate. *At*SEX4 removed all the remaining glucan-bound radiolabeled phosphate. After incubation with *At*SEX4, the reaction was stopped as before with SDS and the reaction was centrifuged to separate the soluble and insoluble fractions. The C6-phosphate released into the supernatant by *At*SEX4 was then quantified using a scintillation counter. The results of this assay will provide a percent of phosphate released from each position giving an indirect method to characterize site-specificity of glucan dikinases.

94
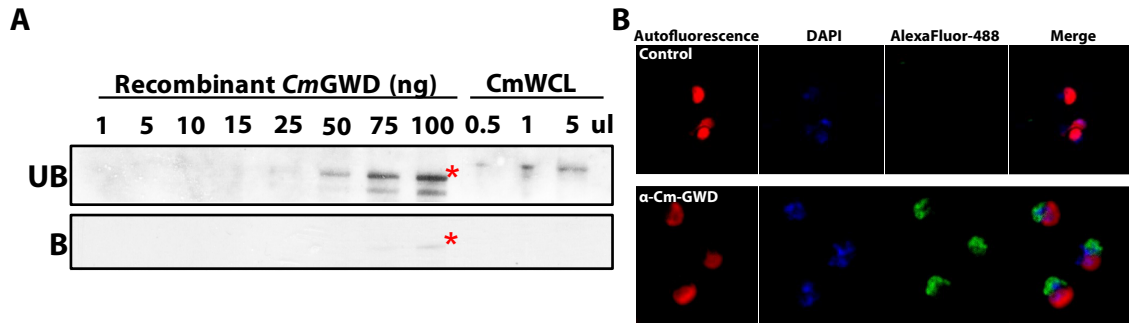
Figure 3-6 α-Cm-GWD validation and endogenous *Cm*GWD localization
A) Excess blocking peptide validation of α-Cm-GWD rabbit polyclonal antibody against recombinant *Cm*GWD protein and endogenous *Cm*GWD in whole-cell lysates. Varying dilutions of purified recombinant *Cm*GWD protein and whole-cell lysates of WT *C. merolae* were run on two identical SDS-PAGE gels. The gels were transferred to PVDF membranes and then one membrane (B) was blocked with 200 molar excess recombinant *Cm*GWD protein prior to adding the primary α-Cm-GWD antibody. Both membranes were then incubated with α-Cm-GWD primary and a goat anti-rabbit secondary then imaged using a ChemiDoc BioRad Imager. The unblocked immunoblot (UB) exhibits detection of both recombinant, down to ~25 ng, and endogenous protein at the lowest density (0.5 μL). The blocked immunoblot was barely able to detect the highest amount of recombinant protein therefore validating that the α-Cm-GWD antibody is specific for *Cm*GWD. Red asterisk, *Cm*GWD protein migration **B)** Immunofluorescence of WT *C. merolae* cells. Cells were fixed and incubated with pre-immune serum (control, top panels) or α-Cm-GWD antibody (bottom panels) and probed with a AlexaFluor-488 conjugated α-rabbit secondary antibody. DAPI stain was used to visualize DNA. Plastids were visualized by their autofluorescence in the CY5 channel (red). Images were merged to observe localization of *Cm*GWD in the cytosol of *C. merolae* cells.
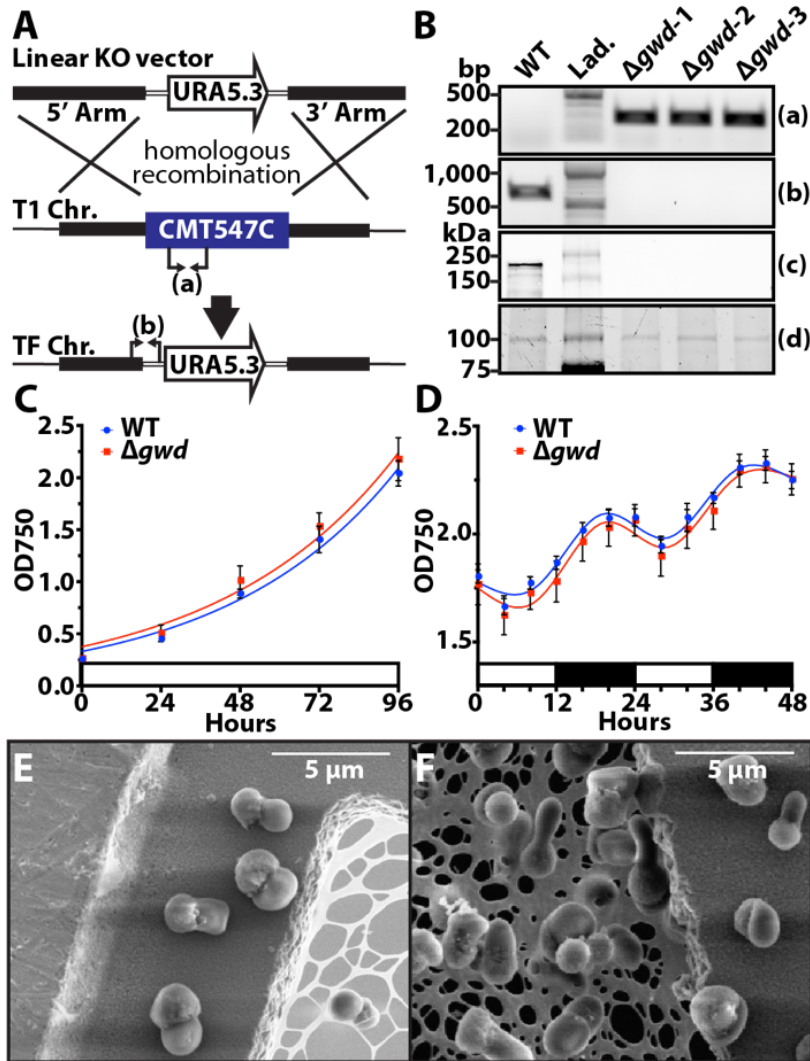
Figure 3-7 *C. merolae* GWD knockout strategy, validation, and initial phenotypic characterization.
A) A gene-targeted knockout strategy was utilized based on Taki et al. 2015. The *URA5.3* gene was introduced into the T1 strain to replace the CMT547C (Cm*GWD*) gene locus. A linear DNA vector containing the *URA5.3* gene flanked by 2 kb homologous arms bordering CMT547C was generated. **B)** Potential Δ*gwd* lines were screened and validated by PCR. One primer set **(a)** screened for the incorporation of the *URA5.3* gene. A second primer set **(b)** screened for the presence/absence of the CMT547C gene. Whole cell lysates **(c)** of wildtype (WT) and putative *gwd* knockouts (Δ*gwd*-1, Δ*gwd*-2, Δ*gwd*-3) were analyzed by immunoblotting with a polyclonal α-Cm-GWD antibody. Total protein load **(d)** was analyzed on a stain-free TGX gel and imaged with a BioRad Imager. **C)** Growth curve of WT and Δ*gwd* cells grown in continuous light growth for 96 hours. **D)** Growth curve of WT and Δ*gwd* cells were grown in diurnal light (12h light/12h dark) for 48 hours. E-F) Representative scanning electron microscopy (SEM) images of WT *C. merolae* cells **(E)** and Δ*gwd* cells **(F)**.
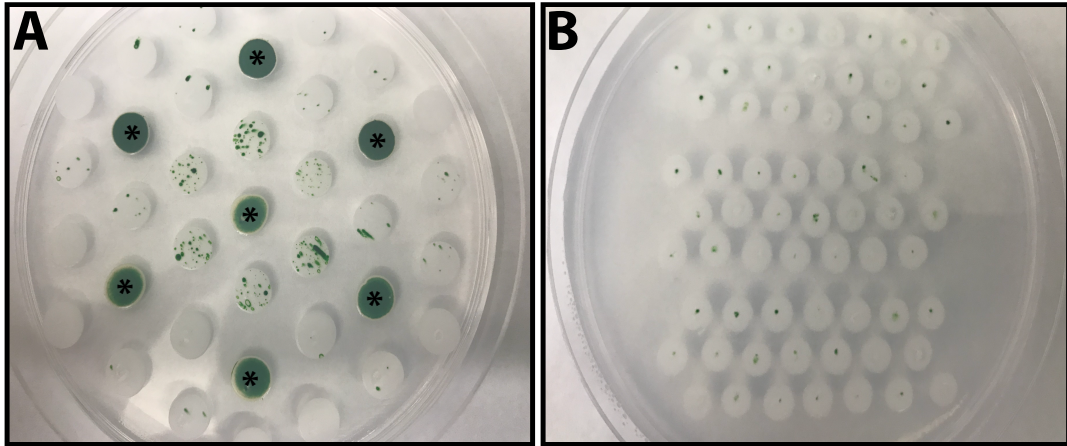
Figure 3-8 Transformant colony formation and isolation.
A) Colony formation after 21 days on a gellan gum plate without uracil grown at 42˚C under continuous light (50 μmol m-2 sec-1) and 2% CO2. Wildtype Nurse cells (*) **B)** Further isolated colonies for an additional three days.

End of Day   **End of Night**
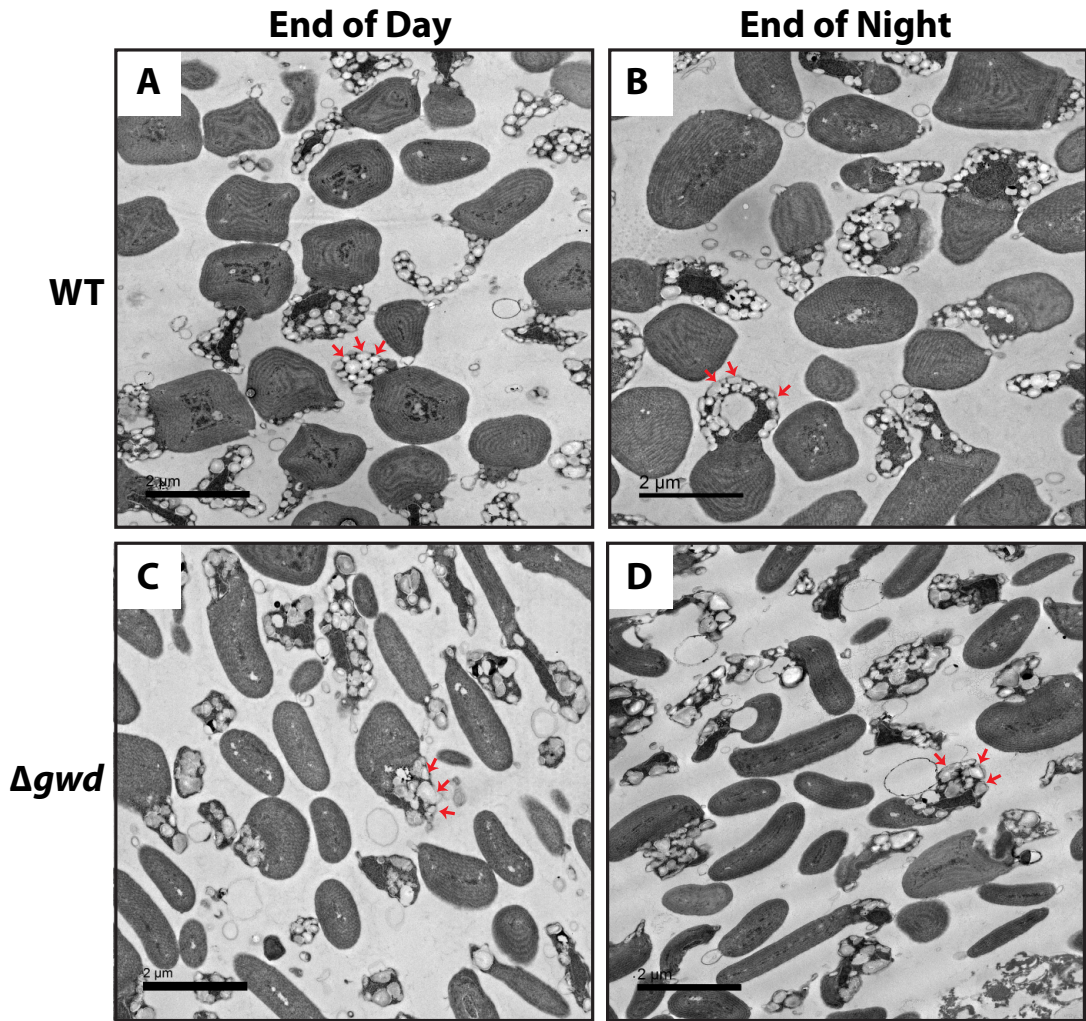
Figure 3-9 TEM images of ultrathin sections of *C. merolae* cells under diurnal growth

TEM images of ultrathin sections of WT (**A, B**) and Δ*gwd* (**C, D**) *C. merolae* cells grown diurnally. Cells were collected at the end of each 12-hour period. Red arrows, starch granules. Osmium-uranyl staining has no effect on polysaccharides therefore they have transparent appearance. Images were taken by Dr. Timothy Meerloo and Ying Jones from the Electron Microscopy Facility at the University of San Diego School of Medicine.
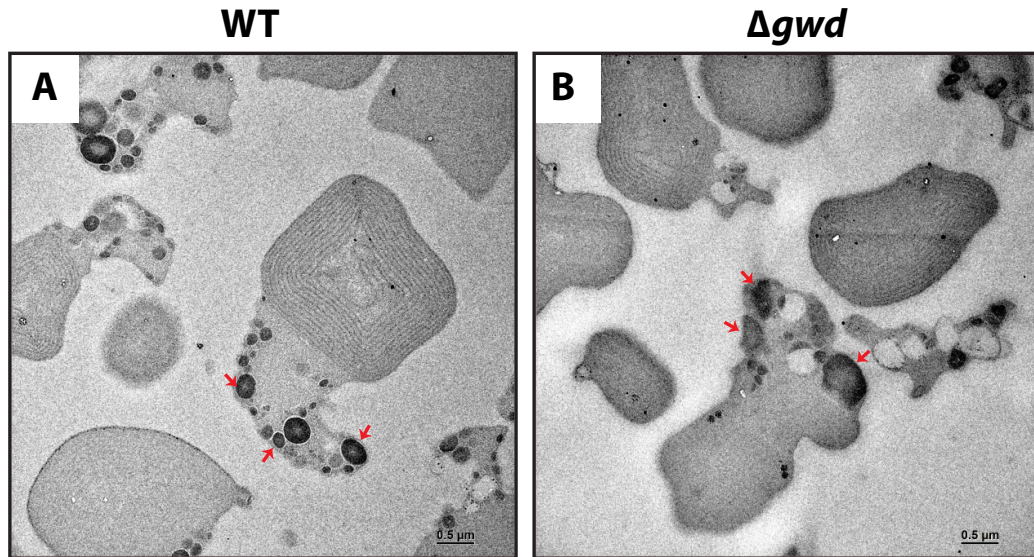
Figure 3-10 TEM images of PATAg stained ultrathin sections of *C. merolae* cells grown in continuous light
TEM images of ultrathin sections of WT (**A**) and Δ*gwd* (**B**) *C. merolae* cells grown in continuous light. Cells were collected at the end of a 48-hour period. Red arrows, starch granules. PATAg selectively stains polysaccharides therefore denser material will have a more electron-dense staining. Images were taken by Dr. Jean-Luc Putaux.
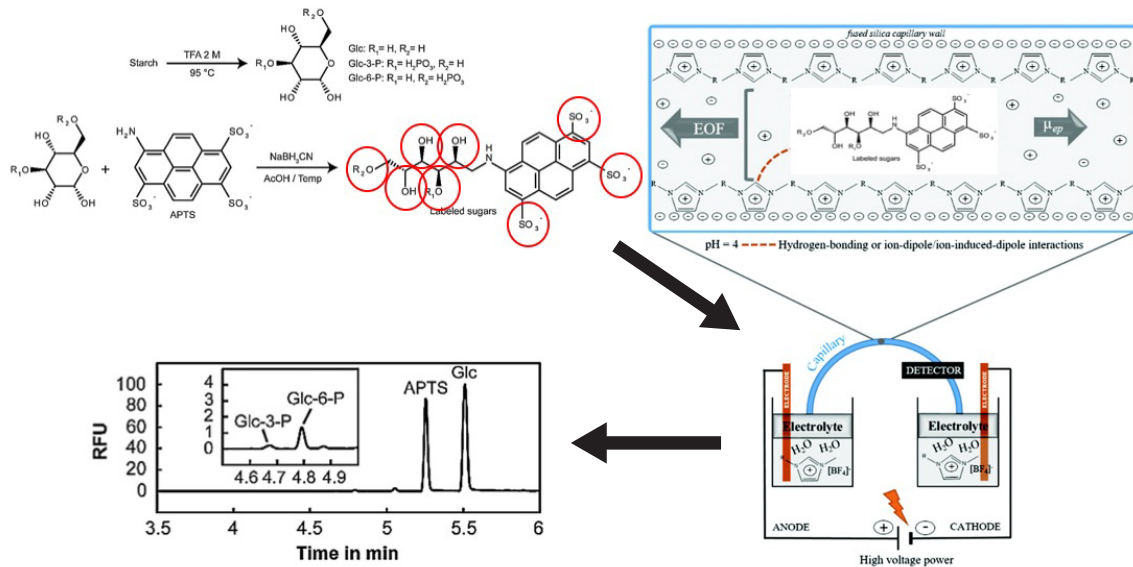
Figure 3-11 Fluorescence-Assisted Capillary Electrophoresis (FACE)
Flowchart of FACE determination of phosphorylated glucose moieties from *C. merolae* floridean starch. Starch was hydrolyzed with a mild TFA acid to preserve the loss of C6- or C3-phosphoesters. After hydrolysis, there were three potential glucose moieties; glucose, C6-glucose, and C3-glucose. These glucose moieties were then dried, labelled with the charged fluorophore, APTS, and derivatized via reductive amination by cyanoborohydride. With the addition of a phosphate this causes the charge of the derivatized glucose to become more negative. This caused a shift in electroosmotic flow (EOF) of the sample or analyte when applied to the electric field. Using standards such as Glucose 3-phosphate and Glucose 6-phosphate, we identified where these phosphorylated glucose molecules eluted. Adapted from Verbeke et al. 2016 (93).
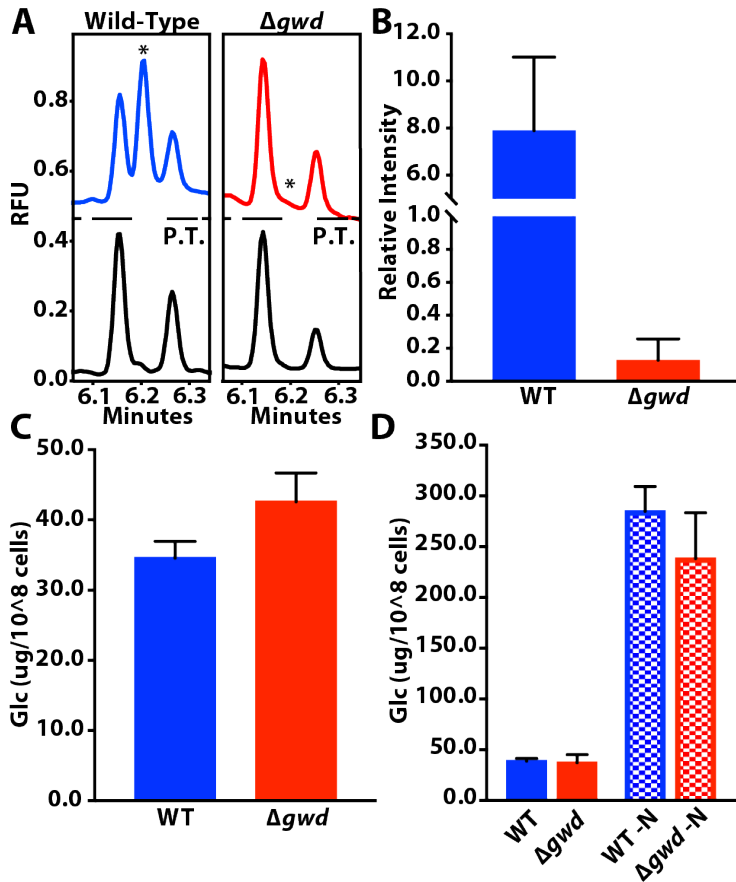
Figure 3-12 Glucose 6-phosphate and floridean starch content under continuous light.
A) Representative electrophoretic profiles of phosphate determination by fluorescence-assisted capillary electrophoresis (FACE). Blue and red profiles signify untreated hydrolyzed floridean starch FACE signal for WT and Δ*gwd*, respectively. Each sample was treated with alkaline phosphatase, the corresponding black FACE signal depicts the removal of the phosphate from the glucose-phosphate species (*). FACE analysis performed by Dr. Nicolas Szydlowski and Stanislas Helle. **B)** Gas chromatography mass spectrometry (GCMS) identification of glucose 6-phosphate in floridean starch purified from WT and Δ*gwd* *C. merolae* cells grown in continuous light. **C)** Floridean starch content in WT and Δ*gwd* cells grown in continuous light. **D)** Floridean starch content in WT and Δ*gwd* cells grown in continuous light after 48 hours with or without nitrogen containing media. MA2 media with nitrogen (+N), solid colored bars; MA2 media without nitrogen (-N), checkered colored bars.

Common Name	Species	Total phosphate content (‰)	Content of Glc-3-P (‰)	Content of Glc-6-P (‰)
Potato[#]	*Solanum tuberosum*	2.73 ± 0.21	0.52 ± 0.03	2.21 ± 0.19
C. merolae	*Cyanidioschyzon merolae*	0.888 ± 0.05	0.048 ± 0.01	0.840 ± 0.049
GWD Knockout	*Cyanidioschyzon merolae*	0.031 ± 0.01	0.002 ± 0.01	0.029 ± 0.04
Arabidopsis[#]	*Arabidopsis thaliana*	0.62 ± 0.04	0.072 ± 0.01	0.55 ± 0.03
Maize[#]	*Zea mays*	0.034 ± 0.013	ND	0.034 ± 0.013

Figure 3-13 Starch phosphate content comparisons
Starch phosphate content between various model organisms via FACE. #, values from Verbeke et al. 2016 (93). Performed by Dr. Nicolas Szydlowski and Stanislas Helle from the Universitè de Lille.
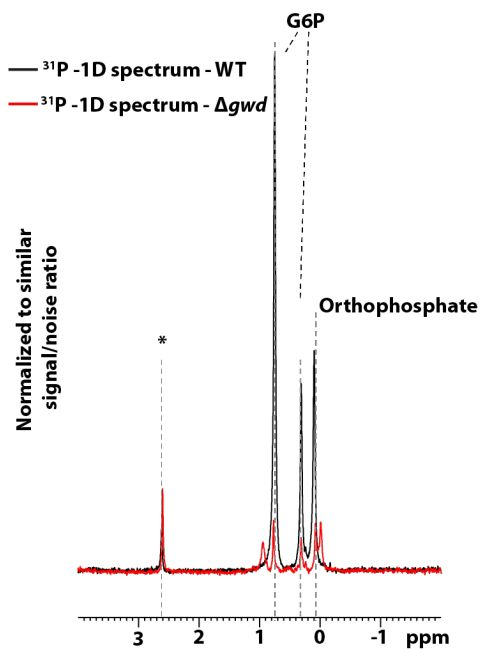
Figure 3-14 Phosphate content by ^{31}P-NMR analyses.
Normalized 1D spectrum of WT and Δ*gwd* floridean starch. Asterisk (*) represents non-glucosyl attached phosphate as determined by HMBC. G6P values were determined enzymatically to be about 0.9 and 0.03 mmol/mol glucose in WT and Δ*gwd* floridean starch, respectively. NMR analyses were performed by Dr. Felix Nitschke.
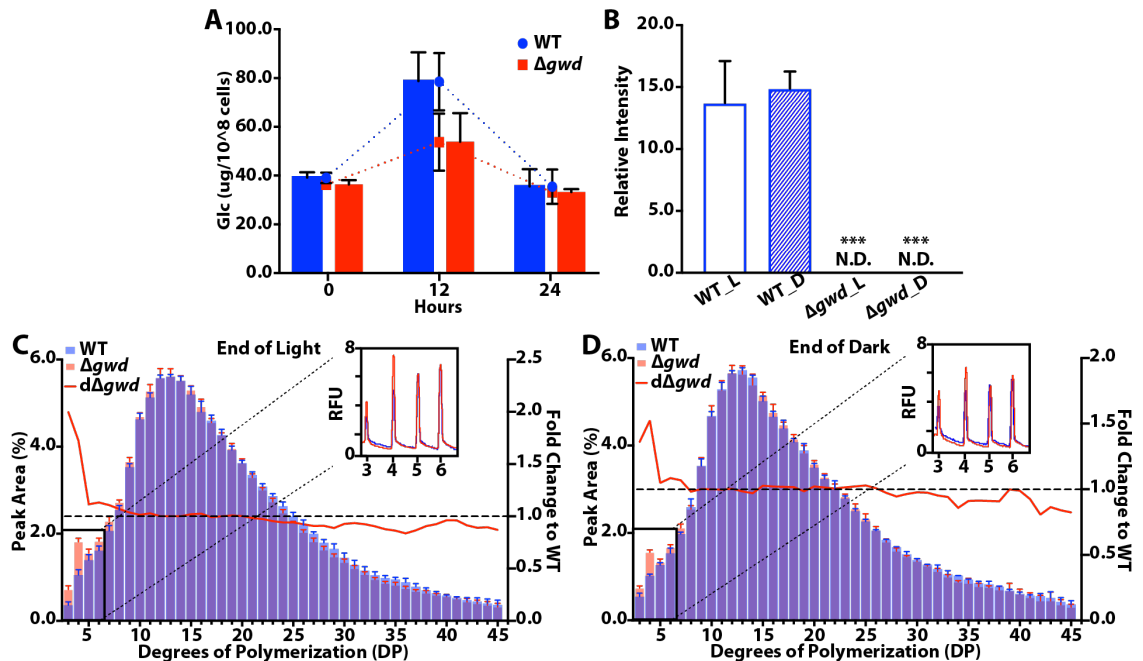
Figure 3-15 Degree of phosphorylation, floridean starch content, and amylopectin structure under diurnal growth
A) Floridean starch content from *C. merolae* WT (Blue) and Δ*gwd* (Red) cells grown under diurnal conditions for 24 hours. Rates of synthesis and degradation are presented by dashed lines. **B)** GCMS quantification of glucan-derived glucose 6-phosphate after 12 hours light (day, open bars) and 12 hours dark (night, shaded bars). **C-D)** Quantification of chain-length distribution from WT (blue bars) and Δ*gwd* (red bars) *C. merolae* granules using FACE at the end of 12 hours light **(C)** and dark **(D)**. Peak area fold change (red line) of Δ*gwd* compared to WT peak area percentages of chain lengths. Inset, representative electrophoretic profile of Δ*gwd* (red) DP 3-6 compared to profile of WT (blue) in relative fluorescent units, RFU. Each value for **A-D** is the mean of 3 WT or Δ*gwd* lines ± SD.
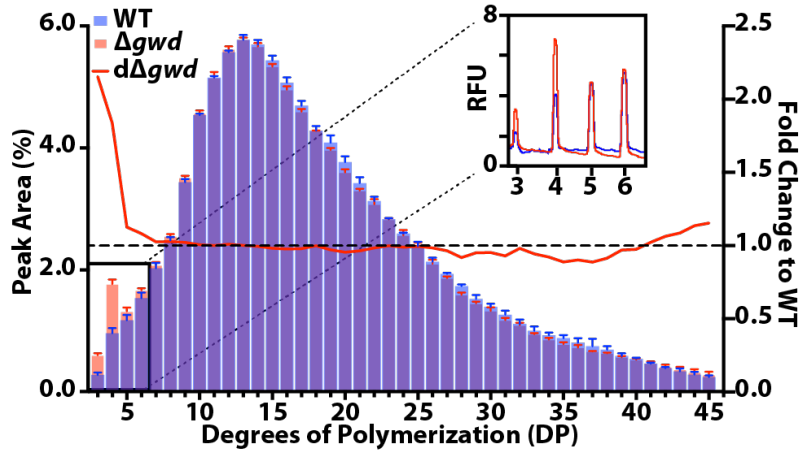
Figure 3-16 Amylopectin structure under continuous light growth.
Quantification of chain-length distribution from WT (blue bars) and Δ*gwd* (red bars)
C. merolae floridean starch granules using FACE after 48 hours continuous light.
Peak area fold change (red line) of Δ*gwd* compared to WT peak area percentages
of chain lengths. Inset, representative electrophoretic profile of Δ*gwd* (red) DP 3
and 4 compared to profile of WT (blue) in relative fluorescent units, RFU. Each
value is a mean of three WT or Δ*gwd* lines ± SD.
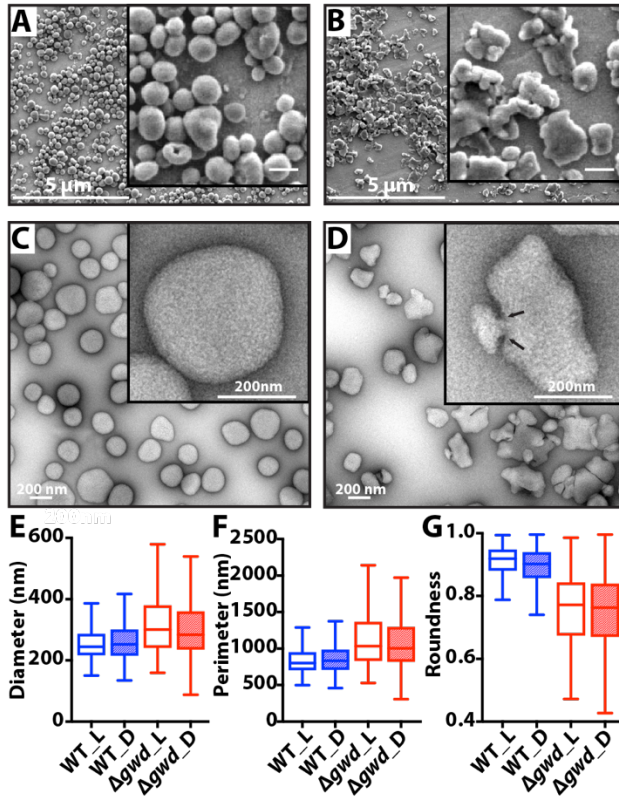
Figure 3-17 Morphology of floridean starch granules from *C. merolae* WT and Δ*gwd* cells grown in diurnal light.
Scanning electron micrographs of native granules from WT **(A)** and Δ*gwd* **(B)** cells grown under diurnal conditions. Granules were isolated after a 12h photoperiod. Inset micrograph scale bar = 200 nm. Transmission electron micrographs of negative-stained granules from WT **(C)** and Δ*gwd* **(D)** cells after 12h period of light. Black arrows in **D**, highlight regions of depression observed in Δ*gwd* granules. **E-G)** Quantification of transmission electron micrographs with respect to diameter (**E**, nm), perimeter (**F**, nm), and roundness (**G**, scale 0 – 1.0). Shaded boxes represent granules collected at the end of a 12-hour period of darkness while open boxes represent granules collected at the end of a 12-hour period of light. Analyses were processed with the Tukey method to identify outliers below the 25th percentile minus 1.5 times IQR (inter-quartile range) and above the 75th percentile plus 1.5 times IQR. Images were taken by Dr. Jean-Luc Putaux.

106
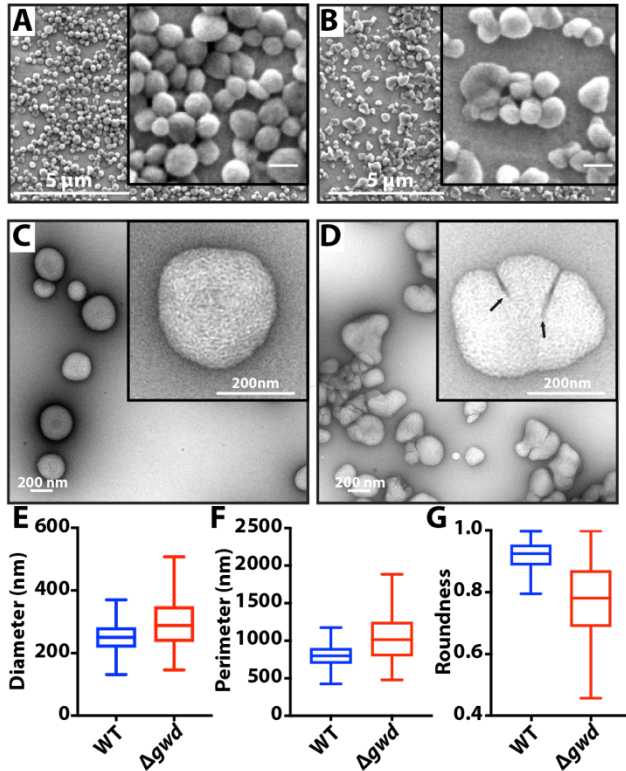
Figure 3-18 Morphology of floridean starch granules from *C. merolae* WT and Δ*gwd* cells grown in continuous light.

Scanning electron micrographs of native granules from WT **(A)** and Δ*gwd* **(B)** cells grown under continuous light conditions. Granules were isolated after 48 hours. Inset micrograph scale bar = 200 nm. Transmission electron micrographs of negative-stained granules from WT **(C)** and Δ*gwd* **(D)** cells after 48 hours continuous light. Black arrows in **D**, highlight regions of depression observed in Δ*gwd* floridean starch granules. **E-G)** Quantification of transmission electron micrographs with respect to diameter (**E**, nm), perimeter (**F**, nm), and roundness (**G**, scale 0 – 1.0). Analyses were processed with the Tukey method to identify outliers below the 25th percentile minus 1.5 times IQR (inter-quartile range) and above the 75th percentile plus 1.5 times IQR. Images were taken by Dr. Jean-Luc Putaux.
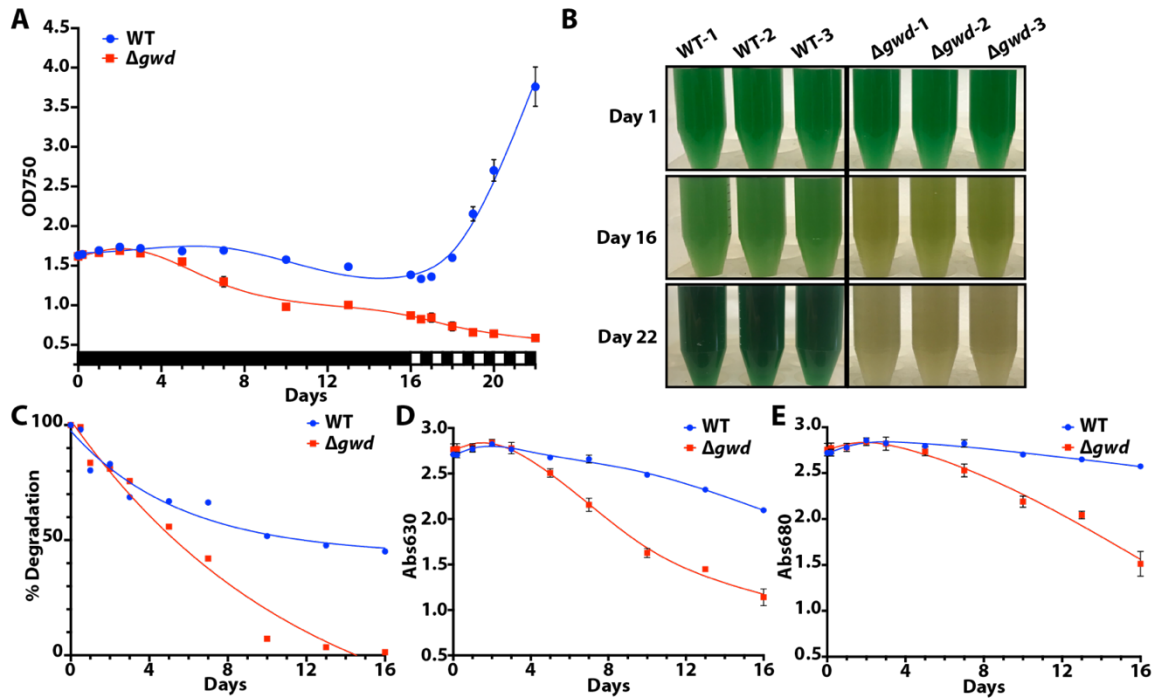
Figure 3-19 Survival and recovery after prolonged dark stress
A) Optical density (OD750) of cells cultured under 16 days of continuous dark stress followed by reintroduction of diurnal light regime. Black bar segments along x-axis represent periods of darkness while white bar segments represent periods of light. **B)** Changes in the culture color during the experimental period. Day 1; starting cultures, day 16; cultures at the end of prolonged dark stress, day 22; and cultures at the end of diurnal light reintroduction. **C)** Percentage of initial starch levels using amyloglucosidase-dependent hydrolysis. **D)** Phycocyanin absorption levels at 630 nm. **E)** Chlorophyll α absorption levels at 680 nm. All values represent the mean $\pm$ SD of three lines of WT and Δgwd cultures.

CHAPTER 4. ABERRANT POLYGLUCAN STRUCTURE, GRANULE MORPHOLOGY, AND NUTRIENT-SCAVENGING: EVIDENCE TOWARDS THE ROLE OF LAFORIN IN *CYANIDIOSCHYZON MEROLAE*

4.1 Introduction

Polysaccharides are glucose-rich biopolymers that are one of the most efficient forms of energy storage molecules throughout all kingdoms of life (228). Glycogen is a polysaccharide made up of short linear chains (~13 on average) of glucose residues linked by α-1,4-glycosidic bonds with continuous α-1,6 branches throughout (55). The short linear chains and the branching pattern of glycogen can allow up to ~55,000 glucose residues to be stored in a water-soluble state (55).

Similar to glycogen, amylopectin is also an α-1,4-linked polymer; however, it has clustered α-1,6 branches and is the main constituent of starch (70-90%). Starch is widely produced in the plastids of green algae and land plants and is comprised of two glucose polymers, amylopectin and amylose. The average length of linear α-glucan chains of amylopectin typically range from 20-25 glucose residues, consequentially the longer, clustered chains form double helices with neighboring chains, producing crystalline layers (lamellae) (95). The semi-crystalline layers of adjacent double helices exclude water rendering the starch granule water-insoluble. Amylose, the minor component of starch (10-30%), is a predominantly linear α-1,4-linked polymer with rare α-1,6 branch points and is thought to intwine through the spaces between semi-crystalline regions of amylopectin (60, 63, 68).

Another key characteristic of starch and glycogen is the presence of covalently bound phosphate located at the C2-, C3-, and C6-hydroxyls of glucose residues; however, C2 phosphorylation has not been routinely detected in starch analyses (82, 85, 89, 90). Phosphorylation is the only known natural covalent starch modification which has been shown to occur during synthesis and degradation of starch, but the levels of phosphorylation are much higher during degradation (160, 229, 230). On the other hand, increased phosphorylation activity during degradation may not lead to a change in overall total phosphate content (160). Phosphate groups are also predominantly linked to the semi-crystalline

amylopectin species of starch therefore influencing the structure of starch, such as crystallinity and other physicochemical properties (231, 232).

Starch-like semi-crystalline polysaccharides (also called polyglucans) are also found in the cytosol of red algae, termed floridean starch, which generally contain lower amounts of amylose much like that of *waxy* mutant starches and different branching patterns compared to Chloroplastida starch (233, 234). Floridean starch resembles a unique class of polyglucans, intermediate of higher plant starch and mammalian glycogen (73). The insolubility aspect of semi-crystalline polyglucans contained in red algae, green algae, and higher plants requires a subset of specialized enzymes to access, catabolize, and utilize the energy cache to maintain growth in times where photosynthesis is absent (i.e., dark periods) (69, 171). Reversible glucan phosphorylation has been found to be essential in facilitating normal degradation of starch in many higher plant model organisms; however, there is a significant gap in knowledge in regards to floridean starch metabolism and the role of reversible glucan phosphorylation in floridean starch-producing organisms (158, 230).

One such organism that produces floridean starch is the thermophilic red microalga, *Cyanidioschyzon merolae,* which has been rapidly advancing as a model organism for many fundamental photosynthetic processes. Due to its simple cellular structure and ease of cell cycle synchronicity, *C. merolae* began as a model organism to understand mechanisms of organelle division (25, 208-212). Since the whole genome sequence was available in the early 2000s, *C. merolae* has also been a part of large multiple comparative genomic studies (8, 22, 23, 235). *C. merolae* has one of the smallest eukaryotic genomes (~16.5 Mbp) due to genome reduction and horizontal gene transfers (HGT) resulting in a remarkable nonredundant genome (100, 236). The simple gene composition and low genetic redundancy of *C. merolae* has driven extensive improvements on genetic, molecular biology, and biochemical techniques, including the ability to produce stable gene-targeted knockouts (26, 28, 29, 197). Moreover, several studies have shown that *C. merolae* contains a minimal set of genes required to metabolize a polyglucan called semi-amylopectin floridean starch (containing no amylose) in the

110

cytosol (69, 73, 102). In this chapter, the term 'polyglucan' will be utilized to refer to the polysaccharide produced by *C. merolae.* Amongst these conserved genes, a single glucan phosphatase (laforin, CMT465C) and a putative glucan dikinase (GWD, CMT547C) were identified, suggesting that reversible glucan phosphorylation may also be present in *C. merolae* as a means to metabolize their polyglucan (185). Therefore, we proposed that the genetically manipulatable *C. merolae,* would be an excellent model to study the underlying mechanisms of reversible glucan phosphorylation.

Access to the starch has been shown to occur via a cyclic process of phosphorylation, amylolysis, and dephosphorylation known as reversible glucan phosphorylation (68, 95, 158). Initiation of starch degradation is catalyzed by two glucan dikinases, α-glucan, water dikinase (GWD) and phosphoglucan, water dikinase (PWD) which phosphorylate the C6- and C3-hydroxyls of glucose residues on the outer granular surface, respectively (90). Phosphorylation disrupts the amylopectin helices which permits access to the starch granule for amylolytic enzymes such as β-amylases and isoamylases (123, 158). Although phosphorylation can facilitate amylolytic degradation, the presence of phosphate groups can also prevent further degrading activity (164, 237). Removal of the phosphate groups by glucan phosphatases is necessary to progress normal starch degradation and essentially 'resets' the cycle (164). The glucan phosphatases Starch EXcess4 (SEX4) and Like Sex Four2 (LSF2) have different dephosphorylation specificities to preferentially remove phosphate groups at either the C6- or C3-position, respectively (Figure 4-1C) (175, 179, 181). The importance of reversible glucan phosphorylation is revealed by the loss of function in any of the genes encoding GWD, PWD, or SEX4 resulting in a starch excess phenotype in multiple higher plants (144, 146, 150, 164, 172, 173).

Upon the discovery that the SEX4 gene encodes a glucan phosphatase, the Dixon lab reported that the human protein laforin also dephosphorylates complex carbohydrates such as amylopectin (173, 238). Laforin is the founding member of glucan phosphatases and is the only phosphatase encoded in the human genome containing a carbohydrate binding module (CBM) (185). Laforin is a member of the

protein tyrosine phosphatase (PTP) superfamily and belongs to a diverse subgroup of enzymes, called dual-specificity phosphatases (DSPs), capable of dephosphorylating phosphate esters at both serine/threonine and tyrosine residues of proteinacious substrates in addition to non-protein substrates such as polysaccharides, lipids, and nucleotides (166). DSPs share a conserved catalytic CX_5R motif and substrate specificity varies amongst DSPs based on the design of their catalytic site (169). Human laforin is a bimodular protein consisting of a CBM of the family 20 (CBM20) followed by a DSP domain. Alternatively, SEX4 contains a chloroplast targeting peptide (cTP), followed by a DSP domain, a CBM of the family 48 (CBM48), and a carboxy-terminal (CT) motif (173, 239-241). SEX4 and laforin proteins have similar domain structure; however, these glucan phosphatases are not orthologues of each other based on domain orientation and class of CBM (**Figure 4-1A**) (171, 185). Although the glucan phosphatases; SEX4, LSF2, and laforin are classified as a DSP, these glucan phosphatases have a signature DSP motif in the active site comprised of a Cysteine, hydrophilic, Alanine, Glycine, long chain aliphatic, Glycine, Arginine ($C\zeta AG\Psi GR$) (169). Similarly, the signature DSP motif is highly conserved in *Cm*laforin (**Figure 4-1B**).

Intriguingly, the starch excess phenotype in *sex4* mutant *Arabidopsis* plants is analogous to the cellular phenotype found in Lafora disease (LD) patients with mutations of laforin (238). LD is a rare and fatal autosomal recessive neurodegenerative disorder resulting in severe epilepsy. Mutations of the gene encoding laforin (*EPM2A*) cause an accumulation of hyperphosphorylated insoluble polyglucans known as Lafora bodies (LBs) in the cytoplasm of nearly all cell types (183, 242-244). A recent report showed that LBs are remarkably similar to that of amylopectin of starch in plants based on their infrequent branching, level of phosphorylation, and longer α-glucan chains (245). Furthermore, human laforin fused to a cTP (to gain access to starch granules in the chloroplast) rescued the starch excess phenotype when transformed into *sex4-3 A. thaliana* plants (185). This work defined laforin as a functional equivalent of SEX. In the same study, a laforin-like orthologue was discovered in *C. merolae* through bioinformatic analyses which demonstrated that laforin is not solely found in vertebrates as

112

originally thought. This study hypothesized that *C. merolae* laforin activity is likely required to regulate insoluble carbohydrate metabolism in the organism.

C. merolae laforin, *Cm*laforin (CMT465C), is the only glucan phosphatase encoded by the *C. merolae* genome. It is a 532-amino acid protein comprised of a N-terminal predicted unstructured region, two CBM20s, and a DSP domain. Although *Cm*laforin is only 25% identical to its human laforin orthologue, both CBM20s contain four invariant aromatic residues that are a critical characteristic of a CBM20. In addition, the DSP domain contains the signature (CζAGΨGR) motif where the catalytic cysteine residue performs nucleophilic attack on the phosphorylated substrate (**Figure4-1B**). Due to the orientation of the CBMs to the DSP and the family of CBMs (CBM20 instead of CBM48), this protein is predicted to be more laforin-like than SEX4-like (185).

Utilizing biochemical analyses and cell biology, we demonstrate that *Cm*laforin has SEX4-like dephosphorylation specificity and is actively involved in the dephosphorylation of polyglucans in *C. merolae*. Mutants lacking laforin (Δ*laforin*) exhibit a significant increase of glucan-bound glucose 6-phosphate and this appears to have an impact on both synthesis and degradation of polyglucans. Additionally, Δ*laforin* polyglucan has an aberrant chain-length distribution profile and a drastically altered granule morphology compared to wild-type. Lastly, under light deprivation Δ*laforin* cells rapidly deplete major carbon and nitrogen reserves such as photosynthetic pigments (phycocyanin and chlorophyll α). However, the Δ*laforin* cells struggle to degrade their polyglucans in response to energy deprivation. Consequently, Δ*laforin* cells are unable to recover alongside their wild-type counterparts after losing their photosynthetic pigments, ultimately leading to cell death as opposed to cellular adaptation as seen in wild-type cells.

4.2   Results

4.2.1   *Cm*laforin characterization

Using ClustalW (195), the 532-amino acid sequence of *Cm*laforin was aligned with the smaller 331-amino acid human laforin (*Hs*laforin) to identify regions of disorder and domain boundaries similar to that described in Gentry et al. 2007

(185). Alignment with *Hs*laforin revealed a large 157 to 162-amino acid N-terminal region bearing no similarity to *Hs*laforin (**Figure 4-2**). Initial secondary structure prediction via Jpred (246) showed no secondary structure within the first 162 amino acids of *Cm*laforin (**Figure 4-2**). There was also a span rich in β-strands (162-358, *Cm*laforin numbering) that divvied up the CBM20 sequence of *Hs*laforin. We took the CBM20 sequence from *Hs*laforin and aligned it with stepwise regions from *Cm*laforin from 162-336. The CBM20 sequence of *Hs*laforin aligned with both of these region's sequences which led us to believe there are two CBM20s in *Cm*laforin (**Figure 4-3**). Both of the putative CBM20 regions of *Cm*laforin shared invariant glucan binding residues with *Hs*-CBM20 (**Figure 4-3**, highlighted in gray). The putative CBM20 regions also have two key residues conserved that are necessary for glucan binding in *Hs*laforin, W32 and K87 (**Figure 4-3**, highlighted in red). Interestingly, the second putative CBM20 has an Arginine residue in place of the Lysine residue at position 338 which likely serves the same purpose as both amino acid side chains are similar in properties.

Full-length *Cm*laforin was inputted into several secondary structure prediction servers, PredictProtein (247), and RaptorX (248), in order to verify that the first 157 amino acids of *Cm*laforin were unstructured as predicted initially by Jpred. All three secondary structure prediction servers identified that the ~157 N-terminal region of *Cm*laforin was highly disordered (**Figure 4-4A, B**). Based on these analyses, we cloned full-length *Cm*laforin as well as truncated constructs deleting the first 157 amino acids of the N-terminus (157-C) which conserved both CBM20s and DSP domain, and may aid in purifying stable protein (**Figure4-1A**, red asterisk).

4.2.2 *Cm*laforin displays SEX4-like specificity

The full-length and truncated *Cm*laforin protein were cloned into a pET28b expression vector fused to a N-terminal His$_6$-tag and expressed in BL21 (DE3) competent *E. coli*. The full-length *Cm*laforin protein was largely insoluble after lysing induced *E. coli* cells. The truncated 157-C protein was robustly expressed and the majority of protein was soluble. After separating the soluble protein from the insoluble protein and cell debris, the soluble protein was purified via affinity

chromatography followed by size-exclusion chromatography. The typical yield of recombinant *Cm*laforin (157-C) was ~20 mg/L *E. coli.*

As mentioned previously, human laforin dephosphorylates the C3- and C6-position of glucosyl residues of substrates; however, the C3-position is preferred (**Figure 4-1C**). Utilizing a novel radiolabeling assay, we can define the specificity of glucan phosphatases (**Figure 4-5**) (169, 174, 179, 181, 194). We used *A. thaliana sex1-3* phosphate-free starch as the substrate for phosphorylation and dephosphorylation. First, two separate reactions are set up with equal amounts of phosphate-free starch. In one pool, starch is incubated with GWD from *S. tuberosum* with $^{33}\beta$-ATP ('HOT'), then PWD from *A. thaliana* with unlabeled ATP ('COLD'). In the other pool, starch is incubated with GWD from *S. tuberosum* with unlabeled ATP ('COLD'), then PWD from *A. thaliana* with $^{33}\beta$-ATP ('HOT'). Each of these pools are phosphorylated at both the C6- and C3-positions; however, only one position is radiolabeled representing either C6-radiolabeled starch or C3-radiolabeled starch (**Figure 4-5**). As a control, we utilized recombinant *At*SEX4 protein that has been shown to preferentially dephosphorylate the C6-position (175). Results of the dephosphorylation assay confirm the C6-preference of SEX4 (**Figure 4-6**). Intriguingly, *Cm*laforin also dephosphorylates the C3- and C6-position of glucosyl residues, and it largely prefers the C6-position (**Figure 4-6**). The specificity of *Cm*laforin resembles that of the plant glucan phosphatase SEX4. Importantly, these data align with data presented in the previous chapter regarding *Cm*GWD. I previously demonstrated that GWD phosphorylates the C6-position and that WT *C. merolae* polyglucan contains phosphate at the C6-position. Thus, all data are in agreement regarding the importance of C6-phosphorylation of the *C. merolae* polyglucan.

4.2.3 Gene-targeted laforin knockout strain

To assess the function of laforin in semi-amylopectin metabolism, we created a targeted knockout strain that lacks the *Cmlaforin* gene (CMT465C). Approximately 2 kb linear fragments upstream (5'-end) and downstream (3'-end) of *Cmlaforin* were amplified by PCR from wild-type *C. merolae* genomic DNA. In

addition, a third linear DNA fragment amplifying the *URA5.3* gene (CMK046C) was produced with primers that are complementary to both the 5'-end and 3'-end *Cmlaforin* fragments. This complementation allowed us to generate a single ~6.7 kb linear DNA construct via an overlap extension PCR. The final knockout DNA construct contains ~2 kb of genomic DNA 5' to *Cm*laforin, the *URA5.3* gene, and ~2 kb of genomic DNA 3' to *Cm*laforin (**Figure 4-7A**). We used the recently developed *URA5.3* null, uracil auxotrophic strain T1 (33) as the parental strain for polyethylene glycol (PEG) transformation (28). After successful isolation and propagation of potential laforin knockout strains (Δ*laforin*), we screened for the incorporation of the gene-targeted knockout construct and the corresponding loss of laforin at the DNA and protein level of three independent lines (Figure 4-3B). Potential *laforin* knockout lines were first screened via PCR for both the incorporation of *URA5.3* and loss of *Cmlaforin* (**Figure 4-7B-a and -b**). The primers for incorporation of *URA5.3* were specific towards the gene-targeted knockout construct used for transformation. Therefore, the primers were designed to target a piece of the 5'-fragment of *Cmlaforin* and a piece of the incorporated *URA5.3* gene which would not be found in WT cells (**Figure 4-7B-a**). The second PCR was designed for an internal region of *Cmlaforin* (**Figure 4-7B-b**). Lines positive for *URA5.3* and negative for *Cmlaforin* via PCR were then assessed by immunoblot analysis. Using an α-Cm-laforin antibody previously generated (185), *C. merolae* cell lysate from WT and putative Δ*laforin* cells was probed by immunoblotting (**Figure 4-7B-c and -d**). Immunoblot analysis recognized endogenous laforin only in the wild-type *C. merolae* strain at the expected mass of 58 kDa validating the successful knockout of laforin in Δ*laforin* lines (**Figure 4-7B**).

4.2.4 Cell growth of Δ*laforin* lines in continuous and diurnal light

The three independent Δ*laforin* lines were grown under continuous and diurnal (12-hour photoperiod) conditions to evaluate cell proliferation. Under both conditions, cultures were supplied with 2% atmospheric CO_2 and photoperiods had a light intensity of 50 μmol m^{-2} sec^{-1}. There were no apparent disparities in the growth rate for the Δ*laforin* lines compared to wild-type under continuous and

diurnal conditions (**Figure 4-7C, D**). Although growth-rates were similar between Δ*laforin* and wild-type, cell imaging using brightfield and fluorescent microscopy showed a slight reduction in Δ*laforin* cell size (**Figure 4-7E**). Similar observations are seen in regards to *Arabidopsis* plants deficient in *sex4* which display reduced fresh weight of shoots compared to wild-type plants (172). These results show that laforin-deficient cells do not effect cell growth under continuous and diurnal conditions; however, the cells display a reduced overall cell size when compared to wild-type *C. merolae* cells.

4.2.5 Laforin-deficient polyglucan characterization

The role of laforin has been focused largely towards degradation/maintenance of glycogen similarly to that of SEX4 to starch in higher plants (80, 164, 165, 173, 174, 185). Therefore, we hypothesized that under synthesizing conditions such as continuous light or accumulating conditions such as nitrogen deprivation, laforin-deficient cells would not display a starch-excess phenotype. Asynchronous WT and Δ*laforin* cells were grown under continuous light, glucans were extracted by sonication (73), amyloglucosidase digested, and quantified by the R Biopharm Inc. D-Glucose Kit (Fisher). Strikingly, we observed a dramatic ~80% decrease in polyglucans compared to wild-type cells (**Figure 4-8A**). The *C. merolae* polyglucan was also analyzed by a recently developed novel gas chromatography mass spectrometry (GCMS) technique (201) to assess C6-phosphate levels. This method utilizes mild acid hydrolysis and a two-step derivatization protocol to create volatile glucosyl species which can then be separated by gas chromatography (201). While Δ*laforin* cells produced far lower levels of polyglucan, there was a sizable 4-fold increase in C6-phosphate levels when normalized to total glucose (**Figure 4-8B**).

Altered phosphate concentrations have been shown to correlate with altered chain-lengths of starch and glycogen in potato tubers and in LD mice models, respectively (80, 87, 203, 249). In addition, expressing the R1 protein (GWD) from *S. tuberosum* in glycogen-producing *E. coli* causes an increase in glycogen-bound phosphate and an altered chain-length distribution (CLD) towards smaller degrees

117

of polymerization (DP) (250). To assess the CLD profile of Δ*laforin* polyglucans, cells were grown under continuous light for 48 hours, the polyglucan was extracted by sonication and purified by a 80% percoll gradient (73). We then performed CLD analysis using FACE to determine whether there were differences in the structure of amylopectin. The purified polyglucans were debranched via *Pseudomonas sp.* isoamylase after a brief solubilization at 98 °C for 10 minutes. Following isoamylase treatment, the debranched glucans were dried, APTS-labelled, and derivatized in a similar fashion to the acid-hydrolyzed glucose moieties to detect phosphate levels in **Chapter 3** (93, 199). The polyglucans produced in continuous light conditions of Δ*laforin* cells displayed an altered CLD profile which revealed an abnormal abundance of short chains from DP 4-10 while long chains greater than DP 12 showed no considerable decrease compared to wild-type (**Figure 4-8C**). The chain-length of Δ*laforin* polyglucans DP4-10 varied in fold increase, from 1 to ~2-fold, compared to WT polyglucans (**Figure 4-8C**).

4.2.6 Irregular granule morphology of laforin-deficient cell lines

Since there were significant structural alterations of the polyglucans in Δ*laforin* cells, we then hypothesized that this may lead to altered granule morphology. We grew cells under continuous light, purified granules via sonication and percoll gradient, and the native granules were processed and visualized them by scanning (SEM) and transmission (TEM) electron microscopy. Compared to wild-type, the polyglucan granules from Δ*laforin* cells were less spherical in shape and the majority were smaller (**Figure 4-9A, B**, respectively). The median diameter of wild-type granules was 254 ± 52 nm whereas Δ*laforin* granules measured 229 ± 39 nm, a 10% decrease (**Figure 4-15A**). Over 80% of Δ*laforin* granules also had an irregular rough surface and had several regions of depressions or crevices that seemed to originate from the core area (hilum) (**Figure 4-9B, D**).

Under nutrient-deprived stress conditions such as nitrogen deprivation, *C. merolae* accumulates polyglucans rapidly within the first 48 hours as it is the primary carbon sink compared to lipids (189, 191, 193). Therefore, we subjected cells to media absent of a nitrogen source for 96 hours which induced polyglucan

accumulation in both wild-type (5-fold) and Δ*laforin* (7-fold); however, Δ*laforin* cells still accumulated only 55% of that in wild-type cells after 96 hours (**Figure 4-10A**). Furthermore, the Δ*laforin* granule misshapen morphology was exacerbated compared to granules grown in regular media. There are considerable alterations of the granular surface exhibiting bulging protrusions compared to the smooth granular surface of wild-type granules (**Figure 4-10B, C**). The diameter of Δ*laforin* granules were 37% larger whereas wild-type granules were 22% larger compared to those in regular media (**Figure 4-15A**). In addition to the noticeable increase in diameter, there were also dramatic variations in distribution for perimeter and roundness of Δ*laforin* granules while wild-type granules displayed a remarkable conservation of uniform size and shape (**Figure 4-15B, C**). A notable observation was the additional presence of a small population, <20%, of smooth granules in Δ*laforin* samples. These data suggests that phosphate regulation significantly impacts polyglucan structure and granule morphology during accumulating conditions in *C. merolae*.

4.2.7 Morphology via Transmission electron microscopy (TEM)

We visualized the internal ultrastructure of WT and Δ*laforin* cells to provide us more insight on cell and polyglucan granule morphology. Cultures were grown under continuous light for 48 hours with and without nitrogen supplied in the media. An aliquot of cells were taken after the 48-hour period and gently centrifuged and resuspended in a fixative. Our collaborator Dr. Jean-Luc Putaux then processed our samples and post-stained with periodic acid thiosemicarbazide silver proteinate (PATAg) (204). This type of stain is analogous to periodic acid-schiff stain used to detect polysaccharides in histological studies (218, 219). Similar to SEM and TEM analysis of the purified polyglucan granules, the granules found in WT were uniform and spherical throughout the cytosol under nitrogen supplied conditions (**Figure 4-11A**, red arrows). In contrast, the polyglucans of Δ*laforin* cells were dramatically smaller and barely visible with PATAg staining under nitrogen supplied conditions (**Figure 4-11B**, red arrows). Nitrogen deprivation for 48 hours significantly reduces and deforms the plastid and conversely enlarges the

cytoplasm of *C. merolae* cells. Both WT and Δ*laforin* cells showed similar characteristics and a dramatic increase in polyglucan granules (**Figure 4-11C, D**). The intensity of the Δ*laforin* polyglucan granules were reduced compared to WT suggesting these granules may be less-dense.

4.2.8 Polyglucan characterization under diurnal conditions

Glucan phosphatases are critical to remove phosphate groups for progressive amylolytic activity by β-amylases and isoamylases (164). Consequently, SEX4-deficient *A. thaliana* plants, exhibit a progressive starch excess phenotype as the leaves age due to an imbalance of starch synthesis and degradation during diurnal conditions (172, 251). Similar results are found in laforin-knockout mice where glycogen accumulation progresses age-dependently (252). Using physiologically-relevant conditions, we subjected both strains to 12-hour/12-hour diurnal conditions and observed that Δ*laforin* cells underwent dramatically slower rates of glucan synthesis and even slower rates of degradation compared to wild-type (**Figure 4-12A**). The rate of synthesis for Δ*laforin* cells was 78% lower than wild-type cells while the rate of degradation was an astounding 95% lower. These data provide additional insights to the lower levels of total glucan in Δ*laforin* cells. Similar to continuous light growth, analysis of phosphate content by GCMS revealed a 4.33-fold increase in glucan-bound C6-phosphate at the end of the 12-hour photoperiod and a 4.55-fold increase after the 12-hour dark period (**Figure 4-12B**). The branching structure of the polyglucan produced diurnally in Δ*laforin* cells displayed a similar altered CLD profile to that of continuous light growth which revealed an abnormal abundance of short chains from DP 4-10. The long chains greater than DP 20 showed a 0% to 25% decreasing trend as the chain-length increased compared to wild-type polyglucans which was not seen in continuous light (**Figure 4-12C**). These data indicate that under diurnal growth, there is an imbalance in glucan synthesis and degradation, and consequentially, the lack of laforin impacts the proportion of longer DP chains differently than under continuous growth.

Alterations to the structure of Δ*laforin* polyglucan encouraged us to examine the morphology of polyglucan granules collected after each 12-hour period. Morphological analyses under SEM showed wild-type granules were uniformly round and smooth; however, Δ*laforin* granules were smaller in volume with a vast majority of granules displaying bumpy surfaces (**Figure 4-13 A, B**, respectively). Taking a closer look at the granules collected at the end of each 12-hour period under TEM observation unveiled that wild-type granules were consistently round and homogeneous in size (**Figure 4-13 C, E**). In stark contrast, Δ*laforin* granules were very heterogeneous with largely contoured surfaces and visible crevices from deep within the core of the granule (**Figure 4-13 D, F**). There was a minor portion of round, smooth granules found amongst the Δ*laforin* granules collected at the end of both 12-hour periods. Quantification of the morphological differences between wild-type and Δ*laforin* granules did not reflect the visual differences (**Figure 4-16A-C**). For example, wild-type granules had an average diameter of 262 ± 62 nm at the end of the night while Δ*laforin* granules had an average diameter of 258 ± 60 nm. These results may reflect the imperfect nature of quantifying and comparing parameters of larger round granules and smaller ruffled granules.

4.2.9 Laforin-deficient cells employ detrimental nutrient-scavenging in prolonged dark stress

Due to dramatic dysregulation of polyglucan metabolism observed in Δ*laforin* cells under continuous and diurnal conditions, we hypothesized that under a prolonged period of darkness, cells lacking laforin would not be able to utilize their carbon reserves properly. We grew dilute cultures under diurnal growth where all cultures were grown equally to an optical density (OD_{750}) ~1.5 and were similarly vibrant green in color (**Figure 4-14 A, B**, respectively.) We then abruptly introduced extended dark stress to the cultures and culture samples were collected throughout the experiment quickly under minimal light. Collected sampled were analyzed visually by spectral scans and polyglucan levels were defined. A threshold OD_{750} value of 0.9 for all cultures was chosen in which would mark the end of the dark stress to allow cultures to then recover under diurnal conditions.

Based on the experimental data, all cultures were reintroduced to diurnal light after sixteen days of darkness for six days to monitor recovery capabilities. From the onset of the dark period, the OD_{750} and color of the culture did not increase suggesting that cells were not dividing and instead were in a quiescent-like state (**Figure 4-14A**) (12). While the WT cells largely remained at constant levels, the Δ*laforin* cells began rapidly consuming major stores of carbon and nitrogen in the form of light-harvesting proteins such as phycocyanin and chlorophyll a after just one day in darkness (**Figure 4-14C, D**, respectively). After ten days, the Δ*laforin* cultures dropped close to the OD_{750} threshold and remained there for another six days (**Figure 4-14A**). Visually, the color of Δ*laforin* cultures were yellowish-brown after 16 days while wild-type cells were light-green (**Figure 4-14B**). Although Δ*laforin* cells contained 55% less polyglucan at the onset of prolonged dark stress, they were not able to degrade their energy-rich carbon store efficiently, as a means to survive compared to wild-type cells. Consequentially, Δ*laforin* cells retained more than 60% of their starch-like reserves whereas wild-type cells retained only 40%, but Δ*laforin* cells were unable to reenter the proliferative cell cycle upon reintroduction of light (**Figure 4-14E**). After sixteen days, we replenished culture media and reintroduced to 12-hour photoperiod diurnal growth to enable cells to begin cell growth. Wild-type cells began growing after two diurnal cycles and grew exponentially for the next four days with dense green cultures. In stark contrast, Δ*laforin* cultures did not recoup from the prolonged dark stress evident by culture turbidity reaching OD_{750} ~0.5 and the cultures essentially lacked all color (**Figure 4-14B**). The Δ*laforin* culture turbidity decreased 35% from the reintroduction of diurnal growth and there was also evidence that Δ*laforin* cells began lysing around sixteen days as the cell count began to drop rapidly for the following days.

4.3   Discussion

This study is the first to show that glucan dephosphorylation is necessary for normal insoluble carbohydrate metabolism in *Cyanidioschyzon merolae*. Understanding how extremophilic organisms such as *C. merolae* metabolize their 'floridean starch', opens up new avenues into the utilization of these organisms as renewable energy sources as well as translating this knowledge to other suitable

systems. Our data defines that *Cm*laforin preferentially dephosphorylates the C6-position of glucosyl residues of starch very reminiscent to the dephosphorylation specificity of SEX4 found in *A. thaliana* (174, 175). In contrast, human laforin was shown to preferentially dephosphorylate the C3-position of *in vitro* phosphorylated starch (169). Intriguingly, the specificity of glucan phosphatases is due to the orientation-specific binding of the glucan in the active site of the DSP (175, 181, 194, 253). Initially our bioinformatic analyses and domain arrangement led us to hypothesize that CMT547C was more similar to a laforin-like glucan phosphatase. However, our biochemical data suggests otherwise and that the DSP of *Cm*laforin orientates α-glucans so that the C6-hydroxyls are preferentially positioned in the active site, similar to that of SEX4. The signature motif of *Cm*laforin is also identical to *At*SEX4 but the addition of CBM20s to the N-terminal may be unique to *C. merolae* to associate the DSP domain with polyglucans produced by *C. merolae.* In a concurrent report, we found that *C. merolae* has an active GWD which is highly specific toward the C6-position of glucosyl residues as C3 phosphate levels were near or below detection level. Therefore, the presence of elevated C6 monophosphates may be strategic in the formation of semi-crystalline/insoluble carbohydrates.

We generated *C. merolae* lines deficient of laforin to better understand the biological function of laforin in carbohydrate metabolism. Although Δ*laforin* lines did not display a proliferative defect under normal growth conditions, Δ*laforin* cells were ~20% smaller in size compared to wild-type cells. Similarly, SEX4-deficient *Arabidopsis* plants also displayed reduced fresh weight of the shoots under diurnal growth (172). However, in transgenic potato and rice lines where SEX4 was suppressed, there were no observable differences in plant morphology (232, 254). The compilation of these results clearly imply species-specific roles for starch-degradation and utilization. Under normal growth conditions, Δ*laforin* lines displayed a significant decrease in semi-amylopectin levels although the decrease was less substantial under diurnal conditions. This result does not rule out that there may be a very slow progressive accumulation in Δ*laforin* cells if cultured over long periods of time (i.e., several months); although we did not observe this

phenomenon under our experimental conditions. It was surprising that the growth rate was not effected in Δ*laforin* lines under diurnal growth as many other mutants altering starch metabolism, whether an increase or decrease in starch levels, often suppressed growth rates (124, 150, 172, 255, 256). This would suggest that in *C. merolae,* cell proliferation is not dependent on the total size of the starch pool but may require a minimal of ~20% of wild-type levels to maintain growth. Algae have the unique ability to store carbon in other storage forms such as neutral triacylglycerides (TAGs). Several reports demonstrate the accumulation of TAGs in *C. merolae* upon nutrient-stress conditions (191, 226). Less is known about role of floridoside found in *C. merolae* in the 1980s, which is analogous to sucrose in higher plants (52). Floridoside is a main source of soluble carbon of the Cyanidiales. If carbon is allocated to floridoside and soluble sugars, then *C. merolae* can bypass polyglucan storage under laboratory conditions. Much more progress is needed to fully understand polyglucan and carbon metabolism in *C. merolae.*

Glycogen found in LD (*epm2a^-/-*) mouse models, have a progressive increase in phosphate content, 4-fold higher in 3-month old mice (80). Similarly, the phosphate content of Δ*laforin* polyglucan granules were considerably (4-fold) higher than wild-type. In contrast, SEX4-deficient *Arabidopsis* starch displayed a 31% decrease in total phosphate content compared to wild-type starch *in vivo* due to the decrease in amylopectin content and release of phosphorylated starch degradation products (i.e. phospho-oligosaccharides) (164). Multiple studies have reported a correlation between phosphate content and the amylose:amylopectin ratio (Am:Ap) of higher plant starches (150, 163, 164, 257). However, *C. merolae* produces semi-amylopectin type floridean starch without amylose nor the enzyme to synthesize amylose (Granule-Bound Starch Synthase, GBSS) comparable to *waxy* mutant starches. Therefore, the relationship between phosphate content and amylopectin branching/structure are of increasing importance and our work may provide new insights into this relationship. Does the presence of phosphate alter substrate specificity, thus activity of starch synthases and branching enzymes? With a conservative polyglucan metabolism network, it is likely that alterations in

phosphate content dramatically affect starch synthases and branching enzymes in *C. merolae.* The overall semi-amylopectin structure from laforin-deficient lines was substantially altered in both CLD and morphology. The CLD profile of Δ*laforin* semi-amylopectin under normal growth displayed an abnormal abundance of short chains with DP 4-10 while long chains greater than DP 20 showed a decreasing trend only under diurnal conditions compared to wild-type. Intriguingly, α-glucan chains shorter than DP 12 are generally too short to transcend through the semi-crystalline region as well as capable of forming helical arrangements (258).

The altered structure of polyglucan translated to substantial granule-morphology differences between wild-type and Δ*laforin* samples. Compared to wild-type, the semi-amylopectin granules from Δ*laforin* lines were smaller and less spherical in shape. Many granules also had an irregular rough surface, multilobed, and had several fissure-like regions that appeared to originate near the hilum (core). Although fissure-like regions have been seen in previous reports regarding starch synthase III (SSIII) antisense lines, these type of alterations have not been observed in transgenic lines where a glucan phosphatase has been eliminated or suppressed (259, 260). In SSIII antisense lines of potato, there was also a direct positive correlation between reduction of starch synthase activity and phosphate content (259). The CLD profile of SSIII antisense line (line 12) had higher proportions of DP 6-10 similar to a SSII mutant line (*st-3*) in *Chlamydomonas* (261). There is only one UDP-glucose starch/glycogen synthase (CMM317C) as well as one starch branching enzyme (CMH144C) encoded in the *C. merolae* genome for the synthesis and branching of semi-amylopectin. Furthermore, LBs in LD patients also display altered chain-length and branching patterns; however, the mechanism remains unresolved (262). Under nutrient-stress conditions such as nitrogen deprivation that promote semi-amylopectin accumulation in *C. merolae*, Δ*laforin* cells accumulated only 55% of that in wild-type cells after 96 hours. Although Δ*laforin* cells accumulated less carbohydrates compared to wild-type, there was a comparable fold increase to wild-type under these conditions. Furthermore, Δ*laforin* granule morphology was expressively pronounced compared to granules grown in regular media. Therefore, these results suggest the loss of laforin does

not likely decrease the activity of these synthesizing enzymes but more likely alters the specificity and arrangement of their activity. The latter could explain the wide size distribution of granules compared to wild-type. These data suggest that phosphate content maintenance significantly impacts polyglucan structure and granule morphology in *C. merolae*.

Under more physiologically-relevant conditions, Δ*laforin* cells underwent considerably slower rates of polyglucan synthesis and even more dramatically slower rates of degradation compared to wild-type under diurnal conditions. The branching structure of semi-amylopectin produced diurnally in Δ*laforin* cells displayed a similarly altered CLD profile to that of continuous light growth with the addition of a decreasing trend of chains longer than DP 20 compared to wild-type which was not seen in continuous light. These data indicate that under diurnal growth, the loss of laforin further alters the chain-length ratio of short to long chains which is indicative of major restructuring of the semi-amylopectin granule. The morphology of Δ*laforin* granules were very heterogeneous with largely contoured surfaces and visible fissure-like crevices that were more prominent than under continuous light conditions. Plants possess intricate mechanisms to regulate carbon supply in and out of starch under diurnal growth therefore it is unclear if the reduced rate of semi-amylopectin synthesis in Δ*laforin* is a coordinated response to the lack of degradation during the night or due to the altered fine structure of the semi-amylopectin (222, 263).

Literature data on prolonged light deprivation of microalgae is relatively scarce. However, many primitive microorganisms have acquired survival strategies to endure unfavorable environments (264, 265). Under our experimental conditions, *C. merolae* is an obligate photoautotroph therefore prolonged dark stress is a drastic environmental change that reflects significant energy deprivation. Unlike nutrient deprivation conditions such as nitrogen depletion, organisms such as *C. merolae* must utilize the energy stores it has already produced as photosynthesis is absent and requires acclimation processes. Therefore, carbohydrate reserves and light-harvesting complexes serve as the major carbon and nitrogen sources for respiration processes in prolonged darkness. Both wild-type and Δ*laforin*

cultures did not increase in turbidity (OD_{750}) over the period of darkness similarly to that described in Moriyama et al. 2015 suggesting that the cell cycle was in a quiescent-like state (12). Under prolonged light deprivation, Δ*laforin* cells rapidly showed signs of nutrient-scavenging degradation of photosynthetic pigments, phycocyanin (PC) and chlorophyll α, after just one day in darkness where as wild-type cells maintained a relatively constant level throughout the experiment. The balance between photosynthetic and semi-amylopectin degradation under light deprivation was drastically different between wild-type and Δ*laforin* lines. Loss of laforin leads to structural defects in semi-amylopectin ultimately impeding on synthesis and degradation. In this regard, Δ*laforin* cells only were able to access ~ 40% of their small carbon reserve in the form of semi-amylopectin which could have redirected attention to degrading photosynthetic pigments as an adaptation response. Consequentially, Δ*laforin* cells lost their ability for regrowth with the reintroduction of light as our data indicates major photosynthetic pigment loss. Target of Rapamycin (TOR) is a key regulatory protein essential to the nutritional status of *C. merolae* and plays a critical role in semi-amylopectin accumulation (189, 191, 226). TOR-inactivation was recently found to lead to dephosphorylation of glycogenin (*Cm*GLG1), resulting in increased semi-amylopectin synthesis (189). Understanding the regulatory mechanisms behind semi-amylopectin metabolism in *C. merolae* under normal and various stress conditions requires further investigation; however, could lead to new insights into how to modulate carbohydrate metabolism for industrial utilization.
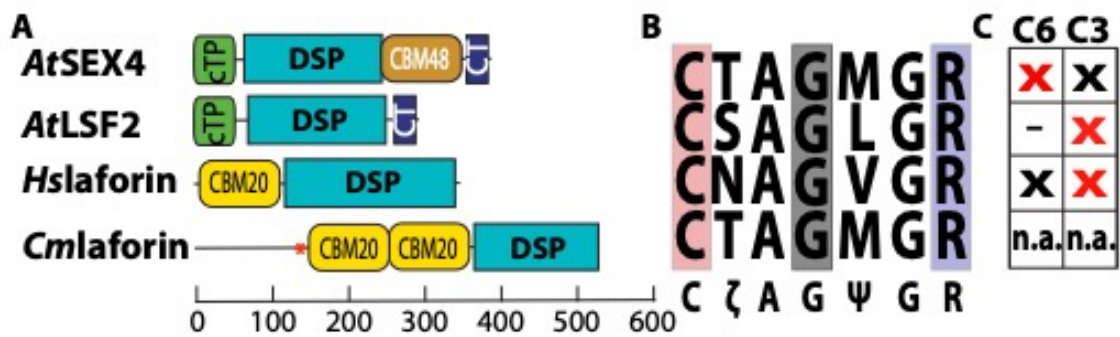
Figure 4-1 Domain structure, DSP active site alignment, and site specificity of glucan phosphatases.
A) Domain structures of SEX4 and LSF2 from *A. thaliana* (*At*) as well as laforin from *H. sapiens* (*Hs*) and *C. merolae* (*Cm*). *Cm*laforin (Δ157) is marked by red asterisk (*). Scale bar is amino acid length **B)** Multisequence alignment of the DSP active site. Catalytic cysteine and arginine residues highlighted in red and blue, respectively. Highly conserved glycine residue found in all PTPs shaded dark gray.
C) Site specificity of glucan phosphatases. Preferential dephosphorylation marked in red. (-) marks no activity for LSF2 on the C-6 position. (n.a.) not available.

```
HsLaforin     ------------------------------------------------------------      0
CmLaforin     MARIRTSDRRNTNDQAGSESRHRVPSMARAPAADSSGAQSTPAARRASEGVSVAEPPSKP     60

Jpred SS

HsLaforin     ------------------------------------------------------------      0
CmLaforin     AADSSGAQSTPAARRASEGVSVAGPPSKPAADSSGAQSTPAARFASEGVSVPEPPSKPAA    120

Jpred SS

HsLaforin     ------------------------------------------MRFRFGVVVPPAVAGARPE     19
CmLaforin     DSSGAQSTPAARGASEDISVPGPPSDIADTISKNDRSVTPTIPTLFRVYCH---TEFGDA    177
                                                        :     * *       :
Jpred SS                                                    ▶                ▶

HsLaforin     LLVVGSRPELGRWEPRGAVRLRPAGTAAGDGALALQEPGLWLGEVELAAEEAAQ------     73
CmLaforin     VVAAGSHDKLGNWEPAKALRLRHQCQVD------TPFRDCWEGEVDLVPETSFEFKFVRL    231
              ::..**: :**.***   *:***    .      . * ***:*. * : :
Jpred SS      ▶                               ▶          ▶

HsLaforin     ------------------------------------------------------------     73
CmLaforin     IGGDPQRALWETGPNRRAVIQRNSKDGCLIEVEWERTRVLFSIYYPTKEKQHLCVTGDLP    291

Jpred SS      ▶       ▶         ▶         ▶       ▶         ▶       ▶    ▬

HsLaforin     ------------------------------DGAEPGRVDTFWYKFLKREP-GGELSW     99
CmLaforin     EIGRWVEPGPVPMALSTTEERLETGGKGRRWSLTVSVPSTVGKFAYRYVLVDDNRQQTIW    351
                                             : *. *..* *::: :     : *
Jpred SS      ▬           ▬                 ▶        ▶

HsLaforin     EGNGPHHDRCCTYNENNLVDGVYCLPIGHWIEATGHTNEMKHTTDFYFNIAGHQAMHYSR    159
CmLaforin     EREPNRY---------------------ATLER----AVNGRLECFDANFVASLEFDE    384
              * :  ::                              :       *:       ::.:..
Jpred SS      ▬          ▬                                            ▬

HsLaforin     ILPNIWLGSCPRQVEHVTIKLKHELGITAVMNFQTEWDIVQNSSGCNRYPEPMTPDTMIK    219
CmLaforin     ICPDIYIGPYPQTPEHVE--MMHEAGITAVLNLQTDEDFAHRSIP---------WSTLME    433
              * *:*::*   *:    *** : ** *****:*:**: *:.:.*         .*:::
Jpred SS      ▬         ▬              ▶

HsLaforin     LYREEGLAYIWMPTPDMSTEGRVQMLPQAVCLLHALLEKGHIVYVHCNAGVGRSTAAVCG    279
CmLaforin     TYTALEMQVIRCPIPDFNAEALMQLLPDAVRALDAALKAKRVVYVHCTAGMGRAPAVVVA    493
               *     :  *   * **:.:*. :*:**:**  *.* *:   ::*****.**:**: *.*  .
Jpred SS      ▶                                            ▶         ▬

HsLaforin     WLQYVMGWNLRKVQYFLMAKRPAVYIDEEALARAQEDFFQKFGKVRSSVCSL    331
CmLaforin     YLVWRRGMTLEDALSHVKARRAVAAPNVTVLEKVLRNPL-------------    532
              :*   *  .*... .: *:* .. :  .* :. .: :
Jpred SS      ▬       ▬           ▬
```

Figure 4-2 Human and *C. merolae* laforin alignment and secondary structure
Using ClustalW, Human (*Hs*) and *C. merolae* (*Cm*) laforin were aligned. Secondary structure prediction of *Cm*laforin by Jpred underneath each aligned segment. Black arrows, β-strands. Gray lines, helices.

```
HsLaforin           MRFRFGVVVPPAVAGARPELLVVGSRPELGRWEPRGAVRLRPAGTAAGDGALALQ-EPGL        59
CmLaforinCBM20-1    IPTLFRVYC---HTEFGDAVVAAGSHDKLGNWEPAKALRLRHQCQV------DTP-FRDC        50
CmLaforinCBM20-2    --VLFSIYYPT---KEKQHLCVTGDLPEIGRWVEPGPVPMALSTTEER---LETGGKGRR        52
                        * :                 : ..*.  ::*.*       : :

HsLaforin           WLGEVELAAEEAAQDGAEPGRVDTFWYKFLKREPG--GELSWEGN---------------       102
CmLaforinCBM20-1    WEGEVDLVPETS------------FEFKFVRLIGGDPQRALWETGPNRRAVIQRNSKDGC        98
CmLaforinCBM20-2    WSLT-----------VSVPSTVGKFAYRYVLVDD-NRQQTIWEREP--------------        86
                    *                       * ::::         .  **

HsLaforin           ----------        102
CmLaforinCBM20-1    LIEVEWERTR        108
CmLaforinCBM20-2    ----------         86
```

Figure 4-3 *Hs*laforin CBM20 alignments reveal two putative CBM20s
Using ClustalW, CBM20 of *Hs*laforin (residues 1-102) were aligned to two
segments of *Cm*laforin revealing two putative CBM20s. Invariant residues
highlighted in gray. Critical CBM20 residues for glucan binding highlighted in red.

A

```
>Cmlaforin
MARIRTSDRRNTNDQAGSESRHRVPSMARAPAADSSGAQSTPAARRASEGVSVAEPPSKPAADSSGAQSTPAARRASEGVSVAGPPSKPAADSSGAQSTPA
****************************************************************************************************
ARFASEGVSVPEPPSKPAADSSGAQSTPAARGASEDISVPGPPSDIADTISKNDRSVTPTIPTLFRVYCHTEFGDAVVAAGSHDKLGNWEPAKALRLRHQC
**********************************************************...........................................
QVDTPFRDCWEGEVDLVPETSFEFKFVRLIGGDPQRALWETGPNRRAVIQRNSKDGCLIEVEWERTRVLFSIYYPTKEKQHLCVTGDLPEIGRWVEPGPVP
....................................................................................................
MALSTTEERLETGGKGRRWSLTVSVPSTVGKFAYRYVLVDDNRQQTIWEREPNRYATLERAVNGRLECFDANFVASLEFDEICPDIYIGPYPQTPEHVEMM
....................................................................................................
HEAGITAVLNLQTDEDFAHRSIPWSTLMETYTALEMQVIRCPIPDFNAEALMQLLPDAVRALDAALKAKRVVYVHCTAGMGRAPAVVVAYLVWRRGMTLED
....................................................................................................
ALSHVKARRAVAAPNVTVLEKVLRNPL
..........................*
```

B
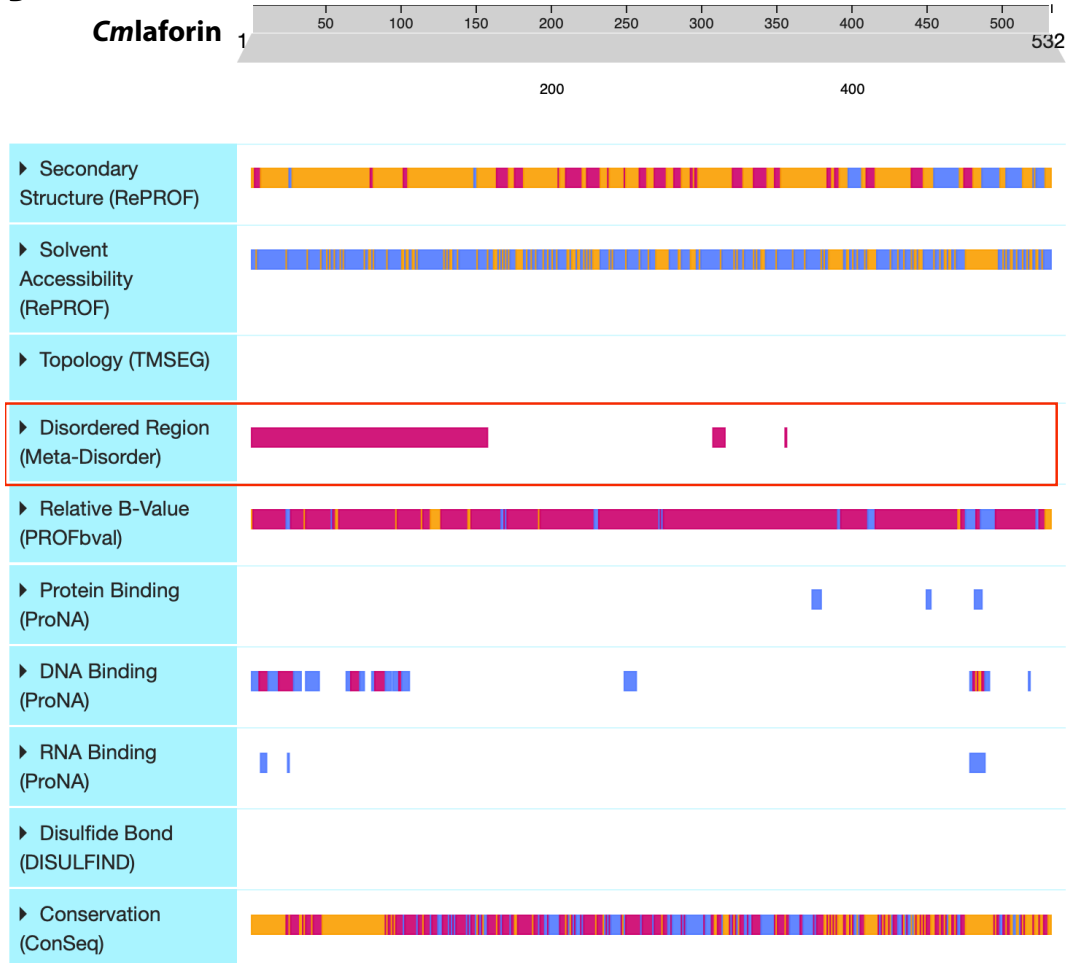
Figure 4-4 Disordered N-terminal region of *Cm*laforin
A) Secondary structure prediction server RaptorX designated highly disordered N-terminal region of *Cm*laforin. Asterisks, disorder. Periods, ordered. **B)** PredictProtein secondary structure server results of *Cm*laforin. Red box highlights regions of disorder. N-terminal region 1-157.
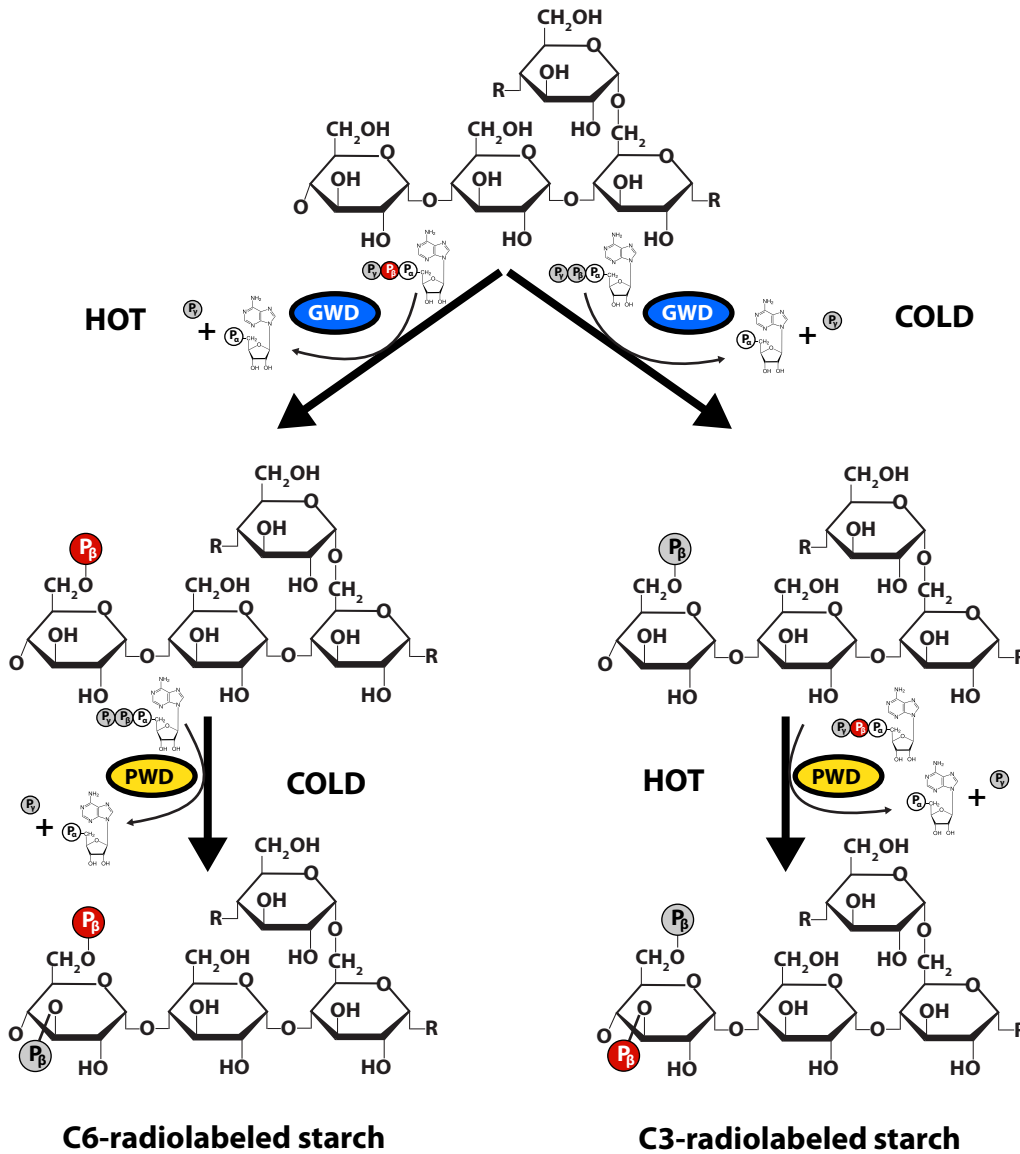
Figure 4-5 *In vitro* starch-radiolabeled site specificity dephosphorylation assay

Flow chart of *in vitro* radiolabeling of *A. thaliana sex1-3* phosphate-free starch for the use of site specificity dephosphorylation assay of glucan phosphatases. One pool of phosphate-free starch is phosphorylated with GWD and $^{33}\beta$-ATP, then phosphorylated with PWD and unlabeled ATP (C6-radiolabeled starch). The other pool of phosphate-free starch is phosphorylated with GWD and unlabeled ATP, then phosphorylated with PWD and $^{33}\beta$-ATP (C3-radiolabeled starch). These two specifically radiolabeled starches are then used as substrates for glucan phosphatases and quantified as percent of phosphate released in relative proportion to radiolabel incorporation by glucan dikinases.
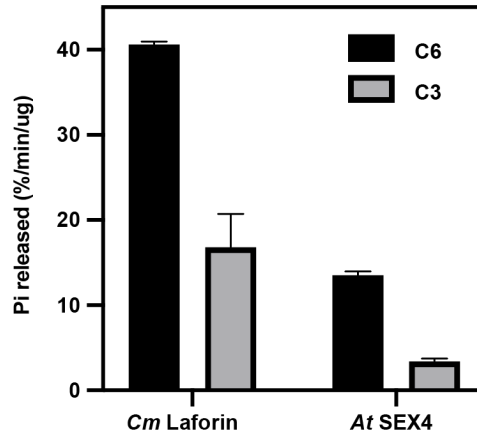
Figure 4-6 Glucan phosphatase dephosphorylation specificity.
Site specificity of *Cm*laforin dephosphorylation activity. *A. thaliana sex1-3* (phosphate-free) starch granules were phosphorylated as previously described in **Figure 4-5** (169, 175) and subsequently dephosphorylated. Black and gray bars represent [33]β-phosphate release (%Pi released•min^{-1}•ug^{-1}) from C6- and C3-positions, respectively. All assays were performed in triplicate; averages ± SD are shown.
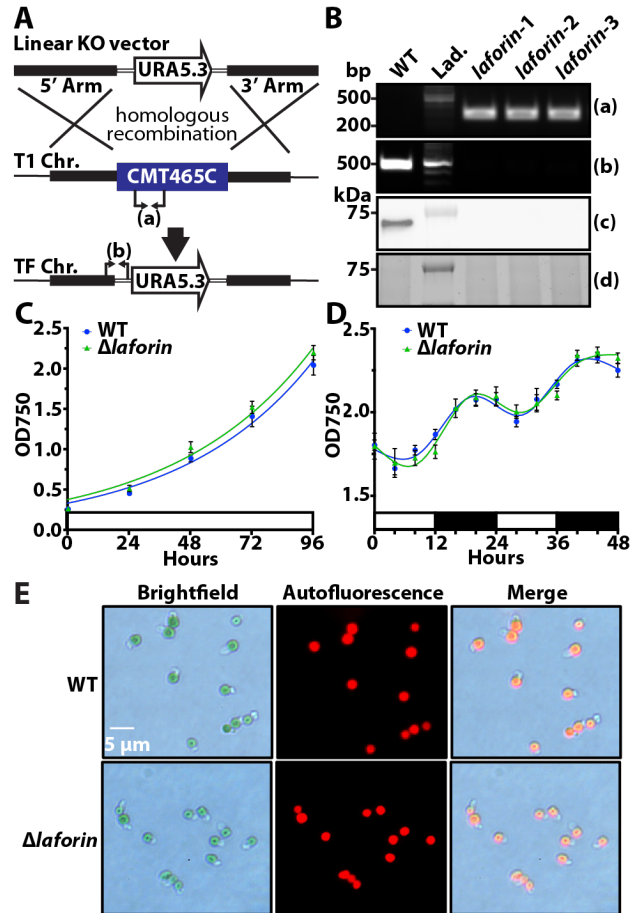
Figure 4-7 *C. merolae* **laforin knockout strategy, validation, and initial phenotypic characterization.**
A) A gene-targeted knockout strategy was utilized based on Taki et al. 2015. The *URA5.3* gene was introduced into the T1 strain to replace the CMT465C (*laforin*) gene locus. A linear DNA vector containing the *URA5.3* gene flanked by 2 kb homologous arms bordering CMT465C was generated. **B)** Putative Δ*laforin* lines were screened and validated by PCR. One primer set **(a)** screened for the incorporation of the *URA5.3* gene. A second primer set **(b)** screened for the presence/absence of *Cm*laforin. Whole cell lysates **(c)** of wildtype (WT) and potential laforin knockout lines (Δ*laforin*-1, Δ*laforin*-2, Δ*laforin*-3) were analyzed by immunoblotting with a polyclonal *Cm*laforin antibody. Total protein load **(d)** was analyzed on a stain-free TGX gel and imaged with a BioRad Imager. **C)** Growth curves of WT and Δ*laforin* cells grown in continuous light growth for 96 hours. **D)** Growth curves of WT and Δ*laforin* cells were grown in diurnal light (12h light/ 12h dark) for 48 hours. **E)** Representative brightfield and fluorescent (autofluorescence of plastids) microscopy images of WT *C. merolae* cells (top row) and Δ*laforin* cells (bottom row). Microscopy images were taken by Savita Sharma.
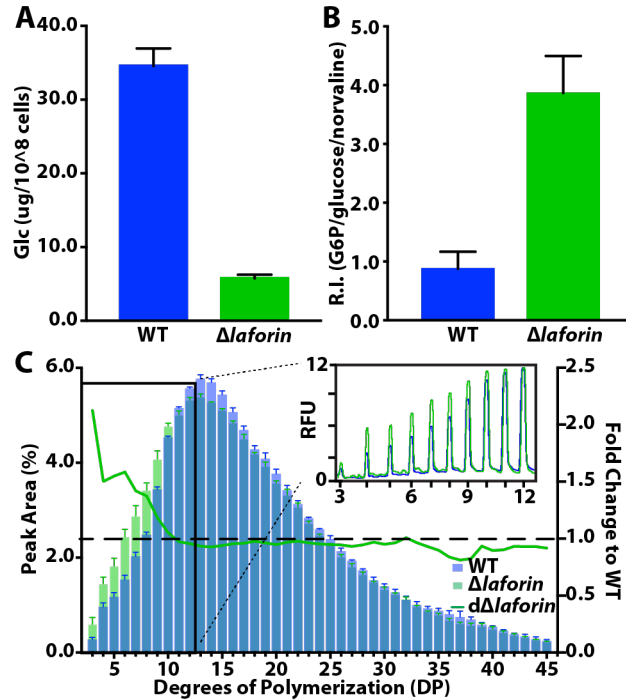
Figure 4-8 Continuous light polyglucan content and characterization
A) Polyglucan content measured by amyloglucosidase digestion and subsequent glucose measurement by the R Biopharm Inc. D-Glucose Kit (Fisher). **B)** Gas chromatography mass spectrometry (GCMS) identification of glucose 6-phosphate in polyglucans purified from WT and Δ*laforin C. merolae* cells grown in continuous light for 96 hours. **C)** Quantification of chain-length distribution from WT (blue bars) and Δ*laforin* (green bars) polyglucan using FACE at the end of continuous light. Peak area fold change (green line) of Δ*laforin* compared to WT peak area percentages of chain lengths. Inset, representative electrophoretic profile of Δ*laforin* (green) DP 3-12 compared to profile of WT (blue) in relative fluorescent units, RFU. Each value for **A-C** are the mean of three WT or Δ*laforin* lines ± SD.
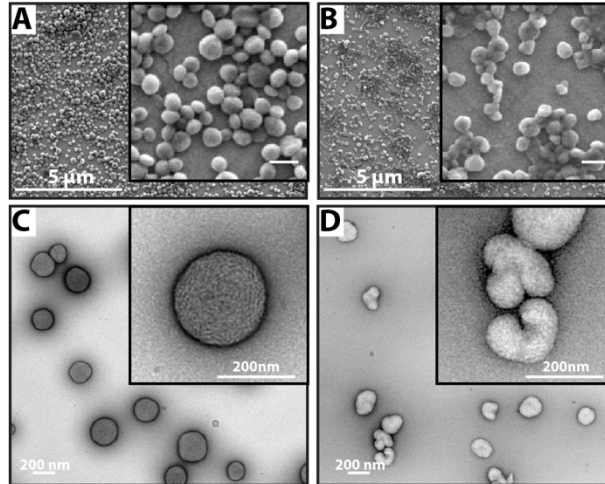
Figure 4-9 Morphology of polyglucan granules from *C. merolae* WT and Δ*laforin* cells grown in continuous light.
Scanning electron micrographs of native granules from WT **(A)** and Δ*laforin* **(B)** cells grown under continuous light conditions. Granules were isolated after 48 hours. Inset micrograph scale bar = 200 nm. Transmission electron micrographs of negative-stained granules from WT **(C)** and Δ*laforin* **(D)** cells after 48 hours continuous light. Images taken by Dr. Jean-Luc Putuax.
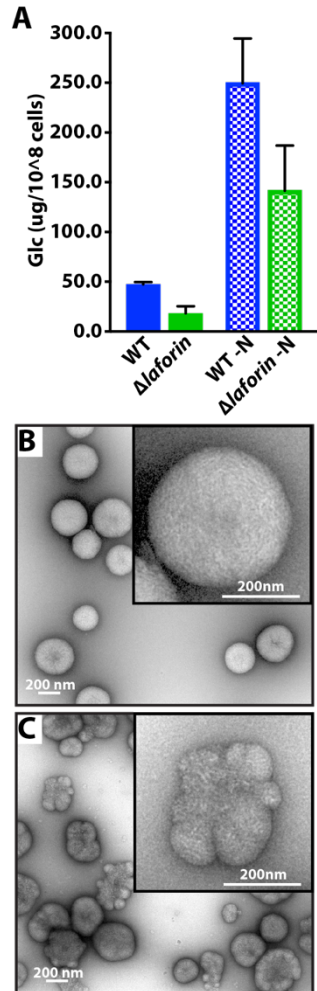
Figure 4-10 Polyglucan content and granule morphology after 96 hours of nitrogen deprivation
A) Polyglucan content in WT and Δ*laforin* grown in continuous light after 96 hours with or without nitrogen containing media. MA2 media with nitrogen (+N), solid colored bars; MA2 media without nitrogen (-N), checkered colored bars. Transmission electron micrograph of WT **(B)** and Δ*laforin* **(C)** granules after 96 hours of nitrogen deprivation, respectively. Images were taken by Dr. Jean-Luc Putaux.
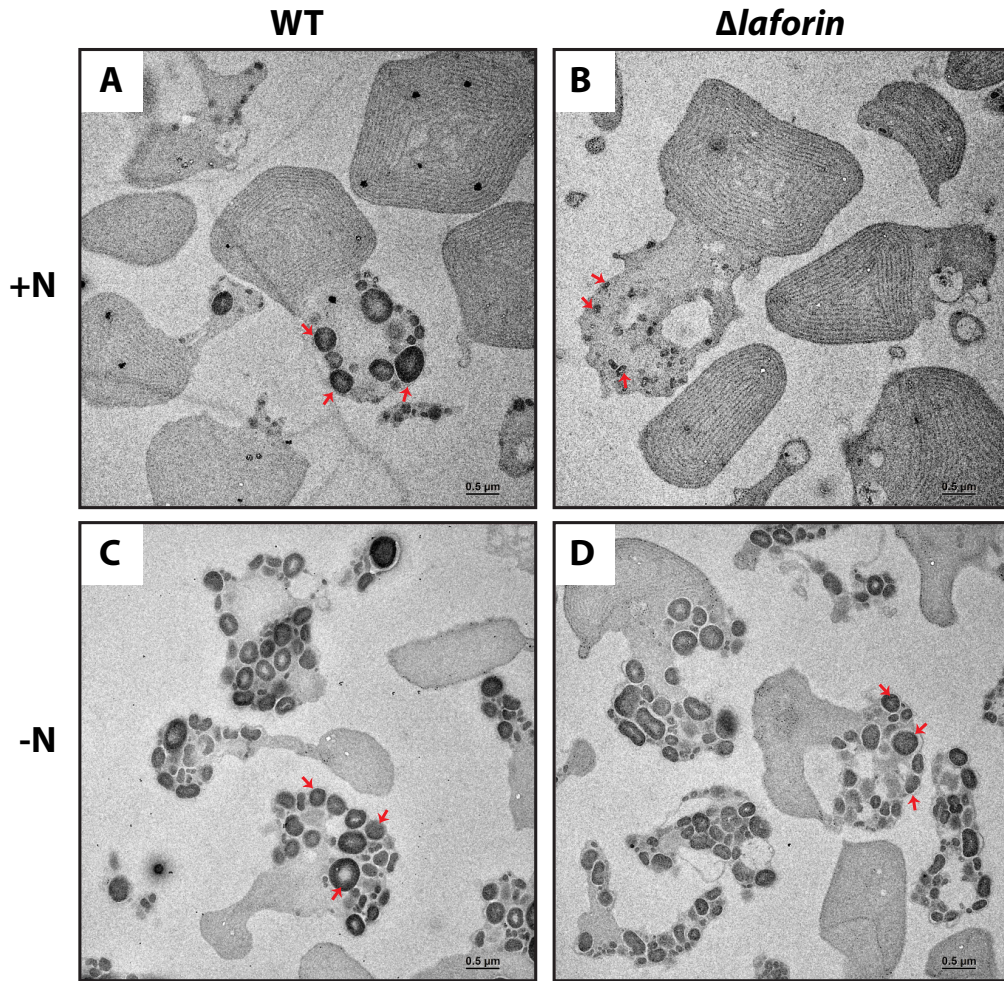
Figure 4-11 TEM images of PATAg stained ultrathin sections of *C. merolae* cells grown in continuous light with and without nitrogen deprivation
TEM images of ultrathin sections of WT (**A**) and Δ*laforin* (**B**) *C. merolae* cells grown in continuous light. TEM images of ultrathin sections of nitrogen-deprived WT (**C**) and Δ*laforin* (**D**) *C. merolae* cells grown in continuous light. Cells were collected at the end of a 48-hour period. Red arrows, starch granules. PATAg selectively stains polysaccharides therefore denser material will have a more electron-dense staining. Cells were processed, stained, and imaged by Dr. Jean-Luc Putuax.
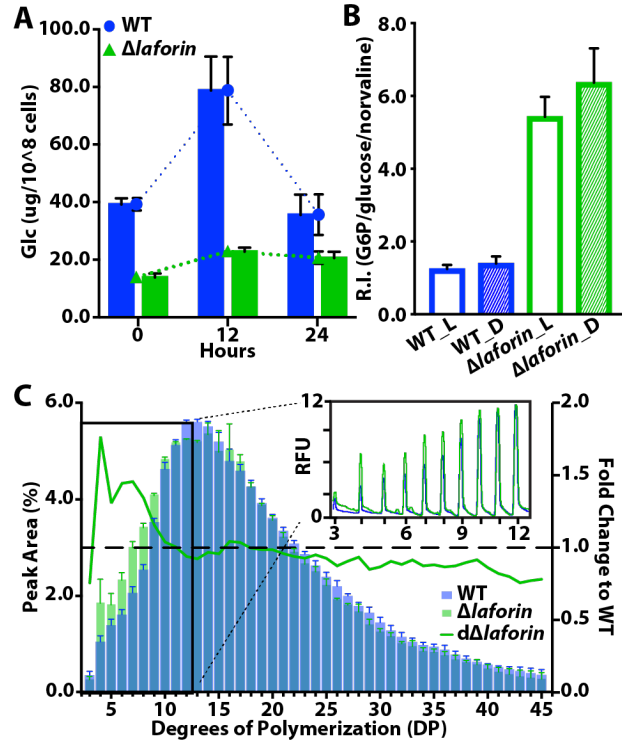
Figure 4-12 Diurnal polyglucan content, glucose 6-phosphate content and chain-length characterization
A) Polyglucan content from *C. merolae* WT (Blue) and Δ*laforin* (Green) cells grown under diurnal conditions for 24 hours. Rates of synthesis and degradation are presented by dashed lines. **B)** GCMS quantification of glucan-derived glucose 6-phosphate after 12 hours light (day, open bars) and 12 hours dark (night, shaded bars). **C)** Quantification of chain-length distribution from WT (blue bars) and Δ*laforin* (green bars) *C. merolae* debranched polyglucan using FACE at the end of 12 hours light. Peak area fold change (green line) of Δ*laforin* compared to WT peak area percentages of chain lengths. Inset, representative electrophoretic profile of Δ*laforin* (green) DP 3-12 compared to profile of WT (blue) in relative fluorescent units, RFU. Each value for **A-C** are the mean of three WT or Δ*laforin* lines ± SD.
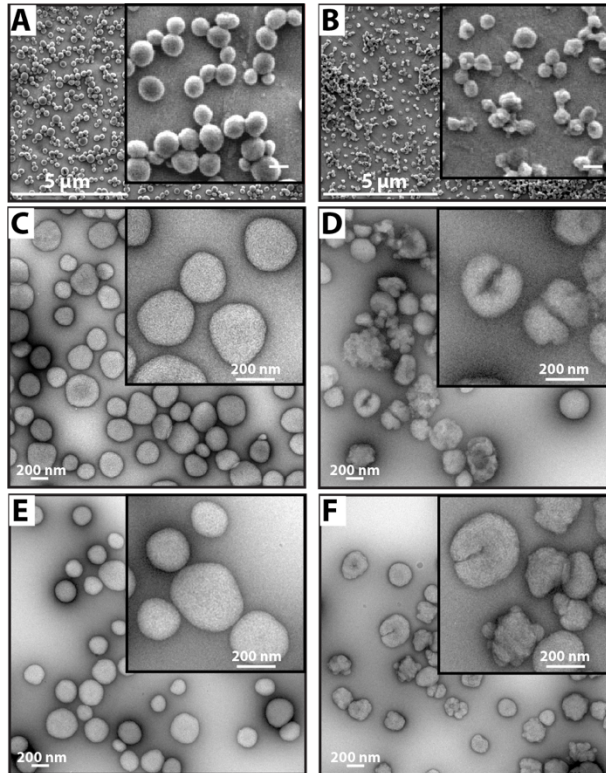
Figure 4-13 Morphology of polyglucan granules from *C. merolae* WT and Δ*laforin* cells grown in diurnal light.
Scanning electron micrographs of native polyglucan granules from WT **(A)** and Δ*laforin* **(B)** cells grown under diurnal conditions. Granules were isolated after a 12h photoperiod. Inset micrograph scale bar = 200 nm. Transmission electron micrographs of negative-stained granules from WT **(C,E)** and Δ*laforin* **(D,F)** cells after 12h period of light and 12h period of dark, respectively. Images were taken by Dr. Jean-Luc Putuax.
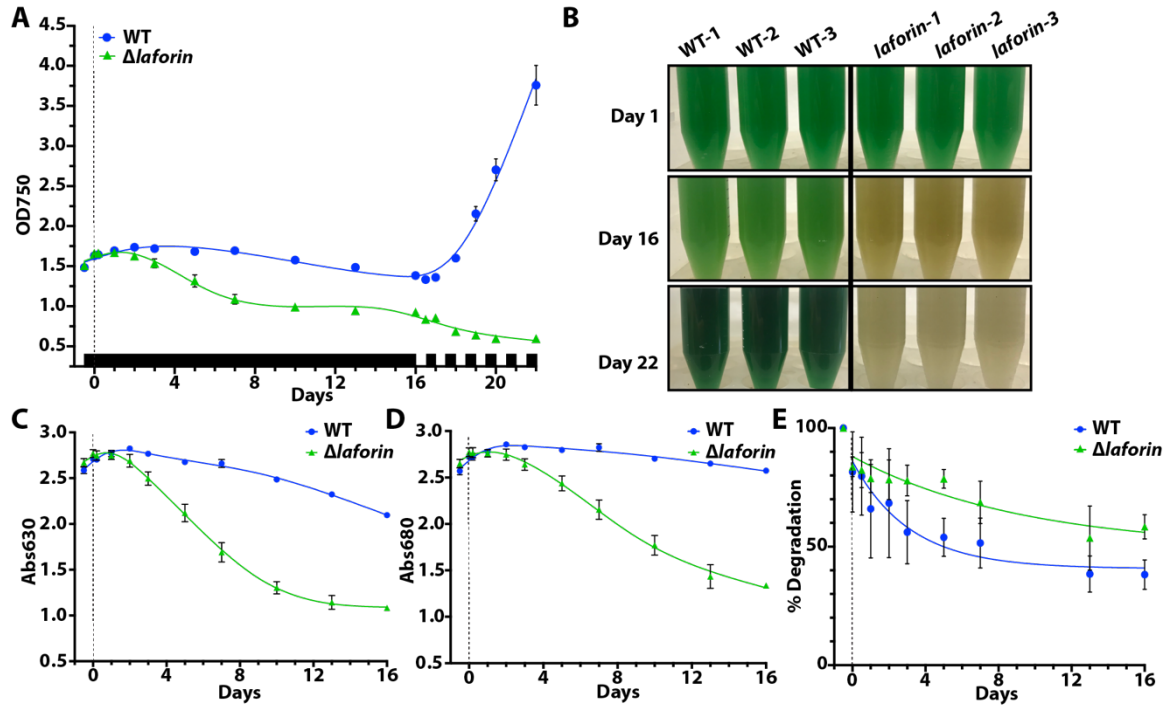
Figure 4-14 Survival and recovery after prolonged dark stress
A) Optical density (OD_{750}) of cells cultured under 16 days of continuous dark stress followed by reintroduction of diurnal light regime. Black bar segments along x-axis represent periods of darkness while white bar segments represent periods of light. **B)** Changes in the culture color during the experimental period. Day 1; starting cultures, day 16; cultures at the end of prolonged dark stress, day 22; and cultures at the end of diurnal light reintroduction. **C)** Phycocyanin absorption levels at 630 nm. **D)** Chlorophyll α absorption levels at 680 nm. **E)** Percentage of degradation from initial polyglucan levels using amyloglucosidase-dependent hydrolysis and glucose measurement by R Biopharm Inc. D-Glucose Kit (Fisher). Vertical dashed line represents start of extended dark stress. All values represent the mean $\pm$ SD of three lines of WT and $\Delta laforin$ cultures.
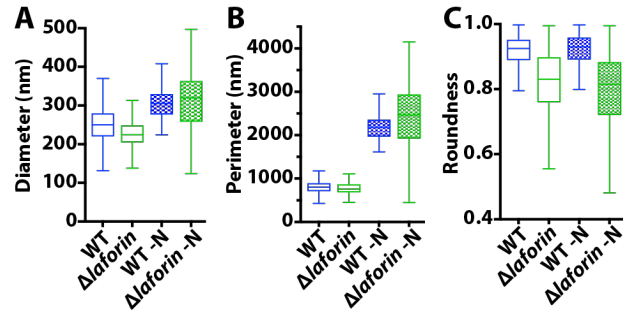
Figure 4-15 TEM polyglucan granule analysis from continuous light with or without nitrogen
A-C) Quantification of transmission electron micrographs with respect to diameter (**A**, nm), perimeter (**B**, nm), and roundness (**C**, scale 0 – 1.0). Analyses were processed with the Tukey method to identify outliers below the 25th percentile minus 1.5 times IQR (inter-quartile range) and above the 75th percentile plus 1.5 times IQR.
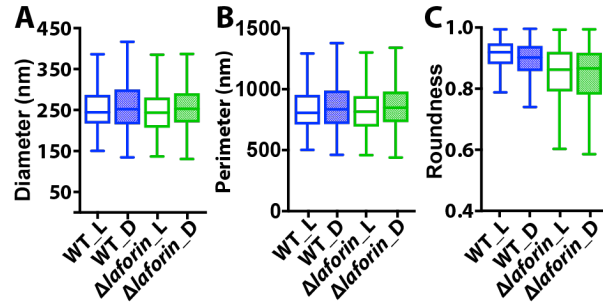
Figure 4-16 TEM polyglucan granule analyses from diurnal growth
A-C) Quantification of transmission electron micrographs with respect to diameter
(**A**, nm), perimeter (**B**, nm), and roundness (**C**, scale 0 – 1.0). Shaded boxes
represent granules collected at the end of a 12-hour period of darkness while open
boxes represent granules collected at the end of a 12-hour period of light. Analyses
were processed with the Tukey method to identify outliers below the 25th
percentile minus 1.5 times IQR (inter-quartile range) and above the 75th percentile
plus 1.5 times IQR.

CHAPTER 5. CARBOHYDRATE BINDING MODULE 45: AN ELUSIVE STRUCTURE NO MORE

5.1 Introduction

Polysaccharide metabolism revolves around networks of enzymes with specific substrate preferences, and in many cases, rely on interactions outside of their respective catalytic sites. As such, these non-catalytic domains can facilitate a multitude of efficient catalytic actions on polysaccharides corresponding to cellulose, starch, and glycogen. Historically, these substrate-recognizing modules were termed cellulose-binding domains (CBDs) as these CBDs were found to enable glycoside hydrolases to bind and act on crystalline cellulose (266). As more variations of substrate preferences (i.e. starch, glycogen, etc.) by enzyme isoforms were identified, the broader term carbohydrate-binding module (CBM) was chosen (266).

CBMs are 50-200 amino acid modules and are generally appended to carbohydrate-active enzymes (CAZymes) which cover almost every aspect surrounding carbohydrate metabolism including synthesis, transport, degradation, and modification (267, 268). CAZymes and their associated CBMs are classified based on their sequence-similarity (CAZy; http://www.cazy.org). Despite significant differences amongst sequences between CBM families, most CBMs exhibit similar secondary and tertiary structures (153). There are currently over 250,000 modules classified into 88 CBM families, of which, only 15 of those families (CBM20, 21, 25, 26, 34, 41, 45, 48, 53, 58, 68, 69, 74, 82 and 83) are specifically classified as starch-binding domains (SBDs) that interact with native starch granules (http://www.cazy.org) (97, 98, 269).

Starch is a product of photosynthesis in most plants and photosynthetic organisms that is accumulated during the day. During the night, accumulated starch is degraded to prevent nocturnal carbon starvation (162). Starch is an energy-dense α-1,4-linked glucose polymer comprised of approximately 10-25% linear amylose and 75-90% branched amylopectin (63). The α-1,6-branches in amylopectin are mostly responsible for the densely packaged double helical structure and semi-crystalline, water-insoluble nature of starch (63, 161). The

insoluble helical chains on the outer granular surface render starch inaccessible to most amylolytic enzymes that are responsible for degrading starch. Much progress has been accomplished on understanding how plants gain access to the energy-dense cache and modifications by means of phosphorylation is essential for this process (68, 95, 123, 158, 229).

Since the identification of phosphoesters in starch in the 1970s, phosphorylation is still the only known *in vivo* covalent starch modification (85, 89, 214, 270). Intriguingly, these phosphoesters were subsequently found to be specifically located mainly on two hydroxyl positions of glucose moieties, the C3 (30%) and C6 (70%) positions by two starch phosphorylating enzymes (85, 89, 90, 142, 143). In addition to the position-specific phosphate groups on glucosyl residues, these phosphate groups are localized to the amylopectin fraction of starch and can vary considerably between plant species (86). Starch phosphate content majorly influences the physico-chemical properties of starch granules which is an enticing avenue for designer starches for industrial purposes (270). Higher phosphate concentrations in starch positively correlate to higher hydration capacities, higher starch gel viscosities, more stable starch pastes, and lower melting enthalpies (energy required for melting) (157, 270, 271). Indeed, reduced phosphate content in potato tuber transgenic lines lead to increased melting enthalpy (258). Most starches used for industrial applications are often chemically phosphorylated post-harvest to improve their processability; however, these chemicals are detrimental to the environment as well as costly for proper disposal (270, 272). Post-harvest modifications are attempting to transition to 'Clean-Tech' using thermostable enzymes found in nature involved in starch metabolism (272). Therefore, understanding enzymatic mechanisms behind starch phosphorylation is not only advantageous for *in planta* starch metabolism but also for cheaper, more eco-friendly industrial applications.

In higher plants, it is now well known that the enzymes responsible for phosphorylation of the C6- and C3-positions are α-glucan, water dikinase (GWD1, EC 2.7.9.4) and phosphoglucan, water dikinase (GWD3/PWD, EC 2.7.9.5), respectively (90). The addition of phosphate by GWD and subsequent

phosphorylation by PWD to the branched and tightly-wound helical chains of amylopectin, leads to chain unwinding, and thus amylopectin solubilization (95, 123). This process renders the glucose chains within starch more solvent accessible and vulnerable to degradation by the successive amylolytic actions of β-amylases and isoamylases (158). In addition, their functional importance is demonstrated by loss of either gene resulting in significantly reduced phosphate level of starch as well as a starch excess phenotype from impaired degradation (143, 144, 146, 150).

Glucan dikinases are widely conserved from land plants to green algae, nonetheless, to date, most of the enzymatic characterization of glucan dikinases has been developed from proteins of two model organisms, *Solanum tuberosum* (*St*GWD) and *Arabidopsis thaliana* (*At*PWD) (179). Both glucan dikinases possess similar domain structure at the C-terminus which contains a PPDK domain with homology to bacterial pyruvate, water dikinase (PPS; EC 2.7.9.2) and pyruvate, phosphate dikinase (PPDK; EC 2.7.9.1) (156, 206). The catalytic PPDK domain is subdivided into two subdomains, the nucleotide-binding (NBD) and phosphohistidine (HIS) domain. Glucan dikinases follow an unique catalytic mechanism using ATP, bound by a nucleotide-binding domain (NBD), as a dual phosphate donor, simultaneously transferring the γ-phosphate to water yielding orthophosphate and AMP, while the β-phosphate is used to autophosphorylate the catalytic histidine residue in the HIS domain and is then transferred to a glucan substrate (78, 145, 156, 206). Furthermore, *St*GWD phosphorylates crystalline substrates such as starch and crystalline maltodextrins; however, cannot phosphorylate water-insoluble substrates (i.e., glycogen, solubilized maltodextrins, etc.) (90, 123, 142). CBMs are an integral part of the dynamic glucan dikinase catalytic mechanism allowing the catalytic domain to come in close contact with the polysaccharides concurrently with a swiveling mechanism, which in the case of GWD and PWD, allow the transfer of the β-phosphate to the C-6 and C-3 hydroxyl of glycosyl residues, respectively (90, 151, 214).

The N-terminal CBMs differ between GWD and PWD as they possess CBMs of family 45 (CBM45) and 20 (CBM20), respectively, and are key identifiers

between the two glucan dikinase isoforms (78). The CBM20 of PWD was one of the earliest identified and is one of the most well-characterized CBMs. It readily exhibits binding towards starch and amylopectin as well as soluble substrates such as glycogen and a variety of oligosaccharides (153, 171, 273). Interestingly, it is proposed that the initial GWD activity creates a phase transition at the starch granule surface that facilitates further action by PWD (95, 158). In contrast to CBM20s, the small CBM45 family is found normally as tandem N-terminal domains in two classes of enzymes: GWD orthologs and plastidial α-amylases (AMYs, EC 3.2.1.1) (130, 214). CBM45s of GWD have not been studied extensively and there is still no three-dimensional structure of a CBM45 nor any part of the binding region (152). Glucan dikinases are very large >150 kDa proteins that are dynamic with multiple domains and they have proven difficult to express and purify to homogeneity (146, 156, 215). In addition, isolated CBM45 domains have proven equally just as challenging as upon purification, the recombinant proteins rapidly precipitate (152). We focused on applying the extensive enzymatic characterization previously reported on the prototypical *St*GWD as guidelines for deconstructing and identifying novel GWD orthologues to elucidate their respective structural features and contributions to the overall enzymatic mechanism of GWD (144, 152, 156, 159, 214).

Using *St*GWD as our query sequence, we performed bioinformatic analyses and recently discovered and characterized a single active GWD (*Cm*GWD) from the extremophilic red alga, *Cyanidioschyzon merolae* (see **Chapter 3**). *C. merolae* produces a semiamylopectin-type floridean starch that lacks amylose and is synthesized in the cytosol instead of in the plastid (see **Chapter 3**). *C. merolae* is naturally found in acid hot springs and optimally grows at 40-55°C in pH 1-3 (26). This microalga began as a model organism to study the mechanistic nature of organelle division (i.e., mitochondrial, plastidial, and nuclear) due to its simplistic cell structure and ease of cell-cycle synchronicity (25, 208-212). *C. merolae* is now rapidly emerging as a potential renewable energy resource as it is genetically-manipulatable and produces high levels of lipids and carbohydrates (28, 29, 189, 191, 226). Due to the extreme habitat that *C. merolae* lives in, it is conceivable that

147

the enzymes involved in starch-like metabolism such as *Cm*GWD could overcome several barriers required for the biochemical and biophysical analyses.

Extensive bioinformatic and biochemical analyses of the N-terminal CBM45s of *Cm*GWD are reported in this chapter. We establish that *Cm*GWD is a unique glucan dikinase with three CBM45s (CBM45-1, CBM45-2, and CBM45-3) separated by ~150 and ~80 amino acid linker regions. All three CBM45s contain well-conserved characteristic aromatic residues associated with glucan binding (152, 214, 269). We deconstructed *Cm*GWD by isolating individual CBM45s and found CBM45-2 to be the most optimal for protein expression, homogeneous purification, and maximum yield. Site-directed mutagenesis was performed on all CBM45-2 conserved aromatic residues to identify which residues were involved with glucan interactions. Using a differential-scanning fluorimetry (DSF)-based thermal shift assay, we quantified the binding and stability of CBM45-2 and W457A mutant to a variety of oligosaccharides. These initial analyses have ultimately led to the first three-dimensional structure of a CBM45 which provides invaluable information on the mechanism behind glucan interactions of CBM45-containing proteins (Dr. Andrea Kuchtova, *in preparation*).

5.2   Results

5.2.1   Bioinformatic analyses of N-terminal *Cm*GWD domains

We initially characterized as a large multi-domain 1,572 amino acid protein comprised of an unstructured N-terminal region, a CBM45, a domain of unknown function (DUF), another CBM45, and a C-terminal PPDK (HIS and NBD) catalytic domain.   The putative 1572 amino acid GWD from *C. merolae* was only 24% identical to the prototypical *St*GWD (**Figure 3-3B**). Despite the low identity, the putative GWD sequence contained two tandem domains containing signature aromatic amino acid profile consistent with that of a CBM45 (152). There was also a DUF (318-469) that was ~150 amino acids long, which upon closer analysis using the secondary structure prediction tool Jpred4 showed the DUF possessed a β-sheet-rich secondary structure similar to that of a CBM (**Figure 5-1A**) (246). Multi-sequence alignments of each CBM45 from *St*GWD and *At*GWD, along with both

recognized *Cm*GWD CBM45s and the DUF, interestingly revealed the DUF contained all five well-conserved aromatic residues that are critical for glucan interactions (**Figure 5-1A**, highlighted in blue) (130, 152, 214). Therefore, based on the size, secondary structure predictions and conserved aromatic residues, we hypothesized that this DUF was a previously unrecognized CBM45.

5.2.2 Biochemical analyses reveal an unrecognized third CBM45 in *Cm*GWD

To investigate whether or not the DUF was indeed a *Cm*GWD CBM45, we generated multiple constructs of each of the three individual domains based on multiple sequence alignments, predicted secondary structure conservation, and regions of disorder (**Table 5-1, Figure 5-1B**). These constructs were cloned in a pET28b (Novagen) bacterial expression system containing an isopropyl β-D-thiogalactopyranoside (IPTG) inducible promoter and fused to a N-terminal His_6 tag to aid in purification. Several constructs were difficult or unable to express; however, we were able to successfully express and purify at least one construct of each domain to >90% homogeneity via affinity chromatography followed by size-exclusion chromatography and analyzed by SDS-PAGE (**Figure 5-1C**). Surprisingly, the DUF constructs were surprisingly the most stable, generated the highest yields ranging from 20-27 mg/L *E. coli* cells, and were the purest proteins (**Table 5-1, Figure 5-1D**). Expression and purification of both DUF-1 and DUF-2 proteins were robust and allowed our group to apply the proteins to many biochemical and biophysical approaches developed and frequently used by our lab, including differential scanning fluorimetry (DSF) and DSF-based thermal shirt assays (169, 194, 274).

Of the five aromatic residues, there are two tryptophan residues corresponding to *St*GWD CBM45-1 (W139 and W194) that have been confirmed as necessary for substrate binding (152, 214). We initially synthesized glycine mutants at each of four aromatic residues of DUF-1 to at positions W375, W385, F447, and W457. Subsequently, we attempted to express and purify each mutant in similar fashion to wildtype DUF constructs (DUF-1 and DUF-2). All mutants were sufficiently expressed via IPTG induction; however, the W375G mutant protein aggregated

rapidly through the size-exclusion process (**Figure 5-2A**, orange line). All other mutants behaved similarly to wildtype DUF-1 and DUF-2 protein and were able to proceed to further biochemical analyses (**Figure 5-2A**).

We utilized differential scanning fluorimetry, to evaluate the effect of the site-directed mutations on the protein stability of the DUF protein. DSF measures the thermal stability of a protein by defining its melting temperature (T_m).   (169, 194, 275, 276). DSF determines the melting temperature of the protein using a fluorophore called SYPRO Orange that nonspecifically binds to hydrophobic regions of proteins. As the temperature is gradually raised, the protein begins to unfold exposing a greater number of hydrophobic residues. The wild-type DUF-1 protein had a T_m of ~57°C whereas the W385G mutant displayed a dramatically decreased stability with a T_m ~40°C (**Figure 5-2B**). Both F447G and W457G mutant proteins did not display any significant destabilizing effects compared to wild-type (**Figure 5-2B**).

To assess the ability of the DUF to bind glucans, we often employ a glucan-binding assay developed in our lab (164, 178, 179, 185, 194, 238, 277). We incubate different types of glucan substrates with Concanavalin A, a lectin extracted from *Canavalia ensiformis*, that is conjugated to an agarose resin. Once the carbohydrate is bound to the resin and the excess carbohydrate is washed away, the carbohydrate-resin is incubated with the protein of interest. The mixture is then centrifuged and the soluble fraction (containing proteins not bound to resin) is separated from the pellet fraction (containing resin and bound proteins). The soluble vs. pellet fractions are then separated by SDS-PAGE and visualized by Western analysis using an anti-His antibody to detect the recombinant proteins (**Figure 5-3A**). CBM45s are very low-affinity domains and proved difficult to assess the binding capabilities of the DUF proteins as we were unable to consistently capture any glucan binding via Concanavalin A.

As an alternative method to study ligand binding, we employed a DSF-based thermal shift assay to assess glucan binding affinity and protein stability towards multiple glucan substrates. One can quantify substrate binding indirectly by monitoring the change in thermal stability (ΔT_m) using DSF upon addition of ligand

(**Figure 5-3B**) (169, 194, 274-276). If the protein binds the carbohydrate, then the melting temperature goes up proportional to the degree of binding. This assay has the advantage of allowing comparisons among chemically defined oligosaccharides, based on differences in the apparent dissociation constant (K_d). In addition, this assay allows for a large number of conditions (e.g., pH, salinity, etc.) to be assayed simultaneously. Firstly, we incubated DUF-1 with increasing concentrations of a potentially physiologically-relevant substrate, potato amylopectin. DUF-1 displayed a significant dose-dependent shift in T_m with increasing concentrations of amylopectin (**Figure 5-3C**). The apparent K_d of DUF-1 for potato amylopectin was 7.61 ± 0.89 mg/mL, which is similar to previous reports of *St*GWD CBM45-1 affinity towards potato starch (214). To determine if the DUF has a binding mechanism similar to CBM45s, we attempted to assess the aromatic residue mutants towards varying glucan substrates. The destabilized W385G mutant showed quite a reduction in apparent K_d of10.68 mM vs 41.19 mM compared to wild-type DUF-1 towards the oligosaccharide, maltohexaose (**Figure 5-3D**). This data indicates that the W385 residue is likely part of the binding mechanism for the DUF similarly to aligned CBM45s from GWD orthologues. These data along with the primary sequence and secondary structure similarities to CBM45s, recognizes the once denoted DUF as a now defined third CBM45 in *Cm*GWD.

Our initial aromatic site-directed mutants were substituted with glycine residues; however, glycine residues are unusually flexible as they only contain a hydrogen as its side chain (278). The original *St*CBM45 glucan-binding residues were identified by mutating the tryptophan residues to alanine. Alanine mutations are more widely used than glycine for identifying residues important for catalytic function or ligand binding due to its inert nature (278). Therefore, we followed the same protocols as with the DUF-1 glycine mutations, from site-directed mutagenesis to DSF-based thermal shift assays, to re-evaluate the binding mechanism of the newly recognized CBM45.

For this portion, we utilized the DUF-2 construct in which was equally robustly expressed and as stable throughout our purification scheme as DUF-1. We

constructed DUF-2 with more concise boundaries based on the secondary structure predictions. The resultant protein was therefore slightly smaller than DUF-1 (23.7 kDa vs 19.6 kDa) and was used throughout the remainder of our biochemical and biophysical characterization pipeline (**Figure 5-1C**). We mutated each of the three tryptophan residues of DUF-2 to alanine by site-directed mutagenesis at positions W375, W385, and W457. Subsequently, we attempted to express and purify each mutant in similar fashion to wildtype DUF-2. The W375A and W385A mutants were sufficiently expressed via IPTG induction; however, both mutant proteins aggregated rapidly throughout the IMAC purification process (**Figure 5-4**) and size-exclusion process (**Figure 5-5A**, orange and red line). W457A behaved similarly to wildtype DUF-2 protein although the yield was significantly less (**Figure 5-4B, 5-5A**; blue line).

In order to compare the DUF to other validated CBM45s, we synthesized CBM45-1 from *St*GWD based off of previous reports (152, 159, 214) and our bioinformatic analyses. Our *St*GWD CBM45-1 construct (GDV109-SGK443) was synthesized by Genscript in the same bacterial expression system fused to a N-terminal His$_6$-tag. This approximately 39 kDa His-tagged protein was stable and eluted just before our DUF-2 construct via size-exclusion (**Figure 5-5A**, green line). We performed the DSF-based thermal shift assay to validate the ability of our *St*GWD CBM45-1 construct to bind to maltooligoaccharides. *St*GWD CBM45-1 had a T$_m$ ≈54°C and the stability of the protein increased with increasing concentration of maltoheptaose (**Figure 5-5B**, blue line). As a negative control, we incubated *St*GWD CBM45-1 with DP2 (maltose) and observed no major stabilizing effect therefore validating that this is a specific effect (**Figure 5-5B**, red line). A similar protocol was used for DUF-2 with increasing concentrations of varying maltooligosaccharides and we observed similar stabilizing effects compared to *St*GWD CBM45-1 (**Figure 5-5C**). We observed a significant dose-dependent response in the ΔT$_m$ of DUF-2 with increasing lengths of maltooligosaccharides (**Figure 5-5C**). In comparison with *St*GWD CBM45-1, the DUF-2 protein ΔT$_m$ along with the highest concentration of maltoheptaose (DP7) was ~7°C higher than *St*GWD CBM45-1 with DP7. We then were able to assess the effect of the W457A

mutation (corresponding to *St*GWD W194) on the binding capabilities of the DUF-2 protein. Incubation with DP7 and potato amylopectin revealed a significant impairment on the ability to bind both substrates (**Figure 5-5D and E**, respectively). These data validate the DUF as being a previously unrecognized third CBM45 in *Cm*GWD. In addition, the two tryptophan residues at positions 385 and 457 are necessary for proper glucan interactions by this CBM45.

5.2.3 Modeling of newly identified *Cm*GWD CBM45-2

We also proposed an initial model of the *Cm*GWD CBM45-2 domain that was generated using the Phyre^2 server, which constructs a three-dimensional structure, based on searching through homologous sequences using PSI-BLAST (279). The highest confident hits were the structures of CBM25-1 from *Paenibacillus polymyxa* (96.4% confidence, 20% i.d.) and from *Bacillus halodurans* (96.4% confidence, 17% i.d.). Although the identity is low compared to the standard threshold of 23%, there is a high similarity between CBM25 and CBM45 secondary structure. Sequence alignment of CBM45 and CBM25 show how different amino acid sequences can be while still maintaining a similar distorted β-barrel topology (**Figure 5-6A**). Figure 5-6A predicts CBM45-2 having eight β-strands; however, the three-dimensional model contains six β-strands (**Figure 5-6B**). These discrepancies highlight that the predicted three-dimensional model is just that, "a model."

Analysis of the predicted three-dimensional structure of CBM45-2 using Pymol reveals that W385 and W457 are likely to interact with carbohydrates (**Figure 5-6C, D**). In addition to the conserved tryptophan residues, there may also be a role for a central histidine residue in the binding region (**Figure 5-6E**). Not surprisingly, CBM25 from *Bacillus halodurans* (PDB code: 2C3W) has two conserved tryptophan residues with a conserved histidine in the main binding region as well (215). Surface models of CBM45-2 show a potential carbohydrate binding pocket configuration as well (**Figure 5-6E**). Representation of the predicted three-dimensional CBM45 structure shows conserved aromatic residues amongst the

signature β-strands with high confidence; however, outside the signature secondary elements, such as loops, are highly variable.

5.3   Discussion

This chapter combined bioinformatic and biochemical techniques to identify a third, previously unrecognized CBM45 in *Cm*GWD. Our analyses revolved around previous work done on the prototypical GWD from *S. tuberosum* where tandem N-terminal domains were identified (152, 159, 214). *Cm*GWD is therefore unique as it contains three CBM45s and is one of four members to contain more than two CBM45s (**Table 5-2**, highlighted in green). Having an extra CBM45 might be a result of the environment of *C. merolae* as a need to compensate for the loss of molecular interaction at higher temperatures (266). The presence of a single glucan dikinase in *C. merolae* is thought to be one of two distinct enzymes that separate crystalline carbohydrate storing organisms from non-crystalline carbohydrate storing organisms (69, 102). It is still unknown what each CBM45 contributes to the overall activity of *Cm*GWD; however, it is likely that each CBM45 does indeed contribute to the overall activity of *Cm*GWD. We also applied new techniques frequently used by our lab to better understand binding mechanisms and structural details. CBM45-2 of *Cm*GWD showed increasing binding affinity to longer maltooligosaccharides and potato amylopectin. Glycine and alanine mutations of the well-conserved aromatic residues in CBM45-2 partly proved difficult to express and purify stable protein as other groups have reported (152). We initially expressed and purified glycine mutants; however, they destabilized and likely altered the structural integrity of CBM45-2. Although alanine mutations were less successful when expressing and purifying protein, we were able to increase the scale of our purifications to get ample W457A mutant protein for DSF-based thermal shift assays. The W457A mutation drastically impaired the ability to bind to varying maltooligosaccharides and potato amylopectin. This data corroborates previous findings that W194 (*St*GWD numbering) is involved in glucan interactions (152, 214).

CBM45-2 showed the most stabilizing effect with maltohexaose (DP6) and maltoheptaose (DP7) in which can be used for crystallization screening conditions.

Structural data is critical to understand the mechanisms behind GWD phosphorylation activity. To date, the three-dimensional structure of CBM45 has not been solved although there have been models proposed recently (215). These initial bioinformatic and biochemical data reported here ultimately have led to the first three-dimensional structure of a CBM45 by my colleagues Dr. Andrea Kuchtova and Tiantian Chen in collaboration with Dr. Craig Vander Kooi (**Figure 5.7**). Exhaustive crystallization screens exploiting countless experimental conditions were used to determine the structure of CBM45-2 of *Cm*GWD. From broad polyethylene glycol screens (PEGII and JCSG+) to heavy-atom soaking to obtain phase information of crystal, my colleagues left no stone unturned in efforts to determine the structure of CBM45-2. The structure of CBM45-2 of *Cm*GWD (previously known as DUF-2 construct) was refined to a resolution of 1.75 Å and exhibits a β-sandwich structure consisting of nine β-strands (**Figure 5-7A**). The structure shows the orientation of the five well-conserved aromatic residues with W385 and W457 displaying the carbohydrate-binding hallmark of the CBM45 family (**Figure 5-7B, C**). Three of the five aromatic residues (W375, F447, and F465) are buried in the hydrophobic core of the CBM45 which corroborates our difficulties purifying these mutants. In addition, W385 likely forms hydrogens bonds with surrounding residues and that is a probable reason why W385G and W385A mutations were destabilizing to the protein. Interestingly, our initial model proposed a potential role of a central histidine residue in the carbohydrate binding region, part of a signature LHWG motif of CBM45s (215). H374 is positioned in the middle of the glucan binding region of the CBM45-2 structure and likely aids in glucan interactions (**Figure 5-7D, E**).

The biochemical and structural data presented here provides invaluable insights into how CBM45-containing enzymes (GWDs and AMYs) recognize and interact with distinct carbohydrates. The specific differences in binding modes can be evaluated between GWD orthologues to determine characteristics pertaining to binding affinities and substrate preferences. Starch phosphorylation frequency is relatively low even amongst the highly phosphorylated potato tuber starch in which one out of every 250 glucose units is phosphorylated (271). Nevertheless, the

presence of phosphate has drastic effects on the physicochemical properties of starch such as hydration capacity, pasting and gelatinization functions (92). The CBM45s that have been investigated so far have lower binding affinities that may reflect the dynamic activity of GWD on the starch granule surface (280). This is similar to CBM20s of *At*GWD3 (PWD) which display a 50-fold lower binding affinity to β-cyclodextrins than a CBM20 of glucoamylase (281). CBM20s generally have two separate binding sites which are supported by three-dimensional structures (153). Structural modelling and sequence comparisons identified a deletion of critical residues associated with binding site 2 that likely results in lowered binding affinities (281). CBM45s are a relatively newly discovered CBM family which could possess novel functions towards starch metabolism. Details of CBM45s from GWDs and AMYs can identify differences in binding modes that correlate to lower binding affinities of GWDs. Although there is no additional structural data of the catalytic domain published for glucan dikinases, structural data for CBM45s allow us to isolate and engineer their activity that could be employed in industrial applications. Engineering chimeric proteins with a granular starch-binding CBM45 may allow for proteins to be targeted to starch and for dynamic activity corresponding to the catalytic function of appended domains.

Much is still unknown about the specificity of glucan dikinases and whether this is due to catalytic domain or CBM differences. It is likely that the C6- or C3-specificity lies within the catalytic HIS domain and the CBM is responsible for the substrate preference. In the case of GWD, generally having tandem CBM45s must have a cooperative effect on plastidial starch whereas deviants are found in organisms with modified variants of storage glucans like semi-amylopectin found in *C. merolae.* The presence of three CBM45s and their relationship to the overall preference and activity of *Cm*GWD is likely specialized to their unique substrate. Further investigation into the novel CBM45 family will help understand the importance of low binding affinities and dynamic interactions at the starch granule surface. Structural data of CBM45-2 from *Cm*GWD opens up new opportunities in a biotechnological point of view as it is a step closer to discovering glucan chain

phosphorylation patterns and substrate specificity for the production of desirable industrial starches.
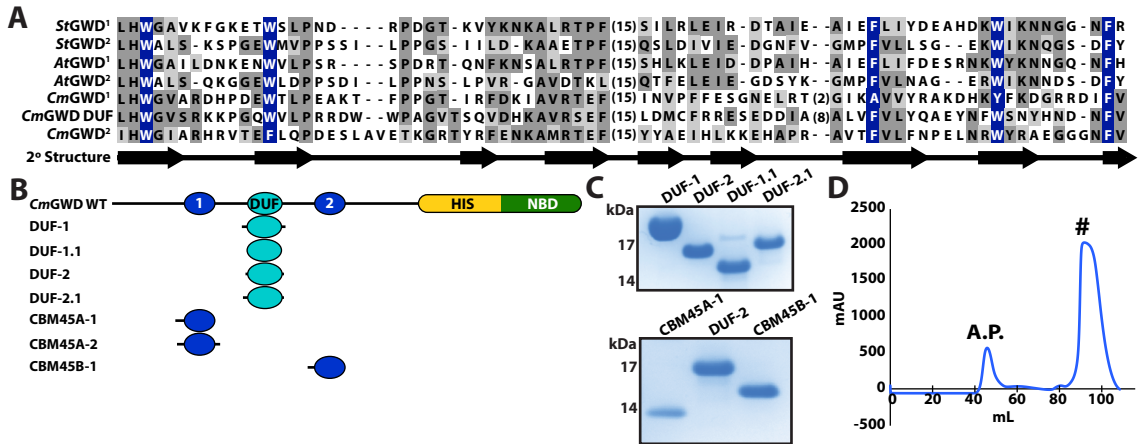
Figure 5-1 Alignments, construction, and purification of N-terminal *Cm*GWD domains.
A) Multisequence alignments of individual CBM45s from *S. tuberosum* GWD1*, A. thaliana* GWD1, and *C. merolae* GWD (locus CMT547C) with *Cm*GWD DUF (318-469). Residues boxed in dark gray are identical, while similar residues are boxed in light gray. Residues boxed in blue are highly conserved amongst the CBM45 family and critical for glucan binding. Secondary structure prediction by Jpred below multisequence alignment, arrows represent predicted β-strands. **B)** Full-length *Cm*GWD domain schematic with corresponding isolated individual domain constructs. **C)** SDS-PAGE of purified individual DUF and CBM45s of *Cm*GWD. **D)** SEC elution profile of DUF-1 construct. A.P. = aggregation peak/void fraction. # = non-aggregated target protein.
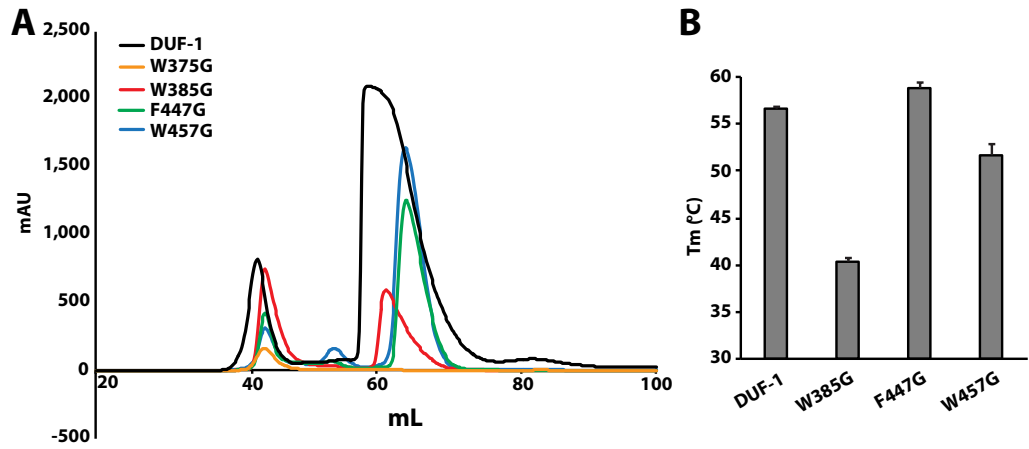
Figure 5-2 Purification of DUF-1 glycine mutants and protein stability
A) SEC elution profiles of wild-type DUF-1 and glycine mutants purified on a S75 column. **B)** DSF thermal stability of DUF-1 and glycine mutants.
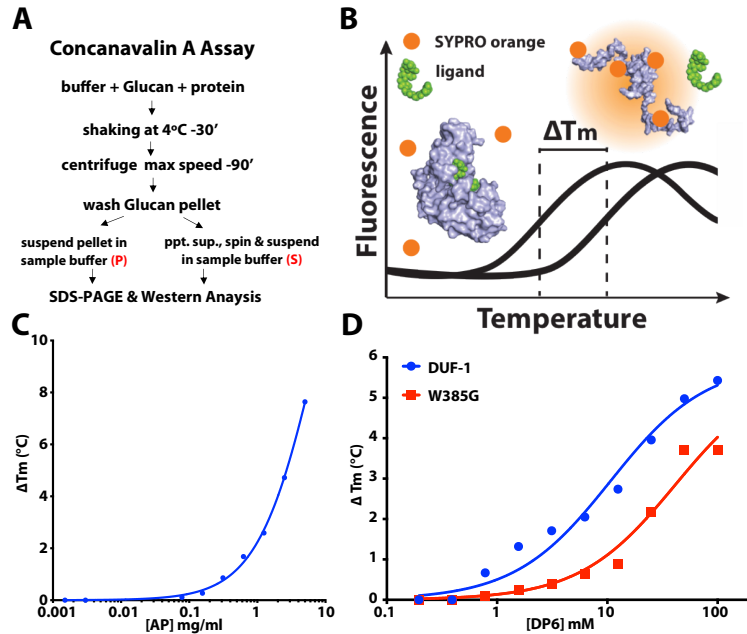
Figure 5-3 Glucan binding assays – Concanavalin A and DSF-based thermal shift

A) Concanavalin A glucan binding assay utilizes a lectin from *C. ensiformis* bound to agarose resin allowing soluble carbohydrates to pellet upon centrifugation. Bound protein will pellet (P) with carbohydrates while unbound protein will be left in the supernatant (S). **B)** DSF-based thermal shift assay measures the change in melting temperature (ΔT_m) of a protein with varying concentrations of carbohydrates. **C)** DSF-based thermal shift assay of the DUF-1 protein with increasing concentrations (mg/mL) of potato amylopectin (AP). **D)** DSF-based comparison between wild-type DUF-1 (blue) and W385G mutant (red) binding affinity to increasing concentrations of maltohexaose (DP6).
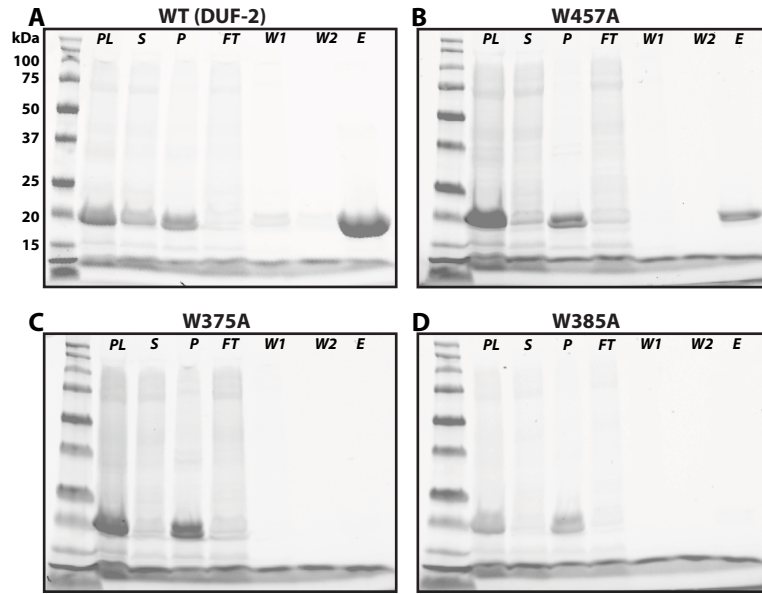
Figure 5-4 Expression and purification of DUF-2 and alanine mutants via Immobilized metal-ion affinity chromatography (IMAC)
A-D) SDS-PAGE analysis of each step throughout the initial purification process via IMAC. PL=post lysis, S= supernatant (soluble protein), P= Pellet (insoluble protein), FT= BioRad Profinia IMAC flowthrough, W1= first wash of His-bound protein, W2= second wash of His-bound protein, E= elution fraction. Gels were ran by Cassadi Cordea.
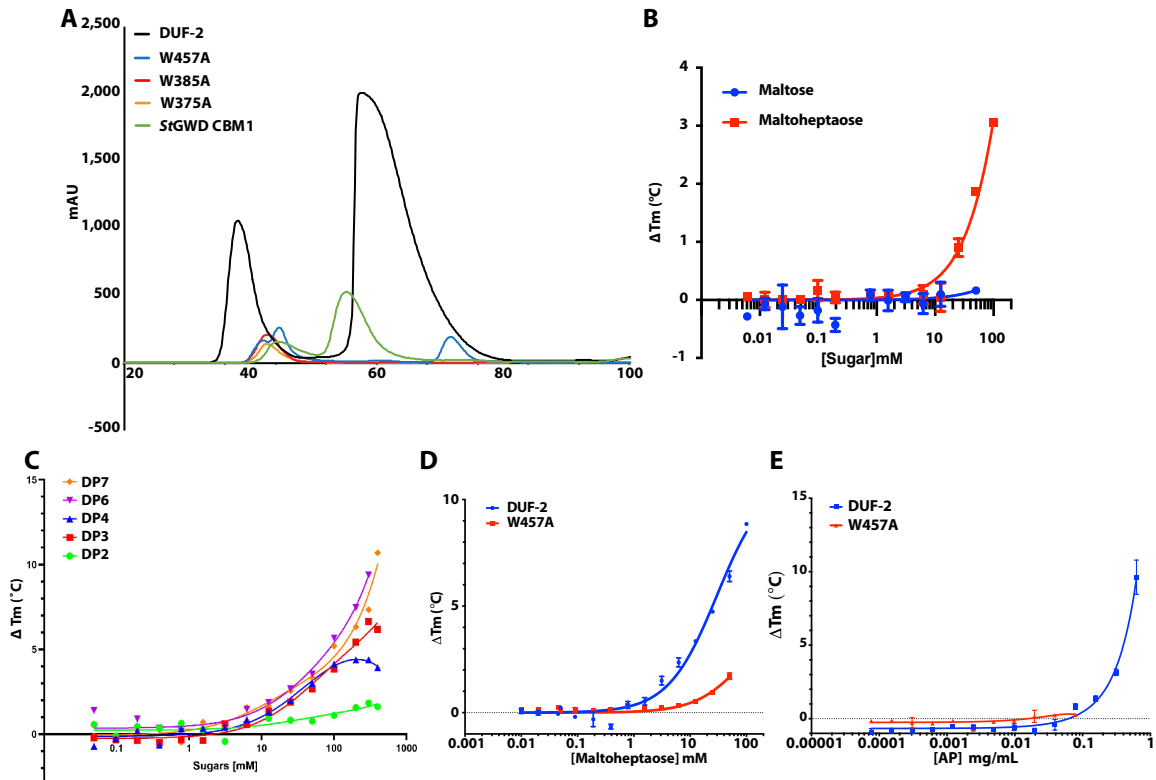
Figure 5-5 SEC purification and DSF-based thermal shift assays of *St*GWD CBM45-1, DUF-2 and alanine mutations
A) SEC elution profile of *St*GWD CBM45-1, DUF-2 and alanine mutants. W375A and W385A mutants showed no non-aggregated protein peak, orange and red lines, respectively. **B)** DSF-based thermal shift assay of *St*GWD CBM45-1 with increasing concentrations of maltose (red) as a negative control and maltoheptaose (DP7, blue). **C)** DSF-based thermal shift assay of DUF-2 with increasing concentrations of varying maltooligosaccharides. Increased binding affinity towards longer maltooligosaccharides DP6 and DP7 (violet and orange, respectively). **D)** Comparison between DUF-2 (blue) and W457A mutant (red) on binding affinity towards increasing concentrations of maltoheptaose (DP7). **E)** Comparison between DUF-2 (blue) and W457A mutant (red) on binding affinity towards increasing concentrations of potato amylopectin. Each DSF-based thermal shift assay was performed in triplicate reactions and displayed as mean ± SD. Protein purification and DSF-bases assays were performed with the help from Dr. Andrea Kuchtova.
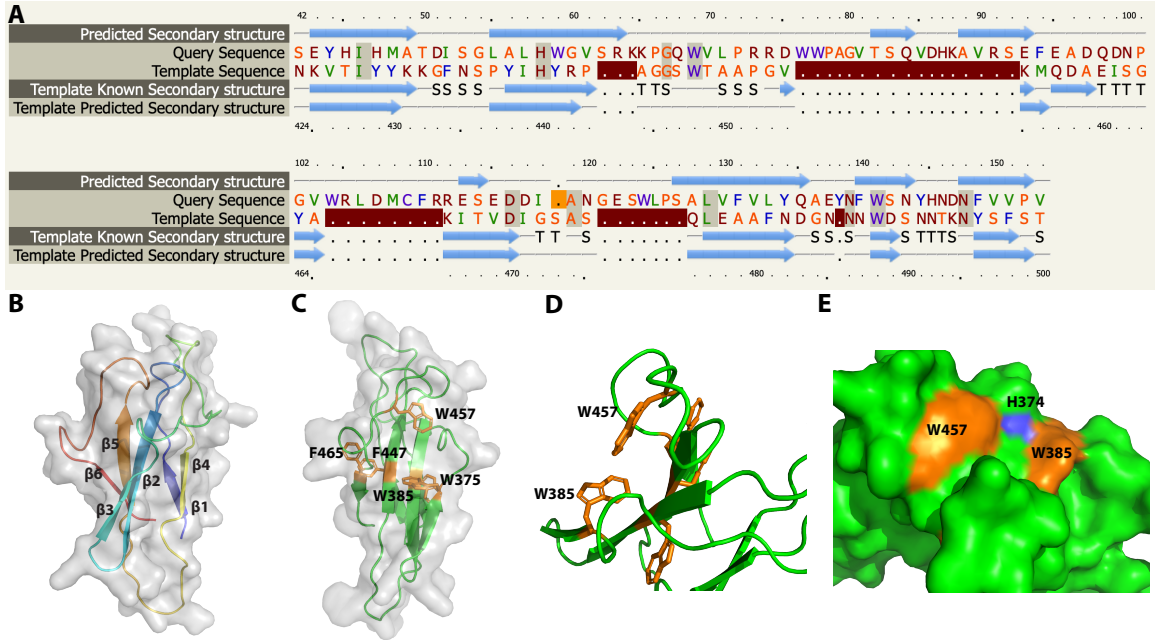
Figure 5-6 Initial modelling of CBM45-2 from *Cm*GWD showing potential carbohydrate binding region and mode
A) Phyre2 secondary structure prediction with best-fitted homologous sequences using PSI-BLAST. **B)** Structural models based off of CBM25-1 from *Paenibacillus polymyxa* (96.4% confidence, 20% i.d.). Model exhibits six β-strands numbered from N-terminus to C-terminus. Surface topology shown overlayed in gray. **C)** Five well-conserved aromatic residues shown in stick form (orange) **D)** Close-up of W385 and W457 showing the most potential for glucan interactions. **E)** Surface topology of binding region revealing a conceivable role of a central histidine residue H374.
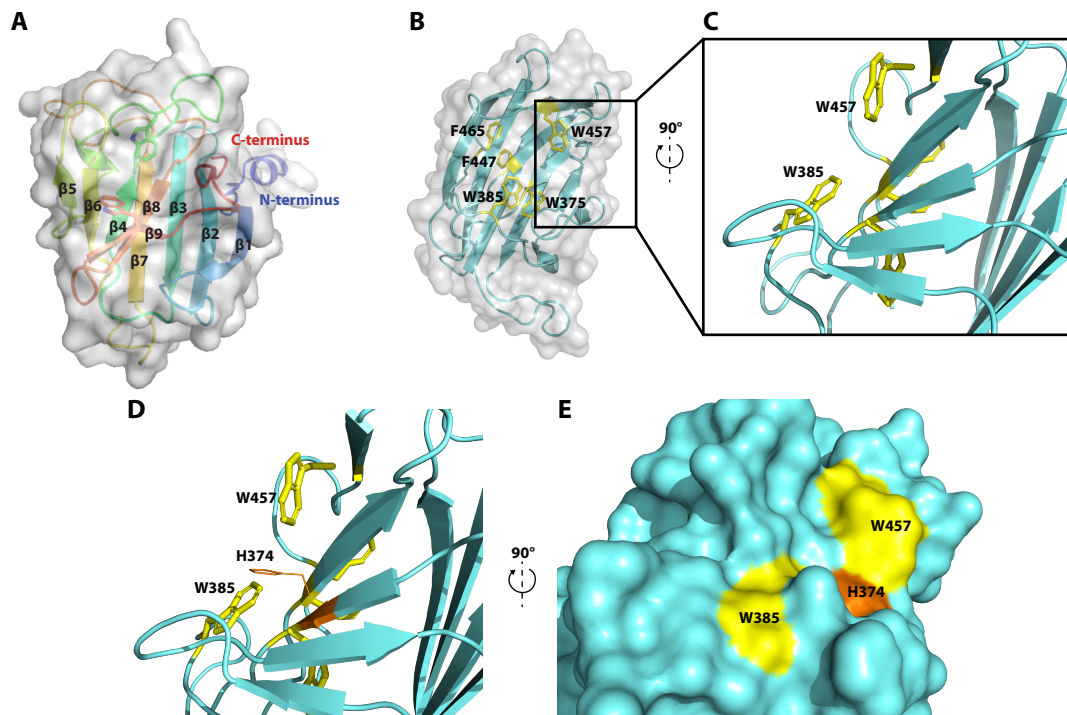
Figure 5-7 Crystal structure of CBM45-2 of *Cm*GWD
A) Structure of CBM45-2 of *Cm*GWD refined to 1.75 Å and exhibits a β-sandwich structure consisting of nine β-strands **B)** Five well-conserved aromatic residues displayed in stick form (yellow). **C)** Close-up of W385 and W457 orientation of the unique carbohydrate-binding hallmark of CBM45 **D)** Sugar interacting central histidine H374 in line form (orange) suggesting possible binding mode **E)** Surface topology exhibiting a carbohydrate-binding groove. Structure and crystallization of CBM45-2 was produced by Dr. Andrea Kuchtova.

Table 5-1 Construct primers of CBM45s and DUF

Construct	Primer Sequences	Amino Acid Boundary	Molecular weight with His tag (kDa)
CBM45-1 #1 (CBM45A-1)		139-216	11.4
Forward Primer	TTTCATATGCTGCATTGGGGCGTGG		
Reverse Primer	TTTTCTCGAGTCAGTCTTTAAAGTATTTGT		
CBM45-1 #2 (CBM45A-2)		139-219	11.8
Forward Primer	TTTCATATGCTGCATTGGGGCGTGG		
Reverse Primer	TTTTCTCGAGTCAGCGACGGCCGTCTTTA		
DUF #10 (DUF-1)		304-493	22.5
Forward Primer	AAACATATGCTGGACCGTCTGGTGAAAG		
Reverse Primer	TTTTCTCGAGTCATTTTTCTTGTTCTTGCA		
DUF #14 (DUF-1.1)		337-493	20
Forward Primer	AAACATATGGGCGGTGTCGGTCG		
Reverse Primer	TTTTCTCGAGTCATTTTTCTTGTTCTTGCA		
DUF #11 (DUF-2)		318-469	18.3
Forward Primer	AAACATATGCTGAAAGCAGTGCGTCGC		
Reverse Primer	TTTTCTCGAGTCACACCGGCACGACGAA		
DUF #13 (DUF-2.1)		337-469	17.4
Forward Primer	AAACATATGGGCGGTGTCGGTCG		
Reverse Primer	TTTTCTCGAGTCACACCGGCACGACGAA		
CBM45-3 #22 (CBM45B-1)		548-645	13.8
Forward Primer	AAAACATATGCTGGTGATTCATTGGGGTA		
Reverse Primer	TTTTCTCGAGTCAGCTAAACGATTCCAGG		

Table 5-2 Results from six BLAST's of *Cm, St,* and *At*GWDs
18 members contain one copy of CBM45 on their N-terminus (highlighted violet). Four members contain three copies of CBM45 on their N-terminus (highlighted green). 64 other members contain two copies of CBM45 on their N-terminus.

No.	Organism	GenBank	UniProt	Length	Domain
CmGWD (M1VD00) – sequences containing at least two CBM45 (results from the first 100 hits)					
1.	*Cyanidioschyzon merolae* strain 10D	**BAM83464.1**	**M1VD00**	**1572**	**Eukaryota – (red algae)**
2.	*Magnetoovum chiemensis*	KJR43545.1	A0A0F2J824	1153	Bacteria - Nitrospirae
3.	*Proteobacteria bacterium*	PIE18029.1	A0A2G6J6D5	1226	Bacteria - Proteobacteria
4.	*Nitrospirae bacterium HCH-1*	KWT83506.1	A0A109CAL8	1168	Bacteria - Nitrospirae
5.	*Aegilops tauschii subsp. tauschii*	XP_020163887.1		1288	Eukaryota – (hard grass)
6.	*Physcomitrella patens*	PNR57280.1	A0A2K1KU47	1415	Eukaryota – (moss)
7.	*Phaseolus vulgaris*	ESW25754.1	V7C6L3	1456	Eukaryota – (green bean)
8.	*Ipomoea nil*	XP_019166631.1		1467	Eukaryota – (ornamental plant)
9.	*Panicum hallii*	PAN30166.1		1301	Eukaryota – (grass)
10.	*Aquilegia coerulea*	PIA61801.1	A0A2G5F1E8	1386	Eukaryota – (flowering plant)
11.	*Oryza sativa Japonica Group*	BAS97907.1	Q0DC10	1414	Eukaryota – (rice)
12.	*Vigna radiata var. radiata*	XP_014523173.1	A0A1S3VXT7	1456	Eukaryota – (mung bean)
13.	*Vigna angularis*	KOM31677.1	A0A0L9TMK8	1456	Eukaryota – (adzuki bean)
14.	*Sesamum indicum*	XP_011086610.1		1466	Eukaryota – (sesame)
15.	*Daucus carota subsp. sativus*	XP_017226386.1		1383	Eukaryota – (wild carrot)
16.	*Populus trichocarpa*	PNT14688.1	B9HTV3	1476	Eukaryota – (poplar)
17.	*Actinidia deliciosa*	AOQ26246.1	A0A1S5RRZ4	1467	Eukaryota – (kiwifruit)
18.	*Erythranthe guttata*	XP_012848069.1		1468	Eukaryota – (monkeyflower)
19.	*Glycine max*	XP_003552035.1	K7MS29	1459	Eukaryota – (soybean)
20.	*Prunus persica*	ONI30396.1	A0A251R324	1468	Eukaryota – (peach)
CmGWD (M1VD00) (excluding all plants) – sequences containing at least one CBM45 (results from the first 50 hits)					
21.	*bacterium BMS3Abin06*	GBD97615.1	A0A2H6F799	1007	Bacteria
22.	*Planctomycetaceae bacterium*	OAI50193.1	A0A177QUH0	1032	Bacteria – Planctomycetes
23.	*bacterium BMS3Bbin05*	GBE31444.1	A0A2H6HYV9	1007	Bacteria
24.	*Desulfobacterales bacterium*	OEU46774.1	A0A1V1WWL2	1039	Bacteria – Proteobacteria
25.	*Magnetobacterium bavaricum*	KJU86800.1	A0A0F3GY57	1011	Bacteria – Nitrospirae
26.	*Magnetobacterium casensis*	WP_040333309.1		1054	Bacteria – Nitrospirae
27.	*Porphyra umbilicalis*	OSX69353.1	A0A1X6NLZ0	1343	Eukaryota – Rhodophyta
28.	*Symbiodinium microadriaticum*	OLP87183.1	A0A1Q9CW69	1698	Eukaryota – Alveolata
29.	*Eimeria mitis*	CDJ32881.1	U6K7V2	1651	Eukaryota – Alveolata
30.	*Guillardia theta*	EKX34264.1	L1IEF4	1066	Eukaryota – Cryptophyta
31.	*Gregarina niphandrodes*	EZG66638.1	A0A023B6M1	1359	Eukaryota – Alveolata
32.	*Klebsormidium nitens*	GAQ90596.1	A0A1Y1IP88	1103	Eukaryota – Viridiplantae
33.	*Auxenochlorella protothecoides*	KFM25761.1	A0A087SJ57	1252	Eukaryota – Viridiplantae
34.	*Cryptosporidium andersoni*	OII71601.1	A0A1J4MBK4	1687	Eukaryota – Alveolata
StGWD (I0DFJ7) – sequences containing at least two CBM45 (results from the first 50 hits)					
35.	*Solanum tuberosum*	**AFH88388.1**	**I0DFJ7**	**1464**	**Eukaryota – potato**
36.	*Solanum lycopersicum*	NP_001234405.2	B5B3R3	1465	Eukaryota – tomato
37.	*Solanum pennellii*	XP_015076014.1		1462	Eukaryota – wild tomato
38.	*Nicotiana attenuata*	XP_019257150.1		1464	Eukaryota – wild tobacco
39.	*Nicotiana sylvestris*	XP_009775339.1	A0A1U7WKY5	1464	Eukaryota – tobacco
40.	*Nicotiana tabacum*	XP_016451036.1	A0A1S3YFK2	1464	Eukaryota – tobacco
41.	*Nicotiana tomentosiformis*	XP_009631515.1		1464	Eukaryota - herbaceous plant
42.	*Capsicum annuum*	NP_001311566.1	A0A0A8K9I6	1464	Eukaryota – peppers
43.	*Coffea canephora*	CDP13198.1	A0A068V035	1465	Eukaryota –cafe
44.	*Handroanthus impetiginosus*	PIN21110.1	A0A2G9HUW1	1466	Eukaryota – pink tree
45.	*Vitis vinifera*	CBI28585.3	D7TDL2	1470	Eukaryota – grape
46.	*Hevea brasiliensis*	XP_021635188.1		1473	Eukaryota – rubber tree
47.	*Juglans regia*	XP_018805215.1	A0A2I4DDI6	1472	Eukaryota – walnut
48.	*Olea europaea*	XP_022892008.1		1498	Eukaryota – olive
49.	*Durio zibethinus*	XP_022735440.1		1470	Eukaryota – durian
50.	*Jatropha curcas*	KDP26632.1	A0A067JRV6	1466	Eukaryota – flowering plant
51.	*Corchorus capsularis*	OMO78306.1	A0A1R3I6S7	1469	Eukaryota – white jute
52.	*Quercus suber*	POE53012.1		1526	Eukaryota – cork oak
StGWD (I0DFJ7) (excluding all plants) – sequences containing at least one CBM45 (results from the first 50 hits)					
53.	*Bathycoccus prasinos*	CCO20386.1	K8EQS6	1502	Eukaryota - Chlorophyta
54.	*Micromonas commoda*	ACO64480.1	C1E8A5	1419	Eukaryota – marine algae

166

55.	*Chlamydomonas eustigma*	GAX78330.1	A0A250X6D3	1526	Eukaryota - Chlorophyta
56.	*Ostreococcus tauri*	CEG01373.1	A0A090M894	1303	Eukaryota – marine green algae
57.	*Coccomyxa subellipsoidea*	EIE24570.1	I0Z1Q1	1384	Eukaryota –green algae
58.	*Chlamydomonas reinhardtii*	PNW80482.1	A0A2K3DIY0	1522	Eukaryota –green algae
59.	*Micromonas pusilla*	EEH54887.1	C1MZK9	1562	Eukaryota – marine algae
60.	*Ostreococcus lucimarinus*	ABO97582.1	A4S125	1043	Eukaryota –green algae
61.	*Chlorella sorokiniana*	PRW33076.1		1553	Eukaryota – freshwater microalga
62.	*Chondrus crispus*	CDF39037.1	R7QKK2	1353	Eukaryota – Irish moss
63.	*Stylonychia lemnae*	CDW81022.1	A0A078AHP3	1127	Eukaryota - Alveolata
64.	*Stentor coeruleus*	OMJ88441.1	A0A1R2CHG0	1029	Eukaryota - Alveolata
65.	*Oxytricha trifallax*	EJY65107.1	J9HJS5	1179	Eukaryota - Alveolata
66.	*Monoraphidium neglectum*	KIZ04120.1	A0A0D2MN16	1390	Eukaryota – single cell algea
AtGWD (Q9SAC6) – sequences containing at least two CBM45 (results from the first 50 hits)					
67.	***Arabidopsis thaliana***	**NP_563877.1**	**Q9SAC6**	**1399**	**Eukaryota – flowering plant**
68.	*Arabidopsis lyrata*	EFH68856.1	D7KLJ1	1396	Eukaryota – flowering plant
69.	*Camelina sativa*	XP_010458437.1		1400	Eukaryota – flowering plant
70.	*Eutrema salsugineum*	XP_006417419.1	V4L0E0	1409	Eukaryota – flowering plant
71.	*Capsella rubella*	XP_023644825.1		1392	Eukaryota - shepherd's-purse
72.	*Brassica napus*	XP_013716410.1		1399	Eukaryota – rape
73.	*Brassica oleracea*	XP_013604660.1	A0A0D3DY28	1399	Eukaryota – oilseed rape
74.	*Raphanus sativus*	XP_018440005.1		1396	Eukaryota – radish
75.	*Brassica rapa*	XP_009144413.1		1395	Eukaryota – rape
76.	*Tarenaya hassleriana*	XP_010553614.1		1477	Eukaryota – flowering plant
77.	*Manihot esculenta*	AFO83529.1	V9K755	1409	Eukaryota – shrub
78.	*Gossypium arboreum*	XP_017622791.1		1471	Eukaryota – tree cotton
79.	*Gossypium raimondii*	KJB15603.1	A0A0D2NPX3	1471	Eukaryota – cotton plant
80.	*Gossypium hirsutum*	XP_016701354.1	A0A1U8KKX0	1471	Eukaryota – cotton plant
81.	*Malus domestica*	XP_017192456.1		1406	Eukaryota – apple
82.	*Fragaria vesca*	XP_011464043.1		1400	Eukaryota – wild strawberry
83.	*Ricinus communis*	EEF34459.1	B9SPI3	1469	Eukaryota – castor oil-plant
AtGWD (Q9SAC6) (excluding all plants) – sequences containing at least one CBM45 (results from the first 50 hits) – Nothing new (all results are already in table)					

CHAPTER 6. CONCLUDING REMARKS

6.1 Summary and Discussion

Starch and glycogen are an essential component for the majority of species and have been developed to maintain energy homeostasis and often determines the vitality of the species (68). Water-soluble glycogen is an excellent source of quick, short-term energy in response to energy demands. In contrast, plants and algae have developed the macromolecule starch that is elegantly suitable for their dependence on external circumstances. Semi-crystalline starch is water-insoluble and inaccessible to many enzymes; thus, plants and algae have developed a coordinated system so that these enzymes can gain access to the denser starch energy cache. Reversible glucan phosphorylation is essential for the proper degradation of starch in higher plants. However, there is a knowledge gap in regards to this process in other starch-containing organisms such as algae. In addition, the relationship between phosphorylation and dephosphorylation activity on the structural consequences of starch are still in their infancy.

Regardless of storage carbohydrate type, it is becoming increasingly clear that the presence of phosphate esters plays an important role in proper glucan structuring and metabolism. Since the discovery of phosphate esters in both glycogen and starch in the 1970-1980s, phosphorylation is still the only known *in vivo* covalent modification (78, 85, 89, 282). Phosphorylation content varies between species; however, even amongst the most highly phosphorylated tuber starches, phosphorylation content is still only ~0.5% of all glucose molecules (214). Despite the relative trace amounts of phosphate content in starch, there is a clear correlation between phosphate content and its effect on the physico-chemical properties of starch (86, 144, 156, 157, 271, 283). In addition, mutations in either the kinases responsible for starch phosphorylation or the phosphatases responsible for starch dephosphorylation generally result in impaired starch degradation, growth, and increased starch accumulation (146, 150, 164, 179). The effect of phosphate content in glycogen has come to light due to an understanding of Lafora disease (LD) where LD patients accumulate hyperphosphorylated

aberrant glycogen in the form of Lafora bodies (LBs) in almost all cell types. These LBs cause neurodegeneration and fatal childhood epilepsy (80, 183, 242, 245). The glycogen phosphatase laforin is required for normal maintenance of glycogen, therefore, loss of function mutations in the gene encoding laforin cause abnormal phosphate build-up leading to altered glycogen structures that become insoluble. The underlying enzymes behind glycogen phosphorylation, especially at the C6-position, is still under investigation. Some results have suggested that glycogen phosphorylation is a mistake incorporated by glycogen synthase (80). While the mechanism of glycogen phosphorylation is still under debate, this is certainly not the case for starch phosphorylation (219).

A hallmark study to screen for mutants with impaired starch degradation using the model organism *A. thaliana* spear-headed research on reversible glucan phosphorylation and aided to identify the enzymes involved (124). Phosphorylation by the glucan dikinases, GWD1 and GWD3/PWD at the C6- and C3-positions respectively increase solubilization at the granule surface allowing amylolytic enzymes better access to glucose polymers releasing mainly maltose and glucose. Dephosphorylation by the glucan phosphatases, SEX4 and LSF2, remove phosphate groups allowing further degradation by amylolytic enzymes and phosphate removal is essential to 'reset' the cycle for subsequent rounds of degradation. The necessity of these enzymes for proper starch metabolism are witnessed when loss of function occurs in any of the genes encoding GWD, PWD, or SEX4 causing a starch-excess phenotype. In addition, the resulting starch is modified with altered phosphate content, granular morphology, and physico-chemical properties which have led to many subsequent studies on modifying starch *in planta* that is relevant to commercial crops such as barley, wheat, cassava, rice, and potato (232, 257, 258, 270, 283-289).

Starch granule morphologies of glucan dikinase and glucan phosphatase mutants have differential effects between species and depending on if the starch is a transitory or storage starch. Although differences in starch granule morphologies of previous studies have been subtle, they can also be drastic and provide invaluable clues into the structuring of the granule and its biological effects.

Starch granules in potato tubers are ovoid in nature and repression of *SEX4* and *LSF2* did not change the overall morphology of the granules (**Figure 6-1A-C**) (254). In contrast, *A. thaliana SEX4* mutants have larger, more spherical granules compared to the naturally flat and discoid granules of wild-type (**Figure 6-1D, E**) (72). Interestingly, LSF1*,* was originally classified as a glucan phosphatase whose role in starch degradation was previously unclear until recently, was shown to act as a scaffold for β-amylases facilitating degradation (182). Additionally, other laboratories have demonstrated that LSF1 is a catalytically dead phosphatase (182). *LSF1* mutant starch however was similar in size and shape compared to wild-type (**Figure 6-1F**). The *LSF1/SEX4* double mutant displayed a similar morphology to the large, spherical *SEX4* mutant starch (**Figure 6-1G**). Recently, the effect of altering phosphate content in the root crop cassava has been of increased interest due to its wide commercial cultivation in parts of Asia (290). Cassava granules are irregularly shaped with polygonal and round granules (**Figure 6-1H**). RNAi silencing lines of LSF2 did not alter the granule morphology in any significant way compared to wild-type (**Figure 6-1I**) (290).

Sex1 (GWD) mutants of *A. thaliana* are larger than wild-type but have similar flat, discoid shapes that is in stark contrast to *SEX4* mutants (**Figure 6-2A-D**). It is still unclear what is the cause of the morphology differences between *GWD* and *SEX4* mutants in *A. thaliana;* however, one could speculate that there could be variations in amylose-amylopectin ratios and interactions as well as altered specificities of synthases and debranching/branching enzymes. More severe starch morphologies are seen in low phosphate starch, resulting from the incidental co-suppression of GWD1 transgene and endogenous GWD1 (**Figure 6-2F, H**) (163). In these granules, there are several regions with rough surfaces unlike wild-type tuber starch as well as fissures that can readily be seen through light microscopy (**Figure 6-2H**). On the other hand, this morphological phenotype is not seen in cassava root or leaf starch (**Figure 6-2I-L**).

Fissures in the starch granule are a marked indicator for major destabilization and suboptimal packing of the granule matrix (163). They are also commonly seen in mutants of key starch synthesizing enzymes (starch synthases (SS) and

branching enzymes (SBEs)) (259, 260, 291-294). Along with fissures, SBE mutants incur a wide variety of other irregularities from longer rod-like shapes to multi-lobed shapes which can be seen in potato tuber antisense SBE (**Figure 6-3A-C**) (294). Similar phenotypes have been observed in potato tuber SSIII antisense lines compared to wild-type starch granules (**Figure 6-3D, E**) (260). Mechanical cracking and partial digestion of SSIII antisense lines with α-amylase, which prefers to act in the amorphous regions of granules showed a complete disruption in the organization of semi-crystalline lamellae (**Figure 6-3F**) (260). Interestingly, when human laforin was overexpressed in potato lines, there was an increase in starch phosphate content due to compensatory effects increasing GWD and PWD expression (257). There were also moderate proportions with significant reductions in amylose content (characterized as red-stained and blue-stained) and irregular starch granule morphologies associated with both groups (**Figure 6-3G-L**) (257). Both iodine-stained groups exhibited bumpy surfaces and cracked/severely fissured granules (**Figure 6-3H, I**). Therefore, alterations in phosphate content clearly have a substantial impact on the amylose:amylopectin ratio and on many other genes involved in starch biosynthesis and degradation.

The work herein is the first to show specific effects of reversible glucan phosphorylation in a red algal system (**Chapter 3 and 4**). In addition, a sole glucan dikinase (GWD) and phosphatase (laforin) are responsible for phosphorylation and dephosphorylation of semi-amylopectin type floridean starch in *C. merolae.* The loss of either enzymatic activity significantly affects the fine structure of amylopectin and thus granule morphology. The granule morphologies were different between GWD and laforin knockout lines as Δgwd granules were meaningfully flatter, larger, and more heterogenous which corroborates previous findings that GWD has an fundamental effect on granule size (295). On the other hand, $\Delta laforin$ granules were similar in size, had irregularly bumpy surfaces, and were slightly less spherical compared to wild-type. Both knockout lines though had several fissure-like regions and bi-lobal areas radiating from the inner granule. Loss of C6-phosphate content of polyglucans in Δgwd lines results in suboptimal organization of amylopectin indicating that C6-phosphate is required for proper

synthesis and degradation in *C. merolae* (**Chapter 3**). In the case of Δ*laforin* lines, without proper maintenance of C6-phosphate, too much C6-phosphate content can equally be as detrimental to amylopectin organization and thus plant vitality (**Chapter 4**).

Much of the work done to better understand the roles of glucan dikinases and phosphatases have been through higher plant systems that contain many isoforms of enzymes involved in starch metabolism (69). *C. merolae* is amongst a few organisms that produce starch-like polyglucans with a limited set of enzymes (69, 100). There is only one starch synthase and starch branching enzyme involved in the biosynthesis of starch in *C. merolae,* therefore, the effect of phosphorylation is likely more severe on the activity of these enzymes compared to higher plants where compensatory mechanisms may be involved. *C. merolae* provides an excellent model organism to study the basic functions of enzymes involved in reversible glucan phosphorylation and how they affect the main constituent of starch. As *C. merolae* contains a semi-amylopectin type floridean starch, this is a natural amylose-free or *waxy*-like starch, albeit a less ordered amylopectin structure (296). C6-phosphate represents the major portion (70%) of total phosphate content in higher plants; however, C6-phosphate is the only phosphate in *C. merolae.* This model can shed light on specific effects of C6-phosphorylation on branching and elongation activities during starch biosynthesis. Proper packing of amylopectin likely has direct biological effects in *C. merolae* as seen through prolonged energy deprivation. Loss of GWD or laforin in *C. merolae* resulted in excessive nutrient-scavenging which led to the depletion of critical photosynthetic pigments required to recover cell proliferation upon reintroduction of light (**Chapter 3 and 4**). Interestingly, Δ*gwd* lines continuously degraded all of their polyglucan over the extended dark period while wild-type lines were able to regulate their polyglucan degradation. Although Δ*laforin* lines consumed their photosynthetic pigments much more rapidly than Δ*gwd* lines, the loss of laforin clearly effected degradation of starch as only 40% was expended. The mechanisms behind the uncontrolled degradation seen in Δ*gwd* lines will need further investigation;

however, we hypothesize that there are several unforeseen regulatory mechanisms involved.

6.2 Future Prospectives

Our work on the enzymes involved in reversible glucan phosphorylation in *C. merolae* opens new opportunities to manipulate carbon metabolism. Initially, we hypothesized that Δ*gwd* and Δ*laforin* lines would exhibit a starch-excess phenotype similar to those seen in *A. thaliana;* however, as described in Chapters 3 and 4, we did not observe such a phenotype. Algae have two main forms of carbon storage, starch and neutral triacylglycerides (TAGs), therefore these knockout lines may be switching their carbon storage to TAGs or altering lipid profiles for specific purposes which can be an enticing avenue for engineering *C. merolae* to produce higher lipid contents. Our observations of lower insoluble polyglucan content in laforin knockout lines may be in correlation to decreases of starch synthesizing activity by UDP-glc starch synthase. Although studies characterizing floridean starch metabolism are severely lacking, these observations are similar to that seen in the low-starch mutant of the heterotrophic dinoflagellate, *Crypthecodinium cohnii* that also produces floridean starch (**Figure 6-4A**). The mutant (*sta1-1*) effectively altered UDP-glc soluble starch synthase activity resulting in lower starch content, a starch granule phenotype (irregular bumpy surfaces, **Figure 6-4B**), and CLD differences similar to Δ*laforin* lines in *C. merolae* (**Figure 6-1K**) compared to wild-type (**Figure 6-1J**) (297).

Another key future prospective in need of exploring is the role of floridoside as an osmolyte in *C. merolae,* analogous to sucrose in higher plants (49). We were able to identify a consistent soluble pool of floridoside in wild-type *C. merolae* through metabolomics but were often unable to observe this in both knockout lines. Metabolomics allows us to identify small molecules known as metabolites, and the metabolites give invaluable insight into the metabolism of an organism. Metabolomics exploits the use of making the metabolites volatile compounds which upon ionization can be separated based on their mass. The synthesis of floridoside and floridean starch comes from the same precursor UDP-glucose substrate and could be a crucial fate determinant of assimilated carbon; however,

there is very limited information regarding floridoside in general for red algae nor its regulation (49). Further optimization of metabolomic techniques will provide invaluable insights into the biological effects that arise from irregular starch metabolism. Recent studies on modulating starch accumulation in *C. merolae* have reported increased starch content in cells with inactivation of target of rapamycin (TOR) (188, 189). TOR plays a major role in both starch and TAG accumulation in *C. merolae,* therefore, investigation of the interactions between TOR and GWD/laforin may provide insights into their regulation.

CBM45s are a relatively newly discovered CBM family which could possess novel functions towards starch metabolism. Engineering chimeric proteins with a granular starch-binding CBM45 may allow for proteins to be targeted to starch and for dynamic activity corresponding to the catalytic function of appended domains. Although there is no additional structural data of the catalytic domain published for glucan dikinases, structural data for CBM45s allow us to isolate and engineer their activity that could be employed in industrial applications. We have initial structural data in regards to the isolated catalytic domain of *St*GWD that is currently being employed to other GWD orthologues. Possessing structural data for CBMs as well as the catalytic domain has an enormous potential to progress the field of starch metabolism and starch engineering. Much is still unknown about the specificity of glucan dikinases and whether this is due to catalytic domain or CBM differences. The presence of three CBM45s in *Cm*GWD and their relationship to the overall preference and activity of *Cm*GWD is likely specialized to their unique substrate. Structural data of CBM45-2 from *Cm*GWD opens up new opportunities in a biotechnological point of view as it is one step closer to discovering glucan chain phosphorylation patterns and substrate specificity for the production of desirable industrial starches (**Chapter 5**). Limited technology is available to decipher glucan chain phosphorylation patterns and their effect on physico-chemical properties of starch; however, our lab along with Dr. Ramon Sun's lab is equipped with a state-of-the-art Matrix-Assisted Laser Desorption/Ionization (MALDI) mass spectrometer that could be utilized to identify specific debranched glucan chains that are phosphorylated as MALDI is more sensitive than the commonly used method of

High-Performance Anion-Exchange Chromatography with Pulsed Amperometric Detection (HPAEC-PAD) (298). Thus, our lab is uniquely positioned to define the dynamics of starch phosphorylation by glucan dikinases and how to manipulate them for biotechnological utilization.

6.3 Conclusion

Starch is an indispensable commodity for humans as it serves as a main staple of our diet and has been an emerging source for renewable energy for decades. These studies highlight the importance and conservation of reversible glucan phosphorylation in floridean starch metabolism and its effect on the fine structure and granular morphology of starch. Understanding the mechanisms of action for glucan dikinases is essential for their unlimited potential in industrial processes. Manipulation of algal starch *in planta* can not only produce profitable designer starches, but it can also lead to new conceivable renewable energy sources that do not compete with feeding our rising population.
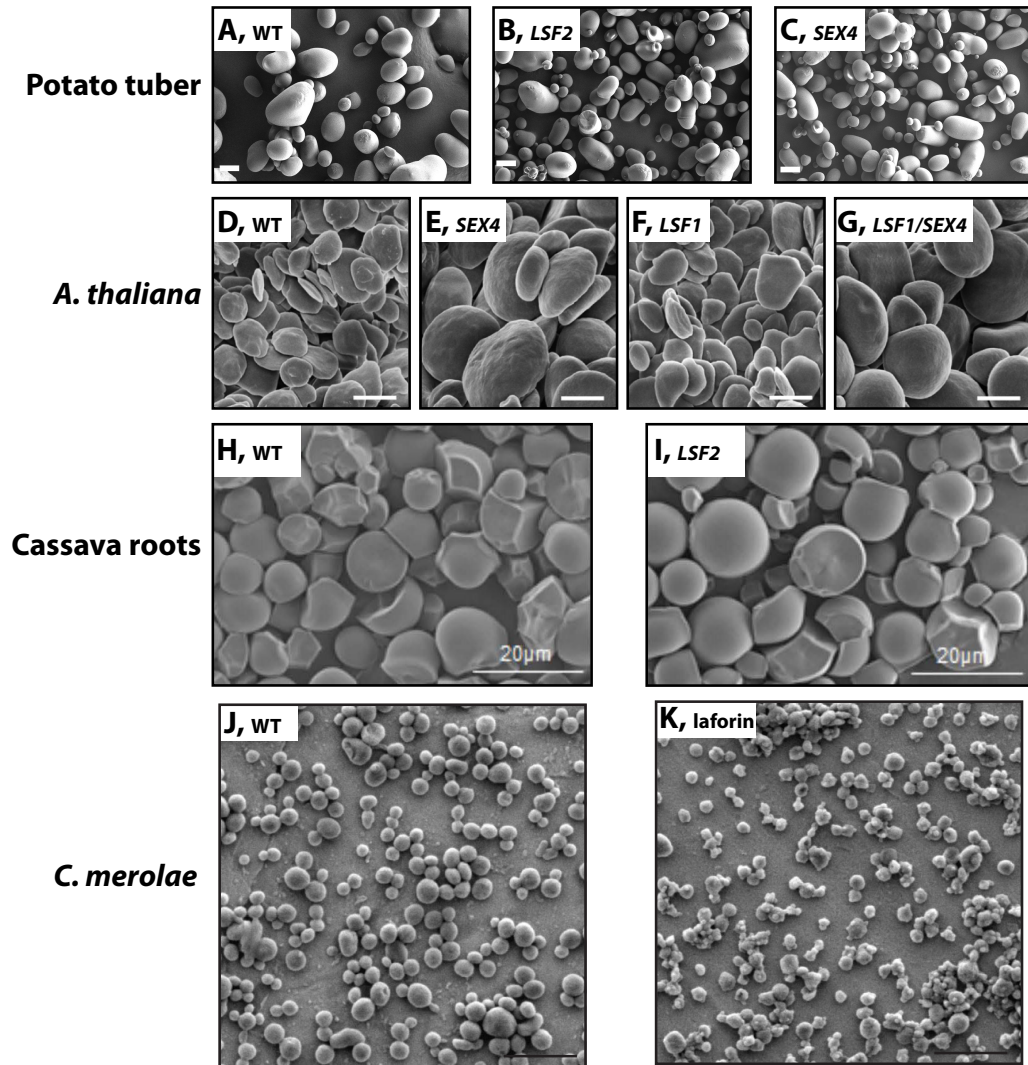
Figure 6-1 Glucan phosphatase mutant starch morphology
A-C) Modified from Samodien et al. 2018 (254). Scale bar = 20 μm. **D-G)** Modified from Comparot-Moss et al. 2010 (180). Scale bar = 2 μm. **H, I)** Modified from Wang et al. 2018 (290). **J, K)** *C. merolae* WT **(J)** and Δ*laforin* **(K)** polyglucan granules.
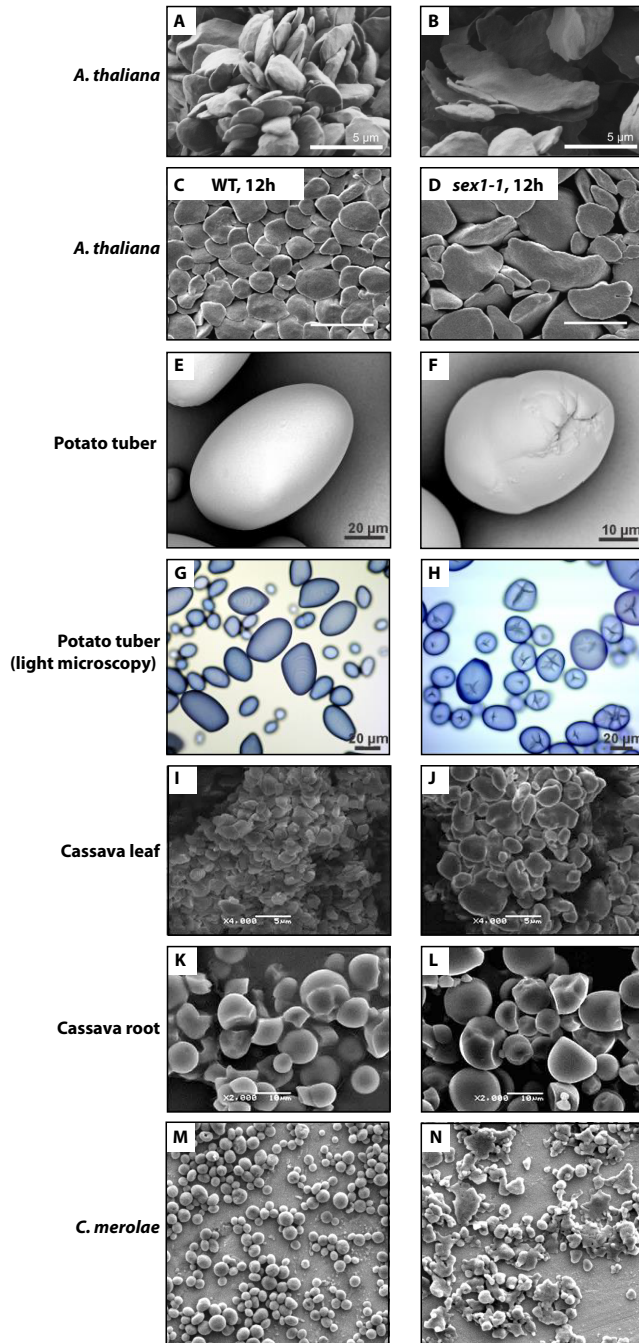
Figure 6-2 GWD mutant starch morphologies
A-D) *A. thaliana* leaf starch of wild-type **(A, C)** and GWD mutants (**B**, *sex1-8*) (**D**, *sex1-1)* collected at the end of 12-hour photoperiod. A, B modified from Mahlow et al. 2014 (161). **C, D** modified from Zeeman et al. 2002 (72). Scale bar = 2 μm. Potato tuber starch from wild-type **(E, G)** and GWD co-suppressed lines **(F, H).** Modified from Xu et al. 2017 (163). **I-L)** Modified from Zhou et al. 2017 (192). Cassava leaf starch granules **(I)** and GWD RNAi line 12 (**J**, G1i-12). Scale bar = 5 μm. Cassava root starch granules from wild-type **(K)** and GWD RNAi line 12 **(L).** Scale bar = 10 μm. **M, N)** *C. merolae* WT **(M)** and Δ*gwd* **(N)** polyglucan granules.
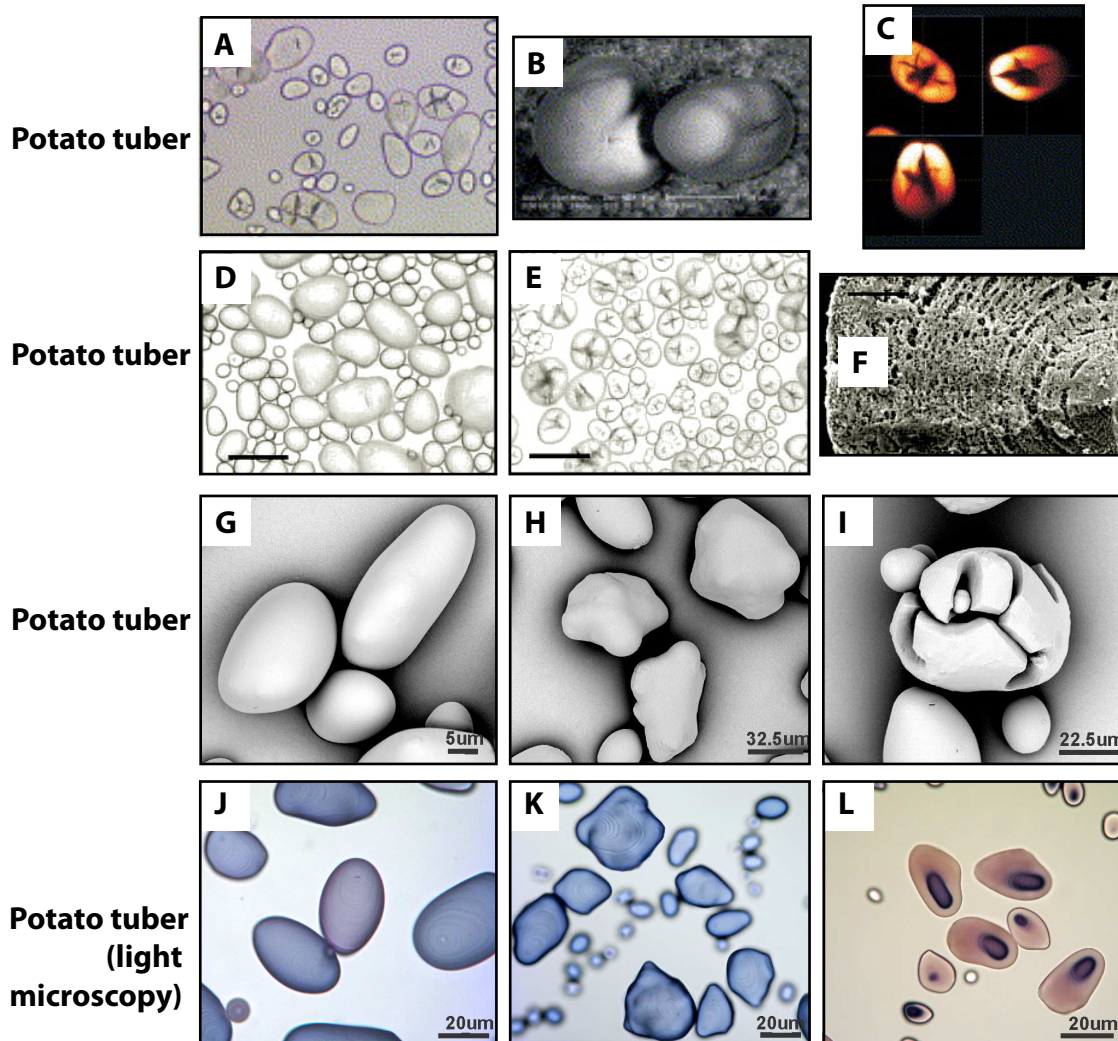
Figure 6-3 Irregular bumpy and fissure-like starch granule morphologies
A-C) Potato tuber starch granules from SBE antisense line viewed through brightfield **(A),** environmental scanning electron **(B),** and confocal laser scanning **(C)** microscopy. Modified from Blennow et al. 2003 (294). **D-F)** Potato tuber starch morphology of wild-type **(D)** and starch synthase III (SSIII) antisense line 18 **(E).** Scale bars = 50 μm. **F)** Internal structure of mechanically cracked and partly digested starch granule of SSIII antisense line 8. Modified from Fulton et al. 2002 (260). **G-I)** SEM of potato tuber starch granules from wild-type **(G)** and two different morphologies in laforin-overexpressed lines **(H and I).** Light micrographs of iodine-stained granules of wild-type **(J)** and two different morphologies in laforin-overexpressed lines (**K and L**). Modified from Xu et al. 2017 (257).
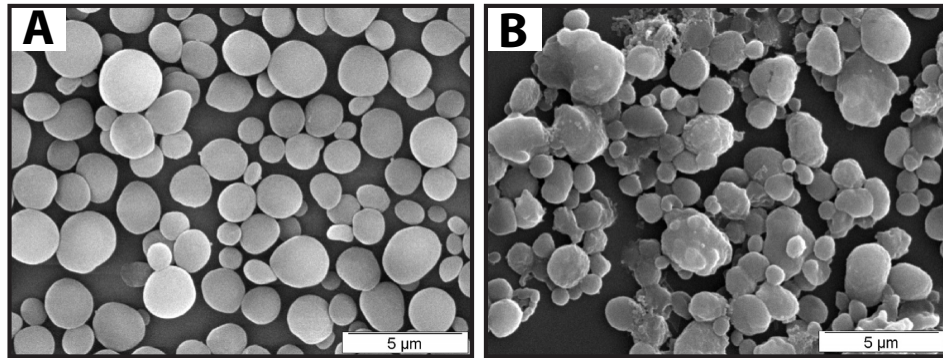
Figure 6-4 Irregular bumpy surface starch granule morphologies
Floridean starch granules from wild-type **(A)** and UDP-glc starch synthase mutant
sta1-1 **(B)** dinoflagellate, *C. cohnii.* Modified from Dauvillee et al. 2009 (297).

REFERENCES

1. De Luca P, Taddei R, Varano L. Cyanidioschyzon merolae- an new alga of thermal acidic environments. Journal of Plant Taxonomy and Geography. 1978;33(1):37-44.

2. Pueschel CM. Cell structure. In: Sheath KMCaR, editor. Biology of the red algae. New York: Cambridge University Press; 1990. p. 7-41.

3. Reeb V, Bhattacharya D. The thermo-acidophilic cyanidiophyceae (cyanidiales). In: Seckbach J, Chapman DJ, editors. Red Algae in the Genomic Age. 13: Springer; 2010. p. 409-26.

4. Albertano P, Ciniglia C, Pinto G, Pollio A. The taxonomic position of *Cyanidium, Cyanidioschyzon,* and *Galdieria*: an update. Hydrobiologia. 2000;433:137-43.

5. Ott FD, Seckbach J. A review on the taxonomic position of the algal genus *Cyanidium* Geitler 1933 and its ecological cohorts *Galdieria Merola* in Merola et al. 1981 and *Cyanidioschyzon* De Luca et al. 1978. In: Seckbach J, editor. Evolutionary Pathways and Enigmatic Algae: *Cyanidium caladium (Rhodophyta)* and Related Cells. The Netherlands: Klewer; 1994. p. 113-32.

6. Miyagishima S, Wei JL, Nozaki H, Hirooka S. Cyanidiales: Evolution and Habitats. In: Kuroiwa T, Miyagishima S, Matsunaga S, Sato N, Nozaki H, Tanaka K, et al., editors. *Cyanidioschyzon merolae:* A New Model Eukaryote for Cell and Organelle Biology. Singapore: Springer Nature; 2017. p. 2-15.

7. Sato N, Moriyama T. Genomic and Biochemical Analysis of Lipid Biosynthesis in the Unicellular Rhodophyte *Cyanidioschyzon merolae:* Lack of a Plastidic Desaturation Pathway Results in the Coupled Pathway of Galactolipid Synthesis. Eukaryotic Cell. 2007;6(6):1006-17.

8. Barbier G, Oesterhelt C, Larson MD, Halgren RG, Wilkerson C, Garavito RM, et al. Comparative Genomics of Two Closely Related Unicellular Thermo-Acidophilic Red Algae, Galdieria sulphuraria and Cyanidioschyzon merolae, Reveals the Molecular Basis of the Metabolic Flexibility of Galdieria sulphuraria and Significant Differences in Carbohydrate Metabolism of Both Algae. Plant Physiol. 2005;137(2):460-74.

9. Merola A, Castaldo R, De Luca P, Gambardella R, Musacchio A, Taddei R. Revision of Cyanidium caldarium. Three species of acidophilic algae. Giornale botanico italiano: Official Journal of the Societa Botanica Italiana. 1981;115(4-5):189-95.

10. Toplin JA, Norris TB, Lehr CR, McDermott TR, Castenholz RW. Biogeographic and Phylogenetic Diversity of Thermoacidophilic Cyanidiales in Yellowstone National Park, Japan, and New Zealand. Applied and Environmental Microbiology. 2008;74(9):2822-33.

11. Gross W, Schnarrenberger C. Heterotrophic growth of 2 strains of the acid-thermophilic red alga *Galdieria sulphuraria.* Plant Cell Physiology. 1995;36:633-8.

12. Moriyama T, Mori N, Sato N. Activation of oxidative carbon metabolism by nutritional enrichment by photosynthesis and exogenous organic

compounds in the red alga C*yanidioschyzon merolae:* evidence for heterotrophic growth. . Springer Plus. 2015;4.

13.   Suzuki K, Ohta N, Kuroiwa T. Isolation of the cell-nuclear, mitochondrial, and chloroplast DNA from the ultra-small eukaryote *Cyanidioschyzon merolae.* Protoplasma. 1992;171:80-4.

14.   Kuroiwa T, Kawazu T, Takahashi H, Suzuki K, Ohta N, Kuroiwa H. Comparison of ultrastructures between the ultra-small eukaryote *Cyanidioschyzon merolae* and *Cyanidium caldarium.* Cytologia. 1994;59:149-58.

15.   Kuroiwa T. The primitive red algae *Cyanidium caldarium* and *Cyanidioschyzon merolae* as model system for investigating the dividing apparatus of mitochondria and plastids. . BioEssays. 1998;20:344-54.

16.   Terui S, Suzuki K, Takahashi H, Itoh R, Kuroiwa T. High synchronization of chloroplast division in the ultramicro-alga *Cyanidioschyzon merolae* by treatment with both light and aphidocolin. J Phycol. 1995;31:958-61.

17.   Suzuki K, Ehara T, Osafune T, Kuroiwa H, Kawano S, Kuroiwa T. Behavior of mitochondria, chloroplasts and their nuclei during the mitotic cycle in the ultramicroalga *Cyanidioschyzon merolae.* Eur J Cell Biology. 1994;63:280-8.

18.   Kuroiwa T, Suzuki K, Itou R, Toda K, O'Keefe TC, Kuroiwa H. Mitochondria-dividing ring: ultra-structural basis for the mechanism of mitochondrial division in *Cyanidioschyzon merolae.* Protoplasma. 1995;186:12-23.

19.   Bi E, Luthkenhaus J. FtsZ ring structure associated with division in *Escherichia coli.* Nature. 1991;354:161-4.

20.   Ohta N, Sato N, Kuroiwa T. Structure and organization of the mitochondrial genome of the unicellular red algae C*yanidioschyzon merolae d*educed from the complete nucleotide sequence. . Nucleic Acids Research. 1998;26:5190-8.

21.   Ohta N, Matsuzaki M, Misumi O, Miyagishima S, Nozaki H, Tanaka K, et al. Complete sequence analysis of the plastid genome of the unicellular red alga *Cyanidioschyzon merolae.* DNA Research. 2003;10:67-77.

22.   Matsuzaki M, Misumi, O., Shin-i, T., Maruyama, S., Takahara, M., et al. Genome sequence of the ultrasmall unicellular red alga Cyanidioschyzon merolae 10D. Nature. 2004;428:653-7.

23.   Misumi O, Matsuzaki M, Nozaki H, Miyagishima S-y, Mori T, Nishida K, et al. Cyanidioschyzon merolae Genome. A Tool for Facilitating Comparable Studies on Organelle Biogenesis in Photosynthetic Eukaryotes. Plant Physiol. 2005;137(2):567-85.

24.   Miyagishima SY, Nishida K, Mori T, Matsuzaki M, Higashiyama T, Kuroiwa H, et al. A Plant-Specific Dynamin-Related Protein Forms a Ring at the Chloroplast Division Site. Plant Cell. 2003;15(3):655-65.

25.   Nishida K, Takahara M, Miyagishima S-y, Kuroiwa H, Matsuzaki M, Kuroiwa T. Dynamic recruitment of dynamin for final mitochondrial severance in a primitive red alga. PNAS. 2003;100(4):2146-51.

26. Minoda A, Sakagami R, Yagisawa F, Kuroiwa T, Tanaka K. Improvement of Culture Conditions and Evidence for Nuclear Transformation by Homologous Recombination in a Red Alga, Cyanidioschyzon merolae 10D. Plant Cell Physiol. 2004;45(6):667-71.

27. Boek JD, Trueheart J, Natsoulis G, Fink GR. 5-Fluoroorotic acid as a selective agent in yeast molecular genetics. Methods Enzymol. 1987;154:164-75.

28. Ohnuma M, Yokoyama T, Inouye T, Sekine Y, Tanaka K. Polyethylene glycol (PEG)-mediated transient gene expression in a red alga, Cyanidioschyzon merolae 10D. Plant Cell Physiol. 2008.

29. Imamura SK, Y.Ohnuma, M.Inouye, T. Sekine, Y.Fujiwara, T.Kuroiwa, T. Tanaka, K. R2R3-type MYB transcription factor, CmMYB1, is a central nitrogen assimilation regulator in *Cyanidioschyzon merolae* PNAS. 2009;106(30):12548-53.

30. Fujiwara T, Kanesaki Y, Hirooka S, Era A, Sumiya N, Yoshikawa H, et al. A nitrogen source-dependent inducible and repressible gene expression system in the red alga *Cyanidioschyzon merolae.* Frontiers in Plant Science. 2015;6.

31. Sumiya N, Fujiwara T, Kobayashi Y, Misumi O, Miyagishima SY. Development of a heat-shock inducible gene expression system in the red alga *Cyanidioschyzon merolae*. PLoS ONE. 2014;9.

32. Fujiwara T, Ohnuma M, Kuroiwa T, Ohbayashi R, Hirooka S, Miyagishima SY. Development of a Double Nuclear Gene-targeting Method by Two-Step Transformation Based on a Newly Established Chloramphenicol-Selection System in the Red Alga *Cyanidioschyzon merolae*. Frontiers in Plant Science. 2017;8.

33. Taki K, Sone T, Kobayashi Y, Watanabe S, Imamura S, Tanaka K. Construction of a URA5.3 deletion strain of the unicellular red alga *Cyanidioschyzonmerolae*: A backgroundless host strain for transformation experiments. J Gen Appl Microbiol. 2015;61:211-4.

34. Gest H. Bicentenary homage to Dr Jan Ingen-Housz MD (1730-1799), pioneer of photosynthesis research. Photosynthesis Research. 2000;63:183-90.

35. Duysens LNM. Photosynthesis. Progress in biophysics and molecular biology. 1964;14:1-104.

36. Blankenship RE, Hartman H. The origin and evolution of oxygenic photosynthesis. Trends in Biochemical Sciences. 1998;23(3):94-7.

37. Archibald J. One plus one equals one. Symbiosis and the evolution of complex life. USA: Oxford University Press; 2014.

38. Pi X, Tian L, Dai HE, Qin X, Cheng L, Kuang T, et al. Unique organization of photosystem I-light-harvesting supercomplex revealed by cryo-EM from a red alga. PNAS. 2018;115(17):4423-8.

39. Sato N, Moriyama T. Photosynthesis. In: Kuroiwa T, Miyagishima S, Matsunaga S, Sato N, Nozaki H, Tanaka K, et al., editors. *Cyanidioschyzon merolae* A New Model Eukaryote for Cell and Organelle Biology. Singapore: Springer Nature; 2017. p. 263-82.

40. Busch A, Nield J, Hippler M. The composition and structure of photosystem I-associated antenna from *Cyanidioschyzon merolae.* The Plant Journal. 2010;62:886-97.

41. Parys E, Krunnik T, Kulak I, Kania K, Romanowska E. Photosynthesis of the *Cyanidioschyzon merolae* cells in blue, red, and white light. Photosynthesis Research. 2021;147:61-73.

42. Liu LN, Aartsma TJ, Thomas JC, Lamers GE, Zhou BC, Zhang YZ. Watching the native supramolecular architecture of photosynthetic membrane in red algae: topography of phycobilisomes and their crowding, diverse distribution patterns. J Biol Chem. 2008;283:34946-53.

43. Barber J, Nield J, Morris EP, Zheleva D, Hankamer B. The structure, function, and dynamics of photosystem two. Physiologia Plantarum. 1997;100:817-27.

44. Gardian Z, Bumba L, Schrofel A, Herbstova M, Nebesarova J, Vacha F. Organization of Photosystem I and Photosystem II in red algae *Cyanidium caldarium*: Encounter of cyanobacteria and higher plant concepts. Biochimica et Biophysica Acta. 2007:725-31.

45. Raven JA, Johnston AM, MacFarlane JJ. Carbon Metabolism. In: Cole KM, Sheath RG, editors. Biology of the Red Algae. New York: Cambridge University Press; 1990. p. 171-202.

46. Moriyama T, Mori N, Sato N. Carbon Metabolism. In: Kuroiwa T, Miyagishima S, Matsunaga S, Sato N, Nozaki H, Tanaka K, et al., editors. *Cyanidioschyzon merolae* A New Model Eukaryote for Cell and Organelle Biology. Singapore: Springer Nature; 2017. p. 297-321.

47. Moriyama T, Sakurai K, Sekine K, Sato N. Subcellular distribution of central carbohydrate metabolism pathways in the red alga *Cyanidioschyzon merolae.* Planta. 2014;240:585-98.

48. Mori N, Moriyama T, Toyoshima M, Sato N. Construction of Global Acyl Lipid Metabolic Map by Comparative Genomics and Subcellular Localization Analysis in the Red Alga *Cyanidioschyzon merolae.* Frontiers in Plant Science. 2016;7.

49. Viola R, Nyvall P, Pedersén M. The unique features of starch metabolism in red algae. Proc R Soc Lond B. 2001;268:1417 - 22.

50. Pade N, Linka N, Ruth W, Weber APM, Hagemann M. Floridoside and isofloridoside are synthesized by trehalose 6-phosphate synthase-like enzymes in the red alga *Galdieria sulphuraria.* New Phytologist. 2015;205:1227-38.

51. Ekman P, Yu, S. K. & Pederse¨ n, M. Effects of altered salinity, darkness and algal nutrient status on floridoside and starch content, alpha-galactosidase activity and agar yield of cultivated Gracilaria sordida. British Phycological Journal. 1991;26:123-31.

52. De Luca P, Moretti A. Floridosides in *Cyanidium caldarium, Cyanidioschyzon merolae,* and *Galdieria suyphuraria* (Rhodophyta, Cyanidiophyceae). J Phycol. 1983;19:368-9.

53. Li S-Y. Fixed Carbon Partitioning in the Red Microalga *Porphyridium* Sp. (Rhodophyta). J Phycol. 2001;37:289-97.

54. Brust H, Orzechowski S, Fettke J. Starch and Glycogen Analyses: Methods and Techniques. Biomolecules. 2020;10.

55. Roach PJ, Depaoli-Roach AA, Hurley TD, Tagliabracci VS. Glycogen and its metabolism: some new developments and old themes. Biochem J. 2012;441(3):763-87.

56. Melendez-Hevia E, Waddell TG, Shelton ED. Optimization of molecular design in the evolution of metabolism: the glycogen molecule. Biochem J. 1993;295 (Pt 2):477-83.

57. Smirnova J, Fernie AR, Steup M. Starch degradation. Starch: Springer; 2015. p. 239-90.

58. Fuentes C, Kang I, Lee J, Song D, Sjoo M, Choi J, et al. Fractionation and characterization of starch granules using filed-flow fractionation (FFF) and differential scanning calorimetry (DSC). Analytical and Bioanalytical Chemistry. 2019;411:3665-74.

59. Manners DJ. Recent developments in our understanding of amylopectin structure. Carbohydrate Polymers. 1989;11:87-112.

60. Buleon A, Colonna P, Planchot V, Ball S. Starch granules: structure and biosynthesis. Int J Biol Macromol. 1998;23(2):85-112.

61. Bertoft E. Understanding Starch Structure: Recent Progress. Agronomy. 2017;7(56).

62. Oostergetel GT, van Bruggen EFJ. The crystalline domains in potato starch granules are arranged in a helical fashion. Carbohydrate Polymers. 1993;21:7-12.

63. Pfister B, Zeeman SC. Formation of starch in plant cells. Cellular and Molecular Life Sciences. 2016;73(14):2781-807.

64. Smith AM. The biosynthesis of starch granules. Biomacromolecules. 2001;2(2):335-41.

65. Buleon A, Veronese G, Putaux JL. Self-Association and Crystallization of Amylose. Aust J Chem. 2007;60:706-18.

66. Wei C, Qin F, Zhou W, Yu H, Xu B, Chen C, et al. Granule Structure and Distribution of Allomorphs in C-Type High-Amylose Rice Starch Granule Modified by Antisense RNA Inhibition of Starch Branching Enzyme. J Agric Food Chem. 2010;58:11946-54.

67. Gerard C, Planchot V, Colonna P, Bertoft E. Relationship between branching density and crystalline structure of A- and B-type maize mutant starches. Carbohydrate Research. 2000;326:130-44.

68. Zeeman SC, Kossmann J, Smith AM. Starch: Its Metabolism, Evolution, and Biotechnological Modification in Plants. Annu Rev Plant Biol. 2010;61:209-34.

69. Coppin A, Varré J, Lienard L, Dauvillée D, Guérardel Y, Soyer-Gobillard M, et al. Evolution of Plant-Like Crystalline Storage Polysaccharide in the Protozoan Parasite Toxoplasma gondii Argues for a Red Alga Ancestry. Journal of Molecular Evolution. 2005;60(2):257-67.

70. Gentry MS, Mattoo S, Dixon JE. Utilizing red algae to understand a neurodegenerative disease. In: Seckbach J, Chapman DJ, editors. Red

Algae in the Genomic Age. Cellular Origin, LIfe in Extreme Habitats and Astrobiology. 13. New York: Springer; 2010. p. 149-70.

71. Myers AM, Morell MK, James MG, Ball SG. Recent Progress toward Understanding Biosynthesis of the Amylopectin Crystal. Plant Physiol. 2000;122(4):989-98.

72. Zeeman SC, Tiessen A, Pilling E, Kato KL, Donald AM, Smith AM. Starch Synthesis in Arabidopsis. Granule Synthesis, Composition, and Structure. Plant Physiol. 2002;129(2):516-29.

73. Hirabaru C, Izumo A, Fujiwara S, Tadokoro Y, Shimonaga T, Konishi M, et al. The primitive rhodophyte Cyanidioschyzon merolae containsa semiamylopectin-type, but not an amylose-type, α -glucan. Plant Cell Physiol. 2010;51(5):682-93.

74. Shimonaga T, Konishi M, Oyama Y, Fujiwara S, Satoh A, Fujita N, et al. Variation in Storage {alpha}-Glucans of the Porphyridiales (Rhodophyta). Plant Cell Physiol. 2008;49(1):103-16.

75. Shimonaga T, Fujiwara S, Kaneko M, Izumo A, Nihei S, Francisco Jr PB, et al. Variation in Storage alpha-Polyglucans of Red Algae: Amylose and Semi-Amylopectin Types in *Porphyridium* and Glycogen Type in. Marine Biotechnology. 2007;9:192-202.

76. Nakamura Y, Takahashi J, Sakurai A, Inaba Y, Suzuki E, Nihei S, et al. Some cyanobacteria synthesize semi-amylopectin type alpha-polyglucans instead of glycogen. Plant Cell Physiology. 2005;46:539-45.

77. Deschamps P, Colleoni C, Nakamura Y, Suzuki E, Putaux JL, Buleon A, et al. Metabolic Symbiosis and the Birth of the Plant Kingdom. Mol Biol Evol. 2008;25(3):536-48.

78. Mahlow S, Orzechowski S, Fettke J. Starch phosphorylation: insights and perspectives. Cellular and molecular life sciences. 2016;73(14):2753-64.

79. Tagliabracci VS, Heiss C, Karthik C, Contreras CJ, Glushka J, Ishihara M, et al. Phosphate incorporation during glycogen synthesis and Lafora disease. Cell Metab. 2011;13(3):274-82.

80. Tagliabracci VS, Girard JM, Segvich D, Meyer C, Turnbull J, Zhao X, et al. Abnormal metabolism of glycogen phosphate as a cause for lafora disease. J Biol Chem. 2008;283(49):33816-25.

81. Tagliabracci VS, Turnbull J, Wang W, Girard JM, Zhao X, Skurat AV, et al. Laforin is a glycogen phosphatase, deficiency of which leads to elevated phosphorylation of glycogen in vivo. Proc Natl Acad Sci U S A. 2007;104(49):19262-6.

82. DePaoli-Roach AA, Contreras CJ, Segvich DM, Heiss C, Ishihara M, Azadi P, et al. Glycogen phosphomonoester distribution in mouse models of the progressive myoclonic epilepsy, Lafora disease. J Biol Chem. 2015;290(2):841-50.

83. Contreras CJ, Segvich DM, Mahalingan K, Chikwana VM, Kirley TL, Hurley TD, et al. Incorporation of phosphate into glycogen by glycogen synthase. Arch Biochem Biophys. 2016;597:21-9.

84. Schoch TJ. Fractionation of Starch by Selective Precipitation with Butanol. Journal of American Chemical Society. 1942;64:2957-61.

85. Hizukuri S, Tabata S, Nikuni Z. Studies on starch phosphate. Part 1. Estimation of glucose-6-phosphate residues in starch and the presence of other bound phosphate(s). Starke. 1970;22:338-43.

86. Blennow A, Bay-Smidt AM, Olsen CE, Moller BL. The distribution of covalently bound phosphate in the starch granule in relation to starch crystallinity. Int J Biol Macromol. 2000;27(3):211-8.

87. Blennow A, Engelsen SB, Munck L, Moller BL. Starch molecular structure and phosphorylation investigated by a combined chromatographic and chemometric approach. . Carbohydrate Polymers. 2000;41(2):163-74.

88. Xu X, Dees D, Dechesne A, Huang X-F, Visser RGF, Trindade LM. Starch phosphorylation plays an important role in starch biosynthesis. Carbohydrate Polymers. 2017;157:1628-37.

89. Tabata S, Hizukuri S. Studies on Starch Phosphate. Part 2. Isolation of Glucose 3-Phosphate and Maltose Phosphate by Acid Hydrolysis of Potato Starch. Starch. 1971;23(8):267-72.

90. Ritte G, Heydenreich M, Mahlow S, Haebel S, Kotting O, Steup M. Phosphorylation of C6- and C3-positions of glucosyl residues in starch is catalysed by distinct dikinases. FEBS Lett. 2006;580(20):4872-6.

91. Lim ST, Kasemsuwan T, Jane JL. Characterization of phosphorus in starch by 31P-nuclear magnetic resonance spectroscopy. Cereal chemistry. 1994;71(5):488-93.

92. Blennow A, Bay-Smidt AM, Wischmann B, Olsen CE, Moller BL. The degree of starch phosphorylation is related to the chain length distribution of the neutral and the phosphorylated chains of amylopectin. Carbohydrate Research. 1998;307:45-54.

93. Verbeke J, Penverne C, D'Hulst C, Rolando C, Szydlowski N. Rapid and sensitive quantification of C3- and C6-phosphoesters in starch by fluorescence-assisted capillary electrophoresis. Carbohydrate Polymers. 2016;152:784-91.

94. Takeda Y, Hizukuri S. Location of phosphate groups in potato amylopectin. Carbohydrate Research. 1982;102:321-7.

95. Blennow A, Engelsen SB. Helix-breaking news: fighting crystalline starch energy deposits in the cell. Trends Plant Sci. 2010;15(4):236-40.

96. Machovic M, Janecek S. Starch-binding domains in the post-genome era. Cell Mol Life Sci. 2006;63(23):2710-24.

97. Cantarel BL, Coutinho PM, Rancurel C, Bernard T, Lombard V, Henrissat B. The Carbohydrate-Active EnZymes database (CAZy): an expert resource for Glycogenomics. Nucleic Acids Res. 2009;37(Database issue):D233-8.

98. Lombard V, Golaconda Ramulu H, Drula E, Coutinho PM, Henrissat B. The carbohydrate-active enzymes database (CAZy) in 2013. Nucleic Acids Res. 2014;42(Database issue):D490-5.

99. Guillen D, Sanchez S, Rodriguez-Sanoia R. Carbohydrate-binding domains: multiplicity of biological roles. Applied Microbiology Biotechnology. 2010;83:1241-9.

100. Ball S, Colleoni C, Arias MC. The transition from glycogen to starch metabolism in cyanobacteria and eukaryotes. In: Nakamura Y, editor. Starch: Metabolism and Structure. Japan: Springer; 2015. p. 93-158.

101. Nakamura Y. Starch: Initiation Process of Starch Biosynthesis. In: Nakamura Y, editor. Starch: Metabolism and Structure. Tokyo: Springer Japan; 2015. p. 315-32.

102. Ball S, Colleoni C, Cenci U, Raj JN, Tirtiaux C. The evolution of glycogen and starch metabolism in eukaryotes gives molecular clues to understand the establishment of plastid endosymbiosis. J Exp Bot. 2011;62(6):1775-801.

103. Bertoft E, Koch K, Aman P. Building block organisation of clusters in amylopectin from different structural types. International Journal of Biological Macromolecules. 2012;50(5):1212-23.

104. Smith AM, Zeeman SC. Starch: A Flexible, Adaptable Carbon Store Coupled to Plant Growth. Annual Review of Plant Biology. 2020;71:217-45.

105. Szydlowski N, Ragel P, Raynaud S, Lucas MM, Roldan I, Montero M, et al. Starch Granule Initiation in *Arabidopsis* Requires the Presence of Either Class IV or Class III Starch Synthases. Plant Cell. 2009;21(8):2443-57.

106. Roldan I, Wattlebled F, Lucas MM, Delvalle D, Planchot V, Jimenez S, et al. The phenotype of soluble starch synthase IV defective mutants of *Arabidopsis thaliana* suggests a novel function of elongation enzymes in the control of starch granule formation. The Plant Journal. 2007;49:492-504.

107. D'Hulst C, Wattebled F, Szydlowski N. Starch Biosynthesis in Leaves and Its Regulation. In: Nakamura Y, editor. Starch: Metabolism and Structure. Tokyo: Springer Japan; 2015. p. 211-38.

108. Denver K, Waite D, Motawia S, Moller BL, Smith AM. Granule-bound starch synthase I in isolated starch granules elongates malto-oligosaccharides processively. Biochem J. 1999;340:183-91.

109. Ball SG, Morell MK. FROM BACTERIAL GLYCOGEN TO STARCH: Understanding the Biogenesis of the Plant Starch Granule. Annual Review of Plant Biology. 2003;54(1):207-33.

110. Nelson OE, Rines HW. The enzymatic deficiency in the waxy mutant of maize. Biochem Biophys Res Commun. 1962;9:297-300.

111. Ball SG, van de Wal MHBJ, Visser RGF. Progress in understanding the biosynthesis of amylose. Trends in Plant Science. 1998;3(12):462-7.

112. Blauth SL, Yao Y, Klucinec JD, Shannon JC, Thompson DB, Guilitinan MJ. Identification of *Mutator* Insertional Mutants of Starch-Binding Enzyme 2a in Corn. Plant Physiology. 2001;125:1396-405.

113. Flipse E, Suurs L, Keetels CJA, Kossmann J, Jacobsen E, Visser RGF. Introduction of sense and antisense cDNA for branching enzyme in the amylose-free potato mutant leads to physico-chemical changes in the starch. Planta. 1996;198:340-7.

114. Kobayashi T, Sasaki S, Utsumi Y, Fujita N, Umeda K, Sawada T, et al. Comparison of Chain-Length Preferences and Glucan Specificities of Isoamylase-Type alpha-Glucan Debranching Enzymes from Rice, Cyanobacteria, and Bacteria. PLoS ONE. 2016:1-21.

115. James MG, Robertson DS, Myers AM. Characterization of the maize gene *sugary1,* a determinant of starch composition in kernels. Plant Cell. 1995;7:417-29.

116. Nakamura Y. Some properties of starch debranching enzymes and their possible role in amylopectin biosynthesis. Plant Science. 1996;121:1-18.

117. Nakamura Y, Umemoto T, Takahata Y, Komae K, Amano E, Satoh H. Changes in structure of starch and enzyme activities affected by s*ugary* mutations in developing rice endosperm. Possible role of starch debranching enzyme (R-enzyme) in amylopectin biosynthesis Physiologia Plantarum. 1996;97(3):491-8.

118. Nakamura Y, Kubo A, Shimamune T, Matsuda T, Harada K, Satoh H. Correlation between activities of starch debranching enzyme and alpha-polyglucan structure in endosperms of *sugary-1* mutants of rice. The Plant Journal. 1997;12(1):143-53.

119. Pan D, Nelson NE. A debranching enzyme deficiency in endosperms of *sugary-1* mutants of maize. Plant Physiology. 1984;74:324-8.

120. Wattebled F, Dong Y, Dumez S, Delvalle D, Planchot V, Berbezy P, et al. Mutants of Arabidopsis Lacking a Chloroplastic Isoamylase Accumulate Phytoglycogen and an Abnormal Form of Amylopectin. Plant Physiology. 2005;138:184-95.

121. Wattebled F, Planchot V, Dong Y, Szydlowski N, Pontoire B, Devin A, et al. Further evidence for the mandatory nature of polysaccharide debranching for the aggregation of semicrystalline starch and for overlapping functions of debranching enzymes in Arabidopsis leaves. Plant Physiology. 2008;148:1309-23.

122. Dinges JR, Colleoni C, James MG, Myers AM. Mutational Analysis of Pullulanase-Type Debranching Enzyme of Maize Indicates Multiple Functions in Starch Metabolism. Plant Cell. 2003;15:666-80.

123. Hejazi M, Fettke J, Haebel S, Edner C, Paris O, Frohberg C, et al. Glucan, water dikinase phosphorylates crystalline maltodextrins and thereby initiates solubilization. Plant J. 2008;55(2):323-34.

124. Caspar T, Lin T-P, Kakefuda G, Benbow L, Preiss J, Somerville C. Mutants of Arabidopsis with Altered Regulation of Starch Degradation. Plant Physiol. 1991;95(4):1181-8.

125. Smith SM, Fulton DC, Chia T, Thorneycroft D, Chapple A, Dunstan H, et al. Diurnal Changes in the Transcriptome Encoding Enzymes of Starch Metabolism Provide Evidence for Both Transcriptional and Posttranscriptional Regulation of Starch Metabolism in Arabidopsis Leaves. Plant Physiol. 2004;136(1):2687-99.

126. Lloyd JR, Kossmann J, Ritte G. Leaf starch degradation comes out of the shadows. Trends in Plant Science. 2005;10(3):130-7.

127. Fulton DC, Stettler M, Mettler T, Vaughan CK, Li J, Francisco P, et al. β -AMYLASE4, a Noncatalytic Protein Required for Starch Breakdown, Acts Upstream of Three Active β -Amylases in A*rabidopsis C*hloroplasts. . The Plant Cell. 2008;20:1040-58.

128. Monroe JD, Breault JS, Pope LE, Torres CE, Gebrejesus TB, Berndsen CE, et al. Arabidopsis b -Amylase2 Is a K + -Requiring, Catalytic Tetramer with Sigmoidal Kinetics. Plant Physiology. 2017;175:1525-35.

129. Monroe JD, Storm AR. Review: The Arabidopsis β-amylase (BAM) gene family: Diversity of form and function. Plant Science. 2018;276:163-70.

130. Yu T-S, Zeeman SC, Thorneycroft D, Fulton DC, Dunstan H, Lue W-L, et al. {alpha}-Amylase Is Not Required for Breakdown of Transitory Starch in Arabidopsis Leaves. J Biol Chem. 2005;280(11):9773-9.

131. Delatte T, Umhang M, Trevisan M, Eicke S, Thorneycroft D, Smith SM, et al. Evidence for distinct mechanisms of starch granule breakdown in plants. J Biol Chem. 2006;281:12050-9.

132. Streb S, Delatte T, Umhang M, Eicke S, Schorderet M, Reinhardt D, et al. Starch granule biosynthesis in Arabidopsis is abolished by removal of all debranching enzymes but restored by subsequent removal of an end-amylase. Plant Cell. 2008;20:3448-66.

133. Fincher GB. Molecular and cellular biology associated with endosperm mobilization in germinating cereal grains. Annual Review Plant Physiology Plant Mol Biol. 1998;40:305-46.

134. Streb S, Zeeman SC. Starch Metabolism in Arabidopsis. The Arabidopsis Book / American Society of Plant Biologists. 2012;10:e0160.

135. Critchley JH, Zeeman SC, Takaha T, Smith AM, Smith SM. A critical role for disproportionating enzyme in starch breakdown is revealed by a knock-out mutation in Arabidopsis. Plant J. 2001;26(1):89-100.

136. Wattebled F, Raj JP, Dauvillee D, Myes AM, James MG, Schlichting R, et al. STA11, a C*hlamydomonas reinhardtii l*ocus required for normal starch granule biogenesis, encodes disproportionating enzyme. Further evidence for a function of a -1,4 glucanotransferases during starch granule biosynthesis in green algae. . Plant Physiology. 2003;132:137-45.

137. Zeeman SC, Thorneycroft D, Schupp N, Chapple A, Weck M, Dunstan H, et al. Plastidial a -Glucan Phosphorylase Is Not Required for Starch Degradation in Arabidopsis Leaves But Has a Role in the Tolerance of Abiotic Stress. Plant Physiology. 2004;135(2):849-58.

138. Steup M, Schachtele C. Mode of glucan degradation by purified phosphorylase forms from spinach leaves. Planta. 1981;153:351-61.

139. Weise SE, Kim KS, Stewart RP, Sharkey TD. b -Maltose is the metabolically active monomer of maltose during transitory starch degradation. . Plant Physiology. 2005;137:756-61.

140. Lu Y, Sharkey TD. The role of amylomaltase in maltose metabolism in the cytosol of photosynthetic cells. Planta. 2004;218:466-73.

141. Chia T, Thorneycroft D, Chapple A, Messerli G, Chen J, Zeeman SC, et al. A cytosolic glucosyltransferase is required for conversion of starch to sucrose in Arabidopsis leaves at night. Plant Journal. 2004;37:853-63.

142. Ritte G, Lloyd JR, Eckermann N, Rottmann A, Kossmann J, Steup M. The starch-related R1 protein is an alpha -glucan, water dikinase. Proc Natl Acad Sci U S A. 2002;99(10):7166-71.

143. Baunsgaard L, Lutken H, Mikkelsen R, Glaring MA, Pham TT, Blennow A. A novel isoform of glucan, water dikinase phosphorylates pre-phosphorylated alpha-glucans and is involved in starch degradation in Arabidopsis. Plant J. 2005;41(4):595-605.

144. Lorberth R, Ritte G, Willmitzer L, Kossmann J. Inhibition of a starch-granule-bound protein leads to modified starch and repression of cold sweetening. Nat Biotechnol. 1998;16(5):473-7.

145. Hejazi M, Steup M, Fettke J. The plastidial glucan, water dikinase (GWD) catalyses multiple phosphotransfer reactions. The FEBS Journal. 2012;279(11):1953-66.

146. Kotting O, Pusch K, Tiessen A, Geigenberger P, Steup M, Ritte G. Identification of a novel enzyme required for starch metabolism in Arabidopsis leaves. The phosphoglucan, water dikinase. Plant Physiol. 2005;137(1):242-52.

147. Ritte G, Steup M, Kossmann J, Lloyd JR. Determination of the starch-phosphorylating enzyme activity in plant extracts. Planta. 2003;216(5):798-801.

148. Glaring MA, Zygadlo A, Thorneycroft D, Schulz A, Smith SM, Blennow A, et al. An extra-plastidial α-glucan, water dikinase from Arabidopsis phosphorylates amylopectin in vitro and is not necessary for transient starch degradation. Journal of Experimental Botany. 2007;58(14):3949-60.

149. Gurrieri L, Merico M, Trost P, Forlani G, Sparla F. Impact of Drought on Soluble Sugars and Free Proline Content in Selected *Arabidopsis* Mutants. Biology. 2020;9.

150. Yu TS, Kofler H, Hausler RE, Hille D, Flugge UI, Zeeman SC, et al. The Arabidopsis sex1 mutant is defective in the R1 protein, a general regulator of starch degradation in plants, and not in the chloroplast hexose transporter. Plant Cell. 2001;13(8):1907-18.

151. Herzberg O, Chen CC, Kapadia G, McGuire M, Carroll LJ, Noh SJ, et al. Swiveling-domain mechanism for enzymatic phosphotransfer between remote reaction sites. PNAS. 1996;93(7):2652-7.

152. Glaring MA, Baumann MJ, Hachem MA, Nakai H, Nakai N, Santelia D, et al. Starch-binding domains in the CBM45 family – low-affinity domains from glucan, water dikinase and α-amylase involved in plastidial starch metabolism. The FEBS Journal. 2011;278(7):1175-85.

153. Christiansen C, Abou Hachem M, Janecek S, Vikso-Nielsen A, Blennow A, Svensson B. The carbohydrate-binding module family 20--diversity, structure, and function. FEBS J. 2009;276(18):5006-29.

154. Kötting O, Pusch K, Tiessen A, Geigenberger P, Steup M, Ritte G. Identification of a Novel Enzyme Required for Starch Metabolism in Arabidopsis Leaves. The Phosphoglucan, Water Dikinase. Plant Physiology. 2005;137(1):242.

155. Hansen PI, Spraul M, Dvortsak P, Larsen FH, Blennow A, Motawia MS, et al. Starch phosphorylation--maltosidic restrains upon 3'- and 6'-phosphorylation investigated by chemical synthesis, molecular dynamics and NMR spectroscopy. Biopolymers. 2009;91(3):179-93.

156. Mikkelsen R, Baunsgaard L, Blennow A. Functional characterization of alpha-glucan,water dikinase, the starch phosphorylating enzyme. Biochem J. 2004;377(Pt 2):525-32.

157. Hejazi M, Fettke J, Paris O, Steup M. The Two Plastidial Starch-Related Dikinases Sequentially Phosphorylate Glucosyl Residues at the Surface of Both the A- and B-Type Allomorphs of Crystallized Maltodextrins But the Mode of Action Differs. Plant Physiology. 2009;150(2):962.

158. Edner C, Li J, Albrecht T, Mahlow S, Hejazi M, Hussain H, et al. Glucan, water dikinase activity stimulates breakdown of starch granules by plastidial beta-amylases. Plant Physiol. 2007;145(1):17-28.

159. Mikkelsen R, Blennow A. Functional domain organization of the potato α-glucan, water dikinase (GWD): evidence for separate site catalysis as revealed by limited proteolysis and deletion mutants. Biochemical Journal. 2005;385(Pt 2):355-61.

160. Ritte G, Scharf A, Eckermann N, Haebel S, Steup M. Phosphorylation of transitory starch is increased during degradation. Plant Physiol. 2004;135(4):2068-77.

161. Mahlow S, Hejazi M, Kuhnert F, Garz A, Brust H, Baumann O, et al. Phosphorylation of transitory starch by alpha-glucan, water dikinase during starch turnover affects the surface properties and morphology of starch granules. New Phytol. 2014;203(2):495-507.

162. Skeffington AW, Graf A, Duxbury Z, Gruissem W, Smith AM. Glucan, Water Dikinase Exerts Little Control over Starch Degradation in Arabidopsis Leaves at Night. Plant Physiol. 2014;165(2):866-79.

163. Xu X, Dees D, Dechesne A, Huang XF, Visser RGF, Trindade LM. Starch phosphorylation plays an important role in starch biosynthesis. Carbohydrate Polymers. 2017;157:1628-37.

164. Kotting O, Santelia D, Edner C, Eicke S, Marthaler T, Gentry MS, et al. STARCH-EXCESS4 Is a Laforin-Like Phosphoglucan Phosphatase Required for Starch Degradation in Arabidopsis thaliana. Plant Cell. 2009;21(1):334-46.

165. Silver DM, Kotting O, Moorhead GB. Phosphoglucan phosphatase function sheds light on starch degradation. Trends Plant Sci. 2014;19(7):471-8.

166. Pulido R, Hooft van Huijsduijnen R. Protein tyrosine phosphatases: Dual-specificity phosphatases in health and disease. FEBS J. 2008;275:848-66.

167. Tonks NK. Protein tyrosine phosphatases: from genes, to function, to disease. Nat Rev Mol Cell Biol. 2006;7(11):833-46.

168. Tonks NK. Protein tyrosine phosphatases--from housekeeping enzymes to master regulators of signal transduction. FEBS J. 2013;280(2):346-78.

169. Meekins DA, Raththagala M, Auger KD, Turner BD, Santelia D, Kotting O, et al. Mechanistic Insights into Glucan Phosphatase Activity against Polyglucan Substrates. Journal of Biological Chemistry. 2015;290(38):23361-70.

170. Patterson KI, Brummer T, O'Brien PM, Daly RJ. Dual-specificity phosphatases: critical regulators with diverse cellular targets. Biochem J. 2009;418(3):475-89.

171. Emanuelle S, Brewer MK, Meekins DA, Gentry MS. Unique carbohydrate binding platforms employed by the glucan phosphatases. Cell Mol Life Sci. 2016.

172. Zeeman SC, Northrop F, Smith AM, Rees T. A starch-accumulating mutant of Arabidopsis thaliana deficient in a chloroplastic starch-hydrolysing enzyme. Plant J. 1998;15(3):357-65.

173. Niittyla T, Comparot-Moss S, Lue W-L, Messerli G, Trevisan M, Seymour MDJ, et al. Similar protein phosphatases control starch metabolism in plants and glycogen metabolism in mammals. J Biol Chem. 2006;281(17):11815-8.

174. Hejazi M, Fettke J, Kotting O, Zeeman SC, Steup M. The Laforin-like dual-specificity phosphatase SEX4 from Arabidopsis hydrolyzes both C6- and C3-phosphate esters introduced by starch-related dikinases and thereby affects phase transition of alpha-glucans. Plant Physiol. 2010;152(2):711-22.

175. Meekins DA, Raththagala M, Husodo S, White CJ, Guo HF, Kotting O, et al. Phosphoglucan-bound structure of starch phosphatase Starch Excess4 reveals the mechanism for C6 specificity. Proc Natl Acad Sci U S A. 2014;111(20):7272-7.

176. Meekins DA, Vander Kooi CW, Gentry MS. Structural Mechanisms of Plant Glucan Phosphatases in Starch Metabolism. FEBS J. 2016.

177. Wilkens C, Auger KD, Anderson NT, Meekins DA, Raththagala M, Abou Hachem M, et al. Plant alpha-glucan phosphatases SEX4 and LSF2 display different affinity for amylopectin and amylose. FEBS Lett. 2016;590(1):118-28.

178. Vander Kooi CW, Taylor AO, Pace RM, Meekins DA, Guo HF, Kim Y, et al. From the Cover: Structural basis for the glucan phosphatase activity of Starch Excess4. Proc Natl Acad Sci U S A. 2010;107(35):15379-84.

179. Santelia D, Kotting O, Seung D, Schubert M, Thalmann M, Bischof S, et al. The phosphoglucan phosphatase like sex Four2 dephosphorylates starch at the C3-position in Arabidopsis. Plant Cell. 2011;23(11):4096-111.

180. Comparot-Moss S, Kotting O, Stettler M, Edner C, Graf A, Weise SE, et al. A putative phosphatase, LSF1, is required for normal starch turnover in Arabidopsis leaves. Plant Physiol. 2010;152(2):685-97.

181. Meekins DA, Guo HF, Husodo S, Paasch BC, Bridges TM, Santelia D, et al. Structure of the Arabidopsis glucan phosphatase like sex four2 reveals a unique mechanism for starch dephosphorylation. Plant Cell. 2013;25(6):2302-14.

182. Schreier TB, Umhang M, Lee S-K, Lue W-L, Shen Z, Silver D, et al. LIKE SEX4 1 Acts as a b-Amylase-Binding Scaffold on Starch Granules during Starch Degradation. The Plant Cell. 2019;31:2169-86.

183. Minassian BA. Lafora's disease: towards a clinical, pathologic, and molecular synthesis. Pediatr Neurol. 2001;25(1):21-9.

184. Sakai M, Austin J, Witmer F, Trueb L. Studies in myoclonus epilepsy (Lafora body form). II. Polyglucosans in the systemic deposits of myoclonus epilepsy and in corpora amylacea. Neurology. 1970;20(2):160-76.

185. Gentry MS, Dowen RH, 3rd, Worby CA, Mattoo S, Ecker JR, Dixon JE. The phosphatase laforin crosses evolutionary boundaries and links carbohydrate metabolism to neuronal disease. J Cell Biol. 2007;178(3):477-88.

186. Pitcher J, Smythe C, Cohen P. Glycogenin is the priming glucosyltransferase required for the initiation of glycogen biogenesis in rabbit skeletal muscle. Eur J Biochem. 1988;176(2):391-5.

187. Chatterjee M, Berbezy P, Vyas D, Coates S, Barsby T. Reduced expression of a protein homologous to glycogenin leads to reduction of starch content in *Arabidopsis* leaves. Plant Science. 2005;168:501-9.

188. Pancha I, Tanaka K, Imamura S. Overexpression of a glycogenin, CmGLG2, enhances floridean starch accumulation in the red alga *Cyanidioschyzon merolae.* Plant Signaling and Behavior. 2019;14(6).

189. Pancha I, Shima H, Higashitani N, Igarashi K, Higashitani A, Tanaka K, et al. Target of rapamycin-signaling modulates starch accumulation via glycogenin phosphorylation status in the unicellular red alga *Cyanidioschyzon merolae* The Plant Journal. 2019;97:485-99.

190. Roach PJ, Skurat AV. Self-Glucosylating Initiator Proteins and Their Role in Glycogen Biosynthesis. Progress in Nucleic Acid Research and Molecular Biology. 1997;57:289-316.

191. Imamura S, Kawase Y, Kobayashi I, Sone T, Era A, Miyagishima S, et al. Target of rapamycin (TOR) plays a critical role in triacylglycerol accumulation in microalgae. Plant Mol Biol. 2015.

192. Zhou W, He S, Naconsie M, Ma Q, Zeeman SC, Gruissem W, et al. Alpha-Glucan, Water Dikinase 1 Affects Starch Metabolism and Storage Root Growth in Cassava (Manihot esculenta Crantz). Scientific Reports. 2017;7:9863.

193. Takusagawa M, Nakajima Y, Saito T, Misumi O. Primitive red alga C*yanidioschyzon merolae* accumulates storage glucan and triacylglycerol under nitrogen depletion. J Gen Appl Microbiol. 2016;62:111-7.

194. Raththagala M, Brewer MK, Parker MW, Sherwood AR, Wong BK, Hsu S, et al. Structural Mechanism of Laforin Function in Glycogen Dephosphorylation and Lafora Disease. Molecular Cell. 2015;57(2):261-72.

195. Thompson JD, Higgins DG, Gibson TJ. CLUSTAL W: improving the sensitivity of progressive multiple sequence alignment through sequence weighting, position-specific gap penalties and weight matrix choice. Nucl Acids Res. 1994;22(22):4673-80.

196. Kobayashi Y, Ohnuma M, Kuroiwa T, Tanaka K, Hanaoka M. The basics of cultivation and molecular genetic analysis of the unicellular red alga *Cyanidioschyzon merolae*. Journal of Endocytobiosis and Cell Research. 2010;20:53-61.

197. Fujiwara T, Ohnuma M. Procedures for Transformation and Their Applications in *Cyanidioschyzon merolae* In: Kuroiwa T, Miyagishima S, Matsunaga S, Sato N, Nozaki H, Tanaka K, et al., editors. *Cyanidioschyzon merolae:* A New Model Eukaryote for Cell and Organelle Biology. Singapore: Springer Nature; 2017. p. 87-103.

198. Nishida K, Misumi O, Yagisawa F, Kuroiwa H, Nagata T, Kuroiwa T. Triple Immunofluorescent Labeling of FtsZ, Dynamin, and EF-Tu Reveals a Loose Association Between the Inner and Outer Membrane Mitochondrial Division Machinery in the Red Alga Cyanidioschyzon merolae. J Histochem Cytochem. 2004;52(7):843-9.

199. Morell MK, Samuel MS, O'Shea MG. Analysis of starch structure using fluorophore-assisted carbohydrate electrophoresis. *Electrophoresis*. 1998;19:2603-11.

200. Sun RC, Dukhanda VV, Zhou Z, Young LEA, Emanuelle S, Brainson CF, et al. Nuclear Glycogenolysis Modulates Histone Acetylation in Human Non-Small Cell Lung Cancers. Cell Metabolism. 2019;30(5):903-16.

201. Young LEA, Brizzee CO, Macedo JKA, Murphy RD, Contreras CJ, DePaoli-Roach AA, et al. Accurate and sensitive quantitation of glucose and glucose phosphates derived from storage carbohydrates by mass spectrometry. Carbohydrate Polymers. 2020;230.

202. Nitschke F, Wang P, Schmieder P, Girard JM, Awrey DE, Wang T, et al. Hyperphosphorylation of glucosyl C6 carbons and altered structure of glycogen in the neurodegenerative epilepsy Lafora disease. Cell Metab. 2013;17(5):756-67.

203. Sullivan MA, Nitschke S, Skwara EP, Wang P, Zhao X, Pan XS, et al. Skeletal Muscle Glycogen Chain Length Correlates with Insolubility in Mouse Models of Polyglucosan-Associated Neurodegenerative Diseases. Cell Reports. 2019;27:1334-44.

204. Gallant D, Guilbot A. Etude de l'ultrastructure du grain d'amidon à l'aide de nouvelles méthodes de préparation en microscopie électronique. . *Die stärke* 1969;6:156-63.

205. Hejazi M, Mahlow S, Fettke J. The glucan phosphorylation mediated by alpha-glucan, water dikinase (GWD) is also essential in the light phase for a functional transitory starch turn-over. Plant Signal Behav. 2014;9.

206. Ritte G, Lloyd JR, Eckermann N, Rottmann A, Kossmann J, Steup M. The starch-related R1 protein is an α-glucan, water dikinase. Proceedings of the National Academy of Sciences of the United States of America. 2002;99(10):7166-71.

207. Pirone C, Gurrieri L, Gaiba I, Adamiano A, Valle F, Trost P, et al. The analysis of the different functions of starch-phosphorylating enzymes during the development of Arabidopsis thaliana plants discloses an unexpected role for the cytosolic isoform GWD2. Physiologia Plantarum. 2017;160(4):447-57.

208. Miyagishima S-y, Itoh R, Aita S, Kuroiwa H, Kuroiwa T. Isolation of dividing chloroplasts with intact plastid-dividing rings from a synchronous culture of the unicellular red alga Cyanidioschyzon merolae. Planta. 1999;209(3):371.

209. Miyagishima S-y, Takahara M, Mori T, Kuroiwa H, Higashiyama T, Kuroiwa T. Plastid Division Is Driven by a Complex Mechanism That Involves Differential Transition of the Bacterial and Eukaryotic Division Rings. Plant Cell. 2001;13(10):2257-68.

210. Nishida K, Yagisawa F, Kuroiwa H, Nagata T, Kuroiwa T. Cell Cycle-regulated, Microtubule-independent Organelle Division in Cyanidioschyzon merolae. Mol Biol Cell. 2005;16(5):2493-502.

211. Yoshida Y, Kuroiwa H, Misumi O, Yoshida M, Ohnuma M, Fujiwara T, et al. Chloroplasts divide by contraction of a bundle of nano filaments consisting of polyglucan. Science. 2010;329(5994):949-53.

212. Yoshida Y, Kuroiwa H, Shimada T, Yoshida M, Ohnuma M, Fujiwara T, et al. Glycosyltransferase MDR1 assembles a dividing ring for mitochondrial proliferation comprising polyglucan nanofilaments. . PNAS. 2017;114:284-9.

213. Altschul SF, Madden TL, Schaffer AA, Zhang J, Zhang Z, Miller W, et al. Gapped BLAST and PSI-BLAST: a new generation of protein database search programs. Nucleic Acids Res. 1997;25(17):3389-402.

214. Mikkelsen R, Suszkiewicz K, Blennow A. A Novel Type Carbohydrate-Binding Module Identified in alpha -Glucan, Water Dikinases Is Specific for Regulated Plastidial Starch Metabolism. Biochemistry. 2006;45:4674-82.

215. Orzechowski S, Grabowska A, Sitnicka D, Siminska J, Felus M, Dudkiewicz M, et al. Analysis of the expression, subcellular and tissue localisation of phosphoglucan, water dikinase (PWD/GWD3) in Solanum tuberosum L.: a bioinformatics approach for the comparative analysis of two α-glucan, water dikinases (GWDs) from Solanum tuberosum L. Acta Physiologiae Plantarum. 2013;35(2):483-500.

216. Emanuelsson O, Nielsen H, Heijne G. ChloroP, a neural network-based method for predicting chloroplast transit peptides and their cleavage sites. Protein Science. 1999;8(5):978-84.

217. Mikkelsen R, Baunsgaard L, Blennow A. Functional characterization of alpha-glucan,water dikinase, the starch phosphorylating enzyme. Biochemical Journal. 2004;377(Pt 2):525-32.

218. Ganesh S, Tsurutani N, Suzuki T, Hoshii Y, Ishihara T, Delgado-Escueta AV, et al. The carbohydrate-binding domain of Lafora disease protein targets Lafora polyglucosan bodies. Biochem Biophys Res Commun. 2004;313(4):1101-9.

219. Gentry MS, Guinovart JJ, Minassian BA, Roach PJ, Serratosa JM. Lafora disease offers a unique window into neuronal glycogen metabolism. Journal of Biological Chemistry. 2018;293(19):7117-25.

220. Wang ZT, Ullrich N, Joo S, Waffenschmidt S, Goodenough U. Algal Lipid Bodies: Stress Induction, Purification, and Biochemical Characterization in Wild-Type and Starchless *Chlamydomonas reinhardtii*. Eukaryotic Cell. 2009;8(12):1856-68.

221. Park JJ, Wang H, Gargouri M, Dashpande RR, Slepper JN, Holguin FO, et al. The response of *Chlamydomonas reinhardtii* to nitrogendeprivation: a systems biology analysis. The Plant Journal. 2015;81:611-24.

222. Smith AM, Stitt M. Coordination of carbon supply and plant growth. Plant, Cell and Environment. 2007;30:1126-49.

223. Toyoshima M, Mori N, Moriyama T, Misumi O, Sato N. Analysis of triacylglycerol accumulation under nitrogen deprivation in the red alga *Cyanidioschyzon merolae* Microbiology. 2016;162:803-12.

224. Delvalle D, Dumez S, Wattebled F, Roldan I, Planchot V, Berbezy P, et al. Soluble starch synthase I: a major determinant for the synthesis of amylopectin in *Arabidopsis thaliana* leaves The Plant Journal. 2005;43:398-412.

225. Rigden DJ, Michels PA, Ginger ML. Autophagy in protists: Examples of secondary loss, lineage-specific innovations, and the conundrum of remodeling a single mitochondrion. Autophagy. 2009;5(6):784-94.

226. Imamura S, Kawase Y, Kobayashi I, Shimojima M, Ohta H, Tanaka K. TOR (target of rapamycin) is a key regulator of triacylglycerol accumulation in microalgae. Plant Signaling & Behavior. 2016;11(3).

227. Yagisawa F, Nishida K, Yoshida M, Ohnuma M, Shimada T, Fujiwara T, et al. Identification of novel proteins in isolated polyphosphate vacuoles in the primitive red alga *Cyanidioschyzon merolae*. The Plant Journal. 2009;60:882-93.

228. Damager I, Engelsen SB, Blennow A, Moller BL, Motawia MS. First principles insight into the alpha-glucan structures of starch: their synthesis, conformation, and hydration. Chemical Reviews. 2010;110(4):2049-80.

229. Blennow A. Phosphorylation of the Starch Granule. In: Nakamura Y, editor. Starch: Metabolism and Structure. Tokyo: Springer Japan; 2015. p. 399-424.

230. Mahdi H, Fettke J, Steup M. Starch phosphorylation and dephosphorylation: The consecutive action of starch-related dikinases and phosphatases2012. 279-309 p.

231. Jane J-L, Kasemsuwan T, Chen JF, Juliano B. Phosphorus in rice and other starches 1,21996. 827-32 p.

232. Huang L-F, Liu Y-K, Su S-C, Lai C-C, Wu C-R, Chao T-J, et al. Genetic engineering of transitory starch accumulation by knockdown of *OsSEX4* in rice plants for the enhanced bioethanol production. Biotechnology and Bioengineering. 2020;117:933-44.

233. McCracken DA, Cain JR. Amylose in Floridean Starch. New Phytologist. 1981;88(1):67-71.

234. Yu S, Blennow A, Bojko M, Madsen F, Olsen CE, Engelsen SB. Physico-chemical characterization of Floridian starch of red algae. Starch. 2002;54:66-74.

235. Misumi O, Yoshida Y, Nishida K, Fujiwara T, Sakajiri T, Hirooka S, et al. Genome analysis and its significance in four unicellular algae, Cyanidioshyzon merolae, Ostreococcus tauri, Chlamydomonas reinhardtii, and Thalassiosira pseudonana. J Plant Res. 2008;121(1):3-17.

236. Schonknecht G, Chen WH, Ternes CM. Gene transfer from bacteria and archaea facilitated evolution of an extremophilic eukaryote. Science. 2013;339:1207-10.

237. Takeda Y, Hizukuri S. Studies on starch phosphate. Part; 1981.

238. Worby CA, Gentry MS, Dixon JE. Laforin: A dual specificity phosphatase that dephosphorylates complex carbohydrates. J Biol Chem. 2006;281(41):30412-8.

239. Wang J, Stuckey JA, Wishart MJ, Dixon JE. A unique carbohydrate binding domain targets the lafora disease phosphatase to glycogen. J Biol Chem. 2002;277(4):2377-80.

240. Denu JM, Stuckey JA, Saper MA, Dixon JE. Form and Function in Protein Dephosphorylation. Cell. 1996;87(3):361.

241. Minassian BA, Lee JR, Herbrick JA, Huizenga J, Soder S, Mungall AJ, et al. Mutations in a gene encoding a novel protein tyrosine phosphatase cause progressive myoclonus epilepsy. Nat Genet. 1998;20(2):171-4.

242. Minassian BA. Progressive myoclonus epilepsy with polyglucosan bodies: Lafora disease. Adv Neurol. 2002;89:199-210.

243. Lafora GR. Uber des Vorkommen amyloider KJrperchen im innern der Ganglienzellen. Virchows Arch f Path Anat. 1911;205:295.

244. Collins GH, Cowden RR, Nevis AH. Myoclonus epilepsy with Lafora bodies. An ultrastruc- tural and cytochemical study. Arch Pathol. 1968;86(3):239-54.

245. Brewer MK, Putaux J-L, Rondon A, Uittenbogaard A, Sullivan MA, Gentry MS. Polyglucosan body structure in Lafora disease. Carbohydrate Polymers. 2020;240.

246. Drozdetskiy A, Cole C, Procter J, Barton GJ. JPred4: a protein secondary structure prediction server. Nucleic Acids Research. 2015.

247. Bernhofer M, Dallago C, Karl T, Satagopam V, Heinzinger M, Littmann M, et al. PredictProtein - Predicting Protein Structure and Function for 29 Years. bioRxiv. 2021.

248. Wang S, Li W, Liu S, Xu J. RaptorX-Property: a web server for protein structure property prediction. Nucleic Acids Research. 2016.

249. Blennow A, Nielsen TH, Baunsgaard L, Mikkelsen R, Engelsen SB. Starch phosphorylation: a new front line in starch research. Trends Plant Sci. 2002;7(10):445-50.

250. Vikso-Nielsen A, Hao-Jie Chen P, Larsson H, Blennow A, Moller BL. Production of highly phosphorylated glycopolymers by expression of R1 in Escherichia coli. Carbohydr Res. 2002;337(4):327-33.

251. Zeeman SC, Rees TA. Changes in carbohydrate metabolism and assimilate export in starch-excess mutants of *Arabidopsis.* Plant, Cell and Environment. 1999;22:1445-53.

252. Nitschke S, Chow n EE, Zha o X, Gabrielia n S, Petkovi c S, Guiss o DR, et al. An inducible glycogen synthase-1 knockout halts but does not reverse Lafora disease progression in mice. The Journal of Biological Chemistry. 2021;296:100150.

253. Meekins DA, Vander Kooi CW, Gentry MS. Structural Mechanisms of Plant Glucan Phosphatases in Starch Metabolism. The FEBS journal. 2016;283(13):2427-47.

254. Samodien E, Jewell JF, Loedolff B, Oberlander K, George GM, Zeeman SC, et al. Repression of *Sex4* and *Like Sex Four2* Orthologs in Potato Increases

Tuber Starch Bound Phosphate With Concomitant Alterations in Starch Physical Properties. Frontiers in Plant Science. 2018;9.

255. Wang ZT, Ulrich N, Joo S, Waffenschmidt S, Goodenough U. Algal Lipid Bodies: Stress Induction, Purification, and Biochemical Characterization in Wild-Type and Starchless C*hlamydomonas reinhardtii.* . Eukaryotic Cell. 2009;8(12):1856-68.

256. Lin TP, Caspar T, Somerville C, Preiss J. Isolation and characterization of a starchless mutant of A*rabidopsis thaliana (*L.) Heynh. lacking ADPglucose pyrophosphorylase activity. . Plant Physiology. 1988;86:1131-5.

257. Xu X, Huang X-F, Visser RGF, Trindade LM. Engineering Potato Starch with a Higher Phosphate Content. . PLoS ONE. 2017;12(1).

258. Kozlov SS, Blennow A, Krivandin AV, Yuryev VP. Structural and thermodynamic properties of starches extracted from GBSS and GWD suppressed potato lines. Int J Biol Macromol. 2007;40(5):449-60.

259. Lloyd JR, Landschutze V, Kossmann J. Simultaneous antisense inhibition of two starch-synthase isoforms in potato tubers leads to accumulation of gross modified amylopectin. Biochem J. 1999;338:515-21.

260. Fulton DC, Edwards A, Pilling E, Robinson HL, Fahy B, Seale R, et al. Role of Granule-bound Starch Synthase in Determination of Amylopectin Structure and Starch Granule Morphology in Potato. The Journal of Biological Chemistry. 2002;277:10834-41.

261. Fontaine T, D'Hulst C, Maddelein M-L, Routier F, Pepin TM, Decq A, et al. Towards the understanding of the biogenesis of the starch granule. Evidence that C*hlamydomanas s*oluble starch synthase II controls the synthesis of intermediate size glucans of amylopectin. . The Journal of Biological Chemistry. 1993;268(22):16223-30.

262. Wang W, Lohi H, Skurat AV, Depaoli-Roach AA, Minassian BA, Roach PJ. Glycogen metabolism in tissues from a mouse model of Lafora disease. Arch Biochem Biophys. 2007;457(2):264-9.

263. Stitt M, Zeeman SC. Starch turnover: pathways, regulation and role in growth. Current Opinion in Plant Biology. 2012;15(3):282-92.

264. Klotz A, Georg J, Bucinska L, Watanabe S, Reimann V, Januszewski W, et al. Awakening of a Dormant Cyanobacterium from Nitrogen Chlorosis Reveals a Genetically Determined Program. . Current Biology. 2016;26(21):1139-41.

265. Valcourt JR, Lemons JMS, Haley EM, Kojima M, Demuren OO, Coller HA. Staying Alive. Cell Cycle. 2012;11(9):1680-96.

266. Boraston AB, Bolam DN, Gilbert HJ, Davies GJ. Carbohydrate-binding modules: fine-tuning polysaccharide recognition. The Biochemical Journal. 2004;382:769-81.

267. Boraston AB, Healey M, Klassen J, Ficko-Blean E, Lammerts van Bueren A, Law V. A structural and functional analysis of alpha-glucan recognition by family 25 and 26 carbohydrate-binding modules reveals a conserved mode of starch recognition. J Biol Chem. 2006;281(1):587-98.

268. Terrapon N, Lombard V, Drula E, Coutinho PM, Henrissat B. The CAZy Database/the Carbohydrate-Active Enzyme (CAZy) Database: Principles

and Usage Guidelines. In: Aoki-Kinoshita KF, editor. A practical guide to using glycomics databases. Japan: Springer; 2017. p. 117-31.

269. Janecek S, Marecek F, MacGregor EA, Svensson B. Starch-binding domains as CBM families - history, occurrence, structure, function and evolution. Biotechnology Advances. 2019.

270. Carciofi M, Shaik SS, Jensen SL, Blennow A, Svensson JT, Vincze É, et al. Hyperphosphorylation of cereal starch. Journal of Cereal Science. 2011;54(3):339-46.

271. Vikso-Nielsen A, Blennow A, Jorgensen K, Kristensen KH, Jensen A, Moller BL. Structural, Physicochemical, and Pasting Properties of Starches from Potato Plants with Repressed *r1*-Gene. Biomacromolecules. 2001;2:836-43.

272. Blennow A, Jensen SL, Shaik SS, Skryhan K, Carciofi M, Holm PB, et al. Future Cereal Starch Bioengineering: Cereal Ancestors Encounter Gene Technology and Designer Enzymes. Cereal Chemistry. 2013;90(4).

273. Janecek S, Svensson B, MacGregor EA. Structural and evolutionary aspects of two families of non-catalytic domains present in starch and glycogen binding proteins from microbes, plants and animals. Enzyme Microb Technol. 2011;49(5):429-40.

274. Niesen FH, Berglund H, Vedadi M. The use of differential scanning fluorimetry to detect ligand interactions that promote protein stability. Nat Protoc. 2007;2(9):2212-21.

275. Layton CJ, Hellinga HW. Quantitation of protein-protein interactions by thermal stability shift analysis. Protein Science: a publication of the protein society. 2011;20(8):1439-50.

276. Matulis D, Kranz JK, Salemme FR, Todd MJ. Thermodynamic stability of carbonic anhydrase: measurements of binding affinity and stoichiometry using ThermoFluor. Biochemistry. 2005;44(13):5258-66.

277. Gentry MS, Pace RM. Conservation of the glucan phosphatase laforin is linked to rates of molecular evolution and the glycogen metabolism of the organism. BMC Evol Biol. 2009;9(1):138.

278. Betts MJ, Russell RB. Amino Acid Properties and Consequences of Substitutions. In: Barnes MR, Gray IC, editors. Bioinformatics for Geneticists: John Wiley & Sons; 2003. p. 289-316.

279. Kelley LA, Mezulis S, Yates CM, Wass MN, Sternberg MJE. The Phyre2 web portal for protein modelling, prediction and analysis. Nature Protocols. 2015;10(6):845-58.

280. Wilkens C, Svensson B, Moller MS. Functional Roles of Starch Binding Domains and Surface Binding Sites in Enzymes Involved in Starch Biosynthesis. Frontiers in Plant Science. 2018;9.

281. Christiansen C, Hachem MA, Glaring MA, Vikso-Nielsen A, Sigurskjold BW, Svensson B, et al. A CBM20 low-affinity starch-binding domain from glucan, water dikinase. FEBS Letters. 2009;583(7):1159-63.

282. Fontana JD. The presence of phosphate in glycogen. FEBS Lett. 1980;109(1):85-92.

283. Chen Y, Sun X, Zhou X, Hebelstrup KH, Blennow A, Bao J. Highly phosphorylated functionalized rice starch produced by transgenic rice expressing the potato GWD1 gene. Scientific Reports. 2017;7:3339.

284. Bowerman AF, Newberry M, Dielen A-S, Whan A, Larroque O, Pritchard J, et al. Suppression of glucan, water dikinase in the endosperm alters wheat grain properties, germination and coleoptile growth. Plant Biotechnology Journal. 2015;14(1):398-408.

285. Ral J-P, Bowerman AF, Li Z, Sirault X, Furbank R, Pritchard JR, et al. Down-regulation of Glucan, Water-Dikinase activity in wheat endosperm increases vegetative biomass and yield. Plant Biotechnology Journal. 2012;10:871-82.

286. Shaik SS, Obata T, Hebelstrup KH, Schwahn K, Fernie AR, Mateiu RV, et al. Starch Granule Re-Structuring by Starch Branching Enzyme and Glucan Water Dikinase Modulation Affects Caryopsis Physiology and Metabolism. PLOS ONE. 2016;11(2):e0149613.

287. Carpenter MA, Joyce NI, Genet RA, Cooper RD, Murray SR, Noble AD, et al. Starch phosphorylation in potato tubers is influenced by allelic variation in the genes encoding glucan water dikinase, starch branching enzymes I and II, and starch synthase III. Frontiers in Plant Science. 2015;6:143.

288. Hirose T, Aoki N, Harada Y, Okamura M, Hashida Y, Ohsugi R, et al. Disruption of a rice gene for α-glucan water dikinase, OsGWD1, leads to hyperaccumulation of starch in leaves but exhibits limited effects on growth. Frontiers in Plant Science. 2013;4:147.

289. Zhou W, He S, Naconsie M, Ma Q, Zeeman SC, Gruissem W, et al. Alpha-Glucan, Water Dikinase 1 Affects Starch Metabolism and Storage Root Growth in Cassava (*Manihot esculenta* Crantz). Scientific Reports. 2019.

290. Wang W, Hostettler CE, Damberger FF, Kossmann J, Lloyd JR, Zeeman SC. Modification of Cassava Root Starch Phosphorylation Enhances Starch Functional Properties. Frontiers in Plant Science. 2018;9.

291. Craig J, Lloyd JR, Tomlinson K, Barber L, Edwards A, Wang TL, et al. Mutations in the gene encoding starch synthase II profoundly alter amylopectin structure in pea embryos. The Plant Cell. 1998;10:413-26.

292. Edwards A, Fulton DC, Hylton CM, Jobling SA, Gidley M, Rossner U, et al. A combined reduction in activity of starch synthase II and III of potato has novel effects on the starch of tubers. The Plant Journal. 1999;17(3):251-61.

293. Marshall J, Sidebottom C, Debet M, Martin C, Smith AM, Edwards A. Identification of the major starch synthase in the soluble fraction of potato tubers. The Plant Cell. 1996;8:1121-35.

294. Blennow A, Hansen M, Schulz A, Jorgensen K, Donald AM, Sanderson J. The molecular deposition of transgenically modified starch in the starch granule as imaged by functional microscopy. Journal of Structural Biology. 2003;143:229-41.

295. Malinova I, Fettke J. Reduced starch granule number per chloroplast in the dpe2/phs1 mutant is dependent on initiation of starch degradation. PLoS ONE. 2017;12(11).

296. Sawada T, Nakamura Y, Ohdan T, Saitoh A, Francisco Jr. PB, Suzuki E, et al. Diversity of reaction characteristics of glucan branching enzymes and the fine structure of a-glucan from various sources. Archives of Biochemistry and Biophysics. 2014;562:9-21.

297. Dauvillee D, Deschamps P, Ral J-P, Plancke C, Putaux J-L, Devassine J, et al. Genetic dissection of floridean starch synthesis in the cytosol of the model dinoflagellate *Crypthecodinium cohnii.* PNAS. 2009.

298. Broberg S, Koch K, Kenne AL. A comparison between MALDI-TOF mass spectrometry and HPAEC-PAD analysis of debranched starch. Carbohydrate Polymers. 2000;43:285-9.

VITA

Corey Owen Brizzee

EDUCATION

University of Rochester, Rochester, NY May 2012
Bachelor of Arts in Biology

RESEARCH EXPERIENCE

University of Rochester, Rochester, NY 2012- 2014
Research Assistant, Department of Anesthesiology

PUBLICATIONS

1. **Corey O. Brizzee**, Savita Sharma, Nico Sydlowski, Keiko Taki, Ying Jones, Jean-Luc Putaux, Sousuke Imamura, Kan Tanaka, Ramon Sun, Craig Vander Kooi, and Matthew S. Gentry. Abolishing glucan-water dikinase phosphorylation of semi-amylopectin in *Cyanidioschyzon merolae,* results in altered granule morphology and flux of carbon. *Plant Cell.* 2021 *IN PREPARATION*

2. **Corey O. Brizzee**, Savita Sharma, Jean-Luc Putaux, Sousuke Imamura, Kan Tanaka, Ramon Sun, Craig Vander Kooi, and Matthew S. Gentry. Aberrant Polyglucan Structure, Granule Morphology, and Nutrient-Scavenging: Evidence Towards the Role of Laforin in *Cyanidioschyzon merolae*. *Plant Cell.* 2021 *IN PREPARATION*

3. Andrea Kuchtova, **Corey O. Brizzee**, Tiantian Chen, Matthew S. Gentry and Craig Vander Kooi. Structure of a CBM45 of α-Glucan, Water Dikinase from the Red Alga, *Cyanidioschyzon merolae.* TBD 2021 *IN PREPARATION*

4. Lyndsay E.A. Young, **Corey O. Brizzee**, Jessica K. A. Macedo, Robert D. Murphy, Christopher J. Contreras, Anna A. DePaoli-Roach, Peter J. Roach, Matthew S. Gentry, and Ramon C. Sun. Accurate and sensitive quantitation of glucose and glucose phosphates derived from storage carbohydrates by mass spectrometry. *Carbohydrate Polymers.* 2020 Feb (230).

5. Lei Z, **Brizzee C**, Johnson GV. BAG3 facilitates the clearance of endogenous tau in primary neurons*. Neurobiology of Aging.* 2015 Jan;36(1): 241-248.

AWARDS AND HONORS

ASBMB Graduate Travel Award, $1,000 2016
Max Steckler Award, $8,350 2018